Global Carbon Budget ~~2025~~2026

Pierre ~~Friedlingstein[1~~Friedlingstein[1,2]~~],~~ Michael ~~O'Sullivan[1], Matthew W. Jones[3],~~O'Sullivan[1], Robbie M. ~~Andrew[4], Dorothee C. E. Bakker[5],~~Andrew[3], Judith ~~Hauck[6~~Hauck[4,5], Matthew W. Jones[6,7]~~],~~ Peter ~~Landschützer[8],~~Landschützer[8], Corinne Le ~~Quéré[3],~~Quéré[6], Hongmei ~~Li[9~~Li[9,10]~~],~~ Ingrid T. ~~Luijkx[11],~~Luijkx[11], Are Olsen[12,13], Glen P. ~~Peters[4],~~Peters[3], Wouter ~~Peters[11,12],~~Peters[11,14], Julia ~~Pongratz[13,10],~~Pongratz[15], Clemens ~~Schwingshackl[13],~~Schwingshackl[15], Stephen ~~Sitch[1],~~Sitch[1], Josep G. ~~Canadell[14],~~Canadell[16], Philippe ~~Ciais[15],~~Ciais[17], Kjetil ~~Aas[4],~~Aas[3], Simone R. ~~Alin[16], Peter Anthoni[17], Leticia Barbero[18],~~Alin[18], Vivek Arora[19], Nicholas R. ~~Bates[19,20],~~Bates[20,21], Kimberly Bedard[22], David Martin Belda[23], Nicolas ~~Bellouin[21],~~Bellouin[24], Alice Benoit-~~Cattin[22],~~Cattin[25], Carla F. ~~Berghoff[23], Raffaele Bernardello[24],~~Berghoff[26], Sarah Berthet[27], Laurent ~~Bopp[2],~~Bopp[2], Ida Bagus Mandhara ~~Brasika[1,25],~~Brasika[1,28], Eleanor Burke[29], Leon Casse[30,31], Matthew A. ~~Chamberlain[26], Naveen Chandra[27],~~Chamberlain[32], Frédéric ~~Chevallier[15],~~Chevallier[17], Louise P. ~~Chini[28], Nathan O. Collier[29], Thomas H. Colligan[30],~~Chini[33], Margot ~~Cronin[31], Laique M. Djeutchouang[32,33,34], Xinyu Dou[35], Matt P. Enright[19,20],~~Cronin[34], Susan E. Curless[35,18], Tim DeVries[36], Tobias Ehmen[12,13], Matthew P. Enright[20], Kazutaka ~~Enyo[36],~~Enyo[37], Michael ~~Erb[37,38],~~Erb[38,39], Wiley ~~Evans[39], Richard A. Feely[16], Liang Feng[40,41],~~Evans[22], Amanda R Fay[40], Ben Felzer[41], Daniel J. ~~Ford[1],~~Ford[1], Adrianna ~~Foster[42],~~Foster[42], Filippa ~~Fransner[43,44], Thomas Gasser[45],~~Fransner[12,13], Agneta Fransson[43], Andrew Friedman[44], Thomas Gasser[45], Marion ~~Gehlen[15],~~Gehlen[17], Thanos ~~Gkritzalis[8], Jefferson Goncalves De Souza[1],~~Gkritzalis[8], Giacomo ~~Grassi[46],~~Grassi[46], Luke ~~Gregor[47~~Gregor[47,48]~~],~~ Nicolas ~~Gruber[47], Bertrand Guenet[49],~~Gruber[47], Özgür ~~Gürses[6],~~Gürses[4], Wensu Hao[49], Kirsty ~~Harrington[50], Ian Harris[51],~~Harrington[50], Jens ~~Heinke[52],~~Heinke[51], George C. ~~Hurtt[28], Yosuke Iida[36],~~Hurtt[33], Tatiana ~~Ilyina[53,9,10],~~Ilyina[9], Akihiko ~~Ito[54],~~Ito[52], Andrew R. ~~Jacobson[55,56],~~Jacobson[53,54], Atul K. ~~Jain[57],~~Jain[55], Rajesh R. Janardanan[56], Tereza ~~Jarníková[3],~~Jarníková[6], Annika ~~Jersild[30],~~Jersild[57], Fei ~~Jiang[58], Steve D. Jones[8],~~Jiang[58], Zhe Jin[59], Linus Kamb[35,18], Etsushi ~~Kato[59],~~Kato[60], Ralph F. ~~Keeling[60],~~Keeling[61], Kees Klein ~~Goldewijk[61],~~Goldewijk[62], Jürgen ~~Knauer[62], Yawen Kong[63,64],~~Knauer[63], Jan Ivar ~~Korsbakken[4], Charles Koven[65],~~Korsbakken[3], Taro ~~Kunimitsu[4],~~Kunimitsu[3], Xin ~~Lan[55,56],~~Lan[53,54], Vladimir Lapin[64], Siv K. Lauvset[65,13], Simone Le Chevère[4], Woo-Sung Lee[66], Enhui Liao[67], Junjie ~~Liu[66,67], Zhiqiang Liu[68],~~Liu[68,69], Zhu ~~Liu[69], Claire Lo Monaco[70],~~Liu[70], Sebastiaan Luyssaert[71], Lei ~~Ma[28],~~Ma[33], Suman Maity[56], Gregg ~~Marland[37,38],~~Marland[38,39], Patrick C. ~~McGuire[71], Galen A. McKinley[72], Joe R. Melton[73],~~McGuire[72], Nicolas Metzl[73], Juliette Mignot[73], Natalie ~~Monacci[74], Erwan Monier[75,76],~~M. Monacci[74], Eric J. ~~Morgan[60], David R. Munro[55,56],~~Morgan[61], Jens D. ~~Müller[Müller[75,76,77]~~],~~ David R. Munro[53,54], Miaki Muramatsu[37], Shin-Ichiro ~~Nakaoka[78], Lorna R. Nayagam[78], Yosuke Niwa[78], Tobias Nutzel[13], Are Olsen[43,44], Abdirahman M. Omar[79,44], Naiqing Pan[80],~~Nakaoka[56], Craig Neill[32], Tobias Nützel[15], Léa

Formatted: Font: 36 pt

Formatted: Superscript

Formatted: Space After: 10 pt

Formatted: Numbering: Continuous

Formatted: Superscript

Formatted: Superscript

Formatted: Superscript

Formatted: Superscript

Olivier[4,15], Timothy Osborn[78], Xosé A. Padín[79], Paul I Palmer[80,81], Sudhanshu ~~Pandey[66],~~Pandey[68], Denis ~~Pierrot[81],~~Pierrot[82], Ben Poulter[83], Zhangcai ~~Qin[82], Pierre Regnier[83],~~Qin[84], Yumou Qiu[85], Gregor ~~Rehder[84],~~Rehder[86], Laure ~~Resplandy[85], Alizée Roobaert[8], Thais M. Rosan[1],~~Resplandy[87], Christian ~~Rödenbeck[86],~~Rödenbeck[88], Alizée Roobaert[8], Thais M. Rosan[1], Simone Rossi[46], Jörg ~~Schwinger[44,79],~~Schwinger[13,65], Gereon Seeberg[15], Roland Séférian[27], Elisabeth H. Shadwick[32,89], Ingunn ~~Skjelvan[79,44],~~Skjelvan[65,13], Karolina Slominska-Durdasiak[88], T. Luke ~~Smallman[40,41], Victoria Spada[87],~~Smallman[80,81], Mohanan G. ~~Sreeush[6],~~Sreeush[4], Qing ~~Sun[88],~~Sun[90,76,77], Adrienne J. ~~Sutton[16],~~Sutton[18], Colm ~~Sweeney[56], Didier Swingedouw[89], Roland Séférian[90],~~Sweeney[54], Shintaro ~~Takao[78],~~Takao[56], Hiroaki ~~Tatebe[91~~Tatebe[91,92]~~],~~, Jens Terhaar[76,77], Hanqin ~~Tian[80], Xiangjun Tian[93,94],~~Tian[49], Bronte ~~Tilbrook[26,95], Hiroyuki Tsujino[96],~~Tilbrook[32,89], Takahiro Toyoda[93], Joaquin A. Triñanes[94], Francesco ~~Tubiello[97], Erik van Ooijen[26],~~Tubiello[30], Guido R. van der Werf[11], Auke M. van der ~~Werf[11],~~Woude[11], Sebastiaan J. van de ~~Velde[98,99],~~Velde[95,96], Anthony P. ~~Walker[100],~~Walker[97], Rik ~~Wanninkhof[81],~~Wanninkhof[82], Xiaojuan ~~Yang[100],~~Yang[97], Wenping ~~Yuan[101],~~Yuan[59], Xu ~~Yue[102],~~Yue[98], Jiye ~~Zeng[78]~~Zeng[56], Ning Zheng[33], and Bo Zheng[99]

~~1: Faculty~~

[1]Faculty of Environment, Science and Economy, University of Exeter, Exeter, EX4 4QF, UK

~~2: Laboratoire~~[2]Laboratoire de Météorologie Dynamique, Institut Pierre-Simon Laplace, CNRS, École Normale Supérieure, Université PSL, Sorbonne Université, École Polytechnique, Paris, France

~~3: Tyndall~~[3]CICERO Center for International Climate Research, Oslo 0855, Norway

[4]Alfred-Wegener-Institut, Helmholtz-Zentrum für Polar- und Meeresforschung, Am Handelshafen 12, 27570 Bremerhaven, Germany

[5]FB02 Biology/Chemistry Bremen, Universität Bremen, Bremen, Germany

[6]Tyndall Centre for Climate Change Research, School of Environmental Sciences, University of East Anglia, Norwich Research Park, Norwich NR4 7TJ, UK

~~4: CICERO Center for International Climate Research, Oslo 0349, Norway~~

~~5: School~~[7]School of Geography, Earth and Environmental Sciences, University of ~~East Anglia, Norwich NR4 7TJ~~Birmingham, Edgbaston, Birmingham, B15 2TT, UK

~~6: Alfred-Wegener-Institut, Helmholtz-Zentrum für Polar- und Meeresforschung, Am Handelshafen 12, 27570 Bremerhaven~~

~~7: Universität Bremen, FB02 Biology/Chemistry Bremen, Germany~~

~~8: Flanders~~[8]Flanders Marine Institute (VLIZ), Jacobsenstraat 1, 8400, Ostend, Belgium

~~9: Helmholtz~~[9]Max Planck Institute for Marine Microbiology, Celsiusstraße 1, 28359 Bremen, Germany

[10]Helmholtz-Zentrum Hereon, Max-Planck-Straße 1, 21502 Geesthacht, Germany

Formatted: Superscript

Formatted: Superscript

Formatted: Space After: 2 pt

Formatted: Space After: 2 pt

Formatted: Space After: 2 pt

Formatted: Space After: 2 pt

Formatted: Space After: 2 pt

~~10: Max Planck Institute for Meteorology, Bundesstraße 53, 20146 Hamburg, Germany~~

~~11:~~ [11]Environmental Sciences Group, Wageningen University, ~~Environmental Sciences Group,~~ P.O. Box 47, 6700AA, Wageningen, ~~The~~the Netherlands

~~12:~~ [12]Geophysical Institute, University of ~~Groningen,~~Bergen, Allégaten 70, 5007 Bergen, Norway

[13]Bjerknes Centre for Climate Research, Bergen, Norway

[14]Centre for Isotope Research, University of Groningen, Groningen, ~~The~~the Netherlands

~~13: Ludwig~~[15]Ludwig-Maximilians-Universität München, Luisenstr. 37, 80333 München, Germany

~~14: CSIRO Oceans and Atmosphere~~[16]CSIRO Environment, Canberra, ACT 2101, Australia

~~15: Laboratoire~~[17]Laboratoire des Sciences du Climat et de l'Environnement~~,~~ (LSCE~~/IPSL,~~), CEA-, CNRS-, UVSQ, Université Paris-Saclay, ~~F-~~91190~~91~~191 Gif-sur-Yvette, France

~~16: National~~[18]National Oceanic and Atmospheric Administration, Pacific Marine Environmental Laboratory (NOAA/PMEL), 7600 Sand Point Way NE, Seattle, WA 98115, USA

[19]Climate Research Division, Environment and Climate Change Canada, Victoria, BC, Canada

[20]ASU-BIOS, 17 Biological Lane, Ferry Reach, St. Georges, GE01, Bermuda

~~17: Karlsruhe~~[21]School of Ocean Futures (SOF), Arizona State University (ASU), Tempe, Arizona, USA

[22]Hakai Institute, 1713 Hyacinthe Bay Rd, Heriot Bay, BC, V0P 1H0, Canada

[23]Karlsruhe Institute of Technology, Institute of Meteorology and Climate Research/Atmospheric Environmental Research, 82467 Garmisch-Partenkirchen, Germany

~~18: Rosenstiel School of Marine Atmospheric and Earth Science, Cooperative Institute for Marine and Atmospheric Studies (CIMAS), University of Miami, 4600 Rickenbacker Causeway, Miami, FL, USA~~

~~19: Arizona State University, Tempe, Arizona, AZ 85287-5502, USA~~

~~20: Bermuda Institute of Ocean Sciences (BIOS), 17 Biological Lane, St.~~ [24]Department~~Georges, GE01, Bermuda~~

~~21: Department~~ of Meteorology, University of Reading, Reading, RG6 6BB, UK

~~22: Marine~~[25]Marine and Freshwater Research Institute, ~~Reykjavik~~Hafnarfjörður, Iceland

~~23: Instituto~~[26]Instituto Nacional de Investigación y Desarrollo Pesquero (INIDEP), Paseo Victoria Ocampo ~~N°~~No 1, B7602HSA, Mar del Plata, Argentina

~~24: Barcelona Supercomputing Center, Barcelona, Spain~~

~~25: Faculty~~[27]Centre National de Recherches Météorologiques, Université de Toulouse, Météo-France, CNRS, UMR 3589, Toulouse, France

[28]Faculty of Marine Science ~~&~~and Fisheries, Udayana University, Denpasar, Bali, 80361, Indonesia

~~26: CSIRO~~[29]Met Office Hadley Centre, FitzRoy Road, Exeter, EX1 3PB, UK

[30]Statistics Division, Food and Agriculture Organization of the United Nations, Via Terme di Caracalla, Rome 00153, Italy

Formatted: Space After: 2 pt

Formatted: Space After: 2 pt

Formatted: French (France)

Formatted: French (France)

Formatted: Space After: 2 pt

Formatted: Space After: 2 pt

Formatted: Space After: 2 pt

Formatted: French (France)

Formatted: French (France)

Formatted: Space After: 2 pt

[31]Environmental Engineering, School of Civil Engineering, The University of Sydney, Sydney, NSW, Australia

[32]CSIRO Environment, Castray Esplanade, Hobart, Tasmania 7004, Australia

~~27: Research Institute for Global Change, JAMSTEC, 3173-25 Showa-machi, Kanazawa, Yokohama, 236-0001, Japan~~

~~28: Department~~[33]Department of Geographical Sciences, University of Maryland, College Park, MD 20742, USA

~~29: Computer Science and Engineering Division, Oak Ridge National Laboratory, Oak Ridge, TN 37831, USA~~

~~30: Earth System Science Interdisciplinary Center, University of Maryland, College Park, MD 20740, USA~~

~~31: Marine~~[34]Marine Institute, Rinville, Oranmore, Co Galway H91 R673, Ireland

~~32: School~~[35]Cooperative Institute for Climate, Ocean and Ecosystem Studies, ~~Stellenbosch~~ University~~, Private Bag X1, Matieland, Stellenbosch, 7602, South Africa~~ of Washington, 3737 Brooklyn Ave NE, Seattle, WA 98105, USA

~~33: Southern Ocean Carbon – Climate Observatory, CSIR, Rosebank, Cape Town, 7700, South Africa~~

~~34: Engr. Computer Science~~[36]Department of Geography, University of California, ~~Davis~~Santa Barbara, CA ~~95616~~93106, USA

~~35: Department of Earth System Science, Stanford University, Stanford, CA 94305, USA~~

~~36: Japan~~[37]Japan Meteorological Agency, 3-6-9 Toranomon, Minato City, Tokyo, 105-8431, Japan

~~37: Research~~[38]Research Institute for Environment, Energy, and Economics, Appalachian State University, Boone, North Carolina, USA

~~38: Department~~[39]Department of Geological and Environmental Sciences, Appalachian State University, Boone, North Carolina, USA

~~39: Hakai Institute, 1713 Hyacinthe Bay Rd, Heriot Bay, BC, V0P 1H0, Canada~~

~~40: National Centre for~~ [40]Lamont-Doherty Earth ~~Observation,~~Observatory, Columbia University, New York, NY, USA

[41]Department of ~~Edinburgh, Edinburgh, EH9 3FE, UK~~Earth and Environmental Sciences, Lehigh University, Bethlehem, PA 18015, USA

~~41: School of Geosciences, University of Edinburgh, Edinburgh, EH9 3FE, UK~~

~~42: Climate~~[42]Climate and Global Dynamics Laboratory, National Center for Atmospheric Research, Boulder, CO 80305, USA

~~43: Geophysical~~[43]Norwegian Polar Institute, ~~University of Bergen, Allégaten 70, 5007 Bergen~~9296 Tromsø, Norway

~~44: Bjerknes~~[44]National Centre for ~~Climate~~Atmospheric Science (NCAS), Climatic Research~~, Bergen, Norway~~ Unit, University of East Anglia, Norwich, NR4 7TJ, UK

Formatted: Space After: 2 pt

Formatted: Space After: 2 pt

Formatted: Space After: 2 pt

Formatted: Space After: 2 pt

Formatted: Space After: 2 pt

Formatted: Space After: 2 pt

Formatted: Space After: 2 pt

45: International[45]International Institute for Applied Systems Analysis (IIASA), Schlossplatz 1 A-, 2361 Laxenburg, Austria

46: European[46]European Commission, Joint Research Centre (JRC), Ispra, Italy

47: Environmental[47]Environmental Physics Group, Institute of Biogeochemistry and Pollutant Dynamics and Center for Climate Systems Modeling (C2SM), ETH Zürich, Zurich, Switzerland

48: Swiss[48]Swiss Data Science Center, 8050 Zurich, Switzerland

49: Laboratoire de Géologie, Ecole Normale Supérieure, CNRS UMR 8538, Institut Pierre-Simon Laplace, PSL Research University, Paris, France

50: Smith[49]Schiller Institute of Integrated Science and Society, Department of Earth and Environmental Sciences, Boston College, Chestnut Hill, MA 02467, USA

[50]Smith School for Enterprise and the Environment, University of Oxford, Oxford, UK

51: NCAS-Climate, Climatic Research Unit, School of Environmental Sciences, University of East Anglia, Norwich Research Park, Norwich, NR4 7TJ, UK

52: Potsdam[51]Potsdam Institute for Climate Impact Research (PIK), member of the Leibniz Association, P.O. Box 60 12 03, 14412 Potsdam, Germany

53: Universität Hamburg, Bundesstraße 55, 20146 Hamburg, Germany

54: Graduate[52]Graduate School of Agricultural and Life Sciences, University of Tokyo, Tokyo, Japan

55: Cooperative[53]Cooperative Institute for Research in Environmental Sciences (CIRES), University of Colorado Boulder, Boulder, CO 80305, USA

56: National[54]National Oceanic and Atmospheric Administration Global Monitoring Laboratory (NOAA/GML), 325 Broadway R/GML, Boulder, CO 80305, USA

57: Department[55]Department of Climate, Meteorology and Atmospheric Sciences, University of Illinois, Urbana, IL 61801, USA

58: Jiangsu[56]Earth System Division, National Institute for Environmental Studies (NIES), 16-2 Onogawa, Tsukuba Ibaraki, 305-8506, Japan

[57]Earth System Science Interdisciplinary Center, University of Maryland, College Park, MD 20740, USA

[58]Jiangsu Provincial Key Laboratory for Advanced Remote Sensing and Geographic Information Technology, International Institute for Earth System Science, Nanjing University, Nanjing, 210023, China.

59:[59]Institute of Carbon Neutrality, Sino-French Institute for Earth System Science, College of Urban and Environmental Sciences, Peking University, Beijing, China

[60]Institute of Applied Energy (IAE), Minato-ku, Tokyo 105-0003, Japan

60: University[61]University of California, San Diego, Scripps Institution of Oceanography, La Jolla, CA 92093-0244, USA

Formatted: Space After: 2 pt

Formatted: Space After: 2 pt

Formatted: Space After: 2 pt

Formatted: Space After: 2 pt

Formatted: Space After: 2 pt

~~61: Utrecht~~[62]Utrecht University, Faculty of Geosciences, Department IMEW, Copernicus Institute of Sustainable Development, Heidelberglaan 2, P.O. Box 80115, 3508 TC, Utrecht, the Netherlands

~~62: School~~[63]School of Life Sciences, Faculty of Science, University of Technology Sydney, Ultimo, NSW 2007, Australia

~~63: State~~[64]Barcelona Supercomputing Center, Barcelona, Spain

[65]NORCE Research, Jahnebakken 5, 5007 Bergen, Norway

[66]Climate Modelling Research Division, Environment and Climate Change Canada, Victoria, BC, Canada

[67]State Key Laboratory of ~~Remote Sensing and Digital Earth, Aerospace Information Research Institute, Chinese Academy of Sciences, Beijing 100101, China~~

~~64: Ministry of Education Key Laboratory for Earth System Modeling, Department of Earth System Science, Tsinghua~~Submarine Geoscience, School of Oceanography, Shanghai Jiao Tong University, ~~Beijing 100084~~Shanghai 200240, China

~~65: Lawrence Berkeley National Laboratory, USA~~

~~66: Jet~~[68]Jet Propulsion Laboratory, California Institute of Technology, Pasadena, CA, USA

~~67: Division~~[69]Division of Geological and Planetary Sciences, California Institute of Technology, Pasadena, CA, USA

~~68: CMA Key Open Laboratory of Transforming Climate Resources to Economy, Chongqing Institute of Meteorological Sciences, Chongqing 401147, China~~

~~69: Department~~[70]Department of Earth System Science, Tsinghua University, Beijing, China

~~70: LOCEAN Laboratory (Sorbonne Université, CNRS, IRD, MNHN), 4 Place Jussieu, F-75005 Paris, France~~

~~71: Department~~[71]A-LIFE, Vrije Universiteit Amsterdam, Amsterdam, the Netherlands

[72]Department of Meteorology and National Centre for Atmospheric Science, University of Reading, Reading, UK

~~72: Lamont-Doherty Earth Observatory, Columbia University, New York, NY, USA~~

~~73: Climate Research Division, Environment and Climate Change Canada, Victoria, BC, Canada~~

~~74: College~~[73]LOCEAN Laboratory (Sorbonne Université, CNRS, IRD, MNHN), 4 Place Jussieu, 75005 Paris, France

[74]College of Fisheries and Ocean Sciences, University of Alaska Fairbanks, Fairbanks, Alaska 99775-7220, USA

~~75: Department of Land, Air and Water Resources, University of California, Davis, CA 95616, USA~~

~~76: Climate Adaptation Research Center, University of California, Davis, CA 95616, USA~~

~~77: Carbon~~[75]Carbon to Sea Initiative, Washington D.C., USA

~~78: Earth System Division, National Institute for Environmental Studies (NIES), 16-2 Onogawa, Tsukuba Ibaraki, 305-8506, Japan~~

Formatted: Space After: 2 pt

Formatted: Space After: 2 pt

Formatted: Space After: 2 pt

Formatted: Space After: 2 pt

Formatted: Space After: 2 pt

~~79: NORCE~~[76]Climate and Environmental Physics, Physics Institute, University of Bern, Bern, Switzerland

[77]Oeschger Centre for Climate Change Research, ~~Jahnebakken 5, 5007 Bergen, Norway~~

~~80: Schiller Institute of Integrated Science and Society, Department~~University of ~~Earth and~~Bern, Bern, Switzerland

[78]Climatic Research Unit, School of Environmental Sciences, ~~Boston College, Chestnut Hill, MA 02467, USA~~University of East Anglia, Norwich Research Park, Norwich, NR4 7TJ, UK

~~81: National~~[79]Instituto de Investigacións Mariñas (IIM-CSIC), Eduardo Cabello 6, 36208 Vigo, Spain

[80]National Centre for Earth Observation, University of Edinburgh, Edinburgh, EH9 3FE, UK

[81]School of Geosciences, University of Edinburgh, Edinburgh, EH9 3FE, UK

[82]National Oceanic and Atmospheric Administration, Atlantic Oceanographic ~~&~~and Meteorological Laboratory (NOAA/AOML), 4301 Rickenbacker Causeway, Miami, FL 33149, USA

~~82: School~~[83]Spark Climate Solutions, Covina, CA, USA

[84]School of Atmospheric Sciences, Sun Yat-sen University, Zhuhai 519000, China

~~83: Department of Geoscience, Environment & Society-BGEOSYS, Université Libre de Bruxelles, 1050 Brussels, Belgium~~

~~84: Leibniz~~[85]School of Mathematical Sciences and Center for Statistical Science, Peking University, Beijing, China

[86]Leibniz Institute for Baltic Sea Research Warnemünde (IOW), Seestrasse 15, 18119 Rostock, Germany

~~85: Princeton~~[87]Princeton University, Department of Geosciences and Princeton Environmental Institute, Princeton, NJ, USA

~~86: Max~~[88]Max Planck Institute for Biogeochemistry, P.O. Box 600164, Hans-Knöll-Str. 10, 07745 Jena, Germany

~~87: Canadian Centre~~[89]Australian Antarctic Program Partnership, University of Tasmania, Hobart, Australia

[90]Wyss Academy for ~~Climate Modelling and Analysis, Environment and Climate Change Canada, Victoria, BC, Canada~~

~~88: Institute for Climate and Environmental Physics~~Nature, University of Bern, Bern, Switzerland

~~89: Environnements et Paléoenvironnements Océaniques et Continentaux (EPOC) UMR CNRS 5805 EPOC - OASU, Université de Bordeaux, Allée Geoffroy Saint Hilaire, 33615 Pessac, France~~

~~90: Centre National de Recherches Météorologiques, Université de Toulouse, Météo-France, CNRS, UMR 3589, Toulouse, France~~

~~91: Research~~[91]Research Center for Environmental Modeling and Application, Japan Agency for Marine-Earth Science and Technology, Yokohama, Japan

Formatted: Space After: 2 pt

Formatted: Space After: 2 pt

Formatted: Space After: 2 pt

Formatted: Space After: 2 pt

Formatted: Space After: 2 pt

~~92: Advanced~~[92]Advanced Institute for Marine Ecosystem Change, Japan Agency for Marine-Earth Science and Technology, Yokohama, Japan

~~93: State Key Laboratory of Tibetan Plateau Earth System and Resource Environment, Institute of Tibetan Plateau Research, Chinese Academy of Sciences, Beijing 100101, China~~

~~94: University of Chinese Academy of Sciences, Beijing 101408, China~~

~~95: Australian Antarctic Partnership Program, University of Tasmania, Hobart, Australia~~

~~96: JMA~~[93]JMA Meteorological Research Institute, Tsukuba, Ibaraki, Japan

~~97: Statistics Division, Food and Agriculture Organization of the United Nations, Via Terme di Caracalla, Rome 00153, Italy~~

~~98: Earth Sciences New Zealand, Wellington, New Zealand~~

~~99: Department~~[94]Department of Electronics and Computer Science, Universidade de Santiago de Compostela, Santiago de Compostela, Spain

[95]Department of Marine Science, University of Otago, Ōtepoti Dunedin, 9016, Aotearoa New Zealand

[96]Earth Sciences New Zealand, Te Whanganui-a-Tara Wellington, 6021, Aotearoa New Zealand

~~100: Climate Change Science Institute and Environmental~~[97]Environmental Sciences Division, Oak Ridge National Laboratory, Oak Ridge, TN 37831, USA

~~101: Institute of Carbon Neutrality, College of Urban and Environmental Sciences, Peking University, Beijing 100091, China~~

~~102: School~~[98]School of Environmental Science and Engineering, Nanjing University of Information Science and Technology (NUIST), Nanjing, 210044, China

[99]Shenzhen Key Laboratory of Ecological Remediation and Carbon Sequestration, Institute of Environment and Ecology, Tsinghua Shenzhen International Graduate School, Tsinghua University, Shenzhen, China

Correspondence to: Pierre Friedlingstein ~~(p.friedlingstein@exeter.ac.uk)~~(p.friedlingstein@exeter.ac.uk)

Formatted: Space After: 2 pt

Formatted: Space After: 2 pt

Formatted: Space After: 2 pt

Formatted: Left, Space Before: 12 pt, After: 7 pt, Line spacing: Multiple 1.15 li

Abstract

Accurate assessment of anthropogenic carbon dioxide (CO_2) emissions and their ~~redistribution~~partitioning among the atmosphere, ocean, and terrestrial biosphere in a changing climate is critical to better understand the global carbon cycle, ~~support~~supporting the development of climate policies, and project future climate change. Here we describe and synthesise datasets and methodologies to quantify the five major components of the global carbon budget and their uncertainties. Fossil CO_2 emissions (E_{FOS}) are based on energy and cement production data. Emissions

from land-use change (E_{LUC}) are estimated by bookkeeping models based on land-use data. The global atmospheric CO_2 growth rate (G_{ATM}) is computed from changes in concentration measured at surface stations. The global net uptake of CO_2 by the ocean (S_{OCEAN}) is estimated with global ocean biogeochemistry models and observation-based fCO_2-products. The global net uptake of CO_2 by the land (S_{LAND}) is estimated with dynamic global vegetation models. Additional lines of evidence are provided by atmospheric inversions, atmospheric oxygen measurements, ocean interior observation-based estimates, and Earth System Models. ~~This year, we introduced corrections on the E_{LUC}, S_{OCEAN} and S_{LAND} estimates.~~ The sum of all sources and sinks results in the carbon budget imbalance (B_{IM}), a measure of imperfect data and incomplete understanding of the contemporary carbon cycle. All uncertainties are reported as ±1σ.

For the year ~~20242~~2025, E_{FOS} increased by 1.~~1~~2% relative to ~~20232~~2024, with fossil emissions at 10.~~3~~5 ± 0.5 GtC yr^{-1} (including the cement carbonation sink, 0.2GtC yr^{-1}), E_{LUC} was 1.~~3~~2 ± 0.7 GtC yr^{-1}, for total anthropogenic CO_2 emissions of 11.~~6~~7 ± 0.9 GtC yr^{-1} (42.~~4~~8 ± 3.2 $GtCO_2$ yr^{-1}). Also, for ~~20242~~2025, G_{ATM} was ~~7.9~~4.4 ± 0.2 GtC yr^{-1} (~~3.73~~2.06 ± 0.1 ppm yr^{-1}), ~~2.2~~3.6 GtC ~~above~~lower than the ~~2023~~record high 2024 growth rate. S_{OCEAN} was 3.~~4~~2 ± 0.~~4~~7 GtC yr^{-1} and S_{LAND} was ~~1~~3.6 ± 0.9 ~~± 1.1~~ GtC yr^{-1}, ~~leaving~~with a ~~large negative~~small B_{IM} ~~(-1.7 GtC yr^{-1}), suggesting that the total sink or G_{ATM} is strongly overestimated in 2024.~~(0.5 GtC yr^{-1}). The global atmospheric CO_2 concentration averaged over ~~20242~~2025 reached ~~422.8~~425.6 ± 0.1 ppm. Preliminary data for ~~2025~~2026 suggest ~~an increase~~a decrease in E_{FOS} relative to ~~20242~~2025 of ~~+~~0.40% (-1.~~0% (0.2~~5% to ~~1.7~~+0.6%) globally, and atmospheric CO_2 concentration increasing by 2.~~1~~2 ppm reaching ~~425.6~~427.7 ppm, ~~53~~54% above the pre-industrial level (around 278 ppm in 1750). Overall, the mean and trend in the components of the global carbon budget are consistently estimated over the period 1959-~~20242~~2025, with a ~~near-zero~~small positive overall budget imbalance, (0.6 GtC yr^{-1} averaged over the period 1959-2025), although discrepancies of up to around 1 GtC yr^{-1} persist for the representation of annual to decadal variability in CO_2 fluxes. Comparison of estimates from multiple approaches and observations shows: (1) a persistent large uncertainty in the estimate of land-use change emissions, (2) a low agreement between the different ~~methods~~estimates on the magnitude of the land CO_2 flux, particularly in the northern extra-tropics, and (3) a discrepancy between the different ~~methods~~estimates on the mean ocean sink and its trend.

This living data update documents changes in methods and datasets applied to this most-recent global carbon budget as well as evolving community understanding of the global carbon cycle. The data presented in this work are available at https://doi.org/10.18160/GCP-~~2025~~2026 (Friedlingstein et al., ~~2025e~~2026b).

Formatted: Normal, Indent: Left: 0.11 cm, Hanging: 0.05 cm

Executive Summary

Global fossil CO_2 emissions (including cement carbonation) are expected to ~~further increase~~ decrease in ~~2025~~2026 by ~~1.~~ -0.4% relative to ~~2024~~2025 (range ~~0.2~~ -1.5% to ~~1.7~~+0.6%), bringing fossil emissions to an expected 10.4 GtC yr^{-1} (38.~~1~~2 $GtCO_2$ yr^{-1}) [1]. Emissions from ~~coal,~~ oil and gas in ~~2025~~2026 are ~~all~~ expected to be ~~above~~below their ~~2024~~2025 levels (by -1.~~0%, 1.1~~9% and ~~1.~~ -0.3% respectively~~).~~), with these decreases partly compensated by an expected growth in emissions from coal (0.6%). These preliminary estimates are based on available data for ~~2025~~2026. Consolidated data confirm a growth of 1.~~1~~2% in ~~2024~~2025 relative to ~~2023~~2024, with fossil CO_2 emissions of 10.~~3~~5 ± 0.5 GtC yr^{-1} (~~37.8~~38.4 ± 1.8 $GtCO_2$ yr^{-1}) in ~~2024~~2025.

Regionally, fossil emissions are projected to ~~grow in 2025~~decrease in 2026 in China, the USA ~~and be nearly flat in,~~ the European Union~~, reversing long-term decreases,~~ and Japan, and to grow in ~~China and~~ India~~, albeit more slowly compared to recent trends.~~. The ~~increase~~decrease in fossil emissions in ~~2025~~2026 relative to ~~2024~~2025 is projected to be -0.~~4% (-0.1~~9% (-2.6% to +0.~~9~~8%) for China, ~~2.5% (2.2~~-1.3% (-3.4% to ~~2~~+0.8%) for the United States, ~~1.1% for India.~~ -1.5% (-4.0% to +0.9%) for the European Union, and -1.0% (-2.5% to +0.6%) for Japan. However, 2025 emissions for ~~the European Union~~India are projected to ~~decrease by -0.1%. Projected emissions in Japan, provided this year for the first time, are for a decrease of -0.9%.~~increase by 4.4% (1.7% to 7.1%). Emissions are also projected to ~~increase~~decrease by ~~6.7~~-1.0% for both international aviation and ~~by 2.0%~~ for international shipping, and to ~~increase~~decrease by -0.7% (-2.9% ~~(-1.0%~~ to ~~3.0~~+1.5%) for the rest of the world in aggregate.

Fossil CO_2 emissions decreased (p<0.05) in 40 countries with growing GDP (p<0.05) during the decade 2016-2025. The list of decarbonising economies is considerably longer than in the previous decade (2006-2015; 22 countries). These 40 decarbonising economies contribute 2.8 GtC yr^{-1} (10.1 $GtCO_2$) fossil fuel CO_2 emissions over the last decade in aggregate, representing 26% of the world CO_2 fossil emissions. The global carbon intensity of energy has consistently decreased over the past decade (-0.~~7~~4% yr^{-1}), indicating decarbonisation of the energy system in China (-~~1.4~~0.8% yr^{-1}), the European Union (-1.~~5~~1% yr^{-1}), and the USA (-1.~~3~~1% yr^{-1}), but no decline in India ~~and an increase in~~; the intensity of the rest of the world in aggregate~~.~~ also declined (-0.3% yr^{-1}). These trends are not sufficient to offset the growth in global energy demand, which is driven by growing GDP globally and a weakening decline in energy per GDP, particularly in China and the ~~US.~~ USA.

~~**Fossil CO_2 emissions decreased (p<0.05) in 35 economies with growing GDP (p<0.05) during the decade 2015-2024.** The list of decarbonising economies nearly doubled since the previous decade (2005-2014; 18 countries). These 35 decarbonising economies contribute 2.7 GtC yr^{-1} (9.7 $GtCO_2$)~~

[1] All growth rates use a leap year adjustment that corrects for the extra day in 2024.

Formatted: No widow/orphan control

Formatted: Not Strikethrough

~~fossil fuel CO_2 emissions over the last decade in aggregate, representing 27% of the world CO_2 fossil emissions.~~

Global net CO_2 emissions from land use averaged 1.~~3~~ ± 0.7 GtC yr^{-1} (~~4 ± 0.7 GtC yr^{-1} (5.0~~.9 ± 2.6 $GtCO_2$ yr^{-1}) for the ~~2015–2024~~2016-2025 period. Emissions from ~~deforestation~~clearing of forest and other vegetation, the main driver of global gross emissions, remain high at around ~~1.9~~2.2 GtC yr^{-1} over the ~~2015–2024~~2016-2025 period, highlighting the strong potential of halting deforestation for emissions reductions. Sequestration of 1.~~3~~6 GtC yr^{-1} through re-/afforestation and forest regrowth in shifting cultivation cycles offsets more than two ~~third~~thirds of the deforestation emissions. In addition, smaller net emissions are due to wood harvest & forest management, peat drainage and peat fire. Regionally, the highest net emitters during ~~2015–2024~~2016-2025 were Brazil, Indonesia, and the Democratic Republic of the Congo, with these 3 countries contributing 0.7 GtC yr^{-1}, more than half of global land-use CO_2 emissions. Net carbon dioxide removals ~~(CDR)~~ from re-/afforestation were highest in China, the ~~USA~~EU27, and the ~~EU27~~USA, with combined removals of 0.~~3~~2 GtC yr^{-1} during ~~2015–2024~~2016-2025.

Since the late-1990s, emissions from land use show a statistically significant decrease at a rate of around 0.2 GtC per decade, with a larger drop within the most recent decade. Preliminary data for ~~2025~~2026 suggest emissions ~~decreased~~ to be around 1.~~1~~4 GtC (~~4~~yr^{-1} (5.1 $GtCO_2$ yr^{-1}), ~~mainly attributable~~0.2 GtC above the 2025 level, partly due to ~~the end of~~increased emissions from Southeast Asia in response to the emerging El Niño ~~conditions~~.

Besides conventional carbon dioxide removal (CDR) through re/afforestation and storage in long-lived harvested wood products, novel CDR occurs through a variety of methods. Vegetation-based CDR methods, primarily biochar and bioenergy with carbon capture and storage, account for removals of about 0.0006 GtC yr^{-1} in 2025. Non-vegetation-based CDR transfers carbon from the atmosphere to the geosphere and amounts to about 0.000003 GtC yr^{-1}, primarily through enhanced rock weathering and alkalinity enhancement of water bodies, with a smaller contribution from direct air carbon capture and storage. Non-vegetation-based CDR represents less than one millionth of current fossil CO_2 emissions.

Total anthropogenic emissions (fossil and land use, including the carbonation sink) were 11.~~6~~7 ± 0.9 GtC yr^{-1} (42.~~8~~ ± 3.2 $GtCO_2$ yr^{-1}) in ~~2024~~2025, with a ~~slightly lower~~ preliminary estimate of 11.~~5~~8 GtC yr^{-1} (~~42.2~~43.3 $GtCO_2$ yr^{-1}) for ~~2025~~2026. Total anthropogenic emissions have grown more slowly over the last decade (0.3% yr^{-1} over the ~~2015–2024~~2016-2025 period) compared to the previous decade (1.~~9~~7% yr^{-1} over ~~2005–2014~~2006-2015).

The remaining carbon budget from the beginning of ~~2026~~2027 for a 50% likelihood to limit warming to 1.5°C is nearly exhausted (~~50~~40 GtC, ~~170~~150 $GtCO_2$ left, equivalent to ~~around~~less than 4 years at the ~~2025~~2026 emissions levels), consistent with the warming of the planet

Formatted: Superscript

attributed to human activities, which reached 1.~~36°C in 2024.~~ ~~Each additional cumulative emission of about 180 GtCO$_2$ will lead to approximately 0.1°C of warming.~~37°C in 2025. The remaining carbon budgets to limit warming to 1.7°C and 2°C above the 1850-1900 level have been reduced to ~~145~~140 GtC (~~525~~510 GtCO$_2$, 12 years) and ~~290~~280 GtC (~~1055~~1035 GtCO$_2$, ~~25~~24 years) respectively.

The concentration of CO$_2$ in the atmosphere is set to reach ~~425.6~~427.7 ppm in ~~2025~~2026, 53% above pre-industrial levels. The atmospheric CO$_2$ growth rate was 5.~~64~~ ± 0.02 GtC yr^{-1} (2.~~65~~ ppm) during the decade ~~2015-2024 (50~~2016-2025 (~~48~~% of total CO$_2$ emissions). ~~2024 had a record-high growth rate of 7.9 ± 0.02 GtC yr^{-1} (3.7 ppm) mainly due to the 2023/2024 El Niño conditions.~~ The preliminary ~~2025~~2026 growth rate estimate is 4.~~4~~6 GtC (2.~~1~~2 ppm).

The ocean sink, the global ~~net~~ uptake of anthropogenic CO$_2$ by the ocean, has taken up ~~29~~27% of the total emissions in the past decade~~, after being re-evaluated upwards based on new evidence and process understanding~~. The ocean sink has been stagnant since 2016, largely in response to climate variability modulating the growing sink trend~~, but further affected by the ocean heatwave of 2023-2024 in the Northern Hemisphere.~~. The ocean CO$_2$ sink was 3.~~2 ± 0~~.4 ± 0.6 GtC yr^{-1} during the decade ~~2015-2024~~2016-2025, with a preliminary estimate of 3.~~2~~1 GtC yr^{-1} for ~~2025~~2026, slightly below ~~2024~~2025 levels~~, due to the end of the El Niño conditions in 2024 and associated reduced atmospheric CO$_2$ growth rate~~.

The land sink, which is the global net uptake of CO$_2$ by the land excluding land use, has taken up ~~21~~22% of the total emissions in the past decade~~, after being re-evaluated downwards based on improved process representation~~. The land sink has been relatively stagnant since 2000, largely in response to climate variability and climate change offsetting the CO$_2$ induced growth. The land CO$_2$ sink was 2.~~4~~5 ± 0.8 GtC yr^{-1} during the ~~2015-2024~~2016-2025 decade but was ~~reduced~~increased to ~~1.9~~3.6 GtC ± 0.8 GtC yr^{-1} in ~~2024.~~2025, recovering from the El Niño induced reduced sink in 2024. The preliminary estimate for the land sink in ~~2025~~2026 is ~~an~~a further increase to ~~34~~.1 GtC~~, recovering entirely from its strong drop during the 2023-2024 El Niño conditions~~.

The effects of climate change and climate variability act to reduce the ocean and land ~~and ocean~~ CO$_2$ sinks by ~~25~~8% and ~~7.1~~19% respectively, on average for the ~~2015-2024~~2016-2025 period. Since 1960, the effect of climate change on the ocean and land sinks has contributed 7.3 ± 4.5 ppm (7%) to the observed atmospheric CO$_2$ increase ([6.6%]). The land sink is negatively affected by warming with decreased tropical plant productivity and enhanced ecosystem respiration globally. The ocean sink is negatively affected by altered oceanic circulation and surface warming which decreases CO$_2$ solubility.

So far in ~~2025~~2026, global fire ~~CO$_2$~~carbon emissions have been ~~approximately 20% lower than~~ close to the ~~2015-2024~~2016-2025 average ~~due to low fire activity in Africa and the tropics, reaching 1.2-1.4 GtC globally during~~. Compared with fire CO$_2$ emissions for January-September~~.~~

Formatted: Font: Not Bold

Formatted: Font: Bold

Formatted: Not Superscript/ Subscript

Formatted: Font: Not Bold

~~This contrasts with the~~ periods throughout 2016-2025, global emissions of 2026 were between 8% below average in GFED5.1 and 3% above average ~~fire emissions~~ in ~~2023 (1.7-2.1 GtC yr^{-1})~~GFAS. Large positive emissions anomalies were seen in Southeast Asia,, while negative anomalies were seen in South America and ~~2024 (1.6-2.2 GtC yr^{-1}) due to extensive fires in Canada (2023) and Brazil and Bolivia (2024). These~~North America. Our fire emissions estimates should not be directly compared with ~~the~~ land-use emissions or the land sink~~,~~ because they represent a gross carbon flux to the atmosphere and do not account for post-fire recovery. They also do not distinguish between natural, climate-driven~~,~~ and land-use-related fires.

1 Introduction

Formatted: Outline numbered + Level: 1 + Numbering Style: 1, 2, 3, … + Start at: 1 + Alignment: Left + Aligned at: 0 cm + Indent at: 0.76 cm

The concentration of carbon dioxide (CO_2) in the atmosphere has increased from approximately 278 parts per million (ppm) in 1750 (Gulev et al., 2021), the beginning of the Industrial Era, to ~~422.8~~425.6 ± 0.1 ppm in ~~2024~~2025 (Lan et al., ~~2025~~2026; Figure 1). The atmospheric CO_2 increase above pre-industrial levels was, initially, primarily caused by the release of carbon to the atmosphere from deforestation and other land-use change activities (Canadell et al., 2021). While emissions from fossil fuels started before the Industrial Era, they became the dominant source of anthropogenic emissions to the atmosphere from around 1950 and their relative share has continued to increase until present. Anthropogenic emissions occur on top of an active natural carbon cycle that circulates carbon between the reservoirs of the atmosphere, ocean, and terrestrial biosphere on time scales from sub-daily to millennial, while exchanges with geologic reservoirs occur on longer timescales (Archer et al., 2009).

The global carbon budget (GCB) presented here refers to the mean, variations, and trends in the perturbation of CO_2 in the environment, referenced to the beginning of the Industrial Era (defined here as 1750). This paper describes the components of the global carbon cycle over the historical period with a stronger focus on the recent period (since 1959, onset of robust atmospheric CO_2 measurements), the last decade (~~2015-2024~~2016-2025), the last year (~~2024~~2025) and the current year (~~2025~~2026). Finally, it provides cumulative emissions from fossil fuels and land-use change since the year 1750, and since the year 1850 (the reference year for historical simulations in IPCC).

We quantify the input of CO_2 to the atmosphere by emissions from human activities, the growth rate of atmospheric CO_2 concentration, and the resulting changes in the storage of carbon in the land and ocean reservoirs in response to increasing atmospheric CO_2 levels, climate change and variability, and other anthropogenic and natural changes (Figure 2). An understanding of this perturbation budget over time and the underlying variability and trends of the natural carbon cycle is necessary to understand the response of natural sinks to changes in climate, CO_2 and land-use change drivers, and to quantify emissions compatible with a given climate stabilisation target.

The components of the CO_2 budget that are reported annually in this paper include separate and independent estimates for the CO_2 emissions from (1) fossil fuel combustion and oxidation from all energy and industrial processes; also including cement production and carbonation (E_{FOS}; GtC yr^{-1}) and (2) the emissions resulting from deliberate human activities on land, including those leading to land-use change (E_{LUC}; GtC yr^{-1}); and their partitioning among (3) the growth rate of atmospheric CO_2 concentration (G_{ATM}; GtC yr^{-1}), and the uptake of CO_2 (the 'CO_2 sinks') in (4) the ocean (S_{OCEAN}; GtC yr^{-1}) and (5) on land (S_{LAND}; GtC yr^{-1}). The CO_2 sinks as defined here conceptually include the response of the land (including inland waters and estuaries) and ocean (including coastal and marginal seas) to

elevated CO_2 and changes in climate and other environmental conditions, although in practice not all processes are fully accounted for (see Section 2.10). Note that the term sink means that the net transfer of carbon is from the atmosphere to land or the ocean, but it does not imply any permanence of that sink in the future.

Global emissions and their partitioning among the atmosphere, ocean and land are in mass balance in the real world. Due to the combination of imperfect spatial and/or temporal data coverage, errors in each estimate, and smaller terms not included in our budget estimate (discussed in Section 2.10), the GCB independent estimates (1) to (5) above do not necessarily add up to zero. We hence estimate a budget imbalance (B_{IM}), which is a measure of the mismatch between the estimated emissions and the estimated changes in the atmosphere, land, and ocean, as follows:

$$B_{IM} = E_{FOS} + E_{LUC} - (G_{ATM} + S_{OCEAN} + S_{LAND}) \quad (1)$$

G_{ATM} is usually reported in ppm yr^{-1}, which we convert to units of carbon mass per year, GtC yr^{-1}, using 1 ppm = 2.124 GtC (Ballantyne et al., 2012; Table 1). Units of gigatonnes of CO_2 (or billion tonnes of CO_2) used in policy are equal to 3.664 multiplied by the value in units of GtC.

We also assess a set of additional lines of evidence derived from global atmospheric inversion system results (Section 2.7), observed changes in oxygen concentration (Section 2.8) and Earth System Models (ESMs) simulations (Section 2.9), all these methods closing the global carbon balance (zero B_{IM}).

We further quantify E_{FOS} and E_{LUC} by country, including both territorial and consumption-based accounting for E_{FOS} (see Section 2), and discuss missing terms from sources other than the combustion of fossil fuels (see Section 2.10). We also assess carbon dioxide removal (CDR) (see Sect. 2.2 and 2.3). Land-based CDR is significant, but already accounted for in E_{LUC} in equation (1) (Sect 3.2.2). Other CDR methods, not based on vegetation, are currently several orders of magnitude smaller than the other components of the budget (Sect. 3.3), hence these are not included in equation (1), or in the global carbon budget tables or figures (except for Figure 2 where CDR is shown primarily for illustrative purpose).

The global CO_2 budget has been assessed by the Intergovernmental Panel on Climate Change (IPCC) in all assessment reports (Watson et al., 1990; Schimel et al., 1995; Prentice et al., 2001; Denman et al., 2007; Ciais et al., 2013; Canadell et al., 2021), and by others (e.g., Ballantyne et al., 2012). The Global Carbon Project (GCP, www.globalcarbonproject.org, last access: ~~23~~30 October ~~2025~~2026) has coordinated this cooperative community effort for the annual publication of global carbon budgets for the year 2005 (Raupach et al., 2007; including fossil emissions only), year 2006 (Canadell et al., 2007), year 2007 (GCP, 2008), year 2008 (Le Quéré et al., 2009), year 2009 (Friedlingstein et al., 2010), year 2010 (Peters et al., ~~2012a~~2012), year 2012 (Le Quéré et al., 2013; Peters et al., 2013), year 2013 (Le Quéré et al., 2014), year 2014 (Le Quéré et al., 2015a; Friedlingstein et al., 2014), year 2015 (Jackson

et al., 2016; Le Quéré et al., 2015b), year 2016 (Le Quéré et al., 2016), year 2017 (Le Quéré et al., 2018a; Peters et al., 2017a), year 2018 (Le Quéré et al., 2018b; Jackson et al., 2018), year 2019 (Friedlingstein et al., 2019; Jackson et al., 2019; Peters et al., 2020), year 2020 (Friedlingstein et al., 2020; Le Quéré et al., 2021), year 2021 (Friedlingstein et al., 2022a; Jackson et al., 2022), year 2022 (Friedlingstein et al., 2022b), the year 2023 (Friedlingstein et al., 2023), ~~and most recently~~ the year 2024 (Friedlingstein et al., 2025a), and most recently the year 2025 (Friedlingstein et al., 2026a). Each of these papers updated previous estimates with the latest available information for the entire time series.

We adopt a range of ±1 standard deviation (σ) to report the uncertainties in our global estimates, representing a likelihood of 68% that the true value will be within the provided range if the errors have a gaussian distribution, and no bias is assumed. Note that when less than 10 individual data are available for an estimate (e.g., atmospheric inversions, ~~f CO_2 products~~ESMs), we provide the full range, as opposed to the standard deviation. The choice of reporting a ±1 σ ~~r~~ reflects the difficulty of characterising the uncertainty in the CO_2 fluxes between the atmosphere and the ocean and land reservoirs individually, particularly on an annual basis, as well as the difficulty of updating the CO_2 emissions from land-use change. A likelihood of 68% provides an indication of our current capability to quantify each term and its uncertainty given the available information. The uncertainties reported here combine statistical analysis of the underlying data, assessments of uncertainties in the generation of the datasets, and expert judgement of the likelihood of results lying outside this range. The limitations of current information are discussed in the paper and have been examined in detail elsewhere (Ballantyne et al., 2015; Zscheischler et al., 2017). We also use a qualitative assessment of confidence level to characterise the annual estimates from each term based on the type, amount, quality, and consistency of the different lines of evidence as defined by the IPCC (Stocker et al., 2013).

This paper provides a detailed description of the datasets and methodology used to compute the global carbon budget estimates for the industrial period, from 1750 to ~~2025~~2026, and in more detail for the recent period since 1959. This paper is updated every year using the format of 'living data' to keep a record of budget versions and the changes in new data, revision of data, and changes in methodology that lead to changes in estimates of the carbon budget. All underlying data used to produce the budget and additional materials associated with the release of each new version are available via the Global Carbon Budget website (https://globalcarbonbudget.org/ , last access: ~~23~~30 October ~~2025~~2026), with emissions also available through the Global Carbon Atlas (http://www.globalcarbonatlas.org, last access: ~~23 October 2025),~~30 October 2026) and Our World in Data ((https://ourworldindata.org/co2-emissions, last access: 30 October 2026). See data availability section for more information. With this approach, we aim to provide the highest transparency and traceability in the reporting of CO_2, the key driver of climate change.

2 Methods

Multiple organisations and research groups around the world generated the original measurements and data used to complete the global carbon budget. The effort presented here is thus mainly one of synthesis, where results from individual groups are collated, analysed, and evaluated for consistency. We facilitate access to original data with the understanding that primary datasets will be referenced in future work (see Table 2 for how to cite the datasets, and Section on data availability). Descriptions of the measurements, models, and methodologies follow below, with more detailed descriptions of each component provided as Supplementary Information (Supplement Tables S1 to S5). In the GCB, when possible, we account for adjustments and corrections to the components estimates. We refer to 'adjustments' when accounting for known processes not included in one estimate (~~ex~~e.g. river ~~correction~~adjustment for atmospheric inversions and fCO_2 products), while we refer to 'corrections' when addressing known biases in one estimate (~~ex. replaced sinks~~e.g. warm layer and ~~sources~~cool skin effect correction for ~~DGVMs~~/CO_2-products).

This is the ~~20th~~21th version of the global carbon budget and the ~~14th~~15th revised version in the format of a living data update in Earth System Science Data. It builds on the latest published global carbon budget of Friedlingstein et al. (~~2025a~~2026a). The main changes this year are: the inclusion of (1) data to year ~~2024~~2025 and a projection for the global carbon budget for year ~~2025~~2026; (2) ~~transient carbon densities in the~~ a new methodology to estimate ~~of E_{LUC}, (3) a correction on~~ S_{LAND} ~~to account~~from DGVMs, accounting for the historical changes in forest cover, ~~(4) a correction on S_{OCEAN} to account for the underestimation of the sink by GOBMs~~ and (3) an extended model evaluation to determine the scaling factor for the ocean ~~temperature gradients in the fCO_2 products estimate, (5) an estimate of the atmospheric CO_2 growth rate derived from satellite observations, and (6) decadal estimates of change in the dissolved inorganic carbon inventory in the interior ocean~~models. Other methodological differences are summarised in Table 3 and previous changes since 2006 are provided in Table S10.

2.1 Fossil CO_2 emissions (E_{FOS})

2.1.1 Historical period 1850-~~2024~~2025

The estimates of global and national fossil CO_2 emissions (E_{FOS}) include the oxidation of fossil fuels through both combustion (e.g., transport, heating) and chemical oxidation (e.g., carbon anode decomposition in aluminium refining) activities, and the decomposition of carbonates in industrial processes (e.g. the production of cement). We also include CO_2 uptake from the cement carbonation process. Several emissions sources are not estimated or not fully covered: coverage of emissions from lime production are not global, and decomposition of carbonates in glass and ceramic production are included only for the "Annex 1" countries of the United Nations Framework Convention on Climate Change (UNFCCC) for lack of activity data. These omissions are considered to be minor. Short-cycle

Formatted: Outline numbered + Level: 1 + Numbering Style: 1, 2, 3, … + Start at: 1 + Alignment: Left + Aligned at: 0 cm + Indent at: 0.76 cm

Formatted: Font: 10 pt

Formatted: Font: 10 pt

Formatted: Font: 10 pt

Formatted: Font: 10 pt, Italic

Formatted: Font: 10 pt

Formatted: Font: 10 pt, Subscript

Formatted: Font: 10 pt

Formatted: Font: 10 pt

Formatted: Font: 10 pt

Formatted: Font: 10 pt

Formatted: Outline numbered + Level: 2 + Numbering Style: 1, 2, 3, … + Start at: 1 + Alignment: Left + Aligned at: 0 cm + Indent at: 1.02 cm

Formatted: Outline numbered + Level: 3 + Numbering Style: 1, 2, 3, … + Start at: 1 + Alignment: Left + Aligned at: 0 cm + Indent at: 1.27 cm

carbon emissions - for example from combustion of biomass - are not included here but are accounted for in the CO_2 emissions from land use (see Section 2.2).

Our estimates of fossil CO_2 emissions rely on data collection by many other parties. Our goal is to produce the best estimate of this flux, and we therefore use a prioritisation framework to combine data from different sources that have used different methods, while being careful to avoid double counting and undercounting of emissions sources. ~~The~~ We begin with official reporting from Annex 1 countries' official submissions to the UNFCCC, add in data for earlier years and other countries from the CDIAC-FF emissions dataset, itself derived largely from UN energy data, ~~forms the foundation,~~ and ~~we~~ extend emissions to ~~2024~~2025 using energy growth rates reported by the Energy Institute ~~(a dataset formerly produced by BP). We~~ . We add process emissions from cement production from Andrew (2026) as well as lime-production emissions for some key countries, and then ~~proceed to~~additionally replace estimates using data from what we consider to be superior sources~~, for example Annex 1 countries' official submissions to the UNFCCC.~~. All data points are potentially subject to revision, not just the latest year. For full details see Andrew and Peters (~~2025~~2026).

Other estimates of global fossil CO_2 emissions exist, and these are compared by Andrew (2020a). The most common reason for differences in estimates of global fossil CO_2 emissions is a difference in which emissions sources are included in the datasets. Datasets such as those published by the Energy Institute, the US Energy Information Administration, and the International Energy Agency's 'CO_2 emissions from fuel combustion' are all generally limited to emissions from combustion of fossil fuels. In contrast, datasets such as PRIMAP-hist, CEDS, EDGAR, and GCP's dataset aim to include all sources of fossil CO_2 emissions. See Andrew (2020a) for detailed comparisons and discussion.

Cement products absorb CO_2 from the atmosphere over their lifetimes, a process known as 'cement carbonation'. We estimate this CO_2 sink, from 1931 onwards, as the average of ~~two~~three studies in the literature (Cao et al., 2020; ~~Guo~~Niu et al., ~~2021). Both studies use the same model, developed by Xi~~2025; Xiao et al~~ (2016),~~., 2026). These three datasets differ in magnitude, with ~~different parameterisations and input data, with the estimate of Guo and colleagues being a revision of Xi~~Xiao et al. ~~(2016).~~(2026) having much lower values due partly to the intentional omission of mortar and end-of-life phases. The trends of the ~~two~~three studies are very similar~~. Since~~, which can be explained by their strong dependence on annual cement production data. The estimates by Cao et al. (2020) have not been updated, but since carbonation is a function of both current and previous cement production, we extend these estimates to ~~2024~~2025 by using the growth rate derived from the smoothed cement emissions (10-year smoothing) fitted to the carbonation ~~data~~estimates. In the present budget, we always include the cement carbonation carbon sink in the fossil CO_2 emission component (E_{FOS}) unless explicitly stated otherwise.

We use the Kaya Identity for a simple decomposition of CO_2 emissions into ~~the~~ key drivers (Raupach et al., 2007). While there are variants (Peters et al., 2017b), we focus here on a decomposition of CO_2 emissions into population, GDP per person, energy use per unit of GDP, and CO_2 emissions per unit of energy. Multiplying these individual components together returns the CO_2 emissions. Using the decomposition, it is possible to attribute the change in CO_2 emissions to the change in each of the drivers. This method gives a first order understanding of what causes CO_2 emissions to change each year.

2.1.2 ~~2025~~2026 projection

We provide a projection of global fossil CO_2 emissions in ~~2025~~2026 by combining separate projections for China, USA, EU, India, Japan, and for all other countries combined. The methods are different for each of these. For China we use growth rates from the 2026 edition of the National Bureau of Statistics' Statistical Communique along with cement clinker trade data and estimated changes in lime production. For the USA our projection is taken directly from the Energy Information Administration's (EIA) Short-Term Energy Outlook (EIA, 2026), combined with the year-to-date growth rate of cement clinker production. For the EU we use monthly energy data through July/August from Eurostat to derive estimates of monthly CO_2 emissions ~~through December (~~using updated methods after Andrew~~,~~ (2021~~).~~), with extensions of natural gas using daily demand estimates derived from ENTSOG using the method of Fernández-Blanco et al., (2024) and of coal using daily power generation data from ENTSO-E. EU cement emissions are based on available production data through ~~December~~August from three of the largest producers, Germany, Poland, and Spain, as well as production indices for Italy and France. India's projected emissions are derived from monthly estimates through ~~December~~August/September using the methods of Andrew (2020b~~).~~), while Japan's emissions are ~~based on~~derived from monthly estimates through ~~December.~~July using the methods of Kunimitsu & Andrew (2026). Emissions from international transportation (bunkers) are estimated separately for aviation and shipping. Changes in aviation emissions are derived ~~primarily from OECD~~ by analysis of monthly ~~estimates, extrapolated using the growth rates of global flight miles from Airportia.~~IATA data. Shipping emissions are derived ~~from~~ by analysis of estimates of sales of bunker fuels ~~provided by Ship~~ and ~~Bunker (Ship and Bunker, 2026).~~estimates of emissions from OECD. Emissions for the rest of the world are derived for coal and cement using projected growth in economic production from the IMF (~~2025~~2026) combined with extrapolated changes in emissions intensity of economic production; for oil using a global constraint from EIA; and for natural gas using a global constraint from IEA. More details on the E_{FOS} methodology and its ~~2025~~2026 projection can be found in Supplement S.1.

We compare our ~~2025~~2026 projection with the Carbon Monitor (~~2025~~2026). Carbon Monitor is a dataset of daily emissions constructed using hourly to daily proxy data (e.g., electricity consumption, travel patterns, etc) instead of energy use data (Liu et al., 2020a; Liu et al., 2020b). Emissions estimates

Formatted: Outline numbered + Level: 3 + Numbering Style: 1, 2, 3, … + Start at: 1 + Alignment: Left + Aligned at: 0 cm + Indent at: 1.27 cm

~~from January to December~~through July are combined with a projection to give a full-year ~~2025~~2026 estimate.

2.2 CO_2 emissions from land-use~~, land use~~ change and ~~forestry~~land management (E_{LUC})

2.2.1 Historical period 1850-~~2024~~2025

The net CO_2 flux from land-use~~, land use~~ change and ~~forestry~~land management (E_{LUC}, ~~called~~hereafter referred to as net land-use change emissions ~~in the rest of the text)~~) accounts for CO_2 emissions and removals resulting from anthropogenic land-use activities. It includes ~~CO_2~~ fluxes from deforestation and clearing of other natural vegetation, afforestation, logging~~,~~ and forest degradation (including harvest activity), shifting cultivation (cycle of cutting forest for agriculture, then abandoning), regrowth of forests and other natural vegetation (following wood harvest or agriculture abandonment), peat burning~~,~~ and peat drainage, and transitions between cropland, pasture and urban areas.

Updated estimates from the three bookkeeping models ~~are used to quantify gross emissions, gross removals, and the resulting net E_{LUC}:~~ BLUE (Hansis et al., 2015), LUCE (Qin et al. 2024), and OSCAR (Gasser et al., 2020~~). An important improvement compared to previous GCBs is the use of transient~~) are used to quantify gross emissions, gross removals, and the resulting net E_{LUC}. Bookkeeping models track changes in vegetation and soil carbon ~~densities by all trees~~stocks following land-use transitions and due to land management, accounting for carbon losses through decay, carbon transfer to harvested wood products, and carbon uptake through regrowth (see Supplement S.2 for a detailed methodological description). The bookkeeping models~~, i.e., they~~ consider the effects of environmental changes, such as atmospheric CO_2 increase, on vegetation and soil carbon densities, to estimate E_{LUC} (Gasser et al., 2020; Dorgeist et al., ~~2024). The GCB assessments have for a long time also (and initially exclusively) used estimates from the bookkeeping model H&C2023 (Houghton and Castanho, 2023), its predecessor H&N2017 (Houghton and Nassikas, 2017), and earlier versions. However, H&C2023 does not consider transient carbon densities and only provides data up to 2020, which implies the need to extrapolate its data to the time after 2020. As the model does thus not incorporate the most recent developments in bookkeeping modeling, it is not used anymore in GCB2025.~~

2024). Emissions from peat burning and peat drainage are added from external datasets (see Supplement S.2.2): peat fire emissions from the Global Fire Emission Database (~~GFED4s~~GFED5.1; van der Werf et al., ~~2017~~2025) and peat drainage emissions averaged from estimates of the Food Agriculture Organization (Conchedda and Tubiello, 2020; FAO, ~~2025a~~2026a) and from simulations with the DGVM ORCHIDEE-PEAT (Qiu et al., 2021) and the DGVM LPX-Bern (Lienert and Joos, 2018; Müller and Joos, 2021). GFED5 represents a major revision of GFED4, with the most substantial change being improved accounting for burned area from small fires (Chen et al., 2023). Other improvements include a revised fuel consumption scheme and the use of higher-resolution input data,

Formatted: Outline numbered + Level: 2 + Numbering Style: 1, 2, 3, … + Start at: 1 + Alignment: Left + Aligned at: 0 cm + Indent at: 1.02 cm

Formatted: Outline numbered + Level: 3 + Numbering Style: 1, 2, 3, … + Start at: 1 + Alignment: Left + Aligned at: 0 cm + Indent at: 1.27 cm

collectively resulting in a 65% increase in estimated fire carbon emissions compared with GFED4, although changes in deforestation and peatland fire emissions are smaller (van der Werf et al., 2025).

Uncertainty estimates were derived from the Dynamic Global Vegetation Models (DGVMs) ensemble for the time period prior to 1960, and using for the recent decades an uncertainty range of ±0.7 GtC yr^{-1}, which is a semi-quantitative measure for annual and decadal emissions and reflects our best value judgement that there is at least 68% chance (±1σ) that the true land-use change emission lies within the given range, for the range of processes considered here.

The GCB E_{LUC} estimates follow the CO_2 flux definition of global carbon cycle models and differ from IPCC definitions of land use, land-use change and forestry (LULUCF) adopted in ~~National GHG Inventories~~national greenhouse gas inventories (NGHGI) for reporting under the UNFCCC. The latter typically include terrestrial fluxes occurring on all land that countries define as managed, following the IPCC managed land proxy approach (Grassi et al., 2018). This partly includes fluxes due to environmental change (e.g., atmospheric CO_2 increase), which are part of S_{LAND} in our definition. As a result, global emission estimates are smaller for NGHGI than for the global carbon budget definition (Grassi et al., 2023). ~~The same is the case for the FAO estimates of carbon fluxes on forest land, which include both anthropogenic and natural fluxes on managed land (Tubiello et al., 2025; FAO, 2025b).~~ Using the NGHGI data collected and processed in the LULUCF data hub ~~V3~~(V4.1~~(~~.0, Melo et al. ~~2025),~~2026) and estimates of natural fluxes in managed forests from DGVMs, we translate the GCB and NGHGI definitions to each other~~,~~ (see Supplement S.2.4), to provide a comparison of the anthropogenic carbon budget as reported in GCB to the official country reporting to the UNFCCC convention. We further compare these estimates with the net atmosphere-to-land flux from atmospheric inversion systems (see Section 2.7), averaged over managed land only. We also show Food and Agriculture Organization (FAO) estimates of CO_2 land fluxes, comprised of emissions from net forest conversion (proxy of deforestation) and net fluxes on forest land (Tubiello et al., 2026), and emissions from peat drainage (Conchedda and Tubiello, 2020) and peat fires (Prosperi et al., 2020). See Supplementary S.2.4 for more details.

E_{LUC} contains a range of fluxes that are related to Carbon Dioxide Removal (CDR). CDR is defined as the set of anthropogenic activities that remove CO_2 from the atmosphere, in addition to the Earth's natural processes (such as carbon uptake in response to atmospheric CO_2 increase), and store it in durable form, such as in forest biomass, soils, long-lived products, oceans or geological reservoirs. Here, we quantify vegetation-based CDR that is implicitly or explicitly captured by land-use fluxes (CDR not based on vegetation is discussed in Section 2.3). We quantify CDR through re/afforestation from the three bookkeeping estimates by separating permanent increases in forest cover, which counts as CDR, from forest regrowth in shifting cultivation cycles (not part of CDR; see Supplement S.2.2). It should be noted that the permanence of the storage under climate risks such as fire is increasingly questioned. Other CDR activities related to land use by using biomass from terrestrial plants as input

but not fully accounted for in our E_{LUC} estimate include the transfer of carbon to harvested wood products (HWP), bioenergy with carbon capture and storage (BECCS), ~~and~~ biochar ~~production~~soil amendment, biomass burial, bio-oil storage, and biomass sinking (when it uses land-grown biomass) (Babiker et al., 2022; ~~Smith~~Edwards et al., ~~2024~~2026). The different bookkeeping models all represent HWP but with varying details concerning product usage and their lifetimes. ~~BECCS and biochar~~The other CDR methods using terrestrial biomass as input are currently only represented in bookkeeping and DGVM models regarding the CO_2 removal through photosynthesis, without accounting for the durable storage. HWP, BECCS, ~~and~~ biochar soil amendment, biomass burial, bio-oil storage, and biomass sinking are typically counted as CDR once the transfer to the durable storage site occurs and not when the CO_2 is removed from the atmosphere, which complicates a direct comparison to the GCB approach to quantify annual fluxes to and from the atmosphere. We provide estimates for CDR through HWP, BECCS, ~~and~~ biochar soil amendment, biomass burial, bio-oil storage, and biomass sinking based on independent studies in Section 3.2.2. ~~HWP and BECCS estimates reflect updated 2024 data of the State of CDR report (Smith et al., 2024), while biochar estimates correspond to 2023 due to unavailability of newer data.~~ We do not add them to our E_{LUC} estimate to avoid potential double-counting that arises from the partial consideration of ~~HWP, BECCS, and biochar~~these methods in the bookkeeping and DGVM models and to avoid inconsistencies from the temporal discrepancy between transfer to storage and removal from the atmosphere. More details on the E_{LUC} methodology can be found in Supplement S.2.

2.2.2 ~~2025~~2026 Projection

We project the ~~2025~~2026 net land-use emissions for BLUE, OSCAR, and LUCE based on their E_{LUC} estimates for ~~2023~~2025 and adding the anomalies in carbon emissions from peat fires in equatorial Asia and tropical deforestation and degradation fires (2026 emissions relative to 2025 emissions ~~relative to 2023 emissions~~) from ~~GFED4s~~GFED5.1 (van der Werf et al., ~~2017~~2025) estimated using active fire data (MCD14ML; Giglio et al., 2016). ~~2023 is used as base year since the E_{LUC} estimate for the year 2024 is informed by extrapolated land-use data (Supplement S.2.1).~~ Peat drainage is assumed to be unaltered as it has low interannual variability.

2.3 Carbon Dioxide Removal (CDR) not based on vegetation

Some CDR involves CO_2 fluxes via land use~~,~~ (or marine biomass), which is included in our estimate of E_{LUC} (re/afforestation) or provided separately in Section 3.2.2 (HWP, BECCS, biochar~~, HWP,~~ soil amendment, biomass burial, bio-oil storage, and ~~BECCS~~biomass sinking). Other CDR not based on vegetation occurs through CO_2 fluxes directly from the air to the geosphere, which is reported in Section 3.3. The majority of this derives from ~~bio-oil storage in geological reservoirs,~~ enhanced weathering through the application of crushed rock to soils, alkalinity enhancement of water bodies, and the production of solid mineral products with CO_2 captured from the atmosphere~~,~~ (including

Formatted: Outline numbered + Level: 3 + Numbering Style: 1, 2, 3, … + Start at: 1 + Alignment: Left + Aligned at: 0 cm + Indent at: 1.27 cm

Formatted: Outline numbered + Level: 2 + Numbering Style: 1, 2, 3, … + Start at: 1 + Alignment: Left + Aligned at: 0 cm + Indent at: 1.02 cm

Formatted: Not Highlight

biogenic CO_2 from BECCS or biochar soil amendment, if applied this way), with smaller contributions from Direct Air Carbon Capture and Storage (DACCS~~),~~). Note that Friedlingstein et al. (2026a) included bio-oil storage and biomass burial and sinking ~~of terrestrial (e.g., straw) or marine (e.g., macroalgae) biomass into~~within the ~~deep ocean through human intervention, and others like intentional ocean or river alkalinity enhancement. For~~ estimates for CDR not based on vegetation, but given these methods both use biomass to capture CO_2 they have been accounted for in the E_{LUC}. For CDR not based on vegetation, we use updated ~~2024~~2026 data (~~Smith~~Edwards et al., ~~2024~~2026), which compiles and harmonises reported CDR from a combination of existing databases, surveys, and novel research. Currently, there are no internationally agreed methods for reporting these types of CDR, implying that estimates are based on self-disclosure by projects following their own protocols or protocols produced by third party registries. As such, the fractional uncertainty on these numbers should be viewed as substantial, and numbers are liable to change in future years as protocols are harmonised and improved.

2.4 Growth rate in atmospheric CO_2 concentration (G_{ATM})

2.4.1 Historical period 1850-~~2024~~2025

The rate of growth of the atmospheric CO_2 concentration is provided for years 1959-2024 by the US National Oceanic and Atmospheric Administration Global Monitoring Laboratory (NOAA/GML; Lan et al., ~~2025~~2026), which includes recent revisions to the calibration scale of atmospheric CO_2 measurements (WMO-CO2-X2019; Hall et al., 2021). For the 1959-1979 period, the global growth rate is based on measurements of atmospheric CO_2 concentration averaged from the Mauna Loa and South Pole stations, as observed by the CO_2 Program at Scripps Institution of Oceanography (SIO, Keeling et al., 1976). For the 1980-2024 period, the global growth rate is based on the average of multiple stations selected from the marine boundary layer sites with well-mixed background air (Lan et al., 2024), after fitting a smooth curve through the data for each station as a function of time, and averaging by latitude band (Masarie and Tans, 1995). The annual growth rate is estimated by Lan et al. (2025) from atmospheric CO_2 concentration by taking the average of the most recent December-January months corrected for the average seasonal cycle and subtracting this same average one year earlier. To obtain G_{ATM}, the observation-based growth rate in units of ppm yr^{-1} is converted to units of GtC yr^{-1} by multiplying by a factor of 2.124 GtC per ppm, assuming instantaneous mixing of CO_2 throughout the atmosphere (Ballantyne et al., 2012; Table 1). There is high confidence in the observations because they are based on direct measurements from stations distributed around the world (Lan et al., 2024) with all CO_2 measurements consistently measured against the same CO_2 standard scale (WMO X2019) defined by a suite of gas standards (Hall et al., 2021). However, the conversion to estimates of G_{ATM} in GtC yr^{-1} incurs large uncertainty on annual time scale as discussed next.

The uncertainty around G_{ATM} is due to three main factors. First, the network composition of the marine boundary layer sites with some sites being introduced or removed over time, gaps in sites time series,

Formatted: Highlight

Formatted: Highlight

Formatted: Highlight

Formatted: Outline numbered + Level: 2 + Numbering Style: 1, 2, 3, … + Start at: 1 + Alignment: Left + Aligned at: 0 cm + Indent at: 1.02 cm

Formatted: Outline numbered + Level: 3 + Numbering Style: 1, 2, 3, … + Start at: 1 + Alignment: Left + Aligned at: 0 cm + Indent at: 1.27 cm

etc. This uncertainty was estimated with a bootstrap method by constructing 100 "alternative" networks (Steele et al., 1992; Masarie and Tans, 1995; Lan et al., ~~2025~~2026). Second, the analytical uncertainty that describes the short- and long-term uncertainties associated with the CO_2 analyzers. A Monte Carlo method was used to estimate the total analytical uncertainty by randomly selecting errors to add to each observation from a normal distribution of combined short- and long-term uncertainties. Prior to the 1980s when analyzers were less precise and CO_2 measurement scale was slightly less well defined, larger analytical errors were assigned to account for these factors. However, the network uncertainty remains the larger term of uncertainty. The first and second uncertainties are reported as 1-sigma standard deviations (i.e., 68% confidence interval), and summed in quadrature to determine the global surface growth rate uncertainty, which averaged to 0.085 ppm (Lan et al., 2024). Third, the uncertainty associated with using the average CO_2 concentration from a surface network to approximate the true atmospheric average CO_2 concentration (mass-weighted, in 3 dimensions) as needed to assess the total atmospheric CO_2 burden. In reality, CO_2 variations measured at the stations will not exactly track changes in total atmospheric burden, with offsets in magnitude and phasing due to vertical and horizontal mixing (Pandey et al., 2025). This effect must be very small on decadal and longer time scales, when the atmosphere can be considered well mixed. The long-term CO_2 increase in the stratosphere lags the increase (meaning lower concentrations) that we observe in the marine boundary layer, while the continental boundary layer (where most of the emissions take place) leads the marine boundary layer with higher concentrations. These effects nearly cancel each other on decadal time scales, when the growth rate is nearly the same everywhere (Ballantyne et al., 2012). We therefore maintain an uncertainty around the annual growth rate based on the multiple stations dataset ranges between 0.11 and 0.72 GtC yr^{-1}, with a mean of 0.61 GtC yr^{-1} for 1959-1979 and 0.17 GtC yr^{-1} for 1980-2024, when more measurement sites were available (Lan et al., ~~2025~~2026). We estimate the uncertainty of the decadal averaged growth rate after 1980 at 0.02 GtC yr^{-1} based on the annual growth rate uncertainty but stretched over a 10-year interval. For years prior to 1980, we estimate the decadal averaged uncertainty to be 0.07 GtC yr^{-1} based on a factor proportional to the annual uncertainty prior and after 1980 (0.02 * [0.61/0.17] GtC yr^{-1}).

To estimate the total carbon accumulated in the atmosphere since 1750 or 1850, we use an atmospheric CO_2 concentration of 278.0 ± 3 ppm or 287.7 ± 3 ppm, respectively (Gulev et al., 2021). For the construction of the historical budget shown in Figure 3, we use the fitted estimates of CO_2 concentration from Joos and Spahni (2008) to estimate the annual atmospheric growth rate (see Supplement S.7). The uncertainty of ±3 ppm (converted to ±1σ) is taken directly from the IPCC's AR5 assessment (Ciais et al., 2013). Typical uncertainties in the growth rate in atmospheric CO_2 concentration from ice core data are equivalent to ±0.1-0.15 GtC yr^{-1} as evaluated from the Law Dome data (Etheridge et al., 1996) for individual 20-year intervals over the period from 1850 to 1960 (Bruno and Joos, 1997).

2.4.2 Satellite-based (~~2015~~2010-present)

Further opportunities to estimate global CO_2 growth rates are offered by space-based platforms such as GOSAT (since 2010) and OCO-2 (since 2015). Their recorded short-wave infrared spectra allow retrieval of column ~~CO_2 abundances~~ averaged dry-air mole fraction of carbon dioxide (XCO_2) over cloud-free scenes over land and ocean with footprints of 80 (GOSAT) and 3 (OCO-2) km^2 respectively. The columns are not full integrals; the sensitivity to surface and lower-tropospheric CO_2 mole fractions is much higher than to upper tropospheric and stratospheric CO_2. However, for the purpose of calculating atmospheric growth rates, the sensitivity is not limiting, as the pressure-weighted sensitivity is still above 0.5 in the stratosphere (Pandey et al. 2024) and priors used in OCO-2 account for the slow stratospheric-tropospheric exchanges using the age of air (Laughner et al. 2023). Here, we use ~~OCO-2 based~~ whole atmosphere growth rates using the Growth Rate from Satellite Observations (GRESO) approach (Pandey et al., 2024). We specifically note that ~~their~~OCO-2 and GOSAT retrievals are evaluated against surface-based remote sensing (Total Column Carbon Observing Network) data, which in turn are tied to atmospheric observations (from aircraft and using aircore) (Wunch et al., 2017). Furthermore, OCO-2 retrievals use a ~~priori~~ CO_2 mole fraction profiles prior tied to NOAA GML in-situ flask records at Mauna Loa (MLO) and American Samoa (SMO) measurement stations (Laughner et al., 2023). For details on evaluation, bias- correction, and spatiotemporal coverage of the OCO-2 retrievals we refer to ~~O'Dell~~O'Dell et al. (2018~~).~~) and Taylor et al. (2026); the GOSAT retrievals use the same ACOS version 11 algorithm.

Relative to surface observations, the GRESO product typically reflects tropical growth rate anomalies earlier and sees whole atmosphere carbon stock changes with a lower latency. The GRESO growth rates presented here use both land and ocean observations of OCO-2 and GOSAT, providing global sampling of the atmosphere. We used GRESO ~~post 2015~~ to present an alternative quantification of the atmospheric carbon stock changes in G_{ATM}, using the reported 1-sigma uncertainty ~~of~~, which is 0.08–0.13 ppm yr^{-1}~~.~~ for 2015–2025 and 0.13–0.14 ppm yr^{-1} for the GOSAT-only years 2010–2014. The mean ~~differences~~difference between GRESO and surface-data derived G_{ATM} is −0.~~05~~01 ± 0.~~26~~19 ppm yr^{-1} over the ~~2015–2024~~2010–2025 (n=~~10~~16 years) period.

2.4.3 ~~2025~~2026 projection

We provide an assessment of G_{ATM} for ~~2025~~2026 as the average of two methods. First, the GCB regression method models monthly global-average atmospheric CO_2 concentrations and derives the increment and annual average from these. The model uses lagged observations of concentration (Lan et al., ~~2025~~2026): both a 12-month lag, and the lowest lag that will allow model prediction to produce an estimate for the following January, recalling that the G_{ATM} increment is derived from December/January pairs. The largest driver of interannual changes is the ENSO signal (Betts et al.,

Formatted: Outline numbered + Level: 3 + Numbering Style: 1, 2, 3, … + Start at: 1 + Alignment: Left + Aligned at: 0 cm + Indent at: 1.27 cm

Formatted: Font: Gungsuh, Not Superscript/ Subscript

Formatted: Font: Gungsuh

Formatted: Font: Gungsuh

Formatted: Font: Gungsuh

Formatted: Outline numbered + Level: 3 + Numbering Style: 1, 2, 3, … + Start at: 1 + Alignment: Left + Aligned at: 0 cm + Indent at: 1.27 cm

2016), so the monthly ENSO 3.4 index (Huang et al., ~~2023~~2017) is included in the model. Given the natural lag between sea-surface temperatures and effects on the biosphere, and in turn effects on globally mixed atmospheric CO_2 concentration, a lagged ENSO index is used, and we use both a 5-month and a 6-month lag. The combination of the two lagged ENSO values helps reduce possible effects of noise in a single month. To help characterise the seasonal variation, we add month as a categorical variable. Finally, we flag the period affected by the Pinatubo eruption (August 1991 - November 1993) as a categorical variable.

The second method uses the multi-model mean and uncertainty of the ~~2025~~2026 G_{ATM} estimated by the ESMs prediction system (see Section 2.9). We then take the average of the GCB regression and ESMs G_{ATM} estimates, with their respective uncertainty combined quadratically.

Similarly, the projection of the ~~2025~~2026 global average CO_2 concentration (in ppm), is calculated as the average of the estimates from the two methods. For the GCB regression method, it is the annual average of global concentration over the 12 months of ~~2025~~2026; for the ESMs, it is the observed global average CO_2 concentration for ~~2024~~2025 plus the annual increase in ~~2025~~2026 of the global average CO_2 concentration, which is an average of NOAA/GML measurements from January to June (Lan et al., ~~2025~~2026) and predictions of the ESMs multi-model mean from July to December (see Section 2.9).

2.5 Ocean CO_2 sink

2.5.1 Historical period 1850-~~2024~~2025

The reported estimate of the global ocean anthropogenic CO_2 sink S_{OCEAN} is derived as the average of two estimates. The first estimate is derived as the mean over an ensemble of ten global ocean biogeochemistry models (GOBMs, Table 4 and Table S2). The second estimate is obtained as the mean over an ensemble of ~~nine~~ten surface ocean fCO_2-observation-based data-products (Table 4 and Table S3).

The GOBMs simulate both the natural and anthropogenic CO_2 cycles in the ocean. They constrain the anthropogenic air-sea CO_2 flux (the dominant component of S_{OCEAN}) by the transport of carbon into the ocean interior, which is also the controlling factor of present-day ocean carbon uptake in the real world. They cover the full globe and all seasons and were evaluated against surface ocean carbon observations, suggesting they are suitable to estimate the annual ocean carbon sink (Hauck et al., 2020). We derive S_{OCEAN} from GOBMs by using a simulation (sim A) with historical forcing of climate and atmospheric CO_2 from GCB (Section 2.4), accounting for model biases and drift from a control simulation (sim B) with constant atmospheric CO_2 and normal year climate forcing. A third simulation (sim C) with historical atmospheric CO_2 increase and normal year climate forcing is used to attribute the ocean sink

Formatted: Outline numbered + Level: 2 + Numbering Style: 1, 2, 3, … + Start at: 1 + Alignment: Left + Aligned at: 0 cm + Indent at: 1.02 cm

Formatted: Outline numbered + Level: 3 + Numbering Style: 1, 2, 3, … + Start at: 1 + Alignment: Left + Aligned at: 0 cm + Indent at: 1.27 cm

to CO_2 (sim C minus sim B) and climate (sim A minus sim C) effects. A fourth simulation (sim D; historical climate forcing and constant atmospheric CO_2) is used to compare the change in anthropogenic carbon inventory in the interior ocean (sim A minus sim D) to the observation-based ~~estimates~~estimate of ~~Gruber et al. (2019) and~~ Müller et al. (2023) with the same flux components (steady state and non-steady state anthropogenic carbon flux).

~~As there is accumulating evidence for a 10–20% underestimation of S_{OCEAN} by the GOBMs based on ocean interior data (section 3.6.5), atmospheric oxygen (section 3.6.2), atmospheric inversions (section 3.8) and supported by eddy-covariance measurements (Dong et al., 2024), we scale up the global GOBM multi-model mean estimates by 10% when estimating S_{OCEAN} (Friedlingstein et al., 2025b) (see Supplement S3.3). Analysis of Earth System Models and GOBMs indicate that an underestimation by about 10% may be due to biases in ocean carbon transport and mixing from the surface mixed layer to the ocean interior (Goris et al., 2018, Terhaar et al., 2021, Bourgeois et al., 2022, Terhaar et al., 2022), biases in the chemical buffer capacity (Revelle factor) of the ocean (Vaittinada Ayar et al., 2022; Terhaar et al., 2022) and partly due to a late starting date of the simulations (mirrored in atmospheric CO_2 chosen for the pre-industrial control simulation, Table S2, Bronselaer et al., 2017, Terhaar et al., 2022; 2024). GOBMs are evaluated against key metrics and their capability to reproduce various statistical measures of physical and biogeochemical fields using the International Ocean Model Benchmarking (IOMB) Scheme (Fu et al., 2022, Text S3.3).~~

The GOBMs capability to simulate S_{OCEAN} was assessed with the International Ocean Model Benchmarking (IOMB) Scheme (Fu et al., 2022) using various statistical measures of physical and biogeochemical fields (text S3.3), with an evaluation of the simulated inventories of transient tracers (CFC11, CFC12, SF6, Matsumoto et al., 2004, text S3.3) and an emergent constraint approach accounting for biases in circulation and carbonate chemistry in models (Terhaar et al., 2022, text S3.3). These evaluations target the physical-chemical processes that drive anthropogenic carbon uptake (ventilation, carbonate chemistry, solubility of CO_2 in seawater). In addition, we report the interior ocean accumulation of anthropogenic carbon for GOBMs and compare this to observation-based estimates (text S3.6 and section 3.6.5). This process-based evaluation provides evidence in support of the GOBM ensemble average capturing S_{OCEAN} and its driving processes well (ventilation, carbonate system buffer capacity, Goris et al., 2018, Terhaar et al., 2021, Bourgeois et al., 2022, Terhaar et al., 2022, Vaittinada Ayar et al., 2022). Therefore, the scaling factor to account for known model biases that was introduced in GCB2025 is set to 1.0, i.e. the GOBM estimate is scaled by 0% this year (section 3.6.5). This is applied only for the final estimate of S_{OCEAN} (text S3.2)

The fCO_2-products are tightly linked to observations of fCO_2 (fugacity of CO_2, which equals pCO_2 corrected for the non-ideal behaviour of the gas; Pfeil et al., 2013), which carry imprints of temporal and spatial variability, but are also sensitive to uncertainties in gas-exchange parameterizations and data-sparsity (Fay et al., 2021, Gloege et al., 2021, Hauck et al., 2023a). Their asset is the assessment of

the mean spatial pattern of variability and its seasonality (Hauck et al., 2020, Gloege et al. 2021, Hauck et al., 2023a~~).~~, McKinley et al 2026). To ~~benchmark~~better understand biases and trends ~~derived from~~ ~~the~~in fCO_2-products, ~~we update~~the fCO_2-product community conducted a ~~model subsampling exercise following Hauck et al. (2023a~~series of experiments (Roobaert et al 2026, in review, see section S3~~) and~~). Additionally, we use independent measurements from the SOCAT (Surface Ocean CO_2 Atlas) flag E dataset (uncertainty less than 10 µatm) (Bakker et al., 2016) and calculated fCO_2 from the Global Ocean Data Analysis Project GLODAP (Lauvset et al., 2024~~). New in~~) to further benchmark the fCO_2 products. Since GCB2025, ~~we now also include the UExP-FNN-U product in~~submissions that perform a temperature correction to the ~~ensemble mean, which was previously shown but not~~underlying observations are included~~. We include it since~~, as new evidence emerged from field and modelling studies, recommending adopting a temperature correction to the fCO_2 from measurement depth to the surface skin layer where the gas exchange takes place (Dong et al., ~~2024~~2024a, Ford et al., 2024a, Bellenger et al., ~~2022). Furthermore,~~2023, Ford et al 2026a). In GCB2026, three out of ten submissions apply such a ~~second fCO_2-product submitted temperature corrected fCO_2 (~~correction (UExP-FFN-U, JMA-MLR~~) this year, so we now include these corrected estimates in the ensemble mean.~~ and AOML-ET). Additionally, following Friedlingstein et al (2025b), we now also add 0.18 GtC yr^{-1} (multiplied by 7/~~9~~10 as ~~two~~three products already include a temperature correction) to the multi fCO_2-product average when calculating S_{OCEAN} to account for the warm layer and cool skin effect (See Supplement S3.1). This correction is based on a recent field study (Ford et al., 2024a) and broadly consistent in magnitude with a GOBM study (Bellenger et al ~~2022~~. 2023).

The global fCO_2-based flux estimates were adjusted to remove the pre-industrial natural ocean source of CO_2 to the atmosphere of 0.65 ± 0.3 GtC yr^{-1}, arising from the transfer of carbon from land to ocean via rivers (Regnier et al., 2022), to satisfy our definition of S_{OCEAN} (Hauck et al., 2020). This CO_2 outgassing adjustment was distributed over the latitudinal bands using the regional distribution of Lacroix et al. (2020; North: 0.14 GtC yr^{-1}, Tropics: 0.42 GtC yr^{-1}, South: 0.09 GtC yr^{-1}). Acknowledging that this distribution is based on only one model, the advantage is that a gridded field is available, and the adjustment can be calculated for the three latitudinal bands and the RECCAP regions (REgional Carbon Cycle Assessment and Processes ~~(~~, RECCAP2; Ciais et al., ~~2020~~2022, Poulter et al., 2022, DeVries et al., 2023). ~~This dataset~~A new study suggests ~~that more of the river-induced~~a roughly equal share between riverine outgassing ~~occurs in the tropics than in the Southern Ocean and is thus opposed to the previously used dataset of Aumont~~across the three regions (Planchat et al~~. (2001~~., 2025). Accordingly, the regional distribution is associated with an additional uncertainty in addition to the large uncertainty around the global estimate (Crisp et al., 2022; Gruber et al., 2023). Anthropogenic perturbations of river carbon and nutrient transport to the ocean are not represented in the process models used to quantify S_{OCEAN}~~, but an a-posteriori correction is applied to the global S_{OCEAN} estimate (see Section 2.10 and Supplement S.8.3).~~ .

New this year, for the regional analysis (Figures 14 and 15), we also subtract the preindustrial mean state derived from GOBMs, to only show anthropogenic perturbation (See Supplement S3.1). This is not necessary on the global scale, where the preindustrial mean state is zero.

We calculate S_{OCEAN} as the average of the GOBM ensemble mean and the fCO_2-product ensemble mean from 1990 onwards, including the corrections on the ~~GOBM and~~ fCO_2-product ensemble ~~means~~mean as described above. For the 1959-1989 period, it is calculated as the GOBM ensemble mean plus half of the offset between GOBMs and fCO_2-products ensemble means over 1990-2001, also including the above corrections. In addition, two diagnostic ocean models are used to estimate S_{OCEAN} over the industrial era (1781-1958, Khatiwala et al. (2013) and DeVries (2014)).

S_{OCEAN} is ~~evaluated against~~also compared to the change in the total dissolved inorganic carbon inventory in the interior ocean from the observation-based estimates of Keppler et al. ~~(2023) with the same flux components.~~(2023), Müller et al. (2023) and an observationally-constrained ocean inverse model (DeVries, 2022). To facilitate the synthesis of these comparisons into a single mean bias estimate, each of the three ocean interior products was - if needed - adjusted for missing carbon flux components to match the definition of S_{OCEAN} and scaled to full decadal periods reported in Table 6 (details of these adjustments are provided in Supplement S3.6).

We assign ~~an~~a temporally varying uncertainty ~~of~~ranging between ± 0.~~4~~53 to 0.68 GtC yr^{-1} to the ocean sink based on a combination of random (ensemble standard deviation) and systematic uncertainties (GOBMs bias in anthropogenic carbon accumulation, previously reported uncertainties in fCO_2-products~~,~~) that are combined as a Gaussian mixture model (see Supplement ~~S.3.4). While this~~S3.5). This approach is consistent within the GCB, ~~an~~and is close to the independent uncertainty assessment of the fCO_2-products alone ~~suggests a somewhat larger uncertainty~~ of up to 0.~~7~~76 GtC yr^{-1} [range 0.60 to 0.85 Pg C yr^{-1}] (Ford et al. 2024). We assess a medium confidence level to the annual ocean CO_2 sink and its uncertainty because it is based on multiple lines of evidence, it is consistent with ocean interior carbon estimates (see Section 3.6.5~~)~~), new process-based evaluation confirms the GOBMs estimate (section 3.6.5), and the interannual variability in the GOBMs and data-based estimates is largely consistent and can be explained by climate variability. We refrain from assigning a high confidence because of the large standard deviation of the fCO_2-products and the deviation between the GOBM and fCO_2-product trends between around 2002 and 2020 and the higher S_{OCEAN} estimate from O_2:N_2 (section 2.8). More details on the S_{OCEAN} methodology can be found in Supplement S.3.

2.5.2 ~~2025~~2026 Projection

The S_{OCEAN} forecast for the year ~~2025~~2026 is based on (a) the historical (Lan et al., ~~2025~~2026) and our ~~2025~~2026 estimate of atmospheric CO_2 concentration, (b) the historical and our ~~2025~~2026 estimate of global fossil emissions, and (c) the boreal spring (March, April, May) Oceanic Niño Index (ONI)

Formatted: Outline numbered + Level: 3 + Numbering Style: 1, 2, 3, … + Start at: 1 + Alignment: Left + Aligned at: 0 cm + Indent at: 1.27 cm

(NCEP, ~~2025~~2026). Using a non-linear regression approach, i.e., a feed-forward neural network, atmospheric CO_2, ONI, and the fossil emissions are used as training data to best match ~~the corrected~~ S_{OCEAN} from 1959 through ~~2024~~2025 from this year's carbon budget. Using this relationship, the ~~2025~~2026 S_{OCEAN} can then be estimated from the projected ~~2025~~2026 input data using the non-linear relationship established during the network training. To avoid overfitting, the neural network training was done using a Monte Carlo approach, with a variable number of artificial neurons (varying between 2-5) and 20% of the randomly selected training data were withheld for independent internal testing.

Based on the best output performance (tested using the 20% withheld input data), the best performing number of neurons was selected. In a second step, we trained the network 10 times using the best number of neurons identified in step 1 and different sets of randomly selected training data. The mean of the 10 trainings is considered our best forecast, whereas the standard deviation of the 10 ensembles provides a first order estimate of the forecast uncertainty. This uncertainty is then combined with the S_{OCEAN} uncertainty ~~(~~of the year 2025 (±0.4~~68~~ GtC yr^{-1}) to estimate the overall uncertainty of the ~~2025~~2026 projection. As an additional line of evidence, we also assess the ~~2025~~2026 atmosphere-ocean carbon flux from the ESM prediction system (see Section 2.9).

2.6 Land CO_2 sink

2.6.1 Historical Period 1850-~~2024~~2025

The terrestrial land sink (S_{LAND}) is thought to be due to the combined effects of rising atmospheric CO_2, increasing N inputs, and climate change, on plant growth and terrestrial carbon storage. S_{LAND} does not include land sinks directly resulting from land-use and land-use change (e.g., regrowth of vegetation) as these are part of the land-use change emissions (E_{LUC}), although system boundaries make it difficult to attribute exactly CO_2 fluxes on land between S_{LAND} and E_{LUC} (Erb et al., 2013).

S_{LAND} is derived from the multi-model mean of ~~22~~23 DGVMs (Table 4 and Table S1). DGVMs simulations include all climate variability and CO_2 effects over land. In addition to the carbon cycle represented in all DGVMs, 15 models also account for the nitrogen cycle and hence can include the effect of N inputs on S_{LAND}. The DGVMs estimates of S_{LAND} do not explicitly include the export of carbon to aquatic systems or its historical perturbation, which is discussed in Supplement S.8.3. DGVMs need to meet several criteria to be included in this assessment (see Supplement S.4.2). In addition, we use the International Land Model Benchmarking system (ILAMB; Collier et al., 2018) for the DGVMs evaluation (see Supplement S.4.2), with an additional comparison of DGVMs with a data-informed, Bayesian model-data fusion framework (CARDAMOM) (Bloom and Williams, 2015; Bloom et al., 2016). The uncertainty on S_{LAND} is taken from the DGVMs standard deviation. S_{LAND} is no longer calculated based on a transient simulation with fixed pre-industrial land cover, and in GCB2025 corrected for the Replaced Sinks and Sources bias (RSS) (Gitz and Ciais, 2003; Sitch et al., 2005,

Formatted: Outline numbered + Level: 2 + Numbering Style: 1, 2, 3, … + Start at: 1 + Alignment: Left + Aligned at: 0 cm + Indent at: 1.02 cm

Formatted: Outline numbered + Level: 3 + Numbering Style: 1, 2, 3, … + Start at: 1 + Alignment: Left + Aligned at: 0 cm + Indent at: 1.27 cm

Pongratz et al., 2009; Gasser et al., 2020; Obermeier et al. 2021; Dorgeist et al., 2024; Walker et al., 2025; O'Sullivan et al. 2026a). In GCB2026 it is now calculated from DGVM simulations with transient land use change, and transient compared with fixed, pre-industrial climate and atmospheric CO_2 content. A different adjustment is now required to account for the environmental effects on vegetation subsequently converted to agriculture (δL). The δL adjustment is based on bookkeeping model results and estimated at 0.20 +/- 0.07 GtC yr^{-1} for the 2016-2025 period. More details on the S_{LAND} methodology can be found in Supplement S.4. ~~The uncertainty on S_{LAND} is taken from the DGVMs standard deviation.~~

~~New to GCB2025 is a correction applied to the S_{LAND} estimate to account for its overestimation resulting from the assumption of pre-industrial land-use in the DGVM simulations, when in reality a large portion of the land surface has been converted to pasture and cropland, with a lower sink capacity. This bias is termed the Replaced Sinks and Sources 2026(RSS) (Gitz and Ciais, 2003; Sitch et al., 2005, Pongratz et al., 2009; Gasser et al., 2021; Obermeier et al. 2021; Dorgeist et al., 2024). The correction, which is only applied when estimating the global S_{LAND}, utilises results from a subset of DGVMs that were able to supply Net Biome Productivity estimates at a Plant Functional Type basis combined with time-varying PFT area fractions from the simulation with land use and land use change considered (O'Sullivan et al., 2025; Friedlingstein et al. 2025b), see S.4.1 for details on methodology. The corrected S_{LAND} is reduced by 19% globally when accounting for the RSS. More details on the S_{LAND} methodology can be found in Supplement S.4.~~

2.6.2 ~~2025~~ Projection

In previous versions of the GCB, the land sink projection was, like the ocean sink forecast, based on a non-linear regression approach with a feed-forward neural network. This approach, however, resulted in a large uncertainty and underestimated the land sink variability in the past. ~~This year,~~ Since GCB2025, we update the projection and simply calculate the land sink for ~~2025~~2026 as the residual of the projection of the other components of the carbon cycle ($S_{LAND}=E_{FOS}+E_{LUC}-G_{ATM}-S_{OCEAN}$). Hence, by construction the ~~2025~~2026 B_{IM} is set to zero.

Formatted: Outline numbered + Level: 3 + Numbering Style: 1, 2, 3, … + Start at: 1 + Alignment: Left + Aligned at: 0 cm + Indent at: 1.27 cm

2.7 Atmospheric inversion estimate

The world-wide network of in-situ atmospheric measurements and satellite derived atmospheric CO_2 column (XCO_2) observations put a strong constraint on changes in the atmospheric abundance of CO_2. This allows atmospheric inversion methods to constrain the magnitude and location of the combined total surface CO_2 fluxes from all sources, including fossil and land-use change emissions and land and ocean CO_2 fluxes. The inversions assume E_{FOS} to be well known, and they solve for the spatial and

Formatted: Outline numbered + Level: 2 + Numbering Style: 1, 2, 3, … + Start at: 1 + Alignment: Left + Aligned at: 0 cm + Indent at: 1.02 cm

temporal distribution of land and ocean fluxes from the residual gradients of CO_2 between stations that are not explained by fossil fuel emissions. By design, such systems thus close the carbon balance (B_{IM} = 0) and provide an additional perspective on the independent estimates of the ocean and land fluxes.

This year's release includes ~~fourteen~~sixteen inversion systems that are described in Table S4. Each system is rooted in Bayesian inversion principles but uses different methodologies. ~~These differences concern the selection of atmospheric CO_2 data or XCO_2, and the choice of a-priori fluxes to refine.~~ They ~~also differ in spatial and temporal resolution, assumed correlation structures, and mathematical approach of the models (see references in Table S4 for details). Importantly, the systems~~ use a variety of transport models, which ~~was demonstrated to be~~previous studies have identified as a ~~driving factor behind~~major driver of differences in ~~atmospheric~~the latitudinal distribution of inversion-based flux estimates~~, and specifically their distribution across latitudinal bands~~ (Gaubert et al., 2019; Schuh et al., 2019). ~~Six~~Also other choices, such as the a-priori fluxes, inversion ~~systems used surface~~ method of the models, and observations ~~from the global measurement network (Schuldt~~used (see references in Table S4 for details) have been identified as drivers of the inter-system flux differences (van der Woude et al., ~~2024, 2025). Eight~~2026). Eleven inversion systems used satellite XCO_2 retrievals from GOSAT and/or OCO-2, scaled to the WMO 2019 calibration scale, of which ~~three~~five inversions this year used these XCO_2 datasets in addition to the in-situ observational CO_2 mole fraction records.

The original products delivered by the inverse modellers were modified to facilitate the comparison to the other elements of the global budget, specifically on two accounts: (1) global total fossil emissions including cement carbonation CO_2 uptake, (2) and ~~(2)~~ riverine CO_2 transport. For the regional analysis (Figures 14 and 15), we also subtract the preindustrial mean state of the atmosphere-ocean CO_2 fluxes derived from GOBMs, to only show anthropogenic perturbation (Supplement S3.1). We note that with these adjustments the inverse results no longer represent the contemporary net atmosphere-surface exchange over land/ocean areas as sensed by atmospheric observations. Instead, for land, they become the net uptake of CO_2 by vegetation and soils that is not exported by fluvial systems, similar to the DGVMs estimates. For oceans, they become the net uptake of anthropogenic CO_2, similar to the GOBMs estimates.

The inversion systems prescribe global fossil emissions based on e.g., the GCP's Gridded Fossil Emissions Dataset versions ~~2025.1~~2026.0 (GCP-GridFED; Jones et al., ~~2025~~2026), which are updates to GCP-GridFEDv2021 presented by Jones et al. (~~2021b~~2021). GCP-~~GridFEDv2025.1~~GridFEDv2026.0 scales gridded estimates of CO_2 emissions from EDGARv4.3.2 (Janssens-Maenhout et al., 2019) within national territories to match national emissions estimates provided by the GCB for the years 1959-~~2024~~2025, which were compiled following the methodology described in Section 2.1. Small differences between the systems due to for instance regridding to the transport model resolution, or use of different fossil fuel emissions than GCP-~~GridFEDv2025.1~~GridFEDv2026.0, are adjusted in the latitudinal partitioning we present, to ensure agreement with the estimate of E_{FOS} in this budget. We also note that

Formatted: Not Superscript/ Subscript

Formatted: Not Superscript/ Subscript

Formatted: Not Superscript/ Subscript

the ocean fluxes used as prior by ~~8~~11 out of ~~14~~16 inversions are part of the suite of the ocean process model or fCO_2-products listed in Section 2.5. Although these fluxes are further adjusted by the atmospheric inversions (except for Jena CarboScope), it makes the inversion estimates of the ocean fluxes not completely independent of S_{OCEAN} assessed here.

To facilitate comparisons to the independent S_{OCEAN} and S_{LAND}, we used the same adjustments for transport and outgassing of carbon transported from land to ocean, as done for the observation-based estimates of S_{OCEAN} (see Supplement S.5.1).

The atmospheric inversions are evaluated using vertical profiles of atmospheric CO_2 concentrations (Figure ~~S13~~S14). More than 50 aircraft programs over the globe, either regular programs or repeated surveys over at least 9 months (except for SH programs), have been used to assess system performance (with space-time observational coverage sparse in the SH and tropics, and denser in NH mid-latitudes; Table S9). The ~~fourteen~~sixteen systems are compared to the independent aircraft CO_2 measurements between 2 and 7 km above sea level between 2001 and ~~2024~~2025. Results are shown in Figure ~~S13~~S14 and discussed in Supplement S.5.2.

We note that as of GCB2025, the ensemble of inverse models covering a full decade is deemed sufficiently large to report the 1-sigma standard deviation as uncertainty, following the convention of the other components in GCB. More details on the atmospheric inversion methodology can be found in Supplement S.5.

2.8 Atmospheric oxygen based estimate

Formatted: Outline numbered + Level: 2 + Numbering Style: 1, 2, 3, … + Start at: 1 + Alignment: Left + Aligned at: 0 cm + Indent at: 1.02 cm

Long-term atmospheric O_2 and CO_2 observations allow estimation of the global ocean and land carbon sinks, due to the coupling of O_2 and CO_2 with distinct exchange ratios for fossil fuel emissions and land uptake, and uncoupled O_2 and CO_2 ocean exchange (Keeling and Manning, 2014). The global ocean and net land carbon sinks were calculated following methods and constants used in Keeling and Manning (2014) but modified to also include the effective O_2 source from metal refining (Battle et al., 2023). For the exchange ratio of the net land sink a value of 1.05 is used, following Resplandy et al. (2019). For fossil fuels, the following values are used: gas: 1.95 ~~(+/-)~~± 0.04, liquid: 1.44~~, (+/-)~~ ± 0.03, solid: 1.17 ~~(+/-)~~± 0.03, cement: 0 ~~(+/-)~~± 0, gas flaring: 1.98 ~~(+/-)~~± 0.07 (Keeling, 1988). Atmospheric O_2 is observed as $\delta(O_2/N_2)$ and combined with CO_2 mole fraction observations into Atmospheric Potential Oxygen (APO, Stephens et al., 1998). The APO observations from 1990 to ~~2024~~2025 were taken from a weighted average of flask records from three stations in the Scripps O_2 program network (Alert, Canada (ALT), La Jolla, California (LJO), and Cape Grim, Australia (CGO), weighted per Keeling and Manning (2014). Observed CO_2 was taken from the globally averaged marine surface annual mean growth rate from the NOAA/GML Global Greenhouse Gas Reference Network (Lan et al., ~~2025~~2026). The O_2 source from ocean warming is based on ocean heat content from updated data from

NOAA/NCEI (Levitus et al., 2012). The effective O_2 source from metal refining is based on production data from Bray (2020), Flanagan (2021), and Tuck (2022). Uncertainty was determined through a Monte Carlo approach with 20,000 iterations, using uncertainties prescribed in Keeling and Manning (2014), including observational uncertainties from Keeling et al. (2007) and autoregressive errors in fossil fuel emissions (Ballantyne et al., 2015). The reported uncertainty is 1 standard deviation of the ensemble. As for the atmospheric inversions, the O_2 based estimates also closes the carbon balance (B_{IM} = 0) by design and provides another independent estimate of the ocean and land fluxes. Note that the O_2 method requires a correction for global air-sea O_2 flux, which has the largest uncertainty at annual time scales, but which is still non-negligible for decadal estimates (Nevison et al., 2008). The 2016-2025 decadal average net land and ocean sinks from the atmospheric O_2 based constraint are based on provisional data from the first half of 2026. These data have not yet been corrected for long-term drift in primary standards and may be revised at a future date.

2.9 Earth System Models estimate

Formatted: Outline numbered + Level: 2 + Numbering Style: 1, 2, 3, … + Start at: 1 + Alignment: Left + Aligned at: 0 cm + Indent at: 1.02 cm

Reconstructions and predictions from decadal prediction systems based on Earth system models (ESMs) provide a novel line of evidence in assessing the atmosphere-land and atmosphere-ocean carbon fluxes in the past decades and predicting their changes for the current year and years to come. By assimilating physical atmospheric and oceanic data products into the ESMs, the models are able to reproduce the historical variations of the atmosphere-sea CO_2 fluxes, atmosphere-land CO_2 fluxes, and atmospheric CO_2 growth rate (Li et al., 2016, 2019; Lovenduski et al., 2019a,b; Ilyina et al., 2021; Li et al., 2023; Li et al., 2026). Furthermore, the ESM-based predictions have proven their skill in predicting the air-sea CO_2 fluxes for up to 6 years, the air-land CO_2 fluxes and atmospheric CO_2 growth for 2 years (Lovenduski et al., 2019a,b; Ilyina et al., 2021; Li et al., 2023; Li et al., 2026). The reconstructions from the fully coupled model simulations ensure a closed budget within the Earth system, i.e., no budget imbalance term.

Six ESMs have performed the set of prediction simulations. The ensemble size of initialized prediction simulations is 10, and the ensemble mean for each individual model is used here. Each ESM uses a different assimilation method and combination of data products incorporated in the system, more details on the models configuration can be found in Table 4 and Supplement Table S5. Reconstructions of atmosphere-ocean CO_2 fluxes (S_{OCEAN}) and atmosphere-land CO_2 fluxes (S_{LAND}-E_{LUC}) for the time period from 1960-~~2024~~2025 are assessed here. Predictions of the atmosphere-ocean CO_2 flux, atmosphere-land CO_2 flux, and atmospheric CO_2 growth for ~~2025~~2026 are calculated based on the predictions at lead year 1. The predictions of atmosphere-ocean CO_2 flux and atmosphere-land CO_2 flux are bias corrected by removing the climatological mean and linear trend biases from 1981-2021 referring to GCB2022 (Friedlingstein et al., 2022), the atmospheric CO_2 growth (G_{ATM}) is then calculated as the residual of the CO_2 emissions subtracting the carbon sinks into the ocean and the land. With the ESMs simulations, we

also compute the G_{ATM} in another way based on monthly atmospheric CO_2 concentrations at 1000hPa level over the oceans to be comparable to the NOAA/GML global measurements of atmospheric CO_2 concentrations (Lan et al., ~~2025~~2026). The bias correction is done referring to NOAA/GML monthly CO_2 concentrations in recent ~~10~~ years from 2015-~~2024~~2025 regarding mean state and linear trend, a shorter period is used because a non-linear trend for the whole period is observed from both NOAA/GML measurements and model simulations. The ~~2025~~2026 G_{ATM} is then calculated by the increment of atmospheric CO_2 concentration in December ~~2025~~2026 minus that in December ~~2024~~2025 multiplied by 2.124 to convert the unit from ppm to GtC. The prediction of ~~2025~~2026 atmospheric CO_2 concentration is an average of the available NOAA/GML measurements from January to June (Lan et al., ~~2025~~2026) and ESMs' predictions from July to December. Note that the two methods, i.e., one based on the residual of carbon sources and sinks and another based on atmospheric concentration increment, of calculation of G_{ATM} result in different magnitudes, which suggests the consideration of variable ratio rather than a constant value in converting CO_2 concentration to mass. More details on methods of bias correction of decadal predictions can be found in Kharin et al. (2012), Boer et al. (2016) and Li et al. (2023). The ESMs are used here to support the assessment of S_{OCEAN} and net atmosphere-land CO_2 flux (S_{LAND} - E_{LUC}) over the 1960-~~2024~~2025 period, and to provide an estimate of the ~~2025~~2026 prediction of G_{ATM} and atmospheric CO_2 concentration.

2.10 Processes not fully included in the global carbon budget

The contribution of anthropogenic CO and CH_4 to the global carbon budget is not fully accounted for in Eq. (1) and is described in Supplement S.8.1. The contributions to CO_2 emissions of decomposition of carbonates not accounted for is described in Supplement S.8.2. The contribution of anthropogenic changes in river fluxes is conceptually included in Eq. (1) in S_{OCEAN} and in S_{LAND}, but it is not represented in the process models used to quantify these fluxes~~. However,~~, hence a correction of -0.07 GtC yr^{-1} is applied a posteriori to the S_{LAND} estimate for the ~~2015-2024~~2016-2025 period, as proposed in Friedlingstein et al. (2025b). This effect is discussed in Supplement S.8.3.~~Similarly, the Replaced Sinks and Sources effect from reduced forest cover over the historical period is missing from the DGVMs used here to estimate S_{LAND}. However, a correction (~19%) is applied a posteriori to the S_{LAND} estimate from DGVMs, based on O'Sullivan et al. (2025; see Section 2.6 and Supplement S.4.1).~~

3 Results

For each component of the global carbon budget, we present results for three different time periods: the full historical period, from 1850 to ~~2024~~2025, the decades in which we have atmospheric concentration records from Mauna Loa (1959-~~2024),~~2025) with a specific focus on last year (~~2024~~2025), and the projection for the current year (~~2025~~2026). Subsequently, we assess the estimates of the budget components of the last decades against the top-down constraints from inverse modelling of atmospheric observations and the land/ocean partitioning derived from the atmospheric O_2 measurements.

Formatted: Outline numbered + Level: 2 + Numbering Style: 1, 2, 3, … + Start at: 1 + Alignment: Left + Aligned at: 0 cm + Indent at: 1.02 cm

Formatted: Highlight

Formatted: Highlight

Formatted: Indent: Left: 0 cm, First line: 0 cm, Outline numbered + Level: 1 + Numbering Style: 1, 2, 3, … + Start at: 1 + Alignment: Left + Aligned at: 0 cm + Indent at: 0.76 cm

Atmospheric inversions further allow for an assessment of the budget components with a regional breakdown of land and ocean sinks.

3.1 Fossil CO_2 Emissions

3.1.1 Historical period 1850-~~2024~~2025

Cumulative fossil CO_2 emissions for 1850-~~2024~~2025 were ~~495~~510 ± 25 GtC, including the cement carbonation sink (Table 8, with all cumulative numbers rounded to the nearest 5GtC). In this period, 46% of global fossil CO_2 emissions came from coal, 35% from oil, 15% from natural gas, 3% from decomposition of carbonates for cement production, and 1% from flaring. In 1850, the UK stood for 62% of global fossil CO_2 emissions. In 1893 the combined cumulative emissions of the current members of the European Union reached and subsequently surpassed the level of the UK. Since 1917 ~~US~~, USA cumulative emissions have been the largest. Over the entire period 1850-~~2024~~, ~~US~~2025, USA cumulative emissions amounted to 120 GtC (~~24~~23% of world total), the EU's to ~~80~~83 GtC (16%), China's to ~~80~~81 GtC (~~15~~16%), and India's to ~~18~~19 GtC (4%).

In addition to the estimates of fossil CO_2 emissions that we provide here (see Section 2.1), there are three global datasets with long time series that include all sources of fossil CO_2 emissions: CDIAC-FF (Erb and Marland, ~~2025~~2026a, 2026b), CEDS version 2024_~~07_08~~03_18 (Hoesly et al., ~~2024~~2025) and PRIMAP-hist version 2.~~6~~8 (Gütschow et al., 2016; Gütschow ~~et al., 2024~~& Pflüger, 2026), although these datasets are not entirely independent from each other (Andrew, 2020a). CEDS has cumulative emissions over 1750-~~2022~~2023 at ~~480~~500 GtC, CDIAC-FF has ~~481~~489 GtC, GCP ~~484~~494 GtC, PRIMAP-hist CR ~~490~~498 GtC, and PRIMAP-hist TR ~~492~~502 GtC. ~~CDIAC-FF excludes emissions from lime production. CEDS estimates higher emissions from international shipping~~While there are some differences in ~~recent years, while PRIMAP-hist has higher fugitive emissions than the other datasets. However~~coverage, in general these four datasets are in relative agreement as to total historical global emissions of fossil CO_2.

3.1.2 Recent period 1959-~~2024~~2025

Global fossil CO_2 emissions, E_{FOS} (including the cement carbonation sink), have increased every decade from an average of 3.0 ± 0.2 GtC yr^{-1} for the decade of the 1960s to an average of ~~9.8~~10.0 ± 0.5 GtC yr^{-1} during ~~2015-2024~~2016-2025 (Table 7, Figure 2 and Figure 4). The growth rate in these emissions decreased between the 1960s and the 1990s, from 4.~~3~~4% yr^{-1} in the 1960s (1960-1969), 3.1% yr^{-1} in the 1970s (1970-1979), 1.~~5~~6% yr^{-1} in the 1980s (1980-1989), to 1.0% yr^{-1} in the 1990s (1990-1999). After this period, the growth rate began increasing again in the 2000s at an average growth rate of 2.8% yr^{-1}, decreasing to 1.2% yr^{-1} in the 2010s, and 0.~~8~~9% yr^{-1} for the last decade (~~2015-2024~~2016-2025). China's emissions increased by 2.~~5~~7% yr^{-1} on average over the last 10 years dominating the global trend, and

Formatted: Outline numbered + Level: 2 + Numbering Style: 1, 2, 3, … + Start at: 1 + Alignment: Left + Aligned at: 0 cm + Indent at: 1.02 cm

Formatted: Outline numbered + Level: 3 + Numbering Style: 1, 2, 3, … + Start at: 1 + Alignment: Left + Aligned at: 0 cm + Indent at: 1.27 cm

Formatted: Outline numbered + Level: 3 + Numbering Style: 1, 2, 3, … + Start at: 1 + Alignment: Left + Aligned at: 0 cm + Indent at: 1.27 cm

India's emissions increased by 3.65% yr^{-1}, while emissions decreased in EU27 (-2.59% yr^{-1}), and in the USA (-1.20.8% yr^{-1}) (Figure 5a). Figure 6 illustrates the spatial distribution of fossil fuel emissions for the 2015-20242016-2025 period.

E_{FOS} reported here includes the uptake of CO_2 by cement via carbonation which has increased with increasing stocks of cement products, from an average of 2013 MtC yr^{-1} (0.0201 GtC yr^{-1}) in the 1960s to an average of 210MtC150MtC yr^{-1} (0.2115 GtC yr^{-1}) during 2015-20242016-2025 (Figure 5b).

3.1.3 Final year 20242025

Global fossil CO_2 emissions were slightly higher, 1.12%, in 20242025 than in 20232024, with an increase of 0.11 GtC to reach 10.35 ± 0.5 GtC (including the 0.2216 GtC cement carbonation sink) in 2024 (Figure 4), distributed among coal (41%), oil (3233%), natural gas (21%), cement (4%), flaring (1%), and others (1%).%) (Figure 4). Compared to 20232024, the 20242025 emissions from coal, oil, and gas increased by 0.84%, 1.39%, and 2.41.8% respectively, while emissions from cement decreased by 40.6%. All annual growth rates presented are adjusted for the leap year, unless stated otherwise.

In 20242025, the largest absolute contributions to global fossil CO_2 emissions were from China (32%), the USA (13%), India (8%), and the EU27 (6%). These four regions account for 5960% of global fossil CO_2 emissions, while the rest of the world contributed 4140%, including international aviation and marine bunker fuels (3% of the total). Growth rates for these countries from 2023 to 2024 to 2025 were 0.74% (China), -0.62.8% (USA), -2.60.0% (EU27), and 4.01.2% (India), with +1.30.5% for the rest of the world, including international aviation and marine bunker fuels (9.84.7%). The per-capita fossil CO_2 emissions in 20242025 were 1.3 tC person^{-1} yr^{-1} for the globe, and were 3.94.0 (USA), 2.4 (China), 1.5 (EU27) and 0.6 (India) tC person^{-1} yr^{-1} for the four highest emitters (Figure 5c).

3.1.4 Year 20252026 Projection

Globally, we estimate that global fossil CO_2 emissions (including cement carbonation, -0.2115 GtC) grewdeclined by 1.0.4% in 2025 (0.22026 (-1.5% to 1.70.6%) to 10.4 GtC (38.12 $GtCO_2$), an historical record high[2].). The estimates of changes in 20252026 emissions per fuel types, relative to 20242025, are projected to be 1.increase by 0.6% (range -0.26% to 1.7%) for coal, 1.1% (range 0.7% to 1.5decrease by 1.9% (range -2.6% to -1.2%) for oil, 1.to decrease by 0.3% (range -1.6% to 0.1% to 2.49%) for natural gas, and -to decrease by 0.96% (range -2.6% to 1.5% to 0.8%) for cement (Figure 5b).

The uncertainty presented for projections relates only to the estimated growth rate, and excludes the uncertainty of the baseline (i.e., 2024) level. Given that our projection is effectively of what the data

[2] Growth rates in this section use a leap year adjustment that corrects for the extra day in 2024.

Formatted: Outline numbered + Level: 3 + Numbering Style: 1, 2, 3, … + Start at: 1 + Alignment: Left + Aligned at: 0 cm + Indent at: 1.27 cm

Formatted: Outline numbered + Level: 3 + Numbering Style: 1, 2, 3, … + Start at: 1 + Alignment: Left + Aligned at: 0 cm + Indent at: 1.27 cm

~~will show when observations are first available, the uncertainty drops to zero for any country where we already have data reported for all of 2025. This is the case below for both India and Japan, and for Carbon Monitor's estimates of growth in 2025, since they report data through December 2025~~2025) level.

For China, projected fossil emissions in ~~2025~~2026 are expected to have ~~increased slightly~~decreased by 0.~~4~~9% (range ~~-0.1~~2.6% to 0.~~9~~8%) compared with ~~2024~~2025 emissions, bringing ~~2024~~2025 emissions for China around 3.4 GtC yr^{-1} (12.3 $GtCO_2$ yr^{-1}). Our projected changes by fuel for China are 0.3% for coal, ~~3.8~~-4.6% for oil, ~~2.3~~-0.9% for natural gas, and ~~-7.3~~6.2% for cement.

For the USA, using the Energy Information Administration (EIA) emissions estimate for ~~2025~~2026 combined with cement clinker data from USGS, we estimate ~~an increase~~a decrease of ~~2.5~~1.3% (range ~~2.2~~-3.4% to ~~20~~.8%) compared to ~~2024~~2025, bringing USA ~~2025~~2026 emissions to around 1.4 GtC yr^{-1} (5.0 $GtCO_2$ yr^{-1}). Our estimated changes by fuel are ~~10.4~~-6.7% for coal, -1.1% for oil, ~~1.4~~0.5% for natural gas, and ~~-3.1~~6.2% for cement.

For India, our estimate for ~~2025~~2026 is an increase of ~~1.1~~4.4% over ~~2024,~~2025 (range 1.7% to 7.1%), with ~~2025~~2026 emissions around 0.9 GtC yr^{-1} (3.~~2~~3 $GtCO_2$ yr^{-1}). Our projected changes by fuel are ~~1.3~~5.9% for coal, -0.~~5~~9% for oil, ~~-5.7~~2.2% for natural gas, and ~~10.5~~9.0% for cement.

For the European Union, our projection for ~~2025~~2026 is for a decrease of ~~-0.~~1.5% (range ~~-2.6~~4.0% to ~~2.3~~0.9%) relative to ~~2024~~2025, with ~~2025~~2026 emissions around 0.~~7~~6 GtC yr^{-1} (2.4 $GtCO_2$ yr^{-1}). Our projected changes by fuel are -2.~~6~~9% for coal, ~~-0.7% for oil, 2.~~1.8% for oil, -0.1% for natural gas, and -~~0~~1.8% for cement.

~~New this year, we provide a projection for~~ For Japan, ~~with~~we project for 2026 a ~~2025~~ decrease of 1.0~~.9%,~~% (range -2.5% to 0.6%), with ~~2025~~2026 emissions around 0.3 GtC yr^{-1} (1.0~~.9~~ $GtCO_2$ yr^{-1}). Our projected changes by fuel are ~~-0~~1.7% for coal, ~~-0.8% for oil, -1.~~2.2% for oil, -4.0% for natural gas, and ~~-2.9~~3.1% for cement.

International aviation and shipping are expected to ~~have increased~~decrease by ~~4.3~~1% in ~~2025~~2026, reaching 0.3 GtC yr^{-1} (1.2 $GtCO_2$ yr^{-1}), with both international aviation and international shipping projected to be ~~respectively 6.7% and 2.0% over 2024.~~1% below 2025. For the rest of the world, the expected change for ~~2025~~2026 is ~~an increase~~a decrease of 0.~~9~~7% (range ~~-1.1~~2.9% to ~~3.0~~1.5%) with ~~2025~~2026 emissions around 3.7 GtC yr^{-1} (13.~~7~~6 $GtCO_2$ yr^{-1}). The fuel-specific projected ~~2025~~2026 growth rates for the rest of the world are: ~~1.3~~-0.2% for coal, ~~0.3~~-1.6% for oil, ~~1.2~~-0.5% for natural gas, ~~2~~1.6% for cement.

Compared to the GCB estimate, Carbon Monitor estimates an ~~increase~~decrease in global fossil CO_2 emissions of 0.~~7%~~5% (-3.5% to +2.6%) for ~~2025, lower than~~2026 , similar to the GCB projection but

with ~~overlapping~~larger uncertainties. ~~In contrast to GCB,~~ Carbon Monitor projects the ~~2025~~2026 emissions ~~from China~~ to decline by 2.3% (-4.4% to ~~-0.6%. Conversely, Carbon Monitor projects the 2025 emissions to increase by 1.4%~~2%) for China, 1.5% (-6.9% to +3.9%) for the USA, ~~by 0.7% for India, by 0~~1.1% (-6.8% to +4.7%) for the EU27~~, but~~ and 3.7% (-7.5% to ~~decrease by -~~+0.3~~%~~5%) for Japan~~. The Carbon Monitor estimates that~~, but to increase by 5.9% (+2.4% to +9.5%) for India consistent with the GCB projection. For the rest of the world (including international aviation and shipping ~~increased by 3.4% in 2025. For the rest of the world,~~), the estimated change is an increase of ~~1.3%.~~0.5% (-1.2% to +2.2%).

For traceability, Table S6 provides a comparison of annual projections from GCB since 2015 with the actual emissions assessed in the subsequent GCB annual report.

3.2 Emissions from Land-Use Change

3.2.1 Historical period 1850-~~2024~~2025

Cumulative net CO_2 emissions from land-use change and land management (E_{LUC}) for 1850-~~2024~~2025 are ~~250 ± 60~~245 ± 50 GtC (Table 8) with a large spread among individual bookkeeping estimates of ~~210~~205 GtC (OSCAR), 240 GtC (LUCE) and 290 GtC (BLUE). DGVMs show a lower estimate of ~~160 ± 60~~180 ± 50 GtC~~.~~ (excluding emissions from peat drainage and largely omitting those from peat fires which together would add 35 ± 10 GtC). Vegetation biomass observations provide independent constraints on the E_{LUC} estimates over the 1901-2012 period (Li et al., 2017). Over that period, the GCB bookkeeping models' cumulative E_{LUC} amounts to 180 GtC [~~155~~150 to ~~210~~215 GtC] and the DGVM cumulative E_{LUC} to ~~121 ± 45~~135 ± 35 GtC, both not significantly different from the observation-based estimate of 155 ± 50 GtC (Li et al., ~~2017). The substantially lower cumulative E_{LUC} estimates from DGVMs compared to GCB2024 are due to the correction for the RSS bias, which is implemented in this assessment (see Section 2.6.1; O'Sullivan et al., 2025~~2017).

3.2.2 Recent period 1959-~~2024~~2025

~~In contrast to growing fossil emissions, net~~Net CO_2 emissions from land ~~use, land~~-use change~~,~~ and ~~forestry~~land management remained relatively constant (around 1.8 GtC yr^{-1}) over the 1959-1999 period. Since then, they have shown a statistically significant decrease of about 0.2 GtC per decade ($p<0.001$), reaching 1.~~4~~3 ± 0.7 GtC yr^{-1} for the ~~2015-2024~~2016-2025 period (Table 7), with a spread from 1.~~3~~2 to 1.~~6~~5 GtC yr^{-1} across the three bookkeeping estimates (~~Table 5,~~ Figure 4b). ~~Different from the bookkeeping average, the~~The DGVM average ~~grows slightly larger~~ shows relatively constant net emissions over the ~~1980~~1970-2010 period, ~~but~~and as bookkeeping models, ~~DGVMs show~~shows decreasing emissions in the most recent ~~decade, 2015-2024~~decades (Table 5).

Formatted: Outline numbered + Level: 2 + Numbering Style: 1, 2, 3, … + Start at: 1 + Alignment: Left + Aligned at: 0 cm + Indent at: 1.02 cm

Formatted: Outline numbered + Level: 3 + Numbering Style: 1, 2, 3, … + Start at: 1 + Alignment: Left + Aligned at: 0 cm + Indent at: 1.27 cm

Formatted: Outline numbered + Level: 3 + Numbering Style: 1, 2, 3, … + Start at: 1 + Alignment: Left + Aligned at: 0 cm + Indent at: 1.27 cm

Formatted: Highlight

~~Compared to GCB2024, the overall trends in E_{LUC} remained similar but the E_{LUC} estimates increased. The main reason for the larger estimates in this assessment is that the H&C2023 model, included up to GCB2024, is not included anymore (see Section 2.2). H&C2023 had the lowest E_{LUC} estimates among all bookkeeping models (Figure S3). Larger E_{LUC} estimates in the last few decades (compared to GCB2024) are also due to the consideration of transient, instead of constant, carbon densities by all three bookkeeping models (Section 2.2.1). The inclusion of transient carbon densities increases gross fluxes for all E_{LUC} components in the last few decades (Figure S3). Net E_{LUC} increases because emissions from deforestation are still the dominating term.~~

We separate E_{LUC} into five component fluxes to gain further insight into the drivers of net emissions: deforestation~~, forest~~ and clearing of other vegetation, (re-)growth of forest and other vegetation, wood harvest and other forest management, peat drainage and peat fires, and ~~all other~~ transitions between cropland, pasture, and urban areas, with CO_2 emissions to the atmosphere being positive and CO_2 removals from the atmosphere being negative (Figure 7b; Supplement S.2.2). This year's decomposition differs from GCB2025: the clearing and (re-)growth of shrub and herbaceous vegetation, included under 'other transitions' in previous GCBs, is now attributed to 'deforestation and clearing of other vegetation (total)', and '(re-)growth of forest and other vegetation (total)', respectively. We further decompose the terms 'deforestation and ~~the forest (~~clearing of other vegetation (total)' and '(re-)growth ~~term~~of forest and other vegetation (total)' into contributions from shifting cultivation vs permanent ~~forest~~land cover changes (Figure 7c~~).~~), where the term 'permanent' is used to align with the FAO categories 'land under permanent crops' and 'permanent meadows and pastures'. Averaged over the ~~2015–2024~~2016-2025 period and over the three bookkeeping estimates, total fluxes from deforestation and clearing of other vegetation amount to ~~an emission~~emissions of 2.2 [1.9 ~~[1~~to 2.5 ~~to 2.3~~] GtC yr^{-1} (Table 5), of which 1.~~1~~0 [0.9~~,~~ to 1.~~2~~1] GtC yr^{-1} are from permanent deforestation~~. Fluxes from~~, 0.2 [0.2 to 0.2] from permanent clearing of shrub and herbaceous vegetation, and the remainder (1.0 [0.8 to 1.2] GtC yr^{-1}) from deforestation and clearing of other vegetation in shifting cultivation cycles. Total fluxes from (re-)growth of forest ~~(re-)growth~~ and other vegetation amount to a removal of -1.~~3~~6 [-1.~~5~~,8 to -1.~~0~~4] GtC yr^{-1} (Table 5), of which -0.6 [-0.7~~,~~ to -0.~~5~~4] GtC yr^{-1} is from permanent forest (re-)growth due to re/afforestation, -0.2 [-0.2 to -0.2] from permanent (re-)growth of shrub herbaceous vegetation, and the remainder ~~from forest~~(-0.8 [-0.9 to -0.7] GtC yr^{-1}) from regrowth of forest and other vegetation in shifting cultivation cycles. Wood harvest and other forest management causes net emissions of 0.4 [0.1~~,~~ to 0.7] GtC yr^{-1} (with substantial gross fluxes largely compensating each other; see Figure S2). Emissions from peat drainage and peat fires (0.2 [0.2~~,~~ to 0.3] GtC yr^{-1}) and the net flux from ~~other~~ transitions between cropland, pasture and urban areas (0.1 [0.~~1~~,0 to 0.1] GtC yr^{-1}) are of smaller magnitude globally (Table 5).

The split into component fluxes clarifies the potentials for emission reduction and carbon dioxide removal: emissions from permanent deforestation - the largest of our component fluxes - could be

halted (largely) without compromising carbon uptake by forests, contributing substantially to emissions reduction. By contrast, reducing wood harvesting would have limited potential to reduce net emissions as it would be associated with less forest regrowth; removals and emissions cannot be decoupled here on long timescales. A similar conclusion applies to removals and emissions from shifting cultivation, which we have therefore separated out. Carbon Dioxide Removal (CDR) in forests could instead be increased by permanently increasing the forest cover through re/afforestation. Currently, re/afforestation creates a removal of -0.6 [-0.7 to -0.4] GtC yr^{-1} from the atmosphere averaged over ~~2015-2024. This~~2016-2025. Net carbon dioxide removals from re-/afforestation were highest in China, the EU27, and the USA, with combined removals of 0.2 GtC yr^{-1} during 2016-2025. The global value is similar to independent estimates derived from NGHGIs for CDR in managed forests (through re/afforestation plus forest management) for ~~2013-2022~~2014-2023 (-0.~~5~~6 ± 0.2 GtC yr^{-1}, ~~Pongratz~~Smith et al., ~~2024~~2026). In contrast to NGHGIs, bookkeeping estimates do not consider the impacts from natural disturbances (like fires, windthrow, insect outbreaks), which may lead to an overestimation of removals from re/afforestation. Re/afforestation constitutes most of all current CDR (~~Pongratz~~Smith et al., ~~2024~~2026). Though they cannot be compared directly to annual fluxes from the atmosphere and are thus not included in our estimate of E_{LUC}, CDR through transfers between non-atmospheric reservoirs such as in durable HWPs~~, or woody~~ biochar~~, or BECCS~~ comprise much smaller amounts of carbon. ~~218~~213 MtC yr^{-1} have been estimated to be transferred to HWPs, averaged over ~~2013-2022~~ (~~Pongratz~~2014-2023 (Smith et al., ~~2024~~2026). The net flux of HWPs, considering the re-release of CO_2 through their decay, amounts to ~~91~~89 MtC yr^{-1} over that period (~~Pongratz~~Smith et al., ~~2024~~2026). Note that some double accounting between the CDR through HWPs and the CDR through re/afforestation exists if the HWPs are derived from newly forested areas. ~~CDR from Biochar and BECCS in 2024 amount to 0.31 MtC yr^{-1} and 0.18 MtC yr^{-1} respectively.~~CDR from BECCS, biomass burial, and bio-oil storage in 2025 amount to -0.14 MtC yr^{-1}, -0.01 MtC yr^{-1}, and -0.002 MtC yr^{-1} respectively. CDR activity via biochar soil amendment amounted to -0.4 MtC yr^{-1} , of which -0.3 MtC yr^{-1} was derived from woody biomass (and constitutes a transfer between non-atmospheric reservoirs). No CDR has been reported for biomass sinking. A portion of mineralisation projects use biomass-derived carbon to enhance mineralisation reactions; these projects accounted for -0.0006 MtC yr^{-1}. "Blue carbon", i.e., coastal wetland management such as restoration of mangrove forests, saltmarshes, and seagrass meadows, though at the interface of land and ocean carbon fluxes, are counted towards the land-use sector as well. Currently, bookkeeping models do not include blue carbon; however, current CDR deployment in coastal wetlands is small globally, less than -0.003 MtC yr^{-1} (Powis et al., 2023).

The statistically significant decrease in E_{LUC} since the late-1990s, including the larger drop within the most recent decade, is due to the combination of decreasing emissions from deforestation (in particular permanent deforestation) and increasing removals from forest regrowth (with those from re/afforestation stagnating globally in the last decade). Net emissions in ~~2015-2024~~2016-2025 are ~~23~~26% lower than in the late-1990s (1995-2004) and ~~19~~20% lower than in 2005-2014. The ~~steep~~

drop2018 peak in E_{LUC} after 2015 is due to the combined effect frompredominantly driven by a peak in peat fire emissionslarge increase in temporary crop area in 2015 and a long-term decline in deforestation emissions in many countries over the 2010-2020 period.Colombia according to FAO data (FAO, 2026b). The processes behind gross removals, foremost forest regrowth and soil recovery, are all slow, while gross emissions include a large instantaneous component. Short-term changes in gross emissions dynamics, such as a temporary decrease in deforestation, influences E_{LUC} faster than a change in gross removals, which rather act on longer-term timescales. Component fluxes often differ more across the bookkeeping estimates than the net flux (Figure 7b), which is expected due to different process representation; in particular, the treatment of shifting cultivation, which increases both gross emissions and gross removals, differs across models, but also net and gross wood harvest fluxes show high model spread (Figure S2). By contrast, models agree relatively well for emissions from permanent deforestation.

Overall, highest net land-use emissions occur in the tropical regions of all three continents. The top three emitters over 2015-20242016-2025 are Brazil (in particular the Amazon Arc of Deforestation), Indonesia, and the Democratic Republic of the Congo, with these 3 countries contributing 0.87 GtC yr^{-1} or 5754% of the global net land-use emissionsE_{LUC} (average over 2015-20242016-2025; Figure 6b, Figure 7a). This is related to massive expansion of cropland (FAO, 2025c2025), particularly in the last few decades in Latin America, Southeast Asia, and sub-Saharan Africa (Hong et al., 2021), to a substantial part for export of agricultural products (Pendrill et al., 2019). Emission intensity is high in many tropical countries, particularly of Southeast Asia, due to high rates of land conversion in regions of carbon-dense and often still pristine, undegraded natural forests (Hong et al., 2021). Emissions are further increased by peat fires in equatorial Asia (GFED4sGFED5.1, van der Werf et al., 20172025, Chen et al., 2026), contributing substantially to emissions in individual years, typically related to dry conditions during El Niño (0.2 GtC in 2015; 0.03 GtC yr^{-1} averaged over 2015-20242016-2025). Uptake due to land-use change occurs in several regions of the world (Figure 6b) particularly due to re/afforestation. Highest nature-based CDR in the last decade is seen in China, the USA, and the EU27, with combined removals of 0.2 GtC yr^{-1} during 2016-2025, partly related to expanding forest area as a consequence of the forest transition in the 19th and 20th century and subsequent regrowth of forest (Mather 2001; McGrath et al., 2015).; Zhu et al., 2025). Substantial uptake through re/afforestation also exists in other regions such as Brazil, Russia, or Indonesia, or Brazil where, however, emissions from deforestation and other land-use changes dominate the net land-use flux. While the mentioned patterns are robust and supported by independent literature, we acknowledge that model spread is substantially larger on regional than global levels, as has been shown for bookkeeping models (Bastos et al., 2021) as well as DGVMs (Obermeier et al., 2021). Independent assessments exist for selected regions (e.g., for Europe by Petrescu et al., 2020; for Brazil by Rosan et al., 2021; for China by Zhu et al., 2025; and for 8 selected countries/regions in comparison to inventory data by Schwingshackl et al., 2022).

The NGHGI data under the ~~land-use, land-use change, and forestry (~~LULUCF~~)~~ sector (Melo et al. ~~2025) and the LULUCF estimates from FAOSTAT (FAO, 2025d~~2026) differ from the ~~global models'~~GCB definition of E_{LUC} (see Section 2.2.1 and Supplement S.2.4). In the NGHGI reporting, natural land fluxes (S_{LAND}) are counted towards E_{LUC} when they occur on managed land (Grassi et al., ~~2018) whereas FAOSTAT LULUCF estimates generally include natural fluxes in managed and unmanaged forests (Tubiello et al., 2021). To compare our~~2018). To compare the GCB results to the NGHGI approach, we perform a translation of our E_{LUC} estimates by adding S_{LAND} in managed forest from the DGVMs simulations (~~1.9~~2.2 GtC yr^{-1} in ~~2015-2024~~2016-2025) to the ~~bookkeeping~~GCB E_{LUC} estimate from bookkeeping models (following the methodology described in Grassi et al., 2023; see Supplement S.2.4). Adding this sink changes E_{LUC} from being a source of 1.4~~3~~ GtC yr^{-1} to a sink of 0.~~5~~9 GtC yr^{-1}, much closer to the NGHGI estimate reporting a sink of 1.~~0~~2 GtC yr^{-1} (Figure ~~8a~~8c, Table S11). ~~Remaining differences in the bookkeeping and~~ The net flux in managed forests agrees very well, with both NGHGI and the translated GCB estimates ~~are mainly stemming from~~indicating a sink of 1.2 GtC/yr for 2016-2025. However, these values mask some compensating biases in the permanent deforestation and forest components (Figure 8a,b, Table S11). Peat emissions agree well across GCB , NGHGI, and FAO estimates, whereas discrepancies between GCB and NGHGI estimates remain for fluxes due to other transitions ~~and permanent deforestation, whereas peat emissions and the net flux in managed forests agree well (Figure 8b,c).~~ We further apply a mask of managed land to the net atmosphere-to-land flux estimate from atmospheric inversions to obtain inverse estimates that are comparable to the NGHGI estimates and to the translated E_{LUC} estimates from ~~bookkeeping models~~GCB (see Supplement S.2.4). The inversion-based net flux in managed land indicates a sink of 0.~~7~~9 GtC yr^{-1} for ~~2015-2024~~2016-2025, which is in broad agreement with the NGHGI and the translated E_{LUC} estimates (Figure 8, Table S11). Additionally, the interannual variability of the inversion estimates and the translated E_{LUC} estimates show a remarkable agreement (Pearson correlation of 0.~~71~~77 in 2000-~~2024~~2025), which supports the suggested translation approach. Though estimates of NGHGI~~, FAOSTAT,~~ and atmospheric inversions and the translated ~~bookkeeping~~GCB estimates still differ in value and need further analysis, the approach suggested by Grassi et al. (2023), which we adopt here, provides a feasible way to ~~relate~~translate the global models' and NGHGI ~~approach~~definitions to each other and thus link the anthropogenic carbon budget estimates of land-use CO_2 fluxes directly to the Global Stocktake, as part of the UNFCCC Paris Agreement. The translation approach has been shown to be generally applicable also at the country-level (Grassi et al., 2023; Schwingshackl et al., 2022).

We further compare GCB, NGHGI, and inversion estimates to CO_2 fluxes reported by FAO, averaged over 2016-2025 (Figure 8d). FAO estimates of net forest conversion emissions (1.0 GtC yr^{-1} in 2016–2025) agree well with GCB estimates of permanent deforestation emissions (1.0 GtC yr^{-1}) as do the respective peat emission estimates (0.2 GtC yr^{-1}). However, the FAO forest sink (1.7 GtC yr^{-1}) is weaker than the translated GCB sink (2.2 GtC yr^{-1}), despite including fluxes from both managed and

Formatted: Font color: Auto

unmanaged forests (Tubiello et al., 2026). This may reflect incomplete reporting of forest carbon stock changes by countries to FAO (Tubiello et al., 2026). This difference in forest sink strength is also reflected in the FAO and translated GCB net flux LULUCF estimates (removals of 0.4 GtC yr^{-1} and 0.9 GtC yr^{-1}, respectively). It should be noted that FAO does not include non-forest land-use transitions in its LULUCF estimate, which are included in the translated GCB estimate.

3.2.3 Final year ~~2024~~2025

The global CO_2 emissions from land-use change are estimated as 1.~~3~~2 ± 0.7 GtC in ~~2024~~2025, similar to the ~~2023~~2024 estimate. However, confidence in the annual change remains low, as the land-use transition forcing underlying the E_{LUC} estimates was informed directly by data only up to and including 2023~~,~~ (2024 for Brazil, Indonesia, and China), with a trend extrapolation to ~~2024~~2025 (see Supplement Section S.2.1). ~~The impacts of the 2023/2024 droughts linked to El Niño on the 2024 E_{LUC} estimate are thus not captured - while natural fires are not counted towards E_{LUC}, deforestation fires spreading further or drained peatlands burning more vastly because of dry conditions would be part of E_{LUC}. The extent of degradation was anomalously high in the Amazon in 2024 and partly masked relatively low deforestation rates (https://terrabrasilis.dpi.inpe.br). However, this is not captured by our approach that is based on forest cover changes. For degradation it is currently impossible to be separated into effects of land-use activity versus effects of climate variability.~~

3.2.4 Year ~~2025~~2026 Projection

In equatorial Asia, peat fire emissions ~~remained low (1~~increased substantially (157 MtC ~~in 2025~~ through October ~~15, 2025~~24, 2026, after ~~2~~6 MtC in ~~2024; GFED4.1s~~2025; GFED5.1, van der Werf et al., ~~2017~~2025, Chen et al., 2026), as did deforestation and degradation fires (~~4 MtC in 2025; 8 MtC in 2024). South America saw a big reduction in emissions from deforestation and degradation fires, from 334 MtC in 2024 to 35 MtC until October 15, 2025.~~63 MtC in 2026; 4 MtC in 2025), associated with drier conditions linked to the El Niño conditions that started earlier this year. Emissions from deforestation and degradation fires in South America remained low (99 MtC through October 24, 2026 after 78 MtC in 2025). El Niño-related fire impacts in the Amazon are generally expected to peak in the following year, particularly during the July-October dry season in the southern Amazon (Chen et al., 2017). Pantropical ~~2025~~2026 fire emission estimates from deforestation and degradation through October ~~15~~24 are ~~105~~306 MtC, which is ~~not just a massive drop~~about 20% more than the emissions of the full year 2025 (258 MtC). Note that the absolute fire emission estimates changed compared to ~~the anomalously high 2024 emissions, but also only about one third of the long-term average (1997-2024). The reduction in emissions is mainly attributable to anomalously low deforestation and degradation fire emissions in South America, likely connected to the ceasing of the El Niño conditions and their impacts on ecosystems.~~

Formatted: Outline numbered + Level: 3 + Numbering Style: 1, 2, 3, … + Start at: 1 + Alignment: Left + Aligned at: 0 cm + Indent at: 1.27 cm

Formatted: Outline numbered + Level: 3 + Numbering Style: 1, 2, 3, … + Start at: 1 + Alignment: Left + Aligned at: 0 cm + Indent at: 1.27 cm

GCB2025 due to our update from GFED4s to GFED5.1 (see Section 2.2). Since ~~the E_{LUC} estimate for the year 2024 is not informed directly by data on land-use dynamics (Section 3.2.3), we estimate the 2025~~ we use fire emission estimates relative to the previous year for the projections, the absolute changes only slightly affect our E_{LUC} projection ~~based on fire anomalies over the year 2023. We~~.

For 2026 we expect E_{LUC} emissions of around 1.~~1~~4 GtC (~~4~~5.1 $GtCO_2$~~) in 2025,~~), 0.~~1~~2 GtC ~~below~~above the ~~20242~~2025 level (and 0.~~3~~1 GtC ~~below~~above the ~~2015-2024~~2016-2025 average). Note that the confidence in the ~~2025~~2026 E_{LUC} projection remains low, as it is based on deforestation, degradation and peat fire emissions, which are only a proxy for land-use change. Projections in past GCB assessments are only partially confirmed by updated E_{LUC} estimates based on bookkeeping models in the following GCB assessments (Figure ~~S4~~S3). Although our extrapolation includes tropical deforestation and degradation fires, the degradation attributable to selective logging, edge-effects or fragmentation is not captured. Further, deforestation and fires in deforestation zones may become more disconnected, partly due to changes in legislation in some regions. For example, Van Wees et al. (2021) found that the contribution from fires to forest loss decreased in the Amazon and in Indonesia over the period of 2003-2018.

3.3 CDR not based on vegetation

Formatted: Outline numbered + Level: 2 + Numbering Style: 1, 2, 3, … + Start at: 1 + Alignment: Left + Aligned at: 0 cm + Indent at: 1.02 cm

Besides the CDR through land use (Sec. 3.2), the atmosphere-to-geosphere flux of carbon resulting from carbon dioxide removal (CDR) activities in ~~2024 is estimated at 0.011 MtC yr^{-1}. This results primarily from 0.0048 MtC yr^{-1} of biomass direct storage (compressing waste biomass to store underground), 0.003 MtC yr^{-1} and 0.002 MtC yr^{-1} of mineralisation and enhanced weathering projects respectively, and 0.0004 MtC yr^{-1} of DACCS (Pongratz et al., 2024). This represents an increase (267%) in the anthropogenic sink compared to revised estimates for 2023 (0.003 MtC yr^{-1}), although it remains roughly a million times smaller than current fossil CO_2 emissions. Note that the lower DACCS estimates, as well as revised 2023 values, reflect updated CDR tracking methodologies which include drawing on more accurate annual data from registries, indicating that operational projects are currently removing less CO_2 than their expected capacities. Similarly, reported CDR via Enhanced Rock Weathering decreased in 2024; however, this may not indicate a real decline in activity. The decline likely reflects a transition toward third party verification, with some removals not yet appearing on registries. Other novel CDR methods, including ocean and river alkalinity enhancement (0.0003 MtC yr^{-1} and 0.00001 MtC yr^{-1} in 2024 respectively), and bio-oil geological storage (0.0002 MtC yr^{-1}, jointly contributed just over 0.0005 MtC yr^{-1} according to updated 2024 estimates of the State of CDR report (Smith et al., 2024). CDR through intentional biomass sinking into the deep ocean was reported at 0.001 MtC yr^{-1} for 2023, but no activities have been identified for 2024~~2025 that are not based on vegetation is estimated at -0.003 MtC yr^{-1}. This results primarily from -0.001 MtC yr^{-1} each of enhanced rock weathering projects and alkalinity enhancement of water bodies, and -0.0004 MtC yr^{-1} of

DACCS (Smith et al., 2026). The atmosphere-to-geosphere component of mineralisation CDR was -0.0001 MtC yr^{-1}, representing 14% of total mineralisation CDR. The remaining -0.0006 MtC yr^{-1} was derived from mineralisation projects which used biomass derived carbon and is therefore accounted for separately under ELUC (Section 3.2) to avoid double counting. The total estimated atmosphere-to-geosphere CDR flux for 2024 has been revised, from -0.011 MtC yr^{-1} reported in Friedlingstein et al. (2026a) to -0.006 MtC yr^{-1}. This reflects that GBC2025 included bio-oil geological storage and biomass burial (-0.0048 MtC yr^{-1} combined) within the estimates for atmosphere-to-geosphere CDR. Given these methods use biomass to capture CO_2, they are now accounted for in the E_{LUC} values, provided in Section 3.2. Additionally, late reporting of project activity on registries has slightly increased the 2024 estimates for enhanced rock weathering and alkalinity enhancement, but within rounding error. The 2025 estimate of -0.003 MtC yr^{-1} therefore represents a 50% decrease from the revised 2024 estimate, driven primarily by decreases in ERW and mineralisation. However, for these methods, registry reporting can be late in reporting CDR fluxes for a given year, as it takes time to verify removals. Therefore the 2025 estimate may increase as additional project data becomes available. The flux from atmosphere-to-geosphere CDR still remains approximately one million times smaller than current fossil CO_2 emissions.

3.4 Total anthropogenic emissions

Formatted: Outline numbered + Level: 2 + Numbering Style: 1, 2, 3, … + Start at: 1 + Alignment: Left + Aligned at: 0 cm + Indent at: 1.02 cm

Cumulative anthropogenic CO_2 emissions (fossil, including cement carbonation, and land-use change) for 1850-~~2024~~2025 totalled ~~745 ± 65~~755 ± 55 GtC (~~2730 ± 240~~2765 ± 205 $GtCO_2$), of which ~~71% (530~~72% (545 GtC) occurred since 1959 and ~~35% (260GtC~~36% (275GtC) since 2000 (Table 7 and 8). Total anthropogenic emissions more than doubled since the 1960s, from 4.9 ± 0.7 GtC yr^{-1} for the decade of the 1960s to an average of 11.23 ± 0.9 GtC yr^{-1} during ~~2015-2024~~2016-2025 and reaching 11.~~6~~7 ± 0.9 GtC (42.~~4~~8 ± 3.2 $GtCO_2$) in ~~2024~~2025. However, total anthropogenic CO_2 emissions have been almost stable over the last decade (0.3% yr^{-1} average growth rate over the ~~2015-2024~~2016-2025 period), much lower than the 1.~~9~~7% growth rate over the previous decade (~~2005-2014~~2006-2015). This slower growth is due both to the reduced growth in E_{FOS} between the two decades, and to the absolute decrease in ~~emissions from~~ E_{LUC} over the past decade.

During the historical period 1850-~~2024, 67~~2025, 68% of historical emissions were from fossil emissions and ~~33~~32% from land-use change. However, fossil emissions have grown significantly since the 1960s while net land-use change emissions have not, and consequently the contributions of land-use change to total anthropogenic emissions were smaller during recent periods, 21% during the period 1959-2024 and down to 12% over the last decade (~~2015-2024~~2016-2025).

For ~~2025~~2026 we project global total anthropogenic CO_2 emissions from fossil and land-use changes to be around 11.~~5~~8 GtC (~~42.2~~43.3 $GtCO_2$), marginally ~~below~~above the ~~2024~~2025 level ~~due to lower net land-use emissions (-0.13 GtC) compensating the growth in fossil emission (+0.09 GtC).~~.

3.5 Atmospheric CO_2

3.5.1 Historical period 1850-~~2024~~2025

Atmospheric CO_2 concentration was approximately 278 parts per million (ppm) in 1750, reaching 300 ppm in the late 1900s, 350 ppm in the late 1980s, and reaching ~~422.80~~425.6 ± 0.1 ppm in ~~2024~~2025 (Lan et al., ~~2025~~2026; Figure 1). The mass of carbon in the atmosphere increased by 52% from 590 GtC in 1750 to ~~898~~904 GtC in ~~2024~~2025. Current CO_2 concentrations in the atmosphere are unprecedented in the last 2 million years and the current rate of atmospheric CO_2 increase is at least 10 times faster than at any other time during the last 800,000 years (Canadell et al., 2021).

3.5.2 Recent period 1959-~~2024~~2025

The growth rate in atmospheric CO_2 level increased from 1.7 ± 0.07 GtC yr^{-1} in the 1960s to 5.~~6~~4 ± 0.02 GtC yr^{-1} during ~~2015-2024~~2016-2025 with important decadal variations (Table 7, Figure 3 and Figure 4c). During the last decade (~~2015-2024~~2016-2025), the growth rate in atmospheric CO_2 concentration continued to increase, albeit with large interannual variability (Figure 9). This interannual variability is highly consistent between the surface-based CO_2 growth rate and GRESO, the XCO_2-based growth rate (Pearson correlation of 0.~~84~~91), but substantial differences are seen in 2019 and 2022-2024. These reflect differences in the total atmospheric carbon stock seen within the set boundaries of Jan-1 and Dec-31 used to create an annual growth rate, as discussed in Section 2.4.~~2~~1. Especially with large anomalies in tropical regions and close to January 1st, the calculation becomes sensitive to when the change is detected. This affected the 2023 and 2024 growth rates most strongly as they originated from tropical regions, and late in the calendar year (see next section). Figure 9 also shows the total annual fluxes (in GtC yr^{-1}) from the inverse models, which are derived to match the observed atmospheric increase while numerically accounting for the atmospheric transport-related delay in detection. The inversely modeled values generally match the GRESO growth rate better than the surface observations-based growth rate, indicating that the latter is more strongly influenced by the delay between the fluxes occurring and the actual observation of these signals. Note that this effect is mainly important on the annual timescale, and not over longer periods.

3.5.3 Final year ~~2024~~2025

The growth rate in the surface based atmospheric CO_2 concentration was ~~7.9~~4.4 ± 0.2 GtC ~~(3.73~~ yr^{-1} (2.06 ± 0.08 ppm yr^{-1}) in ~~2024~~2025 (Figure 4c; Lan et al., ~~2025~~2026), well ~~above~~below the ~~2023~~2024 growth rate (~~5.7~~8.0 ± 0.2 GtC~~, 2.7~~ yr^{-1}, 3.8± 0.08 ppm yr^{-1}) or the ~~2015-2024~~2016-2025 average (5.~~6~~4 ± 0.02 GtC yr^{-1}, 2.~~6~~5 ± 0.008 ppm yr^{-1}), as to be expected ~~during an~~in a post El Niño year. ~~The 2024 atmospheric CO_2 growth rate was the largest over the 1959-2024 atmospheric observational record, more than 1.5 GtC above the growth rates of 1998, 2015, and 2016 and 1998, all strong El Niño years.~~

Formatted: Indent: Left: 0 cm, First line: 0 cm, Outline numbered + Level: 2 + Numbering Style: 1, 2, 3, … + Start at: 1 + Alignment: Left + Aligned at: 0 cm + Indent at: 1.02 cm

Formatted: Outline numbered + Level: 3 + Numbering Style: 1, 2, 3, … + Start at: 1 + Alignment: Left + Aligned at: 0 cm + Indent at: 1.27 cm

Formatted: Outline numbered + Level: 3 + Numbering Style: 1, 2, 3, … + Start at: 1 + Alignment: Left + Aligned at: 0 cm + Indent at: 1.27 cm

Formatted: Outline numbered + Level: 3 + Numbering Style: 1, 2, 3, … + Start at: 1 + Alignment: Left + Aligned at: 0 cm + Indent at: 1.27 cm

~~In contrast~~Similarly, the satellite-based GRESO growth rate was ~~6.8~~4.2±0.2 GtC yr^{-1} (~~3.20~~1.96±0.09 ppm yr^{-1}) for ~~2024 which was~~2025, also ~~above~~below its ~~2023~~2024 growth rate (~~6.5~~7.2±0.2 GtC yr^{-1}, 3.~~06~~4±0.~~07~~09 ppm yr^{-1}~~) and the highest on its 10-year record. But it shows a more equal split of the anomaly between both years (2023-2024). This likely reflects more accurately that a substantial fraction of the flux anomaly occurred in 2023, but this was only detected by the surface network in 2024. For the interpretation of the annual global budget this has strong implications, as 2024 surface fluxes would need to add up to a smaller anomaly (by 1.1 GtC yr^{-1}) than when using the surface-based annual growth rate. Hence the budget imbalance in 2024 (Table 7) would be reduced from -1.7 GtC to -0.6 GtC if the GRESO growth rate was used for the budget estimate.~~).

~~As the satellite-based GRESO growth rate is more evenly split between 2023 and 2024, so would be the B_{IM}, -0.3 GtC in 2023 and -0.6 GtC in 2024 with GRESO, compared to +0.4 GtC in 2023 and -1.7 GtC in 2024 with the GATM from the surface based network.~~

3.5.4 Year ~~2025~~2026 Projection

The ~~2025~~2026 atmospheric CO_2 concentration, averaged over the year ~~reached~~, is projected to reach the level of ~~425.64~~427.7 ppm, 53% over the pre-industrial level (Lan et al., ~~2025~~2026). We estimate the annual growth in atmospheric CO_2 (G_{ATM}) to be about 4.~~4~~6 GtC (equivalent to a 2.~~1~~2 ppm increase in the global mean concentration), ~~in line with a neutral ENSO year (ENSO 3.4 Index between -0.5 and 0.5). The projected growth rate estimated by the ESMs multi-model mean~~similar to the 2025 growth rate. While 2026 is ~~slightly larger (5.5 GtC, 2.6 ppm).~~ the onset of a large El Niño event, it does not yet translate into a large positive CO_2 growth rate anomaly. Historically, the full effects of strong El Niño events (see 1997/98 and 2015/16 El Niño events) is mainly visible in the following year, thus we expect to see the full El Niño effect on atmospheric CO_2 in 2027.

For traceability, Table S7 provides a comparison of annual projections of the G_{ATM}, S_{OCEAN} and S_{LAND} from GCB since 2021 with the actual estimate assessed in the subsequent GCB annual report.

3.6 Ocean Sink

3.6.1 Historical period 1850-~~2024~~2025

Cumulated since 1850, the ocean sink S_{OCEAN} adds up to 200 ± ~~35~~55 GtC, with more than 70% of this amount (145 ± ~~25~~40 GtC) being taken up by the global ocean since 1959. Over the historical period, the ocean sink increased in pace with the anthropogenic emissions exponential increase (Figure 3). Since 1850, the ocean has removed ~~27~~about 26% of total anthropogenic emissions. (Table 8).

Formatted: Outline numbered + Level: 3 + Numbering Style: 1, 2, 3, … + Start at: 1 + Alignment: Left + Aligned at: 0 cm + Indent at: 1.27 cm

Formatted: Indent: Left: 0 cm, First line: 0 cm, Outline numbered + Level: 2 + Numbering Style: 1, 2, 3, … + Start at: 1 + Alignment: Left + Aligned at: 0 cm + Indent at: 1.02 cm

Formatted: Outline numbered + Level: 3 + Numbering Style: 1, 2, 3, … + Start at: 1 + Alignment: Left + Aligned at: 0 cm + Indent at: 1.27 cm

3.6.2 Recent period 1959-~~20242025~~

S_{OCEAN} increased from 1.3 ± 0.~~4~~5 GtC yr^{-1} in the 1960s to 3.~~2 ± 0~~.4 ± 0.6 GtC yr^{-1} during ~~2015-2024~~2016-2025 (Table 7), with interannual variations of the order of a few tenths of GtC yr^{-1} (Figure 4d, Figure 10b). As described in section 2.5.1, S_{OCEAN} is ~~now~~ corrected for identified biases in the ~~GOBMs and~~ fCO_2 products estimates. Compared to the uncorrected estimate, S_{OCEAN} is increased by 0.~~2~~06 GtC yr^{-1} for the ~~2015-2024~~2016-2025 period.

The ocean-borne fraction ($S_{OCEAN}/(E_{FOS}+E_{LUC})$) has been remarkably constant around 27% on average over the 1959-2025 period, with variations around this mean illustrating the decadal variability of the ocean carbon sink. So far, there is no evidence of a sustained decrease in the ocean-borne fraction from 1959 to ~~2024~~2025 (Figure ~~S16~~S17).

The increase of the ocean sink is primarily driven by the increased atmospheric CO_2 concentration, with the strongest CO_2 induced signal in the North Atlantic and the Southern Ocean (Figure 12a, Figure ~~S10~~S9). The effect of climate change as quantified by the current suite of GOBMs is much weaker, reducing the ocean sink globally by 0.~~20~~22 ± 0.~~05~~07 GtC yr^{-1} (-7.~~1~~8% relative to the simulation that only accounts for the effect of atmospheric CO_2 increase) during ~~2015-2024~~2016-2025 (all models simulate a weakening of the ocean sink by climate change, range -45.2 to -~~10.7~~11.2%). The climate change effect leading to a reduced ocean sink is evident in all large-scale latitudinal bands ~~(north,~~with the largest contribution from the tropics~~, south,~~ and the smallest from the north in the multi model mean (Figure 12b, Figure ~~S10~~S9). This is the combined effect of change and variability in all atmospheric forcing fields, previously attributed to wind and temperature changes (Le Quéré et al., 2010, Bunsen et al., 2024). The effect of warming is smaller than expected from offline calculation due to stabilising feedback from limited exchange between surface and deep waters (Bunsen et al., 2024; Müller et al., 2025).

The global net air-sea CO_2 flux is a residual of large natural and anthropogenic CO_2 fluxes into and out of the ocean with distinct regional and seasonal variations (Figure ~~6c and Figure S5~~S4). Natural fluxes dominate on regional scales, but largely cancel out when integrated globally (Figure S4, Gruber et al., 2009; DeVries et al., 2023). Mid-latitudes in all basins and the high-latitude North Atlantic dominate the ocean CO_2 uptake where low temperatures and high wind speeds facilitate CO_2 uptake at the surface (Figure 6c and Figure S4, Takahashi et al., 2009). In these regions, formation of mode, intermediate and deep-water masses transport anthropogenic carbon into the ocean interior, thus allowing for continued CO_2 uptake at the surface. Outgassing of natural CO_2 occurs mostly in the tropics, especially in the equatorial upwelling region, and to a lesser extent in the North Pacific and polar Southern Ocean, mirroring a well-established understanding of regional patterns of air-sea CO_2 exchange (Figure S4; e.g., Takahashi et al., 2009, Gruber et al., 2009; DeVries et al., 2023). These patterns are also noticeable in the Surface Ocean CO_2 Atlas dataset, where an ocean fCO_2 value above the atmospheric level

Formatted: Outline numbered + Level: 3 + Numbering Style: 1, 2, 3, … + Start at: 1 + Alignment: Left + Aligned at: 0 cm + Indent at: 1.27 cm

indicates outgassing (Figure ~~S5~~S4). This map further illustrates the data-sparsity in the Indian Ocean and the Southern Hemisphere in general.

~~-~~The largest variability in the ocean sink occurs on decadal timescales (Figure 10b). The ensemble means of GOBMs and fCO_2-products show the same patterns of decadal variability, although with a larger amplitude of variability in the fCO_2-products than in the GOBMs. The ocean sink stagnated in the 1990s and strengthened between the early 2000s and the mid-2010s (Figure 10b; Le Quéré et al., 2007; Landschützer et al., 2015, 2016; DeVries et al., 2017; Hauck et al., 2020; McKinley et al., 2020, Gruber et al., 2023). Different explanations have been proposed for the decadal variability in the 1990s and 2000s, ranging from the ocean's response to changes in atmospheric wind systems (e.g., Le Quéré et al., 2007, Keppler and Landschützer, 2019), including variations in upper ocean overturning circulation (DeVries et al., 2017) to variations in atmospheric CO_2 growth rate (McKinley et al., 2020, Terhaar, 2024, Danek & Hauck, 2026) the eruption of Mount Pinatubo in the 1990s (McKinley et al., 2020, Fay et al., 2023). The main origin of the decadal variability is a matter of debate with several studies initially pointing to the Southern Ocean (see review in Canadell et al., 2021 and Gruber et al., 2023), but also contributions from the North Atlantic and North Pacific (Landschützer et al., 2016, DeVries et al., 2019), or a global signal (McKinley et al., 2020) were proposed. The GOBM decomposition into climate and CO_2 effects emphasizes the ~~role~~dominance of the climate effect (that would include cooling signals from volcanic eruptions) over the CO_2 effect for the stagnation in the 1990s until 2002, which are seemingly more pronounced in the tropics and north than in the south (Figure ~~S10~~S9). The atmospheric pCO_2 growth rate is a spatially uniform driver that amplifies with large-scale averaging, while climate exerts spatially heterogeneous effects that cancel with averaging. Thus, climate dominates small-scale flux variability, but is matched on the global mean by the impact of the pCO_2 growth rate (Fay et al., 2024).

Formatted: Font: Italic

~~More recently, the~~The sink ~~seems to have~~ entered a phase of stagnation 2016 - 2022, largely in response to large inter-annual climate variability~~.~~, but has continued to increase in the most recent years. The first-order effect of interannual variability stems from a stronger ocean sink during large El Niño events leading to a reduction in CO_2 outgassing from the Tropical Pacific (e.g., 1997/98, 2015/16) and a weaker sink in neutral years following El Niño (2017) and during La Niña events (2020-2022, Figure 10b; Rödenbeck et al., 2014, Hauck et al., 2020; McKinley et al. 2017). After the triple La Niña event 2020-2022, the ocean sink rebound in 2023 linked to the onset of an El Niño event. Warming in the extratropics, in particular in the Northern Hemisphere, however, weakened the overall increase in the ocean carbon sink (Müller et al., 2025). In the GOBMs, the ocean sink stagnation 2016-2022 is associated with a period of a stronger climate effect reducing the ocean sink, mostly stemming from the tropics, in line with the expected patterns from El Niño and La Niña (Figure ~~S10~~S9). The CO_2 effect has also shown a lower growth rate ~~since around 2016~~2016 - 2023 in line with the atmospheric CO_2 growth rate.

The ensemble means of GOBMs, and fCO_2-products (adjusted for the riverine flux) show a mean offset ~~increasing from 0.28 GtC yr^{-1}~~that was lower in the 1990s ~~(first decade available) to~~ and 2000s (0.47 GtC yr^{-1}, 0.42 GtC yr^{-1}, respectively) than after 2010 (2010s: 0.57 GtC yr^{-1}, 2016-2025: 0.59 GtC yr^{-1}~~in the decade 2015-2024.~~) . The offset is larger than in previous GCB versions in the early decades, because (i) fCO_2-products continue to be corrected for surface temperature effects, whereas a previously applied correction to the GOBMs is not applied this year (ii) two new fCO_2-products are included in GCB2026 (AOML-ET, SJTU-AVIT), while one fCO_2-product is not included this year (CSIR-ML6) and (iii) three fCO_2-products (UExP-FNN-U, JMA-MLR, AOML-ET), that use an adjusted version of the Surface Ocean CO_2 Atlas data ~~to represent the sea surface fCO_2 within the surface skin layer where gas exchange takes place~~ (Ford et al., ~~2025~~2026b), are ~~now~~ included in the GCB2026 fCO_2-product mean~~. Additionally, an update in the SOCAT dataset with regards to Southern Ocean data led to an increase~~, which is one more than in ~~the sink strength in three of the fCO_2-products (VLIZ-SOMFFN, LDEO-HPD, CMEMS-LSCE-FFNN - see section S3.1, Fay et al., 2025).~~GCB2025. In this version of the GCB, the positive trends in the ocean sink estimated by the GOBMs and the fCO_2-products diverges over time by a factor of 1.~~6~~3 since 2002 (GOBMs: 0.27 ± 0.05 GtC yr^{-1} per decade, fCO_2-products: 0.~~46~~36± 0.20 GtC yr^{-1} per decade ~~[0.22 to 0.81 GtC yr^{-1} per decade],~~, corrected S_{OCEAN}: 0.~~38~~32 GtC yr^{-1} per decade), ~~but~~so the ~~uncertainty ranges overlap~~divergence shrinks with a lower fCO_2-product trend than in previous GCB releases, partly because the method with one of the strongest trend in past GCB releases (CSIR-ML6) is not included this year. A hybrid approach recently constrained the trend for 2000 to 2022 to 0.42 ± 0.06 GtC yr^{-1} decade^{-1} (Mayot et al., 2024), which aligns with the updated trend of S_{OCEAN} (0.~~46~~39 GtC yr^{-1} decade^{-1}), and the fCO_2-products (0.44 ± 0.04 GtC yr^{-1} decade^{-1}), while the ~~fCO_2-products exhibit a larger (0.54 [0.29, 0.85] GtC yr^{-1} decade^{-1}) and the~~ GOBMs have a lower trend (0.~~34~~33 ± 0.~~05~~03 GtC yr^{-1} per decade) over the same period.

In the current budget, the discrepancy between the two types of estimates stems from a persistently larger ocean sink in the fCO_2-products in ~~the northern and southern extra-tropics since around 2002 (Figure 14). Note that the discrepancy in the mean flux, which was located in the Southern Ocean in GCB2022 and earlier, was reduced due to the choice of the regional river flux adjustment (Lacroix et al., 2020 instead of Aumont et al., 2001). This comes at the expense of a discrepancy in the mean S_{OCEAN} of about 0.2-0.3 GtC yr^{-1} in the tropics.~~all large-scale latitudinal bands (Figure 14). Likely explanations for the discrepancy in the trends and decadal variability in the high latitudes are data sparsity and uneven data distribution (Bushinsky et al., 2019, Gloege et al., 2021, Hauck et al., 2023a, Mayot et al., 2024~~).~~, Roobaert et al 2026, in review), whereas the discrepancy in the tropics may be related to the regional distribution of the river flux adjustment (Lacroix et al., 2020, Planchat et al., 2025). In particular, two fCO_2-products were shown to overestimate the Southern Ocean CO_2 flux trend by 50 and 130% based on current sampling in a model subsampling experiment (Hauck et al., 2023a) and the largest trends in the fCO_2-products occurred in a data devoid region in the North Pacific (Mayot

et al., 2024). ~~In Supplement S3 we show that the strength of the trends in fCO_2 products may be linked to reconstruction biases of the true trend signal.~~A study of Roobaert et al 2026, that extends an analysis presented in previous GCB releases based on model testbed analysis, confirms previously reported biases identified in Hauck et al. (2023a) within individual fCO_2-products, partly linked to data-sparsity, however, it also shows that the ensemble mean bias is significantly dampened. Similarly, a study using independent observations by McKinley et al. (2026) shows significant biases in the fCO_2-product mean (± 5µatm) and their seasonal cycle representation within large scale regions, again with individual methods having larger errors. In this respect it is highly worrisome that the coverage of fCO_2 observations has declined since 2016/17 (Dong et al., 2022, ~~2024~~2024b; Bakker et al., ~~2025b~~2026b) and is now down to that of the mid-2000s (Figure 10b). The temperature correction applied ~~in two~~ products further worsens the agreement in trends between GOBMs and fCO_2-products. Similarly, model biases likely contribute to the discrepancy between GOBMs and fCO_2-products (as indicated by the comparison with Mayot et al., 2024, and by the large model spread in the South, Figure 14).

The S_{OCEAN} estimate is 2.~~9~~8 ± 0.4~~6~~ GtC yr^{-1} over the period 2004 to 2019, which agrees within the ranges of uncertainty with the ocean interior estimate of 3.2 ± 0.7 GtC yr^{-1} obtained with the MOBO-DIC approach (Keppler et al., ~~2023). The carbon flux components of the observation-based ocean interior estimate match~~2023), which directly matches the definition of S_{OCEAN} used here (Hauck et al., 2020). Furthermore, the decadal S_{OCEAN} estimates agree well (mean offset < 0.1 GtC yr^{-1}) with the corresponding ocean interior estimates for all decades from the 1960s to the 2010s, which represent a composite estimate of three adjusted observation-based products (Table 6).

The S_{OCEAN} estimate agrees within uncertainties with other lines of evidence from atmospheric oxygen-based estimates, atmospheric inversions, and ocean interior observation-based constraints (Table 6). The atmospheric oxygen-based estimate shows a lower estimate than S_{OCEAN} in the 1990s, but a larger estimate over the ~~2015-2024~~2016-2025 period, indicating a strong growth of >1.~~5~~3 GtC yr^{-1} over that period. ESMs with data assimilation result in lower estimates of the ocean sink than all other estimates (Table 6). Also, the atmospheric inversion estimates of the ocean sink ~~are generally lower than~~agree with S_{OCEAN} ~~on average but are~~ within 0.1 GtC yr^{-1} for all decades except the ~~uncertainties of the GOBMs and fCO_2 products~~2000s (0.15 GtC yr^{-1}) .

3.6.3 Final year ~~2024~~2025

The estimated ocean CO_2 sink is 3.42 ± 0.47 GtC for ~~2024~~2025. This is ~~an~~a small increase of <0.1 GtC compared to ~~2023~~2024 (Figure 4d~~).~~ and 10b), which is not significantly different from 2024. The small sink strengthening ~~was expected from~~ is related to rather neutral ENSO conditions in 2025 and the weaker increase in atmospheric CO_2 ~~growth and El Niño conditions in the beginning of the year (January to April). However, the continuation of the anomalous warm conditions in the extra tropics, especially~~compared to 2024. A positive sink anomaly (stronger uptake) occurs throughout most of the

Formatted: Outline numbered + Level: 3 + Numbering Style: 1, 2, 3, … + Start at: 1 + Alignment: Left + Aligned at: 0 cm + Indent at: 1.27 cm

Atlantic Ocean~~, led to a weaker than expected increase in~~ and in the ~~sink~~ North Pacific, whereas a negative sink anomaly (less uptake) is found in the tropical Pacific and in southern extratropics (Figure ~~11c). The~~ 11). Interestingly, the GOBMs suggest that the increase is driven by ~~the anomalously high~~climate effects and dampened by CO_2 effects, suggesting a rebound effect after the strong atmospheric CO_2 growth rate ~~and dampened by climate effects, thus suggesting that warming overcompensated the effect from El Niño (Figure S10). GOBMs and fCO_2-products largely agree on patterns of ocean sink anomalies with a reduced sink in parts of the subtropical and subpolar North Atlantic and North Pacific that coincides with regions of anomalously warm sea surface temperatures~~of 2024 (Figure S9). GOBM and fCO_2-product ensemble mean estimates consistently result in an ~~ocean sink increase~~insignificant change in ~~20242025~~ (GOBMs: ±0.~~13~~06 ±0.~~14~~1 GtC, fCO_2-products: ±0.~~08 [-~~00 ± 0.~~34,0.43~~]16 GtC~~). Eight~~ yr^{-1}~~). Seven~~ GOBMs and ~~six~~four fCO_2-products show an increase in S_{OCEAN}, while ~~only two~~three GOBMs and ~~three~~six fCO_2-products show a decrease in S_{OCEAN}. The fCO_2-products have a larger uncertainty at the end of the reconstructed time series, potentially linked to uncertainties related to fewer available observations in the final year (see e.g. Watson et al 2020, Pérez et al 2024). Specifically, the fCO_2-products' estimate of the last year is regularly adjusted in the following release owing to the tail effect and an incrementally increasing data availability. While the monthly grid cells covered may have a lag of only about a year (Figure 10b inset), the values within grid cells may change with 1-5 years lag (see absolute number of observations plotted in previous GCB releases), potentially resulting in annual changes in the flux magnitude from fCO_2-products.

3.6.4 Year ~~2025~~2026 projection

Formatted: Outline numbered + Level: 3 + Numbering Style: 1, 2, 3, … + Start at: 1 + Alignment: Left + Aligned at: 0 cm + Indent at: 1.27 cm

Using a feed-forward neural network method (see Section 2.5.2) we project an ocean sink of 3.~~3~~1 ±0.~~4~~7 GtC for ~~2025~~2026, which is a declining sink of -0.1 GtC compared to ~~2024 and can be explained by the generally lower ocean CO_2 uptake following the El Niño event ending~~2025. As mentioned in ~~2024, consistent with the projected recovery of the~~ Section 3.5.4 for the 2026 atmospheric ~~CO_2~~ growth rate ~~after a record high in 2024. The,~~we do not predict an El-Niño initiated increase in the global carbon sink for 2026, but we expect to see the full El Niño effect on the ocean sink in 2027. For comparison, the set of ESMs predictions support this estimate with a ~~2025~~2026 ocean sink of around 3.1 [3.0, 3.2] GtC~~. Taking the average of both estimates, we project an ocean sink of 3.2 ±0.4 GtC for 2025~~.

3.6.5 Evaluation of ocean models and fCO_2-products

Formatted: Outline numbered + Level: 3 + Numbering Style: 1, 2, 3, … + Start at: 1 + Alignment: Left + Aligned at: 0 cm + Indent at: 1.27 cm

~~The process-based model evaluation draws a generally positive picture with GOBMs scattered around the observational values for Southern Ocean sea-surface salinity, Southern Ocean stratification index, albeit outliers exist (Section S3.3 and Table S12). The Revelle factor is high in most GOBMs when compared to GLODAP but appears less biased when compared to OceanSODA. However, the Atlantic Meridional Overturning Circulation at 26°N is underestimated by 8 out of 10 GOBMs and overestimated by one GOBM.~~ The process-based model evaluation provides evidence for a good

performance of the GOBM ensemble average. Although individual models have biases, these are typically averaged out in the ensemble mean and models close to the ensemble mean generally perform best in the evaluations (Figures S6 and S7). High sink models that appear to be closer to ocean interior estimates, atmospheric inversions and O_2:N_2 estimates do not perform better than the other models, but rather seem to ventilate too much and too deep (Figures S6 and S7).

IOMB summarizes the GOBMs' performance across physical and biogeochemical data sets and various statistics relative to the GOBM ensemble (Figure ~~S6~~S5). All GOBMs perform better in some variables compared to the other models, and worse in other variables. ~~Despite the indication that GOBMs underestimate the ocean sink, low sink models do not perform generally worse than the other models; and similarly, high sink models do not perform better than the others.~~Models with an ocean sink close to the ensemble mean generally perform best in the IOMB evaluation. The Revelle factor and carbon uptake capacity scatter around the observational value of OceanSODA (Gregor and Gruber, 2021), and are also close to GLODAP (Supplement S3.3 and Table S12). Seven out of ten models are too salty in the Southern Ocean subpolar biome, and the Atlantic Meridional Overturning Circulation at 26°N is underestimated by 9 out of 10 GOBMs and overestimated by one GOBM.

The CFC analysis that is available for seven models further supports the ensemble average (Figure S6). GOBMs that have a high CFC inventory, indicating strong ventilation, also have a large ocean sink. Vice versa, a lower CFC inventory is associated with a lower ocean carbon sink. However, there are smaller deviations from this linear relationship that point to other drivers than ventilation. The ensemble mean of seven GOBMs simulates a CFC-11 inventory of 0.56 ± 0.11 Gmol, which hits the observational estimate of 0.55 ± 0.12 Gmol almost exactly (Willey et al., 2004). The CFC-11 inventory of OCIM (0.55 Gmol) with steady circulation (no climate change) confirms this value and extends the assessment until 2025. Other transient tracers (CFC-12, SF6) confirm this picture (not shown, as no observational estimate and fewer model simulations ~~allow to separate the anthropogenic carbon component and to compare the GOBMs DIC inventory change directly to the interior ocean estimates of Gruber et al. (2019), Müller et al. (2023) and the GOBM anthropogenic surface fluxes to DeVries (2022) without further assumptions (Table S12). The GOBMs ensemble average of~~ are available). OCIM has a higher deep ocean anthropogenic carbon inventory per CFC inventory, which may be partially explained by the earlier starting date of OCIM, which affects total anthropogenic carbon storage, but not the CFC inventory as CFCs only started to increase in the atmosphere in the 1930s. There is no obvious compensation of deep versus upper ocean CFC inventory biases that would suggest a too low accumulation of total C_{ant} inventory in the GOBMs.

The emergent constraint work (Terhaar et al., 2022), which accounts for model biases in ventilation and carbonate buffer capacity provides further evidence for a 0% scaling in the current suite of GOBMs (Figure S7) as ventilation biases from too high Southern Ocean salinities and too weak Atlantic Meridional Overturning Circulation (AMOC) largely compensate, while the simulated carbonate uptake

capacity of surface ocean waters is on average similar to the observation-based one. The constraint yields 2.60 ± 0.22 GtC yr^{-1} for 2016-2025, compared with 2.67 ± 0.30 GtC yr^{-1} unconstrained (Table S13). The uncertainty is only moderately reduced because one model simulates excessive deep North Atlantic convection unrelated to the AMOC. The emergent constraint without this model would yield a similar value of 2.64 ± 0.11 GtC yr^{-1} (for more details, see Supplement S3.3). The same emergent constraint methodology leads to a higher estimate of the ocean sink from Earth System Models (Terhaar, 2025). One hypothesis is that this is related to the different spin-up strategies, with the GOBMs being spun-up with the earliest available reanalysis data (typically 1958 onwards) that already includes some anthropogenic warming. Hence, over the course of the simulation the GOBMs may underestimate warming and enhanced stratification (Huguenin et al., 2022; Takano et al., 2023; Hollitzer et al., 2024). On the other hand, Earth System Models were shown to overestimate stratification due to warming over the historical period (Danek and Hauck, 2026) and data-assimilating ESMs provide a lower ocean sink (Table 6).

The GOBMs estimate a lower S_{OCEAN} and interior carbon accumulation than the composite estimate averaging three observation-based reconstructions (Table 6 and S12). The deviation amounts to 0.25 and 0.23 GtC yr^{-1} in the 1990s and 2000s, respectively, and increases to 0.5 GtC yr^{-1} in the 2010s. The increasing deviation in the last decade is primarily due to the availability and inclusion of MOBO-DIC estimates from Keppler et al. (2023) only in this decade, which is the only observation-based reconstruction that aims to resolve changes ~~1994-2007 amounts to 2.3 GtC yr^{-1} and is thus 10.5% lower than the 2.6 ± 0.3 GtC yr^{-1} estimated by Gruber et al. (2019) although within the uncertainty. Five models fall within the range reported by Gruber et al. (2019). Comparison to the decadal~~in natural carbon storage and suggest a substantially higher accumulation rate than the OCIM and eMLR(C*) estimates ~~of anthropogenic carbon accumulation (Müller et al., 2023)~~ from Devries (2022) and Müller et al. (2023). Comparing the GOBMs to individual ocean interior products, one finds that the GOBM ensemble average of anthropogenic carbon inventory changes are close to the interior ~~ocean data~~ observation-based estimate for the decade 2004-2014 from Müller et al. (2023) (GOBMs sim D minus sim A, 2.65 ± 0.4 GtC yr^{-1}, Müller et al. 2.7 ± 0.3 GtC yr^{-1}), but do not reproduce the supposedly higher anthropogenic carbon accumulation in the earlier period 1994-2004 (GOBMs sim D minus sim A, 2.~~2~~1 ± 0.3 GtC yr^{-1}, Müller et al. 2.9 ± 0.3 GtC yr^{-1}). ~~Finally,~~Four models fall within the ~~mean anthropogenic carbon uptake in GOBMs from 1985 to 2018 amounts to 2.3 GtC yr^{-1}, slightly~~range reported by Müller et al. (2023) for the 2004-2014 period (24.8-29.8 PgC), with one model simulating a higher, and five models a lower inventory change. All models simulate a lower inventory change than the ~~corresponding observation-based uptake rate of 2.4 ± 0.2 Gt yr^{-1} based on OCIM (DeVries, 2022; DeVries et al., 2023). The underestimation of anthropogenic carbon accumulation by 10% in the period 1994 to 2007, in the 1990s and 2000s (Table 6) and by 15% in~~range reported for the 1994-2004 period (26.8-31.8). The GOBMs match the ~~2010s (Table 6) justifies the correction of GOBMs by 10% (Friedlingstein et al., 2025a, section 2.5.1). Interestingly, and in contrast to the uncertainties in the surface CO_2 flux, we~~

~~find the largest mismatch in~~regional interior ocean carbon distribution with roughly half of the accumulation in the tropics~~, with smaller contributions from~~ though with a slight overestimate of the relative accumulation in the north ~~and~~ on the expense of the south ~~(~~, compared to Müller et al. (2023)(Table S12). ~~The large discrepancy in accumulation in the tropics highlights the role of interior ocean carbon redistribution for those inventories (Khatiwala et al., 2009, DeVries et al., 2023~~For the decade 1994-2004 they match the N:T:S split almost exactly (GOBMs: 15:49:36%, obs: 12:49:39%), but they do not agree with the proposed shift towards the tropics for 2004-2014 (GOBMs: 16:47:37%, obs: 9:56:35%; Table S12).

Additional benchmarking of the fCO_2-products with independent data generally shows low and consistent biases and RMSEs, with the exception of the comparison with SOCAT flag E data in the tropics where the biases range from -6.~~6~~4 µatm in JMA-MLR to -10.~~29~~03 µatm in OceanSODA_ETHv2 , (Figure ~~S7~~S8) and the Northern Hemisphere, where biases range from -~~2.68~~3.09 µatm in VLIZ-SOMFFN to -~~40.47~~26.03 µatm in UExP-FNN-U (Figure ~~S7~~S8), although with few measurements covering the latter area. Generally, biases in the northern hemisphere have improved since GCB2025. This is broadly consistent with a study by McKinley et al (2026) that evaluated the bias of 10 fCO_2-products (8 contributing to GCB2026) and their seasonal representation in 5 large scale biome regions with independent datasets (see supplement S3).

Furthermore, ~~we evaluate the trends~~an fCO_2-product testbed study by Roobaert et al 2026 (in review), examines mean biases and trend biases derived from a subset of 9 fCO_2-products by subsampling five GOBMs used in Friedlingstein et al. ~~(2023; covering the period up to the year 2022~~(2023) following the approach of Hauck et al. (2023a) and evaluating the air-sea CO_2 flux trend for the 2001-2021 period, i.e. the period of strong divergence in the air-sea CO_2 exchange excluding the tail effect, against trend biases identified by the GOBM reconstruction. ~~The results indicate a relationship between reconstruction bias and strength of the decadal trends (Figure S8), indicating a tendency of the fCO_2-products ensemble to overestimate the air-sea CO_2 flux trends in agreement with Mayot et al. (2024). This relationship, however, remains uncertain and its sensitivity to the GOBM used needs further investigation~~Results, based on idealized model testbed experiments, indicate significant fCO_2-product biases regionally in individual reconstruction methods, when they reconstruct full model CO_2 fields and air-sea fluxes based on sparse real-world subsampling, consistent with Hauck et al 2023a and Gloege et al 2021. However, Roobaert et al 2026 (in review) also reveal that many of the regional biases are compensated at larger spatial scales and individual trend biases are partly compensated and in the ensemble average of multiple CO_2 products.

3.7 Land Sink

3.7.1 Historical period 1850-~~20242~~2025

Cumulated since 1850, the terrestrial carbon sink S_{LAND} amounts to ~~175 ± 50~~190 ± 40 GtC, ~~24~~25% of total anthropogenic emissions, with ~~more than~~nearly two thirds of this amount (~~120 ± 40~~125 ± 30 GtC) being taken up by the terrestrial ecosystems since 1959. Over the historical period, the land sink increased in pace with the anthropogenic emissions exponential increase (Figure 3). ~~As described in section 2, S_{LAND} estimate now includes the RSS correction.~~

3.7.2 Recent period 1959-~~20242~~2025

S_{LAND} increased from 1.0~~.9~~ ± 0.3 GtC yr^{-1} in the 1960s to 2.~~4~~5 ± 0.~~8~~7 GtC yr^{-1} during ~~2015-2024~~2016-2025, with important interannual variations of up to 2 GtC yr^{-1} generally showing a decreased land sink during El Niño events (Figure 10a), responsible for the corresponding enhanced growth rate in atmospheric CO_2 concentration. The larger land CO_2 sink during ~~2015-2024~~2016-2025 compared to the 1960s is reproduced by all the DGVMs in response to the increase in both atmospheric CO_2, nitrogen deposition, and the changes in climate, and is broadly consistent with the residual estimated from the other budget terms, that is E_{FOS}+E_{LUC}-G_{ATM}-S_{OCEAN} which amounts to 2.~~4~~9 ± 1.1 GtC yr-1 for the last decade (See Table 5). As described in section 2.6.1, S_{LAND} is now ~~corrected~~adjusted for the ~~Replaced Sinks and Sources (RSS)~~δL bias~~. Compared to the uncorrected estimate, S_{LAND} is reduced by 0.6 GtC yr^{-1} for the 2015-2024 period.~~ (see Supplement S4 for details).

Over the historical period, the increase in the global terrestrial CO_2 sink is largely attributed to the CO_2 fertilisation effect (Prentice et al., 2001, Piao et al., 2009, Schimel et al., 2015) and increased nitrogen deposition (Huntzinger et al., 2017, O'Sullivan et al., 2019), directly stimulating plant photosynthesis and increased plant water use in water limited systems, with a smaller negative contribution of climate change (Figure 12). There is a range of evidence to support a positive terrestrial carbon sink in response to increasing atmospheric CO_2 (Walker et al., 2021), including a new synthesis of free-air CO_2-enrichment experiments across forests and ages, which concluded that Net Primary Productivity increased by 22% for a common 41% CO_2 enrichment (Norby 2025). As expected from theory, the greatest CO_2 effect is simulated in the tropical forest regions, associated with warm temperatures and long growing seasons (Hickler et al., 2008) (Figure 12a). However, evidence from tropical intact forest plots indicate an overall decline in the land sink across Amazonia (1985-2011), attributed to enhanced mortality offsetting productivity gains (Brienen et al., 2015, Hubau et al., 2020). During ~~2015-2024~~2016-2025 the land sink is positive in all regions (Figure 6d) with the exception of eastern Brazil, Bolivia, northern Venezuela, Southwest USA~~, central Europe and Central Asia~~ northern Mexico, North and South Africa, and ~~eastern~~western Australia, where the negative effects of climate variability and change (i.e. reduced rainfall and/or increased temperature) counterbalance CO_2 effects. This is clearly

Formatted: Indent: Left: 0 cm, First line: 0 cm, Outline numbered + Level: 2 + Numbering Style: 1, 2, 3, … + Start at: 1 + Alignment: Left + Aligned at: 0 cm + Indent at: 1.02 cm

Formatted: Outline numbered + Level: 3 + Numbering Style: 1, 2, 3, … + Start at: 1 + Alignment: Left + Aligned at: 0 cm + Indent at: 1.27 cm

Formatted: Outline numbered + Level: 3 + Numbering Style: 1, 2, 3, … + Start at: 1 + Alignment: Left + Aligned at: 0 cm + Indent at: 1.27 cm

visible in Figure 12 where the effects of CO_2 (Figure 12a) and climate (Figure 12b) as simulated by the DGVMs are isolated (see also Figure ~~S12~~S13). The negative effect of climate can be seen across the globe, and is particularly strong in most of South America, Central America, Southwest US, Central and Western Europe, western Sahel, central Africa, southern Africa, Southeast Asia and ~~southern~~ China, and eastern Australia (Figure 12b, Figure ~~S12~~S13). Globally, over the ~~2015-2024~~2016-2025 period, climate change reduces the land sink by 0.~~8~~6 ± 0.~~7~~5 GtC yr^{-1} (~~25~~19% of the CO_2 effect, which is 3.~~2 ± 1.1~~3 ± 0.8 GtC yr^{-1} for the corresponding period~~, see Supplement S4.1~~).

Most DGVMs have similar S_{LAND} averaged over ~~2015-2024~~2016-2025, and ~~14/22~~20/23 models, when adjusted for δL and LOAC, fall within the 1σ range of the residual land sink [1.~~4~~8 to ~~3.3~~4.0 GtC yr^{-1}] (see Table 5), and all models ~~but one~~ are within the 2σ range [0.~~5~~7 to ~~4.3~~5.1 GtC yr^{-1}]. ~~The ED model is an outlier, with a land sink estimate of 4.9 GtC yr^{-1} for the 2015-2024 period (accounting for the RSS correction), driven by a strong CO_2 fertilisation effect (6.4 GtC yr^{-1} in the CO_2 only (S1) simulation).~~ There are no direct global observations of the land sink (S_{LAND}), or the CO_2 fertilisation effect, and so we are not yet able to rule out models based on component fluxes if their net land sink (S_{LAND}-E_{LUC}) is within the observational uncertainty provided by O_2 measurements. The important role of non-living carbon pools in carbon budgets has also been recently highlighted from an Earth-observation (EO) perspective, where contrary to DGVMs, EO products do not show an increase in biomass, thus inferring a larger role of dead carbon in land carbon cycle dynamics (Bar-On et al., 2025). However EO-based carbon accumulation in mature forests may be underestimated (Ma et al., 2026).

Since 2020 the globe has experienced La Niña conditions which would be expected to lead to an increased land carbon sink. This 3-year long period of La Niña conditions came to an end by the second half of 2023 and transitioned to an El Niño which lasted until mid-2024. A clear transition from maximum to a minimum in the global land sink is evident in S_{LAND}, from 2022 to 2023 and we find that an El Niño-driven decrease in tropical land sink is offset by a smaller increase in the high-latitude land sink. In the past years several regions experienced record-setting fire events (see also section 3.8.3). While global burned area has declined over the past decades mostly due to declining fire activity in savannas (Andela et al., 2017), forest fire emissions are rising and have the potential to counter the negative fire trend in savannas (Zheng et al., 2021). Noteworthy extreme fire events include the 2019-2020 Black Summer event in Australia (emissions of roughly 0.2 GtC; van der Velde et al., 2021), Siberia in 2021, where emissions approached 0.4 GtC or three times the 1997-2020 average according to GFED4s, Canada in 2023 and 2024 (Byrne et al., 2024), and unprecedented wildfires in Brazil and Bolivia in 2024 (partly related to land-use activity, see Sec. 3.2.3 and 3.2.4) (Bourgoin et al., 2025), partially offset by a negative trend in wildfire over Northern Hemisphere Africa. ~~While other regions, including Western US and Mediterranean Europe, also experienced intense fire seasons in 2021 their emissions are substantially lower.~~Despite these regional negative effects of climate change on S_{LAND},

the efficiency of land to remove anthropogenic CO_2 emissions has remained broadly constant over the last six decades at around 23% (Figure S17).

~~Despite these regional negative effects of climate change on S_{LAND}, the efficiency of land to remove anthropogenic CO_2 emissions has remained broadly constant over the last six decades at around 23% (including the RSS correction) (Figure S16).~~

The combined effect of climate change on S_{LAND} and S_{OCEAN} (assessed in Section 3.6.3), leads to a cumulative sink reduction of 27 ± 21 GtC since 1960 (relative to the counterfactuals that only accounts for the effect of atmospheric CO_2 increase), implying that the carbon-climate feedback has already contributed 7.3 ± 4.5 ppm (7%) to the observed increase in atmospheric CO_2 concentration since 1960.

3.7.3 Final year ~~2024~~2025

The terrestrial CO_2 sink from the DGVMs ensemble S_{LAND} was ~~1.9~~3.6 ± 0.9 GtC in ~~2024, 37% below~~2025, over 50% larger than the ~~2022 La Niña induced strong~~2024 land sink ~~of 3.1 ± 1.~~(2.2 ± 0.9 GtC~~,~~), and ~~below~~above the ~~2015-2024~~2016-2025 average of 2.45 ± 0.87 GtC yr^{-1} (Figure 4e, Table 7). We estimate that the ~~2024~~2025 land sink ~~was the lowest since 2015. The severe reduction in~~is the highest on record. This is a combination of the positive long-term land sink ~~in 2024 is likely driven by the El Niño conditions, leading to a 66% reduction in S_{LAND} in the tropics (30N-30S) from 2.8 GtC in 2022 to 1.0 GtC in 2024. This is~~ trend in all three latitude bands, combined with ~~intense wildfires in Canada, Bolivia and Brazil that led to a significant CO_2 source (see also Section 3.8.3).~~a strong tropical recovery from the 2023/24 climate extremes and a stable northern sink, relative to 2024 (Figures 11 and 14). DGVM results are broadly consistent from those based on atmospheric inversions (Figure 14). We note that the S_{LAND} estimate for ~~2024 of 1.9 ± 0.9 GtC~~2025 is ~~much larger than~~in good agreement with the ~~0.3~~4.1 ± 1.~~0~~1 GtC yr^{-1} estimate from the residual sink from the global budget (E_{FOS}+E_{LUC}-G_{ATM}-S_{OCEAN}, Table 5~~), although the residual sink would be substantially larger (at around 1.4 GtC yr^{-1}) if using the satellite-based GRESO in this equation. A large budget imbalance is often associated with El Niño years (e.g. 1986/87, 1997/98, 2005/06, 2023/24), and the possible underestimation in DGVMs of the tropical land carbon losses in response to drought, high temperature extremes, and fires. Few DGVMs have explicit representation of drought-mortality and only 8 from 22 include some form of forest demography, although recent efforts are underway to fill these critical research gaps (Eekes-Shephard et al., 2025 Yao et al., 2022, 2023).)~~.

~~An overestimate in S_{LAND} in 2024 can in part be attributed to the inability in DGVMs to reproduce extreme fire emissions in 2024. Globally fire emissions as calculated by GFED were 0.43 GtC yr^{-1} higher in 2024 compared to the decadal average (2015-2024), similar to the anomaly in 2023 (0.44 GtC yr^{-1}). This was mainly due to an increase in fire over forests in Boreal North America (0.16 GtC yr^{-1}) and forests, savannahs and grasslands over Southern Hemisphere South America (0.35 GtC yr^{-1}) in~~

Formatted: Outline numbered + Level: 3 + Numbering Style: 1, 2, 3, … + Start at: 1 + Alignment: Left + Aligned at: 0 cm + Indent at: 1.27 cm

Formatted: Font: Times New Roman, 10 pt

~~2024, partly offset by a negative trend in fires over Northern Hemisphere Africa (-0.05 GtC yr^{-1} anomaly). In fact, across the Amazon basin emissions from degradation fires (two thirds Brazil, one third Bolivia) surpassed those from deforestation fires in 2024 (Bourgoin et al., 2025). In contrast DGVMs simulate an anomaly of 0.2 GtC yr^{-1} in 2024, i.e., an underestimate of 0.23 GtC yr^{-1} in fire emissions for 2024. Fire enabled DGVMs simulate a larger reduction in S_{LAND} in 2024 compared to non-fire models (0.6 vs 0.3 GtC), indicating the importance of representing fire extremes when explaining reductions in the land sink.~~

~~Finally, a large uncertainty relates to climate forcing datasets, particularly over the critical carbon-rich tropical forest regions with poor coverage of meteorological stations. For example, there are large differences in climate forcing (e.g., CRUJRA-3Q and ERA5) and downstream DGVM carbon simulations over the Congo basin and tropical central and northern Africa in 2024 (Ke et al., 2025).~~

3.7.4 Year ~~2025~~2026 projection

Calculating the land sink as the residual of the other projections for ~~2025~~2026, we project a land sink of ~~3.1~~4.0 GtC for ~~2025, 1.1~~2026, 0.3 GtC larger than the ~~2024~~2025 estimate, ~~consistent with an expected recovery of the~~potentially still recovering from the reduced land sink after ~~an~~the 2023/24 El Niño event. The ESMs do not provide an additional estimate of S_{LAND} as they only simulate the net atmosphere-land carbon flux (S_{LAND}-E_{LUC}).

3.7.5 Evaluation of land models

~~The evaluation of~~All DGVMs meet the ~~DGVMs shows generally higher agreement across models for runoff, and to a lesser extent for GPP, and ecosystem respiration. These conclusions are supported by a more comprehensive analysis of DGVM performance in comparison with benchmark data (Sitch et al., 2024). A relative comparison of DGVM performance (Figure S11) suggests several DGVMs (CABLE-POP, CLASSIC, OCN, ORCHIDEE) may outperform others at multiple~~ three minimum-realism criteria described in Supplement S.4.2. We further evaluate the DGVMs and CARDAMOM against observational benchmarks for carbon and water cycle ~~benchmarks. However, results from Seiler et al., 2022, also show how~~ variables using the International Land Model Benchmarking system (ILAMB; Collier et al., 2018; Figure S10). The scores in Figure S10 are relative, showing how each model performs compared with the others rather than absolute skill. DGVM differences are often of similar magnitude ~~compared with~~to the range across observational datasets~~. All models~~ (Seiler et al., 2022), and a more comprehensive analysis of DGVM performance against benchmark data is given in Sitch et al. (2024).

On the combined hydrology and carbon cycle score ~~high enough over the metrics tests~~, CABLE-POP, ORCHIDEEv4 and CARDAMOM perform best relative to ~~support their use here. There are a few~~

Formatted: Outline numbered + Level: 3 + Numbering Style: 1, 2, 3, … + Start at: 1 + Alignment: Left + Aligned at: 0 cm + Indent at: 1.27 cm

Formatted: Outline numbered + Level: 3 + Numbering Style: 1, 2, 3, … + Start at: 1 + Alignment: Left + Aligned at: 0 cm + Indent at: 1.27 cm

Formatted: Font color: Auto

Formatted: Font color: Auto

Formatted: Font color: Auto

Formatted: Font color: Auto

Formatted: Font color: Auto, Not Highlight

Formatted: Font color: Auto, Not Highlight

~~anomalously~~ the other models, with CARDAMOM constrained by the observations it assimilates. EDv3 has the lowest overall score, followed by JSBACH and LPJmL. No model performs uniformly well, and most have at least one variable with a low ~~scores~~ relative score: soil carbon for CLM6.0, CLM-FATES and GDSTEM, biomass for ~~individual metrics from a single model, and these can direct the effort to improve~~E3SM and ISAM, leaf area index for LPJmL, LPX-Bern and VISIT, GPP for EDv3 and LPJmL, and evapotranspiration or runoff for IBIS, IQJ, JSBACH and SDGVM. Performance in the carbon and water cycles is not always aligned: IQJ, for example, is among the best models for the ecosystem and carbon cycle but among the weakest for hydrology.

New to GCB2026, we also evaluate the net land flux of the 21 DGVMs that provide monthly NBP against atmospheric CO_2 measured at 38 NOAA stations, comparing the simulated and observed seasonal cycle, interannual variability (IAV) and trend in seasonal amplitude (Figures S11 and S12). Models errors in the simulated seasonal cycle are largest in the northern extratropics, ranging from 1.2 ppm (LPX-Bern) to 5.0 ppm (iMAPLE), and are mostly below 1 ppm in the tropics and Southern Hemisphere. IAV errors vary less between models ~~for use in future budgets (See also Supplement S.4.2).~~, from 0.8-1.0 ppm in the north to 0.3-0.7 ppm elsewhere. At northern stations (north of 30°N), all models misrepresent the observed trend in seasonal amplitude somewhat, with median absolute errors across stations of 0.30-0.75 ppm decade^{-1} (Figure S12). The change in the amplitude of the seasonal cycle is a useful metric to track and help constrain environmental effects (particularly CO_2) on the biological activity of the northern hemisphere biosphere (McGuire et al, 2001, Graven et al., 2013, Forkel et al., 2016). Results suggest a wide performance among DGVMs with large bias at some stations indicative of a misrepresentation of the response of northern ecosystems to environmental change, such as CO_2 fertilisation, warming or land-use change. The ILAMB CO_2 score, which is based on the same emulated CO_2 (Figure S10), gives a consistent picture: LPX-Bern and VISIT-UT score best and CABLE-POP, DLEM and EDv3 score worst, matching the large northern seasonal-cycle errors of CABLE-POP and EDv3 and the large tropical and southern errors of DLEM. Model rankings nevertheless differ between the atmospheric CO_2 metrics and the flux and stock benchmarks. CABLE-POP has the highest overall ILAMB score among the DGVMs but one of the largest northern seasonal-cycle errors, while SDGVM has the smallest error in the amplitude trend but among the largest seasonal and interannual errors in the tropics and south.

3.8 Partitioning the carbon sinks

3.8.1 Global sinks and spread of estimates

In the period ~~2015-2024~~2016-2025, the bottom-up view of global net ocean and land carbon sinks provided by the GCB, S_{OCEAN} for the ocean and S_{LAND}– E_{LUC} for the land, ~~agrees~~agree closely with the top-down global carbon sinks delivered by the atmospheric inversions. This is shown in Figure 13, which visualises the individual decadal mean atmosphere-land and atmosphere-ocean fluxes from each,

Formatted: Font color: Auto, Not Highlight

Formatted: Font color: Auto, Not Highlight

Formatted: Font color: Auto, Not Highlight

Formatted: Outline numbered + Level: 2 + Numbering Style: 1, 2, 3, … + Start at: 1 + Alignment: Left + Aligned at: 0 cm + Indent at: 1.02 cm

Formatted: Indent: Left: 0 cm, First line: 0 cm, Outline numbered + Level: 3 + Numbering Style: 1, 2, 3, … + Start at: 1 + Alignment: Left + Aligned at: 0 cm + Indent at: 1.27 cm

along with the constraints on their sum offered by the global fossil CO_2 emissions flux minus the atmospheric growth rate ($E_{FOS} - G_{ATM}$, 4.~~2~~6 ± 0.5 Gt C yr^{-1}, Table 7, shown as diagonal line in Figure 13). The GCB estimate for net atmosphere-to-surface flux ($S_{OCEAN} + S_{LAND} - E_{LUC}$) during ~~2015-2024~~2016-2025 is 4.2 ± 1.~~1~~2 Gt C yr^{-1} (Table 7), implying a ~~zero~~ budget imbalance (B_{IM}) ~~(~~of 0.4 Gt C yr^{-1} (see Section 3.9). The atmospheric inversions estimate of the net atmosphere-to-surface flux during ~~2015-2024~~2016-2025 is 4.~~3~~5 Gt C yr^{-1}, with a < 0.1 GtC yr^{-1} imbalance, and thus scatter across the diagonal, with inverse models trading land for ocean fluxes in their solution. The independent constraint on the net atmosphere-to-surface flux based on atmospheric O_2 by design also closes the balance and is 4.~~2 ± 6 ± 1~~.0~~.9~~ GtC yr^{-1} over the ~~2015-2024~~2016-2025 period (orange symbol on Figure 13), while the ESMs estimate for the net atmosphere-to-surface flux over that period is ~~4.8~~5.0 [2.~~4~~2, 6.~~0~~3] GtC yr^{-1} (Tables 5 and 6).

The distributions based on the individual models and fCO_2-products reveal substantial spread but converge near the decadal means quoted in Tables 5 to 7. Sink estimates for S_{OCEAN} are mostly non-Gaussian, while the ensemble of DGVMs and inverse models appears more normally distributed justifying the use of a multi-model mean and standard deviation for their errors in the budget. Noteworthy is that the tails of the distributions provided by the land and ocean bottom-up estimates would not agree with the global constraint provided by the fossil fuel emissions and the observed atmospheric CO_2 growth rate. This illustrates the power of the atmospheric joint constraint from the global CO_2 observation capacity.

3.8.1.1 Net atmosphere-to-land flux

The GCB estimate of the net atmosphere-to-land flux ($S_{LAND} - E_{LUC}$), calculated as the difference between S_{LAND} from the DGVMs and E_{LUC} from the bookkeeping models, amounts to a 1.~~0~~2 ± 1.0 GtC yr^{-1} sink during ~~2015-2024~~2016-2025 (Table 5). The estimate of net atmosphere-to-land flux ($S_{LAND} - E_{LUC}$) from the DGVMs alone (1.~~4~~5 ± 0.~~7~~6 GtC yr^{-1}, Table 5, green symbols on Figure 13) is slightly larger, although within the uncertainty of the GCB estimate and ~~within uncertainty of~~agrees well with the ~~global carbon~~ budget constraint ($E_{FOS} - G_{ATM} - S_{OCEAN}$, 1.~~6 ± 0 ± 0.6~~.8 GtC yr^{-1}; Table 7). Also, for ~~2015-2024~~2016-2025, the inversions estimate the net atmosphere-to-land flux is a 1.~~3~~5 ± 0.3 GtC yr^{-1} sink, similar to the mean of the DGVMs estimates (purple versus grey symbols on Figure 13). The independent constraint based on atmospheric O_2 ~~is slightly lower,~~also aligns well with a net sink of 1.3 ± 0.~~7 ± 0.8~~9 GtC yr^{-1} (orange symbol in Figure 13~~), although its uncertainty overlaps with the uncertainty range from other approaches.~~). Last, the ESMs estimate for the net atmosphere-to-land flux during ~~2014-2023~~2016-2025 is a 2.~~3~~4 [-0.~~1~~4, 3.~~6~~9] GtC yr^{-1} sink, larger than all other estimates (Table 5).

As discussed in Section 3.5.3, the atmospheric growth rate of CO_2 derived from the NOAA surface stations was very high in 2024~~, 7.9 GtC (3.73 ppm) the largest on the 65 years long observational~~

Formatted: Indent: Left: 0 cm, First line: 0 cm, Outline numbered + Level: 4 + Numbering Style: 1, 2, 3, … + Start at: 1 + Alignment: Left + Aligned at: 0 cm + Indent at: 1.52 cm

Formatted: Not Highlight

~~record.~~ (8.0 ± 0.2 GtC) but relatively low in 2025 (4.4 ± 0.2 GtC). Both DGVMs and inversions assign this ~~large~~small CO_2 growth rate to a ~~continued reduction of the net atmosphere to~~strong land ~~flux since 2023~~sink, in particular in the tropics (Figures 11 and 14~~), especially pronounced in the inversions.~~). DGVMs simulate ~~a 2024~~the 2025 global net atmosphere-to-land flux ~~of 1.1 GtC yr^{-1}, a 50% decline relative to the 2.2 GtC~~ as a 2.7 ± 0.9 GtC yr^{-1} sink ~~in 2022,~~, while it was a 0.1 ± 0.9 GtC yr^{-1} source in 2024. The 2025 estimate is 80% greater than the 2016-2025 decadal mean (1.5 ± 0.6 GtC yr^{-1}). This is primarily driven by ~~the severe reduction in S_{LAND} (-37%, see Section 3.7.3).~~tropical recovery of S_{LAND} from the climate extremes in 2023/24, with E_{LUC} in 2025 similar to the decadal mean. The tropics (30°N-30°S) ~~are recording~~in DGVMs show a dramatic ~~decrease~~increase in the net atmosphere-to-land flux from a 0.1~~.3~~ GtC yr^{-1} ~~sink~~source in ~~2022~~2024 to a ~~0.2~~1.4 GtC yr^{-1} ~~source~~sink in ~~2024~~2025. The atmospheric inversions show ~~a continued reduction with~~ the global net atmosphere-to-land flux ~~declining~~going from ~~2.9 GtC yr^{-1} in 2022 to~~ near neutral (-0.~~8~~3 GtC yr^{-1} ~~in 2023 to 0.2 GtC yr^{-1}~~) in 2024 ~~(-94% from 2022 to 2024),~~to a strong sink (3.0 GtC yr^{-1}) in 2025, with ~~the tropics turning from a 1.3 GtC yr^{-1} sink in 2022 to a 1.2 GtC yr^{-1} source in 2024. This discrepancy between the DGVMs and inversions estimates of the tropical and hence global atmosphere~~ tropical land ~~flux largely explains the negative B_{IM} in 2024, (see also Section 3.8.2.2 below~~fluxes nearly fully accounting for the extra carbon uptake (+2.7 GtC yr^{-1}).

3.8.1.2 Net atmosphere-to-ocean flux

For the ~~2015-2024~~2016-2025 period, the GOBMs ~~(2.7 ± 0.4 GtC yr^{-1})~~ produce a lower estimate of the ocean sink of 2.7 ± 0.4 GtC yr^{-1} than the $f$$CO_2$-products with 3.3 ~~[2.9, 3.8]~~± 0.6 GtC yr^{-1}, which shows up in Figure 13 as separate peaks in the distribution from the GOBMs (dark blue symbols) and from the $f$$CO_2$-products (light blue symbols). Atmospheric inversions ~~(3.0 ± 0.3 GtC yr^{-1})~~ suggest an ocean uptake ~~more in line with~~of 3.1 ± 0.3 GtC yr^{-1}, close to the average of the GOBMs and $f$$CO_2$-products for the recent decade (Table 6). The inversions are not fully independent as ~~7~~9 out of ~~14~~16 inversions covering the last decade use $f$$CO_2$-products as ocean priors and one uses a GOBM (Table S4). The independent constraint based on atmospheric O_2 (3.~~5~~3 ± 0.~~5~~65 GtC yr^{-1}) ~~is at~~aligns well with the ~~high end~~$f$$CO_2$-products and majority of the ~~distribution of the other methods. However, as mentioned in section 2.8, the O_2 method requires a correction for global air-sea O_2 flux, which induces a non-negligible uncertainty on the decadal estimates (about 0.5 GtC yr^{-1}).~~inversions. The large growth in the ocean carbon sink from O_2 is compatible with the GOBMs and $f$$CO_2$-products estimates when accounting for their uncertainty ranges. Lastly, the ESMs estimate, 2.5 [2.~~2, 2.8~~3, 3.0] GtC yr^{-1}, suggest a lower average ocean carbon sink than the other estimates. We caution that the riverine transport of carbon taken up on land and outgassing from the ocean, accounted for here, is a substantial (0.65 ± 0.3 GtC yr^{-1}) and uncertain term (Crisp et al., 2022; Gruber et al., 2023; DeVries et al., 2023) that separates the GOBMs, ESMs and oxygen-based estimates on the one hand from the $f$$CO_2$-products and atmospheric inversions on the other hand.

Formatted: Not Superscript/ Subscript

Formatted: Indent: Left: 0 cm, First line: 0 cm, Outline numbered + Level: 4 + Numbering Style: 1, 2, 3, … + Start at: 1 + Alignment: Left + Aligned at: 0 cm + Indent at: 1.52 cm

3.8.2 Regional partitioning

Figure 14 shows the latitudinal partitioning of the global atmosphere-to-ocean ~~(S_{OCEAN}),~~and atmosphere-to-land ~~(S_{LAND} – E_{LUC}),~~CO_2 fluxes, and their sum ~~(S_{OCEAN} + S_{LAND} – E_{LUC}),~~ according to the estimates from GOBMs and ocean fCO_2-products ~~(S_{OCEAN}),~~ DGVMs ~~(S_{LAND} – E_{LUC}),~~ and ~~from~~ atmospheric inversions ~~(S_{OCEAN} and S_{LAND} – E_{LUC}). S_{OCEAN}.~~ The ocean fluxes consistently show S_{OCEAN}, so the preindustrial mean and riverine CO_2 fluxes are subtracted from the contemporary flux estimates ~~were not corrected for the regional analysis.~~from fCO_2-products and inversions (see methods). For $fCO2$-products and inversions, reported S_{OCEAN} uncertainties combine model spread and the uncertainty in the preindustrial mean ocean flux estimate (Table S14).

3.8.2.1 North

Despite being one of the most densely observed and studied regions of our globe, annual mean carbon ~~sink~~atmosphere-to-surface flux estimates in the northern extra-tropics (north of 30°N) continue to differ. The atmospheric inversions suggest an ~~atmosphere-to-surface sink (S_{OCEAN} +~~ anthropogenic (S_{LAND} – E_{LUC}) ~~+~~ S_{OCEAN}) atmosphere-to-surface sink for ~~2015–2024~~2016-2025 of 2.~~7 ± 0~~.4 ± 0.5 GtC yr^{-1}, which is higher than the process models' estimate of ~~2.0~~1.5 ± 0.4 GtC yr^{-1} (Figure 14). The GOBMs (~~1.1 ± 0~~.2~~5~~ ± 0.1 GtC yr^{-1}), fCO_2-products (~~1.4 [1~~0.6 ± 0.2 ~~1.6]~~ GtC yr^{-1}), and inversion systems (~~1~~0.5 ± 0.2 ~~± 0.1~~ GtC yr^{-1}) produce largely consistent estimates of the ocean sink. ~~However, the larger flux in the fCO_2-products may be related to data sparsity (Mayot et al., 2024).~~ Thus, the difference mainly arises from the net land flux ~~(S_{LAND} – E_{LUC})~~ estimate, which is 1.~~0.9~~ ± 0.~~34~~ GtC yr^{-1} in the DGVMs compared to 1.5 ± 0.~~4~~5 GtC yr^{-1} in the atmospheric inversions (Figure 14, second row).

Discrepancies in the northern land fluxes conform with persistent issues surrounding the quantification of the drivers of the global net land CO_2 flux (Arneth et al., 2017; Huntzinger et al., 2017; O'Sullivan et al., 2022) and the distribution of atmosphere-to-land fluxes between the tropics and high northern latitudes (Baccini et al., 2017; Schimel et al., 2015; Stephens et al., 2007; Ciais et al., 2019; Gaubert et al., 2019; O'Sullivan et al. 2024).

In the northern extra-tropics, the process models, inversions, and fCO_2-products consistently suggest that most of the interannual variability stems from the land (Figure 14). Inversions generally agree on the magnitude of interannual variations (IAV) over land, more so than DGVMs (0.~~27~~25-0.~~38~~35 vs 0.~~07~~15-0.~~55~~61 GtC yr^{-1}, averaged over 1990-~~2024~~2025).

3.8.2.2 Tropics

In the tropics (30°S-30°N), both the atmospheric inversions and process models estimate a substantial net ~~carbon balance (S_{OCEAN} +~~ anthropogenic (S_{LAND} - E_{LUC}) ~~that is relatively close~~ ~~+~~ S_{OCEAN}) atmosphere-~~to~~ ~~neutral~~ -surface flux over the past decade (inversions: 1.3 ± 0.~~05 ± 0.59~~ GtC yr^{-1}, process

Formatted: Indent: Left: 0 cm, First line: 0 cm, Outline numbered + Level: 3 + Numbering Style: 1, 2, 3, … + Start at: 1 + Alignment: Left + Aligned at: 0 cm + Indent at: 1.27 cm

Formatted: Indent: Left: 0 cm, First line: 0 cm, Outline numbered + Level: 4 + Numbering Style: 1, 2, 3, … + Start at: 1 + Alignment: Left + Aligned at: 0 cm + Indent at: 1.52 cm

Formatted: Indent: Left: 0 cm, First line: 0 cm, Outline numbered + Level: 4 + Numbering Style: 1, 2, 3, … + Start at: 1 + Alignment: Left + Aligned at: 0 cm + Indent at: 1.52 cm

Formatted: Not Superscript/ Subscript

models: 1.5±0.4±0.67 GtC yr^{-1}). The GOBMs (-(1.0.003 ± 0.31 GtC yr^{-1}), fCO_2-products (01.3 [± 0.1, 0.6]3 GtC yr^{-1}), and inversion systems (1.4 ± 0.3 ± 0.1 GtC yr^{-1}) indicate a neutral to positive large S_{OCEAN} sink for the tropical ocean flux (see Figure S56c for spatial patterns). DGVMs indicate a sink for the net land sink (S_{LAND} - E_{LUC})flux of 0.45 ±0.54 GtC yr^{-1}, whereas the inversion systems indicate a small source in the net land flux although with larger model spread (-0.21 ± 0.6 GtC yr^{-1}, Figure 14, third row).

A continuing conundrum is the partitioning of the global atmosphere-land flux between the Northern Hemisphere land and the tropical land (Stephens et al., 20172007; Pan et al., 2011; Gaubert et al., 2019; Stephens et al., 2026). It is of importance because each region has its own history of land-use change, climate drivers, and impact of increasing atmospheric CO_2 and nitrogen deposition. Quantifying the magnitude of each sink is a prerequisite to understanding how each individual driver impacts the tropical and mid/high-latitude carbon balance. We define the North-South (N-S) difference as net atmosphere-land flux north of 30°N minus the net atmosphere-land flux south of 30°N. For the inversions, the N-S difference is 1.7 ± 1.0 GtC yr^{-1} across this year's inversion ensemble. In the ensemble of DGVMs the N-S difference is 0.65 ± 0.56 GtC yr^{-1}, a much narrower range than the one from atmospheric inversions. The smaller spread across DGVMs than across inversions is to be expected as there is no correlation between Northern and Tropical land sinks in the DGVMs as opposed to the inversions where the sum of the two regions being well-constrained by atmospheric observations leads to an anti-correlation between these two regions.

The tropical lands are the origin of most of the atmospheric CO_2 interannual variability (Ahlström et al., 2015), consistently among the process models and inversions (Figure 14). The interannual variability in the tropics tropical ocean is similar among the ocean fCO_2-products (0.0605-0.1815 GtC yr^{-1}) and the GOBMs (0.07-0.1618 GtC yr^{-1}), and the atmospheric inversions (0.08-0.15 GtC yr^{-1}). The DGVMs and inversions indicate that atmosphere-to-land CO_2 fluxes are more variable than atmosphere-to-ocean CO_2 fluxes in the tropics, with interannual variability of 0.34 to 1.13 and 0.962 GtC yr^{-1} for DGVMs and 0.8 to 1.0 GtC yr^{-1} for inversions, respectively for 1990-20242025. The year 2024 saw the largest growth rate in the atmosphere so far, largely caused by reductions in the tropical land sink, similar to earlier extreme years, such as during the 2015-2016 El Niño period. The inversions seem to capture the response of the tropical land sink to a larger degree than the DGVMs, with a 2024 tropical land source of 1.2 ± 0.9 GtC yr^{-1} for the inversions versus a 0.2 ± 0.7 sink for the DGVMs.7 ± 0.8 GtC yr^{-1} for the inversions versus a much smaller source of 0.1 ± 0.7 for the DGVMs. The year 2025 saw a return to more normal climate conditions which caused a rebound of the tropical land sink to 1.0 ± 0.9 GtC yr^{-1} for the inversions and 1.4 ± 0.5 GtC yr^{-1} for the DGVMs (Figure 14).

Formatted: Font: Times New Roman, Not Superscript/ Subscript

3.8.2.3 South

In the southern extra-tropics (south of 30°S), the atmospheric inversions suggest a net anthropogenic (S_{LAND} - E_{LUC} + S_{OCEAN}) atmosphere-to-surface sink ~~(S_{OCEAN}+S_{LAND}-E_{LUC})~~ for ~~2015-2024~~2016-2025 of 1.~~6~~2 ± 0.~~2~~3 GtC yr^{-1}, ~~similar to~~in line with the process models' estimate of 1.~~5~~2 ± 0.~~4~~2 GtC yr^{-1} (Figure 14). An approximately neutral net land flux ~~(S_{LAND}-E_{LUC})~~ for the southern extra-tropics is estimated by both the DGVMs (0.~~05~~04 ± 0.~~1~~06 GtC yr^{-1}) and the inversion systems (0.~~01~~03 ± 0.1 GtC yr^{-1}). This means nearly all carbon uptake is due to oceanic sinks south of 30°S. The Southern Ocean flux in the fCO_2-products (1.~~6 [1.5, 1.9~~3 ± 0.3 GtC~~] yr^{-1}) and)~~, inversion estimates (1.~~6~~2 ± 0.3 GtC yr^{-1}), and GOBMs (1.2 ± 0.2 GtC yr^{-1}) ~~is marginally higher than in the GOBMs (1.5 ± 0.4 GtC yr^{-1})~~agree well (Figure 14, bottom row). This agreement is subject to the choice of the river flux adjustment (Lacroix et al., 2020, Hauck et al., 2023b~~).~~, Planchat et al., 2025). Nevertheless, the time-series of atmospheric inversions and fCO_2-products diverge from the GOBMs. A substantial overestimation of the trends in the fCO_2-products ~~could be explained by~~has been suggested resulting from sparse and unevenly distributed observations, especially in wintertime (Figure ~~S5~~S4; Hauck et al., 2023a; Gloege et al., 2021). Model biases likely contribute as well, ~~with~~although expected biases in mode water formation, stratification, and the chemical buffer capacity ~~known to play a role in Earth System Models~~ (Terhaar et al., 2021, Bourgeois et al., 2022, Terhaar et al., 2022) were not confirmed for the ensemble average of the suite of models used here (section 3.6.5 and Supplement S3.3, Figures S6 and S7). Recently, a high-resolution model study has shown that the Southern Ocean sink is 10% higher when spatial resolution is increased such that mesoscale eddies are resolved (Patara et al., 2026).

The interannual variability in the southern extra-tropics is low because of the dominance of ocean areas with low variability compared to land areas. The split between land (S_{LAND}-E_{LUC}) and ocean (S_{OCEAN}) shows a substantial contribution to variability in the south coming from the land, with no consistency between the DGVMs and the inversions or among inversions. This is expected due to the difficulty of separating exactly the land and oceanic fluxes when viewed from atmospheric observations alone. The S_{OCEAN} interannual variability was found to be higher in the fCO_2-products (0.04-0.~~18~~17 GtC yr^{-1}) compared to GOBMs (0.03 to 0.~~06~~07 GtC yr^{-1}) in 1990-~~2024~~2025. Inversions give an interannual variability of 0.~~13~~06 to 0.~~15~~13 GtC yr^{-1}. Model subsampling experiments recently illustrated that fCO_2-products may overestimate decadal variability in the Southern Ocean carbon sink by 30% and the trend since 2000 by 50-130% due to data sparsity, based on one and two fCO_2-products with strong variability (Gloege et al., 2021, Hauck et al., 2023a). The trend benchmark test using the method of Hauck et al., (2023a) and a subset of ~~6~~9 fCO_2-products confirms the sensitivity of the decadal trends in fCO_2-products to reconstruction biases, particularly in the Southern Ocean~~, indicating an overestimation of the ensemble mean trend (See Supplement S.3.4). However, we~~ (Roobaert et al 2026). However, Roobaert et al (2026) also find compensating positive biases in the ensemble so that the ensemble mean bias is smaller than the bias from some individual fCO_2-products.

Formatted: Indent: Left: -0.08 cm, Hanging: 0.08 cm, Outline numbered + Level: 4 + Numbering Style: 1, 2, 3, … + Start at: 1 + Alignment: Left + Aligned at: 0 cm + Indent at: 1.52 cm

3.8.2.4 RECCAP2 regions

Formatted: Indent: Left: 0 cm, First line: 0 cm, Outline numbered + Level: 4 + Numbering Style: 1, 2, 3, … + Start at: 1 + Alignment: Left + Aligned at: 0 cm + Indent at: 1.52 cm

Aligning with the RECCAP-2 initiative (Ciais et al., 2022; Poulter et al., 2022; DeVries et al., 2023), we provide a breakdown of this GCB paper estimate of the E_{LUC}, S_{LAND}, Net land (S_{LAND} - E_{LUC}), and S_{OCEAN} fluxes over the 10 land, and 5 ocean RECCAP-2 regions, averaged over the period ~~2015-2024~~2016-2025 (Figure 15). The DGVMs and inversions suggest a positive net land sink in all regions, except for South America, Africa, and Southeast Asia, where the inversions indicate a small net source of ~~respectively~~ -0.~~1~~11±0.~~5~~45 GtC yr^{-1}, -0.~~3~~22±0.~~3~~30 GtC yr^{-1}, and -0.~~1~~05±0.~~3~~32 GtC yr^{-1}, respectively, compared to a small sink of 0.~~1~~04±0.~~3~~26 GtC yr^{-1}, 0.~~1~~25±0.~~3~~17 GtC yr^{-1}, and 0.~~0~~308±0.~~1~~11 GtC yr^{-1} for the DGVMs. The uncertainty in the sign of net tropical carbon fluxes is driven by opposing gross fluxes and relatively large uncertainty in the gross fluxes themselves. For South America, DGVMs estimate S_{LAND} of 0.~~4~~45±0.~~4~~29 GtC yr^{-1} and E_{LUC} of 0.~~3~~42±0.~~2~~13 GtC yr^{-1}. Bookkeeping models suggest a larger E_{LUC} source of ~~around~~ 0.~~5~~53±0.01 GtC yr^{-1}. Similarly, in Southeast Asia, the DGVMs estimate an E_{LUC} of 0.~~2~~19±0.~~1~~07 GtC yr^{-1}, compared with the bookkeeping model estimate of 0.~~4~~32±0.02 GtC yr^{-1}. It is worth noting that emissions from peat fires (from GFED5) and drainage (from FAO, LPX-Bern, and ORCHIDEE-Peat) are added to bookkeeping model E_{LUC} estimates (see Supplement S2.2), which increases Southeast Asia E_{LUC} by 0.08 GtC yr^{-1}, over 2016-2025. Importantly, only 2 out of 23 DGVMs include peat fires and none of the DGVMs include peat drainage. Therefore, DGVMs may underestimate E_{LUC} ~~in these regions~~, which could explain the net sink discrepancy with inversions. In Africa, E_{LUC} is similar for DGVMs and bookkeeping models ~~(~~(0.3-0.4 GtC yr^{-1}), and DGVMs estimate an S_{LAND} of 0.~~5~~56±0.~~2~~13 GtC yr^{-1}.

The inversions suggest the largest net land sinks are in North America (0.~~4~~41±0.~~3~~32 GtC yr^{-1}), Russia (0.~~6~~60±0.~~2~~27 GtC yr^{-1}), Europe (0.~~3~~24±0.~~2~~27 GtC yr^{-1}), and East Asia (0.~~2~~27±0.~~3~~32 GtC yr^{-1}). This agrees well with the DGVMs in North America (0.~~4~~39±0.~~1~~16 GtC yr^{-1}), which indicate a large natural land sink (S_{LAND}) of 0.~~4~~44±0.~~2~~16 GtC yr^{-1}, and ~~near-zero~~small net land-use related carbon losses (0.~~0~~205±0.~~1~~07 GtC yr^{-1}). The DGVMs suggest a smaller net land sink in Russia compared to inversions (0.~~3~~34±0.~~1~~15 GtC yr^{-1}), and a similar net sink in East Asia (0.~~2~~20±0.~~1~~11 GtC yr^{-1}).

There is generally a higher level of agreement in the estimates of regional ~~S_{OCEAN}~~ocean anthropogenic carbon sink between the different data streams (GOBMs, fCO_2-products and atmospheric inversions) on decadal scale, compared to the agreement between the different land flux estimates. ~~All~~The data streams agree that the largest contribution to S_{OCEAN} stems from the Southern Ocean due to a combination of high flux density and large surface area, ~~but with important contributions also from~~followed by the Pacific (large area) and Atlantic (high flux density) ~~and Pacific (large area)~~ basins . In the Southern Ocean, GOBMs suggest a sink of ~~1.1±~~0.~~4~~98±0.16 GtC yr^{-1}, in line with the fCO_2-

products (1.~~1 [1.~~03±0,~~1.2]~~.31 GtC yr^{-1}) and atmospheric inversions (~~1.1±~~0.~~2~~96±0.29 GtC yr^{-1}). There is ~~similar~~also agreement within the uncertainties in the Pacific Ocean, with GOBMs, fCO_2-products, and atmospheric inversions indicating a sink of 0.~~6~~83±0.~~1~~10 GtC yr^{-1}, ~~0.7 [0.6,~~1.04±0.~~9]~~25 GtC yr^{-1}, and 0.~~6~~93±0.~~2~~24 GtC yr^{-1}, respectively. However, in the Atlantic Ocean, GOBMs simulate a sink of 0.~~5~~50±0.~~1~~09 GtC yr^{-1}, noticeably lower than both the fCO_2-products (0.~~8 [77±~~0.~~7,0.9]~~13 GtC yr^{-1}) and atmospheric inversions (0.~~8~~77±0.~~1~~14 GtC yr^{-1}). It is important to note the fCO_2-products and atmospheric inversions have a substantial and uncertain river flux adjustment in the Atlantic Ocean (0.3 GtC yr^{-1}) that also leads to a mean offset between GOBMs and fCO_2-products/inversions in the latitude band of the tropics (Figure 14). The Indian Ocean due its smaller size and the Arctic Ocean due to its size and sea-ice cover that prevents air-sea gas-exchange are responsible for smaller but non negligible S_{OCEAN} fluxes (Indian Ocean: ~~(~~0.~~3~~26±0.~~1~~03 GtC yr^{-1}, 0.~~3 [~~29±0.~~3,0.4]~~14 GtC yr^{-1}, and 0.~~3~~31±0.~~1~~14 GtC yr^{-1} for GOBMs, fCO_2-products, and atmospheric inversions, respectively, and Arctic Ocean: ~~(~~0.05±0.~~1±0.03~~02 GtC yr^{-1}, 0.~~2 [~~13±0.~~1,0.3]~~07 GtC yr^{-1}, and 0.~~1~~06±0.04 GtC yr^{-1} for GOBMs, fCO_2-products, and atmospheric inversions, respectively). Note that the S_{OCEAN} numbers presented here deviate from numbers reported in RECCAP-2 where the net air-sea CO_2 flux is reported (i.e. without river flux and preindustrial mean adjustment for fCO_2-products and inversions, and with river flux adjustment subtracted from GOBMs in most chapters, or comparing unadjusted datasets with discussion of uncertain regional riverine fluxes as major uncertainty, e.g. Sarma et al., 2023, DeVries et al., 2023).

3.8.3 Fire emissions in ~~2025~~2026

Formatted: Indent: Left: 0 cm, First line: 0 cm, Outline numbered + Level: 3 + Numbering Style: 1, 2, 3, … + Start at: 1 + Alignment: Left + Aligned at: 0 cm + Indent at: 1.27 cm

Fire emissions so far in ~~2025~~2026 have been ~~below~~close to the average of recent decades, ~~chiefly due to the lowest emissions on record since 2003 across the tropics.~~with high emissions in Southeast Asia offset by relatively low emissions in several other major fire regions, particularly South America and North America. Figure ~~S14~~S15 shows global and regional emissions estimates for the period ~~1st Jan-30th~~1 January-30 September in each year from 2003~~-2025~~ to 2026. Estimates derive from ~~two global fire emissions products: the global fire emissions database (GFED,~~the Global Fire Emissions Database version ~~4.1s~~5.1 (GFED5.1; van der Werf et al., ~~2017),~~2025, Chen et al., 2026) and the ~~global fire assimilation system~~Global Fire Assimilation System (GFAS~~, operated by the Copernicus Atmosphere Service~~; Kaiser et al., 2012). ~~The two products estimate~~ Because the transition to GFED5.1 has substantially revised absolute fire emissions estimates, we report absolute emissions from GFED5.1, while relative anomalies are calculated independently for GFED5.1 and GFAS and reported separately, following Burton et al. (2026). GFED5.1 estimates that global fire emissions ~~from fires~~ were ~~1.~~2~~-1.~~4,55 GtC ~~(the range reflecting the difference between the two fire emission datasets, actual uncertainties are larger, and estimates are likely conservative, see Chen et al. (2023))~~ during January-September ~~2025. These estimates are 19-20% below the 2015-~~2026. Relative to the 2016-2025 average for the same months, global emissions were 8% below average in GFED5.1 but 3% above average in GFAS.

Relative to the full 2003-2025 record, emissions were 7% below average in GFED5.1 and 5% below average in GFAS.

Global fire emissions in 2026 remained well below the high levels of 2023 and 2024 ~~average for the same months (1.5-1.7 GtC). Both the GFED4.1s and GFAS products show the second-lowest~~, when GFED5.1 estimates January-September ~~fire~~ emissions ~~since 2003 (2022 is~~of 3.17 and 3.41 GtC, respectively, but were slightly higher than the ~~lowest year in both products).~~

~~Notably, the year 2025 follows two years with above-average global fire emissions (Figure S14), with global emissions through September totalling 1.7-~~2.~~1~~49 GtC emitted during the same period in 2025. The high global emissions in 2023 and ~~1.6-2.2 GtC in~~ 2024~~. These high emissions totals~~ were ~~caused by~~associated with exceptionally high emissions in North America in 2023, principally in Canada~~; Jones et al., 2024b),~~, and in both North America and South America in 2024 ~~(~~, principally in Canada and Brazil (Jones et al., 2024a; Kelley et al., 2025). ~~For example, in~~In contrast, the global total in 2026 reflects a mixture of strong positive and negative regional anomalies rather than synchronously high emissions across several major fire regions.

The clearest positive regional anomaly in 2026 occurred in Southeast Asia, where GFED5.1 estimates January-September fire emissions of 0.34 GtC. Relative to the 2016-2025 average, emissions were 29% above average in GFED5.1 and 232% above average in GFAS; relative to the full 2003-2025 record, they were 12% above average in GFED5.1 and 131% above average in GFAS. Indonesia showed the strongest national-scale positive anomaly among the countries with high fire emissions shown in Figure S15, with GFED5.1 emissions of 0.13 GtC. Relative to the previous decade, emissions were 433% above average in GFED5.1 and 791% above average in GFAS. The substantially larger anomaly in GFAS may partly reflect differences in remote-sensing approach: GFAS is driven by active fire observations and fire radiative power, whereas GFED5.1 remains more strongly constrained by burned area detection. This distinction may be particularly important for Indonesian peat fires, where persistent and spatially fragmented burning can be difficult to capture completely from burned area but can generate repeated active fire detections, potentially making FRP-based estimates more sensitive to anomalously high fire activity (Mouillot et al., 2014; Wooster et al., 2021; Chen et al., 2024).

These positive anomalies were counterbalanced by low emissions in several other major fire regions. In South America, GFED5.1 estimates January-September ~~2024, GFED4.1s suggests that global emissions totalled 2.2 GtC, the highest total on record for these months and 32% above the average for the decade prior (2014-2023; GFAS~~ fire emissions of 0.17 GtC, with emissions 50% below the 2016-2025 average in GFED5.1 and 29% below average in GFAS. Brazil emitted 0.094 GtC according to GFED5.1, with emissions 54% below average in GFED5.1 and 32% below average in GFAS. In North America, GFED5.1 estimates emissions of 0.22 GtC, 20% below the previous-decade average in GFED5.1 and 40% below average in GFAS. Canada emitted 0.14 GtC, with emissions 7% below average in GFED5.1

and 53% below average in GFAS. Emissions were also ~~suggests that emissions were 11% above~~ below the ~~average for January-September).~~previous-decade average in Australasia, by 8% in GFED5.1 and 19% in GFAS, and across the Southern Hemisphere extratropics, by 26% in GFED5.1 and 44% in GFAS. Across the tropics, GFED5.1 estimates emissions of 1.94 GtC, 12% below the 2016-2025 average, whereas GFAS indicates emissions 16% above average.

~~Despite low global fire emissions so far in 2025, a pattern of extremely high fire emissions from Canada has now persisted for three consecutive years commencing with the record-breaking year in 2023 (Jones et al., 2024b, Byrne et al., 2024; Kelley et al., 2025). In January-September 2025, fire emissions from Canada (0.3-0.4 GtC) were slightly greater than in the same months of 2024 (0.2-0.3 GtC yr^{-1}) and around half as large as those in the same months of 2023 (0.5-0.8 GtC). The emissions totals for Canada in January-September 2025 were 2.2 times the average of January-September periods during the prior decade 2015-2024 and 4-6 times greater than the average of those months in 2003-2022 [excluding the record-breaking year in 2023]; Figure S14). According to GFED4.1s, January-September fire emissions from Canada in just the past three years (1.5 GtC) exceeded the country's total January-September fire emissions throughout the 20 years prior (1.2 GtC during 2003-2022). The continued anomaly in Canada propagated to the Northern Hemisphere, where January-September 2025 emissions of 0.4-0.5 GtC were 13-21% above the average of 2015-2024.~~

~~Fire emissions anomalies in Africa strongly influence global fire emissions totals because the continent typically contributed near 50% of global fire emissions during 2015-2024 (average of January-September periods). For 2025, fire emissions in Africa through September were 0.4-0.6 GtC, 19-25% below the average of 2015-2024 (0.6-0.8 GtC). Synchronously, emissions through September from South America were around 0.1 GtC in both GFED4.1s and GFAS systems, less than half of the average for 2015-2024 (0.2-0.3 GtC), and emissions from Southeast Asia were around 0.05 GtC, also less than half of the average for 2015-2024 (0.1 GtC in both GFED4.1s and GFAS). Low emissions from the tropical parts of Africa, South America, and Southeast Asia contribute to low emissions across the global tropics so far in 2025 (0.7-0.9 GtC), which were only around two-thirds of the average for 2015-2024 (1.1-1.3 GtC) in both GFED4.1s and GFAS.~~

We caution that the fire emissions fluxes presented here should not be compared directly with other fluxes of the budget (e.g., S_{LAND} or E_{LUC}) due to incompatibilities between the observable fire emission fluxes and what is quantified in the S_{LAND} and E_{LUC} components of the budget. The fire emission estimates from global fire products relate to all fire types that can be observed in Earth Observations (Giglio et al., 2018; Randerson et al., 2012; Kaiser et al., 2012), including (i) fires occurring as part of natural disturbance-recovery cycles that would also have occurred in the pre-industrial period (Yue et al., 2016; Keeley and Pausas, 2019; Zou et al., 2019), (ii) fires occurring above and beyond natural disturbance-recovery cycle due to changes in climate, CO_2 and N fertilisation and to an increased frequency of extreme drought and heatwave events (Abatzoglou et al., 2019; Jones et al., 2022; Zheng

et al., 2021; Burton et al., 2024), and (iii) fires occurring in relation to land use and land use change, such as deforestation fires and agricultural fires (van der Werf et al., 2010; Magi et al., 2012). In the context of the global carbon budget, fire emissions associated with (ii) should be included in the S_{LAND} component, fire emissions associated with (iii) should already be accounted for in the E_{LUC} component, while fire emissions associated with (i) should not be included in the global carbon budget as part of the natural carbon cycle. However, it is not currently possible to derive specific estimates for fluxes (i), (ii), and (iii) using global fire emission products such as GFED or GFAS. In addition, the fire emissions estimates from global fire emissions products represent a gross flux of carbon to the atmosphere, whereas the S_{LAND} component of the budget is a net flux that should also include post-fire recovery fluxes. Even if emissions from fires of type (ii) could be separated from those of type (i), these fluxes may be partially or wholly offset in subsequent years by post-fire fluxes as vegetation recovers, sequestering carbon from the atmosphere to the terrestrial biosphere (Yue et al., 2016; Jones et al., ~~2024c~~2024b). Increases in forest fire emissions and severity (emissions per unit area) globally during the past two decades have highlighted the increasing potential for fire emissions fluxes to outweigh post-fire recovery fluxes, though long-term monitoring of vegetation recovery is required to quantify the net effect on terrestrial C storage (Jones et al., ~~2024c~~2024b).

3.9 Closing the global carbon cycle

3.9.1 Partitioning of cumulative emissions and sink fluxes

Emissions during the period 1850-~~20242025~~ amounted to ~~745 ± 65~~755 ± 55 GtC and were partitioned among the atmosphere (~~290~~295 ± 5 GtC; 39%), ocean (200~~ ± 40~~± 55 GtC; ~~27~~26%), and land (~~175 ± 50~~190 ± 40 GtC; ~~24~~25%). The cumulative land sink is lower than the cumulative land-use emissions (~~250 ± 65~~245 ± 50 GtC), making the global land a source of ~~75 ± 80~~55 ± 65 GtC over the whole 1850-~~20242025~~ period (Table 8).

The use of nearly independent estimates for the individual terms of the global carbon budget shows a cumulative budget imbalance of ~~80~~70 GtC (~~11~~9% of total emissions) during 1850-~~20242025~~ (Table 8), which suggests that emissions could be slightly too high by the same proportion or that the combined land and ocean sinks are underestimated (by up to 20%). A large part of the B_{IM} occurs over the first half of the 20th century (Figure 3, red dashed line) and could originate from the estimation of significant increase in E_{FOS} and E_{LUC} between the mid 1920s and the mid 1960s which is unmatched by a similar growth in atmospheric CO_2 concentration as recorded in ice cores (Figure 3). ~~Also, we now correct the S_{LAND} estimate for historical reduction in forest cover (RSS, see Section 2.6). This reduces the S_{LAND} estimate by about 40 GtC over the 1850-2024 period, contributing to the increase of the historical budget imbalance in comparison to GCB2024 (Friedlingstein et al., 2025a).~~

Formatted: Outline numbered + Level: 2 + Numbering Style: 1, 2, 3, … + Start at: 1 + Alignment: Left + Aligned at: 0 cm + Indent at: 1.02 cm

Formatted: Outline numbered + Level: 3 + Numbering Style: 1, 2, 3, … + Start at: 1 + Alignment: Left + Aligned at: 0 cm + Indent at: 1.27 cm

For the more recent 1959-~~20242025~~ period where direct atmospheric CO_2 measurements are available, total emissions ($E_{FOS} + E_{LUC}$) amounted to ~~530~~545 ± 50 GtC, of which ~~420~~430 ± 20 GtC (79%) were caused by fossil CO_2 emissions, and 110 ± 45 GtC (21%) by land-use change (Table 8). The total emissions were partitioned among the atmosphere (~~230~~235 ± 5 GtC; ~~44~~43%), ocean (145 ± ~~30~~40 GtC; ~~27~~26%), and the land (~~120~~125 ± 30 GtC; 23%), with a budget imbalance of ~~35~~40 GtC (7% of total emissions). All components except land-use change emissions have significantly grown since the 1960s, with important interannual variability in the growth rate in atmospheric CO_2 concentration primarily mirrored in the land CO_2 sink (Figure 4), and some decadal variability in all terms (Table 7). Differences with previous budget releases are documented in Figure ~~S15~~S16.

The global carbon budget averaged over the last decade (~~2015-2024~~2016-2025) is shown in Figure 2 and Table 7. For this period, 88% of the total emissions ($E_{FOS} + E_{LUC}$) were from fossil CO_2 emissions (E_{FOS}), and 12% from land-use change (E_{LUC}). The total emissions were partitioned among the atmosphere (~~50~~48%), ocean (~~29~~27%) and land (~~21~~22%), with a ~~near zero~~small positive budget imbalance (~~0.1%, <0.1 GtC yr^{-1}). We note that, compared to GCB2024~~3%). For single years, the ~~corrections on S_{OCEAN} and S_{LAND} largely reduced the B_{IM} over the 2015-2024 period, by about 0.4 GtC, but at the cost of increasing the cumulated B_{IM} over the longer 1959-2024 period, from 17 GtC (uncorrected estimate) to 37 GtC (corrected estimate~~budget imbalance can be larger (Figure 4f).

~~For single years, the budget imbalance can be larger (Figure 4f). For 2024, the combination of our estimated anthropogenic sources (11.6 ± 0.9 GtC yr^{-1}) and partitioning in atmosphere, land and ocean (13.3 ± 0.9 GtC yr^{-1}) leads to a large negative B_{IM} of -1.7 GtC (Table 7), indicating that, despite the lower than average S_{LAND} in 2024, the land sink is still too large to explain the record-high atmospheric CO_2 growth rate of 2024. We note that using the 2024 GRESO atmospheric growth rate of 6.8±0.2 GtC yr^{-1} (Section 3.5.3) would reduce the 2024 B_{IM} to about -0.6 GtC.~~

3.9.2 Trend and variability in the carbon budget imbalance

The carbon budget imbalance (B_{IM}; Eq. 1, Figure 4f) quantifies the mismatch between the estimated total emissions and the estimated changes in the atmosphere, land, and ocean reservoirs. The budget imbalance from 1959 to ~~20242025~~ is relatively small (~~35~~40 GtC cumulated over the period, i.e. 0.~~5~~6 GtC yr^{-1} on average) and shows no significant trend over the 1959-~~20242025~~ period (Figure 4, Table 7). The process models (GOBMs and DGVMs) and *f*CO_2-products have been selected to match observational constraints in the 1990s, but no further constraints have been applied to their representation of trend and variability. Therefore, the small mean and trend in the budget imbalance can be seen as evidence of a coherent community understanding of the emissions and their partitioning on those time scales (Figure 4). However, the budget imbalance shows substantial variability of the order

Formatted: Outline numbered + Level: 3 + Numbering Style: 1, 2, 3, … + Start at: 1 + Alignment: Left + Aligned at: 0 cm + Indent at: 1.27 cm

of ±1 GtC yr^{-1}, particularly over semi-decadal time scales, although most of the variability is within the uncertainty of the individual estimates of the global budget.

We cannot attribute the cause of the budget imbalance with our analysis, we only note that the budget imbalance is unlikely to be explained by errors in the emissions alone because of its large semi-decadal variability component, a variability that is atypical of emissions, and also because the budget imbalance has not increased in the past 60 years despite a near tripling in anthropogenic emissions (Figure 4). Errors in S_{LAND} and S_{OCEAN} are more likely to be the main cause for the budget imbalance, especially on interannual to semi-decadal timescales. For example, underestimation of the S_{LAND} by DGVMs has been reported following the eruption of Mount Pinatubo in 1991 possibly due to missing responses to changes in diffuse radiation (Mercado et al., 2009). Although we account for aerosol effects on solar radiation quantity and quality (diffuse vs direct), most DGVMs only used the former as input (i.e., total solar radiation) (Table S1). Thus, the ensemble mean may not capture the full effects of volcanic eruptions, i.e., associated with high light scattering sulphate aerosols, on the land carbon sink (O'Sullivan et al., 2021), potentially explaining the large positive B_{IM} in 1991-1992. DGVMs are suspected to underestimate the land sink reduction in response to El Niño events (drought, high temperature extremes, and fires) (see Section 3.7.3), which could explain the large negative B_{IM} in 1986-1987, 1997-1998 or 2023-2024. Few DGVMs have explicit representation of drought-mortality and only 6 from 23 include forest demography, although recent efforts are underway to fill these critical research gaps (Eckes-Shephard et al., 2025 Yao et al., 2022, 2023). Quasi-decadal variability in the ocean sink has also been reported, with all methods agreeing on smaller than expected ocean CO_2 sink in the 1990s and a larger than expected sink in the 2000s (Figure 10b; Landschützer et al., 2016, DeVries et al., 2019, Hauck et al., 2020, McKinley et al., 2020, Gruber et al., 2023) and the climate-driven variability could be substantial but is not well constrained (DeVries et al., 2023, Müller et al., 2023). Errors in sink estimates could also be partly driven by errors in the climatic forcing data, particularly precipitation for S_{LAND} and wind for S_{OCEAN}.

~~Although the budget imbalance is near zero for the most recent decade, it could be due to a compensation of errors. We~~Further, we cannot exclude an overestimation of CO_2 emissions, particularly from land-use change, given their large uncertainty, as has been suggested elsewhere (Piao et al., 2018), and/or an underestimate of the land or ocean sinks. A larger estimate of the atmosphere-land CO_2 flux (S_{LAND}-E_{LUC}) over the extra-tropics would reconcile bottom-up model results with inversion estimates (Figure 14). Likewise, a larger S_{OCEAN} is also possible given the higher estimates from the fCO_2-products and the oxygen-based estimates (see Table 6 and Figure 10b), the underestimation of interior ocean anthropogenic carbon accumulation in the GOBMs (Section 3.6.5, Müller et al., 2023), or known biases of ocean models (e.g., Terhaar et al., 2022; 2024). More integrated use of observations in the global carbon budget, either on their own or for further constraining model results, should help resolve some of the budget imbalance.

4 Tracking progress towards mitigation targets

The average growth in global fossil CO_2 emissions peaked at nearly +3% per year during the 2000s, primarily driven by the rapid growth in emissions in China. In the last decade, however, the global growth rate has slowly declined, reaching a low +0.~~8~~9% per year on average over ~~2015–2024~~2016-2025. While this slowdown in global fossil CO_2 emissions growth is welcome, global fossil CO_2 emissions ~~continue~~continued to grow, far from the rapid emission decreases needed to be consistent with the temperature goals of the Paris Agreement.

Since the 1990s, the average growth rate of fossil CO_2 emissions has continuously declined across the group of developed countries of the Organisation for Economic Co-operation and Development (OECD), with emissions peaking in around 2005 and declining at 1.~~5~~4% yr^{-1} in the decade 2015-~~2024~~2025, compared to a decline of 1.0.~~9~~% yr^{-1} during the ~~2005–2014~~2006-2015 period (Table 9). In the non-OECD countries, emissions rose 4.~~6~~1% yr^{-1} from ~~2005–2014~~2006-2015, but growth has lowered to 2.1% yr^{-1} from ~~2015–2024.~~ 2016-2025.

In the decade ~~2015–2024~~2016-2025, territorial fossil CO_2 emissions decreased significantly (at the 95% confidence level) in ~~35 economies~~40 countries whose gross domestic product (GDP) grew significantly (also at the 95% confidence level): ~~Andorra~~Albania, Australia, Austria, Belarus, Belgium, Bosnia and Herzegovina, Bulgaria, Cameroon, Chile, Czechia, Denmark, Estonia, Finland, France, Germany, Greece, Hungary, Ireland, ~~Israel, Jordan~~Italy, Japan, Latvia, Lithuania, Luxembourg, Netherlands, New Zealand, Norway, Poland, Portugal, ~~South Korea,~~ Romania, Serbia, Slovakia, Slovenia, South Korea, Spain, Sweden, Switzerland, ~~Taiwan,~~ Thailand, United Kingdom, ~~and~~ USA, Venezuela (updated from Le Quéré et al., 2019). Altogether, these ~~35 economies~~40 countries emitted 2.~~7~~8 GtC yr^{-1} (~~9.~~710.1 $GtCO_2$ yr^{-1}) on average over the last decade, about ~~27~~26% of ~~world~~2025 global CO_2 fossil emissions. For comparison, over the previous decade (~~2005–2014), 18 economies~~2006-2015), 22 countries showed a significant decrease in territorial fossil CO_2 emissions while significantly growing their GDP (Austria, Belgium, Bulgaria, Czechia, France, Germany, Lithuania, Luxembourg, Malta, Netherlands, North Macedonia, ~~Netherlands, New Zealand~~Poland, Romania, Serbia, Slovakia, Sweden, Switzerland, Tonga, Tuvalu, United Kingdom, USA, Uzbekistan). These ~~18~~22 economies emitted an average 2.~~0~~2 GtC yr^{-1} over ~~2005–2014~~2006–2015, or ~~20~~23% of ~~the~~2015 global ~~total~~ CO_2 fossil emissions. The number of countries reducing their emissions while growing their economies is clearly increasing, with emissions reductions expanding to 59 countries in all continents for the shorter 2019-2025 period, although not all of these trends are significant (Le Quéré et al., 2026).

~~Decomposing~~By decomposing emission changes into the components of growth, a Kaya decomposition~~,~~ helps give an initial understanding of the drivers of emission changes (Peters et al., 2017b). The reduction in growth in global fossil CO_2 emissions in the last decade (~~2015–2024~~2016-2025, 0.~~8~~9% yr^{-1}) relative to the previous decade (~~2005–2014, 2.2~~2006-2015, 1.9% yr^{-1}) is due to

Formatted: Outline numbered + Level: 1 + Numbering Style: 1, 2, 3, … + Start at: 1 + Alignment: Left + Aligned at: 0 cm + Indent at: 0.76 cm

Formatted: Not Highlight

Formatted: Not Highlight

Formatted: Not Highlight

Formatted: Not Highlight

Formatted: Not Highlight

Formatted: Not Highlight

Formatted: Not Highlight

slightly weaker economic growth (3.~~5~~2% yr^{-1} to 2.~~4~~8% yr^{-1}), ~~increasing declines~~a decline in CO_2 emissions per unit of energy ~~((~~+0.~~3~~% yr^{-1} to -0.~~7~~4% yr^{-1}), and ~~weakening~~steady declines in energy per unit of GDP ~~(1.6% yr-1 (-~~1 ~~to 1.3~~.5% yr^{-1} to -1.5% yr^{-1}) (Figure ~~S17).~~ S18). The growth in solar and wind energy in electricity, and to a lesser extent the deployment of electric vehicles, are a dominant contribution to the reduction in emissions growth between the two decades (Le Quéré et al., 2026).

Fossil CO_2 emission declines in the USA and the EU27 are primarily driven by sustained or increasing declines in energy per GDP and CO_2 emissions per unit energy. China has seen emissions growth decline from ~~6~~5.7% yr^{-1} in the ~~2005-2014~~2006-2015 decade to 2.~~5~~7% yr^{-1} from ~~2015-2024~~2016-2025, driven by weaker economic growth (~~five~~four percentage points), offset by a considerable weakening in the rate of reduction in the energy per GDP (~~four~~two percentage points), with sustained improvements in CO_2 emissions per unit energy (Figure ~~S17~~S18). India has had strong economic growth that is not offset by declines in energy per GDP or declines in CO_2 emissions per unit energy, driving up fossil CO_2 emissions. In the rest of the world, economic growth has slowed considerably in the last decade, and carbon intensity has increased, with declines in energy per GDP unable to counteract these increases leading to growing emissions. Despite the high deployment of renewables in some countries (e.g., China, India), fossil energy sources continue to grow to meet growing energy demand (Le Quéré et al., 2019, 2026). In summary, the carbon intensity of energy has consistently decreased over the past decade globally (-0.~~7~~4% yr^{-1}), indicating decarbonisation of the global energy system, with declines in China (-~~1.4~~0.8% yr^{-1}), the European Union (-1.~~5~~3% yr^{-1}), the USA (-~~1.3~~0.9% yr^{-1}), but no change in India ~~and increases (carbonisation).~~ Carbon intensity in the Rest of the World~~:~~ combined, also declined (-0.3%). The global decarbonation trends ~~are~~have not been sufficient to offset the growth in global energy demand, with energy demand growing faster than expected due to weakening declines in energy per GDP in China, US, and globally.

The slower growth of global fossil CO_2 emissions in the last decade is due in part to the emergence of climate policy (Eskander and Fankhauser 2020; Le ~~Quere~~Quéré et al 2019; Hoppe et al., 2023) and technological change, which is leading to a shift from coal to gas and growth in renewable energies, and reduced expansion and utilisation of coal capacity in some countries. At the aggregated global level, decarbonisation shows a strong and growing signal in the last decade, with smaller contributions from lower economic growth and declines in energy per GDP. Altogether, current global fossil CO_2 emissions ~~are still growing,~~growth is far from the reductions needed to meet the ambitious climate goals of the UNFCCC Paris agreement.

Last, we update the remaining carbon budget (RCB) based on two studies, the IPCC AR6 (Canadell et al., 2021) and the revision of the IPCC AR6 estimates (Forster et al., ~~2025~~2026, Lamboll et al., 2023). We update the RCB assessed by the IPCC AR6 (Canadell et al., 2021), accounting for the 2020 to ~~2025~~2026 GCB estimated anthropogenic emissions from fossil combustion (E_{FOS}) and land use change (E_{LUC}). From January ~~2026~~2027, the IPCC AR6 RCB (50% likelihood) for limiting global warming to

Formatted: Not Superscript/ Subscript

1.5°C, 1.7°C and 2°C is estimated to amount to ~~70, 165~~55, 155, and ~~300~~290 GtC (~~250, 600, 1100~~210, 560, 1060 $GtCO_2$). The Forster et al. (~~2025~~2026) study proposed a significantly lower RCB than IPCC AR6, ~~with the largest reduction being~~primarily due to an update of the climate emulator (MAGICC) used to estimate the warming contribution of non-CO_2 agents, and to the warming (i.e. emissions) that occurred over the 2020-~~2024~~2025 period. We update the Forster et al., ~~budget~~(2026) RCB accounting for ~~the 2025 GCB~~our estimated anthropogenic emissions for 2026. From January ~~2026~~2027, the Forster et al., (~~2025~~2026) RCB (50% likelihood) for limiting global warming to 1.5°C, 1.7°C and 2°C is estimated to amount to 25, ~~120~~125, and 275 GtC (~~90, 450, 101~~085, 455, 1005 $GtCO_2$), significantly smaller than the updated IPCC AR6 estimate. Both the original IPCC AR6 and Forster et al. (~~2025~~2026) estimates include the Earth System uncertainty on the climate response to cumulative CO_2 emissions, which is reflected through the percent likelihood of exceeding the given temperature threshold, an additional uncertainty of ±220$GtCO_2$ due to alternative non-CO_2 emission scenarios, and other sources of uncertainties (see Canadell et al., 2021). The two sets of original estimates overlap when considering all uncertainties.

Here, we take the average of our update of both IPCC AR6 and Forster et al. (2025) estimates, giving a remaining carbon budget (50% likelihood) for limiting global warming to 1.5°C, 1.7°C and 2°C of respectively ~~45, 145~~40, 140, and ~~290~~280 GtC (~~170, 525, 1055~~150, 510, 1035 $GtCO_2$) starting from January ~~2026~~2027. We emphasise the large uncertainties, particularly when close to the global warming limit of 1.5°C. These 1.5°C, 1.7°C and 2°C ~~remaining carbon budgets~~RCBs correspond respectively to about ~~4~~3, 12 and ~~25~~24 years from the beginning of ~~2026~~2027, at the ~~2025~~2026 level of total anthropogenic CO_2 emissions. Reaching net-zero CO_2 emissions by 2050 entails cutting total anthropogenic CO_2 emissions by about 0.5 GtC (1.~~78~~ $GtCO_2$~~),~~, 4% of ~~2025~~2026 emissions~~,~~), each year on average, comparable to the decrease in E_{FOS} observed in 2020 during the COVID-19 pandemic. However, ~~this~~ such linear decrease between now and 2050 would lead to cumulative emissions ~~over 2025-2050~~ of 140 GtC (~~520~~515 $GtCO_2$), well above the 40 GtC remaining ~~carbon~~ budget ~~of 50 GtC~~ to limit global warming to 1.5°C, but still ~~within~~compatible to the ~~remaining~~140 GtC budget ~~of 145 GtC~~ to limit warming to 1.7°C (in phase with the "well below 2°C" ambition of the Paris Agreement).

5 Discussion

Each year when the global carbon budget is published, each flux component is updated for all previous years to consider ~~corrections~~revisions that are the result of further scrutiny and verification of the underlying data in the primary input datasets. Annual estimates may be updated with improvements in data quality and timeliness (e.g., to eliminate the need for extrapolation of forcing data such as land use). Of all terms in the global budget, only the fossil CO_2 emissions and the growth rate in atmospheric CO_2 concentration are based primarily on empirical inputs supporting annual estimates in this carbon budget. The carbon budget imbalance, yet an imperfect measure, provides a strong indication of the

Formatted: Indent: Left: 0 cm, First line: 0 cm, Outline numbered + Level: 1 + Numbering Style: 1, 2, 3, … + Start at: 1 + Alignment: Left + Aligned at: 0 cm + Indent at: 0.76 cm

limitations in observations, in understanding and representing processes in models, and/or in the integration of the carbon budget components.

The persistent unexplained variability in the carbon budget imbalance limits our ability to verify reported emissions (Peters et al., 2017a) and suggests we do not yet have a complete understanding of the underlying carbon cycle dynamics on annual to decadal timescales. Resolving most of this unexplained variability should be possible through different and complementary approaches. First, as intended with our annual updates, the imbalance as an error term should be reduced by improvements of individual components of the global carbon budget that follow from improving the underlying data and statistics and by improving the models through the resolution of some of the key uncertainties detailed in Table 10. Second, additional clues to the origin and processes responsible for the variability in the budget imbalance could be obtained through a closer scrutiny of carbon variability in light of other Earth system data (e.g., heat balance, water balance), and the use of a wider range of biogeochemical observations to better understand the land-ocean partitioning of the carbon imbalance such as the constraint from atmospheric oxygen. Finally, additional information could also be obtained through better inclusion of process knowledge at the regional level. The limit for reducing the carbon budget imbalance is yet unclear, but most certainly not yet reached given the possibilities for improvements that lie ahead.

Estimates of global fossil CO_2 emissions from different datasets are in relatively good agreement when the different system boundaries of these datasets are considered (Andrew, 2020a). While estimates of E_{FOS} are derived from reported activity data requiring much fewer complex transformations than some other components of the budget, uncertainties remain, and one reason for the apparently low variation between datasets is precisely the reliance on the same underlying reported energy data. The budget excludes some sources of fossil CO_2 emissions, which available evidence suggests are relatively small (<1%) (see Supplement S.8.2). We ~~have added~~include emissions from lime production in China and the US, but these are still absent in reporting from most other non-Annex I countries, and before 1990 in other Annex I countries.

Estimates of E_{LUC} suffer from a range of intertwined issues (Obermeier et al., 2025), including the poor knowledge of historical land-cover and land-use change (particularly before the 1960s when FAO reporting started), the rudimentary representation of management processes in most models, and the diversity in methodologies and boundary conditions used across methods (e.g., Arneth et al., 2017; Pongratz et al., 2014; Bastos et al., 2021). Uncertainties in current and historical carbon stocks in soils and vegetation also contribute to uncertainty in E_{LUC} estimates. Major efforts are thus necessary to resolve the different issues concerning E_{LUC} (Obermeier et al., 2025). The large uncertainty and limited reliability of E_{LUC} estimates are particularly concerning given the growing importance of E_{LUC} for climate mitigation strategies, and the large issues in the quantification of the cumulative emissions over the historical period that arise from large uncertainties in E_{LUC}.

By adding the natural land sink in managed forests estimated by DGVMs (part of S_{LAND} in this budget) to the budget E_{LUC} estimate, we reconcile most of the large gap between our E_{LUC} estimate and the land-use flux estimates from NGHGIs (Figure 8). This reconciliation (translation) can be used as potential adjustment in the policy context, for instance to help assess the collective countries' progress towards the goal of the Paris Agreement avoiding double-accounting for the natural sink in managed forests. In the absence of this translation, collective progress would appear better than it is (Grassi et al., 2021). A clear understanding of these implications is thus essential for policymakers for developing effective climate targets (Grassi et al., 2025). The application of this translation is also recommended in the UNFCCC Synthesis report for the first Global Stocktake (UNFCCC, 2022) whenever a comparison between LULUCF fluxes reported by countries and the global emission estimates of the IPCC is conducted. However, this translation should be seen as a short-term and pragmatic fix based on existing data, rather than a definitive solution to bridge the differences between global models and national inventories. Platforms for dataset comparisons (e.g., Melo et al., ~~2025~~2026) help strengthening the dialogue across communities and identify the additional steps needed to understand and reconcile the remaining differences, some of which are relevant at the country level (Grassi, et al., 2023, Schwingshackl, et al., 2022).

The comparison of GOBMs, fCO_2-products, and inversions highlights discrepancies in the temporal evolution of S_{OCEAN} in the Southern Ocean and northern high-latitudes (Figure 14, Hauck et al., 2023a) and in the mean S_{OCEAN} in the tropics. A large part of the uncertainty in the mean fluxes stems from the regional distribution of the river flux adjustment term. The current distribution simulates the largest share of the outgassing to occur in the tropics (Lacroix et al., 2020~~).~~) whereas a new study suggests a more equal split between the regions (Planchat et al., 2025). The long-standing sparse data coverage of fCO_2 observations in the Southern compared to the Northern Hemisphere (e.g., Takahashi et al., 2009) continues to exist (Bakker et al., 2016, ~~2025a~~2026a, Figure ~~S5~~S4) and to lead to substantially higher uncertainty in the S_{OCEAN} estimate for the Southern Hemisphere (Watson et al., 2020, Gloege et al., 2021, Hauck et al., 2023a, Heimdal et al 2024, Behncke et al 2026). This discrepancy, which also hampers model improvement, points to the need for increased high-quality fCO_2 observations especially in the Southern Ocean. At the same time, model uncertainty is illustrated by the large spread of individual GOBM estimates (indicated by shading in Figure 14) and highlights the need for model improvement, now also supported by the IOMB benchmarking. The issue of diverging trends in S_{OCEAN} from different methods remains a matter of concern~~.~~, although the magnitude is reduced in this version of the GCB. Recent and on-going work suggests that the fCO_2-products may overestimate the trend although biases in the fCO_2-product ensemble may partly cancel out (Supplement ~~section~~ S3.4). A data-constrained model approach suggests that the GOBMs underestimate the amplitude of decadal variability, but that the fCO_2-products overestimate the trend (Mayot et al., 2024). ~~The various methods, now also including ocean interior observation-based estimates,~~All three process-based GOBM evaluation approaches reject the previous hypothesis that biases in ocean ventilation explain a low

anthropogenic CO_2 uptake in the GOBMs. This reinforces the question of how the larger anthropogenic carbon accumulation in ocean interior estimates can be reconciled with the process models. A potential candidate could be the anthropogenic riverine fluxes. The various methods agree within uncertainties on the mean ocean sink in the last decade, although the independent estimate from atmospheric oxygen measurements still shows the largest sink estimate for the past decade and has a steeper trend (Table 6). However, the estimate is consistent within uncertainties with S_{OCEAN}, with the relatively larger ocean sink in the *f*CO_2-products and some of the GOBMs.

The assessment of the net land-atmosphere exchange from DGVMs and atmospheric inversions also shows substantial discrepancy, particularly for the estimate of the net land flux over the northern extra-tropic. This discrepancy highlights the difficulty to quantify complex processes (CO_2 fertilisation, nitrogen deposition and fertilisers, climate change and variability, land management, etc.) that collectively determine the net land CO_2 flux. Resolving the differences in the Northern Hemisphere land sink will require the consideration and inclusion of larger volumes of observations.

~~The adjustments introduced in this budget for S_{LAND} and S_{OCEAN} to account for known biases (RSS for DGVMs, cold skin/warm layer for *f*CO_2 products, ocean sink underestimation for GOBMs) lead to a smaller net land sink (S_{LAND}-E_{LUC}) and a larger ocean sink (S_{OCEAN}), more in line with the atmospheric inversions and independent oxygen based estimates (Table 7), and also consistent with a recent study based on satellite-derived changes in aboveground biomass over the 2000–2019 period (Randerson et al., 2025).~~

We provide metrics for the evaluation of the ocean and land models and the atmospheric inversions (Figure ~~S6-S8~~S5-S14, Tables S12 and S13~~, Table S12~~). These metrics expand the use of observations in the global carbon budget, helping 1) to support improvements in the ocean and land carbon models that produce the sink estimates, and 2) to constrain the representation of key underlying processes in the models and to allocate the regional partitioning of the CO_2 fluxes. The joint use of process-based metrics in an objective evaluation framework (IOMB) targeted to evaluate the simulation of S_{OCEAN} in the ocean biogeochemistry models together with the introduction of CFC inventories to evaluate the ocean ventilation and the emergent constraint approach is an important advance. This is another step in the endeavour to use a broader range of observations and more stringent model evaluation that we hope will support continued improvements in the models and in the annual estimates of the global carbon budget.

We assessed before that a sustained decrease of –1% in global emissions could be detected at the 66% likelihood level after a decade only (Peters et al., 2017a). Similarly, a change in behaviour of the land and/or ocean carbon sink would take as long to detect, and much longer if it emerges more slowly. To continue reducing the carbon imbalance on annual to decadal time scales, regionalising the carbon budget, and integrating multiple variables are powerful ways to shorten the detection limit and ensure

Formatted: Font color: Auto

Formatted: Font color: Auto

Formatted: Highlight

the research community can rapidly identify issues of concern in the evolution of the global carbon cycle under the current rapid and unprecedented changing environmental conditions.

6 Conclusions

The estimation of global CO_2 emissions and sinks is a major effort by the carbon cycle research community that requires a careful compilation and synthesis of measurements, statistical estimates, and model results. The delivery of an annual carbon budget serves two purposes. First, there is a large demand for up-to-date information on the state of the anthropogenic perturbation of the climate system and its underpinning causes. A broad stakeholder community relies on the datasets associated with the annual carbon budget including scientists, policy makers, businesses, journalists, and non-governmental organisations engaged in adapting to and mitigating human-driven climate change. Second, over the last decades we have seen unprecedented changes in the human and biophysical environments (e.g., changes in the growth of fossil fuel emissions, impact of COVID-19 pandemic, Earth's warming, extreme events, and strength of the carbon sinks), which call for frequent assessments of the state of the planet, a better quantification of the causes of changes in the contemporary global carbon cycle, and an improved capacity to anticipate its evolution in the future. Building this scientific understanding to meet the extraordinary climate mitigation challenge requires frequent, robust, transparent, and traceable datasets and methods that can be scrutinised and replicated. This paper via 'living data' helps to keep track of new budget updates.

7 Data availability

The data presented here are made available in the belief that their wide dissemination will lead to greater understanding and new scientific insights of how the carbon cycle works, how humans are altering it, and how we can mitigate the resulting human-driven climate change. Full contact details and information on how to cite the data shown here are given at the top of each page in the accompanying database and summarised in Table 2.

The accompanying database includes three Excel files organised in the following spreadsheets:

File Global_Carbon_Budget_~~2025v1~~2026v1.0.xlsx includes the following:

1. Summary
2. The global carbon budget (1959-~~2024~~2025);
3. The historical global carbon budget (1750-~~2024~~2025);
4. Global CO_2 emissions from fossil fuels and cement production by fuel type, and the per-capita emissions (1850-~~2024~~2025);

Formatted: Indent: Left: 0 cm, First line: 0 cm, Outline numbered + Level: 1 + Numbering Style: 1, 2, 3, … + Start at: 1 + Alignment: Left + Aligned at: 0 cm + Indent at: 0.76 cm

Formatted: Indent: Left: 0 cm, First line: 0 cm, Outline numbered + Level: 1 + Numbering Style: 1, 2, 3, … + Start at: 1 + Alignment: Left + Aligned at: 0 cm + Indent at: 0.76 cm

Formatted: Indent: Left: 0.12 cm, Outline numbered + Level: 4 + Numbering Style: 1, 2, 3, … + Start at: 1 + Alignment: Left + Aligned at: 4.44 cm + Indent at: 5.08 cm

5. CO_2 emissions from land-use change from the individual bookkeeping models (1959-~~2024~~2025);

6. Ocean CO_2 sink from the individual global ocean biogeochemistry models and fCO_2-products (1959-~~2024~~2025);

7. Terrestrial CO_2 sink from the individual DGVMs (1959-~~2024~~2025);

8. Cement carbonation CO_2 sink (1959-~~2024~~2025).

File National_Fossil_Carbon_Emissions_~~2025v1~~2026v1.0.xlsx includes the following:

1. Summary

2. Territorial country CO_2 emissions from fossil fuels and cement production (1850-~~2024~~2025);

3. Consumption country CO_2 emissions from fossil fuels and cement production and emissions transfer from the international trade of goods and services (1990-2020) using CDIAC/UNFCCC data as reference;

4. Emissions transfers (Consumption minus territorial emissions; 1990-2020);

5. Country definitions.

File National_LandUseChange_Carbon_Emissions_~~2024v1~~2026v1.0.xlsx includes the following:

1. Summary

2. Territorial country CO_2 emissions from Land Use Change (1850-~~2024~~2025) from three bookkeeping models~~;~~.

All three spreadsheets are published by the Integrated Carbon Observation System (ICOS) Carbon Portal and are available at https://doi.org/10.18160/GCP-~~2025 (Friedlingstein et al., 2025c).~~2026 (Friedlingstein et al., 2026b) and via the Global Carbon Budget website (https://globalcarbonbudget.org/, Global Carbon Budget, 2026). National emissions data are also available at https://doi.org/10.5281/zenodo.5569234 (Andrew and Peters, ~~2025~~2026), from the Global Carbon Atlas (http://www.globalcarbonatlas.org/, ~~last access: 23 October 2025~~Global Carbon Atlas, 2026) and from Our World in Data (https://ourworldindata.org/co2-emissions, ~~last access: 23 October 2025~~Our World in Data, 2026).

We also make all gridded data available. Bookkeeping model data: https://doi.org/10.5281/zenodo.23528902 (Schwingshackl et al. 2026); DGVM data: https://doi.org/10.5281/zenodo.23532075 (O'Sullivan et al. 2026b); GOBM and fCO_2 data :

Formatted: Indent: Left: 0.12 cm, Outline numbered + Level: 4 + Numbering Style: 1, 2, 3, … + Start at: 1 + Alignment: Left + Aligned at: 4.44 cm + Indent at: 5.08 cm

https://doi.org/10.5281/zenodo.23723209 (Hauck et al., 2026);inversion models data: doi/10.18160/99Y6-6994 (Naus et al., 2026).

Author contributions

PF, MOS, ~~MWJ, DCEB,~~ RMA, JH, MWJ, PL, CLQ, HL, ITL, AO, GPP, WP, JP, CSc, and SS designed the study, conducted the analysis, and wrote the paper with input from JGC and PC. RMA, GPP, JIK and TK produced the fossil CO_2 emissions and their uncertainties and analysed the emissions data. ME and GM provided fossil fuel emission data. ZL provided the Carbon Monitor fossil emission projection. JP, CSc, TG, ZQ and ~~ZQ~~GS provided the bookkeeping land-use change emissions with synthesis by JP and CSc. LC and QS provided estimates of emissions from peat drainage. GRvdW provided the GFED fire emissions. KH and JDM provided the estimates of non-vegetation CDR fluxes. SB, LB, MAC, NG, ÖG, ~~NG,~~ TI, TJ, LR, JS, ~~RS,~~ and ~~HTs~~TT provided an update of the global ocean biogeochemical models~~; LD~~, with quality control by SLC and an emergent constraint by JT; AFa, DJF, MG, LG, ~~YI,~~ AJ, ~~GMK~~EL, MM, CR, JAT and JZ, ~~and PC~~ provided an update of the ocean fCO_2-data products, with synthesis on both ~~streams~~models and products by JH, PL and AR. AR benchmarked the data products against independent observations. JDM and TD provided estimates of ocean interior carbon storage. SRA, ~~LBa,~~ NRB, KB, AB, CFB, MC, SEC, TE, MPE, KE, WE, ~~RAF~~AFs, TGk, ~~CL~~SKL, NM, NMM, DRM, SN, ~~AO, AMO~~CN, LO, XAP, DP, GR, EHS, IS, AJS, CSw, ST, BT, SJvdV~~, EVO,~~ and RW provided ocean fCO_2 measurements for the year ~~2024~~2025, with synthesis by ~~DCEB~~AO and ~~SDJ~~LK. KA, ~~PA, THC, JHE~~VA, DMB, EB, BF, AFo, ~~BG, JG~~JHe, AI, AKJ, EK, JK, ~~EM, JM~~SL, LM, TN, ~~QS~~BP, RS, KSD, TLS, QS, HT, APW, ~~WY,~~ XYa, ~~XYu~~WY and ~~CK~~XYu provided an update of the Dynamic Global Vegetation Models, with synthesis by SS and MOS. ~~RB,~~ FF, ~~HL, VS, DS,~~VL, WSL, JM and HiT provided estimates of land and ocean sinks from Earth System Models, as well as a projection of the atmospheric growth rate for ~~2025~~2026, with synthesis by ~~HL~~HiL. FC, ~~NC, LF,~~ ARJ, FJ, ~~ITL~~ZJ, JL, ~~LRN, YN~~SM, RRN, PP, YQ, CR, ~~XT, YK~~AvdW, NZ, and ~~ZL~~BZ provided an updated atmospheric inversion~~,~~; WP, FC, AvdW, and ITL developed the protocol and produced the synthesis and evaluation of the atmospheric inversions. EJM and RFK provided the atmospheric oxygen estimate of surface net carbon sinks. RMA provided projections of the ~~2025~~2026 fossil emissions and atmospheric CO_2 growth rate. PL provided the predictions of the ~~2025~~2026 ocean sink. IBMB, LPC, KKG, GCH~~, TMR~~ and ~~GRvdW~~TMR provided forcing data for land-use change. FT, GG and ~~GG~~SR provided data for the land-use change NGHGI ~~harmonisation.~~and FAO comparison, and LC provided FAO estimates of emissions from organic soils. XL provided the surface atmospheric CO_2 data. SP provided the satellite ~~OCO-2~~-based atmospheric CO_2 growth rate~~. MWJ provided the historical atmospheric CO_2 concentration and growth rate. IH~~ (GRESO) from combined GOSAT and OCO-2 retrievals. TO and ARF provided the climate forcing data for the DGVMs. ~~NP~~WH provided the nitrogen fertilizer forcing data for the DGVMs. MOS and NB produced the aerosol diffuse radiative forcing for the DGVMs. PCM provided the ~~iLAMB~~ILAMB evaluation of the DGVMs. ~~NOC and~~ MGS provided the ~~iOMB~~IOMB evaluation of the GOBMs. ~~PR provided the~~

Formatted: Justified, Line spacing: 1.5 lines

Formatted: Font: Not Italic

Formatted: Subscript

historical land carbon export estimate, MWJ provided the emissions prior for use in the inversion systems. XD provided seasonal, with input from YQ to the GridFED fossil emissions data, based on GRACED (Global gridded daily CO_2 emissions dataset), for most recent years for the emission prior. PF, MO and MWJMOS coordinated the effort, revised all figures, tables, text and numbers to ensure the update was clear from the 20242025 edition and in line with the globalcarbonatlas.org.https://globalcarbonatlas.org (last access: 30 October 2026).

Competing interests.

At least one of the authors is a member of the editorial board of Earth System Science Data

Acknowledgements

First, we wish to thank Richard 'Skee' Houghton for his tremendous contribution to the Global Carbon Budget since its inception, pioneering the estimate of land use change emissions with bookkeeping models. We thank all people and institutions who provided the data used in this global carbon budget 20252026 and the Global Carbon Project members for their input throughout the development of this publication. We thank Christian Ethé, Olivier Torres, Xavier Perrot, Damian Loher, Fatemeh Chegini, Fabrice Lacroix, Yangyang Zhao, Paridhi Rustogi, Sarah Berthet, Aurore Voldoire, Laurent Oziel, T. Toyoda, Y.Youcef Amar, Bertrand Decharme, Hiroyuki Tsujino, Yoshiteru Kitamura, K.Katsuya Toyama, H.Hideyuki Nakano, L. S.Shogo Urakawa, Philip Townsend, Nathaniel O. Collier, Min Xu, JamesGalen A. McKinley, Jamie D. Shutler, Andrew J. Watson, T. Holding, I. G. C. Ashton, D. K. Woolf, Lonneke Goddijn-Murphy, and Richard Sims, Stefanie Falk, Pengyue Du, Peter Lawrence, Sean Swenson, Daniel Kennedy, Sam Levis, Erik Kluzek, Lachlan Whyborn, Drew Holzworth, Ian Harman, Naiqing Pan, Shufen Pan for their involvement in the development, use, and analysis of the models and data products used here. ERA5 forcing (Hersbach et al., 2020) was downloaded from the Copernicus Climate Change Service (C3S) Climate Data Store; the results contain modified Copernicus Climate Change Service information 2020, and neither the European Commission nor ECMWF is responsible for any use that may be made of the Copernicus information or data it contains. We thank Kim Currie, Hannelore Theetaert, and Coraline LeseurreLeticia Barbero, Susan Hartman, Anita Flohr, Siyabulela Hamnca, and Melchor González-Dávila, Claire Lo Monaco who contributed to the provision of surface ocean CO_2 observations for the year 20242025 (see Table S8). We also thank Kevin O'Brien and Eugene Burger of NOAA'sNOAA's Pacific Marine Environmental Laboratory and, Alex Kozyr of NOAA'sNOAA's National Centers for Environmental Information, and Steve Jones and Sara Poelmans of the Flanders Marine Institute (VLIZ) for their contribution to surface ocean CO_2 data and metadata

Formatted: Space After: 12 pt

Formatted: Not Superscript/ Subscript

Formatted: Not Superscript/ Subscript

management. We thank the scientists, institutions, and funding agencies responsible for the collection and quality control of the data in SOCAT as well as the International Ocean Carbon Coordination Project (IOCCP) and the Surface Ocean Lower Atmosphere Study (SOLAS) program for their support. ~~ITL and WP thank the CarbonTracker Europe team at Wageningen University, including Remco de Kok, Joram Hooghiem and Auke van der Woude.~~The Surface Ocean CO2 Observing Network (SOCONET), the Surface Ocean CO2 Atlas (SOCAT) and the Surface Ocean CO2 Mapping (SOCOM) program are linked international efforts that, along with additional critical data from satellites, models and re-analysis, enable the routine delivery of ocean carbon and carbonate system data products. The loss of any activity (SOCONET, SOCAT, or SOCOM) or data source (satellite, in situ, or re-analysis) would prevent delivery of data products to global or regional assessments (Global Carbon Budget, IPCC, and others) that guide policy decisions. SOCONET, SOCAT and SOCOM are endorsed by the International Ocean Carbon Coordination Project (IOCCP, an Infrastructural Project of the Scientific Committee on Oceanic Research) and the Global Ocean Observing System (GOOS) Biogeochemistry Panel. The many researchers, funders, and agencies responsible for these activities and data are thanked for their contributions. ITL and WP thank the CarbonTracker Europe team at Wageningen University, including Remco de Kok and Joram Hooghiem. The inverse modelling team thanks all data providers of atmospheric CO2 data provided through multiple ObsPack products. HL thanks ~~Tatiana Ilyina for supporting the coordination of ESMs' contributions to GCBs, and~~ Sebastian Brune and Kristina Frölich for helping with the MPI-ESM1-2-LR assimilation~~.~~ and providing the data. Zhangcai Qin thanks Ziwang Fu ~~and Dr. Yakun Zhu~~ for contributing to the latest LUCE modeling. We thank Ram Alkama ~~and Simone Rossi~~ for helping in filtering SLAND data from DGVMs with managed forest area and Joana Melo for extracting and processing data from NGHGIs. FT ~~acknowledges~~and LC acknowledge support of member countries to the FAO regular budget and FAOSTAT. The conclusions in this paper are the ~~authors'~~authors' only and do not represent FAO views and position on the subject matter. ~~This is PMEL contribution 5802. MC~~The 2025 pCO2 measurements on RV Celtic Explorer were made possible thanks ~~Tobias Steinhoff (MACID),~~to the dedication of the ship's technicians, Lukasz Pawlikowski~~, Ian Murphy~~ and ~~Gordon Furey (P&O Maritime Services),~~Ruahri Strachan, and ~~Aodhan Fitzgerald (Marine Institute) for their~~ the support~~. TG~~ of the Instrumentation and ~~the VLIZ team are thankful to the management group and crew of the research vessels Simon Stevin, Skagerak and Neil Armstrong for all the~~ IT section at P&O Maritime, Galway. WE thanks the Tula Foundation for funding support ~~and help they provided~~. pCO2 measurements on the Marion Dufresne were collected in the frame of the French COOL/OISO long-term monitoring program with support from the National Institute of Sciences of the Universe (INSU), the French Polar Institute (IPEV) and the French Oceanographic Fleet (FOF). ~~AMO thanks the captain and crew on the Sea-Cargo-Express for their help. DP would like to thank Kevin Sullivan for processing and quality controlling AOML data and facilitating submission to SOCATv2025. GR thanks the "Finnmaid science and tech teams" at IOW and SYKE for their support, and is indebted to the crew of the ship and the people involved at Finnlines. IS thanks the captain and crew on the G. O. Sars for their~~

Formatted: Not Superscript/ Subscript

Formatted: Not Superscript/ Subscript

Formatted: Not Superscript/ Subscript

help. BT and EvO thank Australia's Integrated Marine Observing System (IMOS) for sourcing CO_2 data. IMOS is enabled by the National Collaborative Research Infrastructure Strategy (NCRIS). SJV thanks Andrew Marriner for maintaining the pCO_2 underway system on the RV Tangaroa. PCM thanks Tristan Quaife, Eddy Robertson, Emily Black and Anthony Walker for support.The measurements on RV Polarstern are only possible thanks to the dedication of the crew and of Mario Hoppema and Hauke Becker, whom we thank warmly; we also thank Toste Tanhua and skipper Nicolas Lueven for the data collection on Holcim-PRB during the Vendée Globe 2024. Underway data on the RV Sarmiento de Gamboa are collected through the collaboration of the Marine Technology Unit (UTM-CSIC) and the CSIC Interdisciplinary Thematic Platform PTI OCEANS+, together with the involvement of the principal investigators of the MORIA (Leopoldo D. Pena and Isabel Cacho) and DICHOSO (I. Emma Huertas and Antonio Tovar-Sánchez) projects. SJvdV thanks Andrew Marriner of Earth Sciences New Zealand for the maintenance and processing of the underway data collected on board the RV Tangaroa. CFB thanks INIDEP for support. PCM thanks T. Quaife and E. Robertson for support. FC thanks Adrien Martinez who maintained the atmospheric transport model for the CAMS inversion. We acknowledge the contributions of Jeongmin Yun, Anthony Bloom, and Kevin Bowman to the CMS-Flux inversion submission. YNSM thanks Suman Maity who performed theYosuke Niwa for his contribution to the development of NISMON-GOSAT inversion. LFCO2. PP thanks Paul I. Palmer and acknowledges ongoing support fromLiang Feng for his contribution to the National Centre for Earth Observation. UoE inverse framework. We thank Stijn Naus for contributing to the production of CTE2026 and for the inverse model synthesis, and Joram Hooghiem for the development of CTE. Zhe Jin thanks Xiangjun Tian thanks Zhe Jin, Yilong Wang, Hongqin Zhang, Min Zhao, Tao Wang, Jinzhi Ding, and Shilong Piao for their contributions to the GONGGA inversion system. We thank Ning ZengNZ thanks Zhiqiang Liu, Yun Liu, Eugenia Kalnay, and Gassem Asrar for their contributions to the COLA system. CarbonTracker CT2025CT2026 results provided by NOAA GML, Boulder, Colorado, USA from the website at http://carbontracker.noaa.gov.http://carbontracker.noaa.gov (last access: 30 October 2026). FJ thanks Weimin Ju for running the BEPS model. LNRRJ thanks Lorna Nayagam and Shamil Maksyutov, Rajesh Janardanan and Tsuneo Matsunaga for contributingtheir contribution to the NTFVAR inverse model study. YKinversion. BZ acknowledges Bo ZhengYawen Kong from Tsinghua Universitythe Aerospace Information Research Institute for hisher contribution to the THU inversion system. RSA thanks William Merryfield, Woosung Lee, Jason Cole for their help to set up and produce the model runs. The IPSL contribution was achieved thanks to the valuable contributions of Patricia Cadule, Juliette Mignot and Olivier Torres. GAM-GCDAS products. YQ acknowledges contributionsthe help and support of Tianyu Li, Xinyou Chen, Wu Su, Xinru Ding, Shilong Piao and Song Xi Chen. SP thanks Christopher O'Dell for providing the ACOS XCO2 retrievals from Amanda Fay to updating the LDEO-HPD fCO2 product. JRM thanks Gesa Meyer for assistance setting up the DGVM simulations. LMD thanks Pedro. M. S. Monteiro (SCS-SU)OCO-2 and Sandy Thomalla (SOCCO-CSIR) for their continued support to makeGOSAT used to calculate the CSIR-ML6 fCO2 product up-to-date. CFB is grateful to the technicians and crew of the

~~research vessel Víctor Angelescu for all the support and assistance they provided. This is INIDEP contribution 2460~~GRESO CO_2 growth rates.

Financial and computing support

This research was supported by the following sources of funding: ~~Instituto Nacional de Investrigación y Desarrollo Pesquero (~~ INIDEP~~)~~ (Argentina); Joint Technical Commission of the Maritime Front (CTMFM~~,~~) (Argentina-Uruguay~~) (Argentina); Integrated Marine Observing System (IMOS) (Australia);~~); Australian National Environmental Science Program (NESP) (Australia); ~~Research Foundation Flanders (grant no. I001821N) (Belgium); ICOS (~~Integrated ~~Carbon~~Marine Observing System~~) Belgium (Belgium~~ (IMOS, enabled by the National Collaborative Research Infrastructure Strategy, NCRIS) (Australia); Tula Foundation (Canada); National Natural Science Foundation of China (grant no. 42525503); National Natural Science Foundation of China Major Program (grant No. 12292980); National Key Research and Development Program of China (grant no. 2023YFF0805400) (China); ~~Copernicus Atmosphere Monitoring Service, implemented by ECMWF on behalf of the European Commission (Grant no. CAMS2 55 bis) (EC~~National Key R&D Program of China (2025YFF0516904); Ocean Negative Carbon Emissions (ONCE) Program. (China); European Space Agency (OceanSODA project, grant no. 4000112091/14/I-LG) (ESA); European ~~Research Council (~~Space Agency through the OCE Award #2333608. (ESA); THRAC3E (grant no. 4000149569/25/I-AG) (ESA); INFORMA (101060309) (EU); NextGenCarbon (101184989) (EU); SafeNet (101181981) (EU); GreenFeedBack (101056921) (EU); OptimESM (101081193) (EU); ERC-2022-STG OceanPeak~~, grant~~ (Grant 101077209~~) (EC); Horizon Europe (NextGenCarbon: grant no. 101184989) (EC); Horizon Europe (RESCUE: grant no. 101056939) (EC); Horizon 2020 (ESM2025: grant no. 101003536) (EC); Horizon Europe (TRICUSO: grant no. 101199028) (EC); Horizon Europe (GreenFeedBack: grant no. 101056921) (EC); H2020 (JERICO-S3: grant no. 871153) (EC); Horizon Europe (GEORGE: grant no. 101094716) (EC); Horizon Europe (AI4PEX: grant no.101137682) (EC); ; MOB TAC project of the European Copernicus Marine Environment Monitoring Service (EC); Horizon Europe (TipESM: grant no. 101137673) (EC);~~). The work reflects only the authors' view; the European Commission and their executive agency are not responsible for any use that may be made. (EU); This work was funded by the European Union under grant agreement no. 101083922 (OceanICU) and UK Research and Innovation (UKRI) under the UK government's Horizon Europe funding guarantee [grant number 10054454, 10063673, 10064020, 10059241, 10079684, 10059012, 10048179]. Views and opinions expressed are however those of the author(s) only and do not necessarily reflect those of the European Union or European Research Executive Agency. Neither the European Union nor the granting authority can be held responsible for them~~; Climate Space RECCAP 2 (grant no. 4000144908/24/I-LR) (European Space Agency); EO-~~

Formatted: Indent: First line: 0 cm

Formatted: French (France)

Formatted: French (France)

Formatted: Font color: Auto

~~LINCS (European Space Agency); Ocean Carbon for Climate (grant no. 3-18399/24/I-NB) (European Space Agency); Satellite-based observations of Carbon in the Ocean: Pools, Fluxes and Exchanges (grant no. 4000142532/23/I-DT) (European Space Agency); THRAC3E (grant no. 4000149569/25/I-AG) (European Space Agency); ; ICOS~~ . (EU); The Copernicus Marine Environment Monitoring Service implemented by Mercator Ocean on behalf of the European Commission (grant no. 83-CMEMSTAC-MOB). (EU); European Commission (COMFORT project, grant no. 820989) (EU); ClimTip (grant no. 101137601) (EU); GEORGE (Grant id. 101094716) (EU);

Agence Nationale de la Recherche - France 2030 as part of the PEPR TRACCS programme under grant number ANR-22-EXTR-0008 and ANR-22-EXTR-0009. (France); Agence Nationale de la Recherche - France 2030 as part of the PEPR TRACCS programme under grant number ANR-22-EXTR-0009 (France); INSU/CNRS (France); IPEV (France); IFREMER (France); FOF (France); OSU Ecce Terra (France); Deutsche Forschungsgemeinschaft (DFG, German Research Foundation) through TRR 410 WETSCAPES2.0 (grant no. 531801029) (Germany); Deutsches Klimarechenzentrum (DKRZ) (Project: bm0891) (Germany); ~~Federal Ministry of Education and Research (BMBF) (STEPSEC: grant no. 01LS2102A~~Initiative and Networking Fund of the Helmholtz Association (no. VH-NG-19-33) (Germany); BMFTR and BMW (Germany); Helmholtz Association POF-IV (Germany); Icelandic Ministry for the Environment and Natural Resources (Iceland); Department of Agriculture, Food and the Marine ~~Institute~~ (Ireland); ~~Japan~~ Environment Research and Technology Development Fund (ERTDF) of ERCA by Ministry of the Environment of Japan (grant no. JPMEERF24S12206) (Japan); Meteorological ~~Agency~~Research Institute and ~~(Japan); Global Environmental Research Coordination System, Ministry of the Environment (grant nos. E2152 and E2252) (Japan); NIES GOSAT Project (Japan);~~ the Environment Research and Technology Development Fund (JPMEERF24S12200) of the Environmental Restoration and Conservation Agency provided by Ministry of Environment of Japan. (Japan); NIES GOSAT-2 Project, GED (Global Environmental Database) Project and GCP Tsukuba International Office of NIES. (Japan); Global Environmental Research Coordination System, Ministry of the Environment (grant nos. ~~the Environment of Japan (Japan); Environment Research and Technology Development Fund~~MOE1751 and MOE2252) (Japan); Japan Meteorological Agency (Japan); JST CREST (grant no. JPMJCR23J4), JST PRESTO (grant no. JPMJPR23G7), and JSPS KAKENHI (grant no. 23H03516) (Japan); MBIE Strategic Science Investment Fund via the ESNZ Ocean-Climate Interaction programme (New Zeeland); Research Council of Norway (grant no. 352405) (Norway); Norwegian Research Council (grant no. 350390) (Norway); Norwegian Polar Institute (Norway); Research Council of Norway (ICOS-3, grant no. 350341) (Norway); Ministry of Science, Innovation and Universities (projects: MORIA (Grant PID2022-138010OB-I00), DICHOSO (Grant PID2021-125783OB-I00) and FICARAM+ (Grant PID2023-148924OB-I00)) (Spain); ETH Zürich (Switzerland); Schweizerischer Nationalfonds zur Förderung der Wissenschaftlichen Forschung (grant no. PZ00P2_209044 (ArcticECO)) (Switzerland); NERC NCEO (NE/R016518/1) (United Kingdom); Met Office Hadley Centre Climate Programme (HCCP) funded by the UK Department for Business,

Innovation, Science and Trade (DBIST) (United Kingdom); National Centre for Atmospheric Science, a NERC collaborative centre (United Kingdom); Royal Society (grant no. ~~JPMEERF24S12205, Co-PI: P. K. Patra) of the Environmental Restoration and Conservation Agency of Japan, and the Arctic Challenge for Sustainability phase III project (ArCS-3;~~ RSRP\R\241002) (United Kingdom); NERC EXPLANATIONS (grant no. ~~JPMXD1720251001; Co-PI: P. K. Patra) (Japan); Environment Research and Technology Development Fund (grant no. JPMEERF24S12206) of the~~NE/Y005260/1) (United Kingdom); NERC Marine Frontiers (grant no. NE/V011103/1) (United Kingdom); Schmidt Sciences (projects CALIPSO, CLARiTy, and InMOS) (USA); Princeton University High Meadows Environmental ~~Restoration and Conservation Agency of Japan (Japan); Ministry of Business, Innovation and Employment (Strategic Science Investment Fund via the NIWA Ocean-Climate Interaction programme) (New Zealand); Research Council of Norway (ICOS-3, grant no. 350341) (Norway); Research Council of Norway (grant no. 352474) (Norway); Research Council of Norway (grant no. 352204) (Norway); South African Department of Science, Technology and Innovation (grant no. DSI/CON-C3184/2023) (South Africa); UK~~ Institute. We thank Princeton Research Computing, a consortium of groups including the Princeton Institute for Computational Science and Engineering (PICSciE) and the Office of Information Technology's High-Performance Computing Center and Visualization Laboratory at Princeton University. (USA); NOAA, through a University of Miami subaward to the University of Santiago de Compostela under the project "Remote sensing and in situ observations for improved monitoring and forecasting in U.S. near-coastal regions" (Subaward OS00001891). (USA); NOAA grant NA24NESX432C0001 (Cooperative Institute for Satellite Earth System Studies - CISESS) at the University of Maryland/ESSIC (USA); NSF through the LEAP STC (Award #2019625) (USA); NSF National Center for Atmospheric Research ~~and Innovation (Horizon Europe GreenFeedBack: grant no. 10040851) (UK); NCAS at the University of Reading (UK); NERC NE/V011103/1 "Frontiers of instability in marine ecosystems and carbon export"UK Natural Environment~~ , which is a major facility sponsored by the National Science Foundation under Cooperative Agreement No. 1852977 (USA); NASA Land-Cover and Land-Use Change (LCLUC) Program (NASA Grant Nos. 80NSSC24K0920 and 80NSSC25K7497). (USA);

Future of Life Institute (CODEC project) (USA); NOAA Global Ocean Monitoring and Observing Program (Open Funder Registry no. 100018302) (USA); NOAA Ocean Acidification Program (Research Organization Registry (ROR): 02bfn4816) (USA); NOAA Pacific Marine Environmental Laboratory (ROR: 03crn0n59) (USA); NOAA Ocean Acidification Program and Alaska Ocean Observing System (NA21NOS0120094) (USA); NASA Carbon Monitoring System (grant no. 80NSSC25K7221) (USA); NASA Early Career Investigator Program in Earth Science (grant no. ~~Council (NE/V01417X/1) (UK);~~80NSSC24K1632) (USA); NASA GEDI Competed Science Team (grant no. 80NSSC24K0599) (USA);

ORNL Terrestrial Ecosystem Science SFA and Energy Exascale Earth System Model (E3SM) project, funded by the U.S. Department of Energy, Office of Science, Office of Biological and Environmental

Formatted: Space Before: 0 pt, After: 0 pt

Research ~~(USA); NOAA (Global Ocean Monitoring and Observing Program: Open Funder Registry no. 100018302) (USA); NOAA (Ocean Acidification Program: Open Funder Registry no. 100018228) (USA); NOAA (Cooperative Agreement NA20OAR4320472) (USA); NOAA (Cooperative Agreement NA 03 AR4320179) (USA); Alaska Ocean Observing System (USA); NASA Carbon Monitoring System (grant no.~~ Earth Systems Model Development Program area of Earth and Environmental System Modeling. (USA). A portion of this research was carried out~~80NSSC25K7221) (USA); NASA Early Career Investigator Program in Earth Science (grant no. 80NSSC24K1632) (USA); NASA Land Cover and Land Use Change Program (Grants: 80NSSC24K0920 and 80NSSC25K7497) (USA); NSF (Cooperative Agreement No. 1852977) (USA); NASA Orbiting Carbon Observatory Science Team Program (grant no. NNH23ZDA001N OCOST) (USA); NASA Carbon Monitoring System (grant no.NNH22ZDA001N CMS) (USA); Work of J.L. and S.P. was conducted~~ at the Jet Propulsion Laboratory, California Institute of Technology, under ~~a~~contract with the National Aeronautics and Space Administration (80NM0018D0004~~) (USA); NOAA (Cooperative Institute for Marine, Earth and Atmospheric Systems, Award No. NA25NMFX432C0003 T1 01) (USA); NSF (OPP 2329254) (USA); ORNL is managed by UT Battelle, LLC, for the DOE (grant no. DE AC05 1008 00OR22725) (USA); Schmidt Sciences (VESRI CALIPSO) (USA); Schmidt Sciences (OBVI InMOS) (USA); NSF (OPP 1922922) (USA); NOAA grant NA24NESX432C0001 (Cooperative Institute for Satellite Earth System Studies CISESS) (USA); NOAA cooperative agreement NA22OAR4320151 (CIRES: Andrew Jacobson and Xin Lan) (USA); Schmidt Sciences (CLARiTy project, part of the Virtual Institute for the Carbon Cycle) (USA); Schmidt Sciences (COCO2 project, part of the Virtual Institute for the Carbon Cycle) (USA); NSF (LEAP STC Award no 2019625) (USA); NASA (grant no. 80NSSC22K0150) (USA); NOAA (GOMO, grant no. NA24OARX431G0151 T1 01) (USA~~).

~~The US National Science Foundation (grant nos. OPP 1922922, OPP 2329254), a NOAA cooperative agreement, the Cooperative Institute for Marine, Earth and Atmospheric Systems (CIMEAS, grant nos. NA20OAR4320278 T1 01 and NA25NMFX432C0003 T3 01S022); although NSF grants 1922922 and 2329254 and NOAA grants NA20OAR4320278 T1 01 and NA25NMFX432C0003 T3 01S022 have been identified for conflict of interest management based on the overall scope of the project and its potential benefit to the Keeling Curve Foundation, the research findings included in this particular publication may not necessarily relate to the interests of Keeling Curve Foundation. The terms of this arrangement have been reviewed and approved by the University of California, San Diego in accordance with its conflict of interest policies.~~

We also acknowledge support from the following computing facilities: ~~Australian Community Climate and Earth System Simulator National Research Infrastructure (~~

ACCESS-NRI~~) (Australia);~~ and National Computational Infrastructure (NCI) (Australia); ~~High Performance Computing Center (HPCC) of Nanjing University for doing the inversions on its blade cluster system (~~National Large Scientific and Technological Infrastructure: Earth System Numerical

Simulation Facility (China); HPC ~~computing and storage~~ resources ~~by~~from LSCE, IPSL, and GENCI ~~at IDRIS and~~ TGCC ~~thanks to the grant 2024-2201 on the supercomputers Jean Zay's V100 and Joliot Curie's SKL and V100 partitions. (France); The ORCHIDEE simulations were performed using HPC resources from GENCi-TGCC on grant 2024-00006328 (France); IPSL Climate Modelling Centre (https://mesocentre.ipsl.fr) (France); HPC resources~~under grant 06328 from ~~GENCI - TGCC (Grant A005-017403)~~2018 to 2026 (France); Deutsches Klimarechenzentrum (DKRZ) ~~(Projects: bm0891, bm1124 and bg1446)~~granted by its shareholder Max Planck Society under project ID 143 (Germany); NIES Supercomputer system~~, GOSAT Supercomputing Facility (GOCF) (Japan); NEC SX-Aurora TSUBASA at NIES (Japan);Fugaku provided by the RIKEN Center for Computational Science (Project ID: hp250024) (Japan); JAMSTEC's ES4 Super Computer system (Japan);~~ (Japan); UNINETT Sigma2 ~~– the~~, National Infrastructure for High- Performance Computing and Data Storage in Norway (~~Norway); NICIS Centre for High-~~ NN9560K/NS9560K) (Norway); Swiss National Supercomputing Centre (CSCS) under project ID s1323 on Alps (Switzerland); Edinburgh Compute and Data Facility (ECDF, http://www.ecdf.ed.ac.uk/) (United Kingdom); UEA High Performance Computing ~~(South Africa); UK CEDA JASMIN supercomputer (UK);~~cluster (United Kingdom); CEDA JASMIN data analysis facility for environmental science (United Kingdom). This research used resources of the Compute and Data Environment for Science (CADES) at the Oak Ridge National Laboratory ~~(USA); LEAP Pangeo cloud platform (USA);NASA Ames Supercomputers (USA).~~, which is supported by the Office of Science of the U.S. Department of Energy under Contract No. DE-AC05-00OR22725 (USA).

References

Abatzoglou, J. T., Williams, A. P., and Barbero, R.: Global Emergence of Anthropogenic Climate Change in Fire Weather Indices, Geophys. Res. Lett., 46, 326–336, https://doi.org/10.1029/2018GL080959, 2019.

Ahlström, A., Raupach, M. R., Schurgers, G., Smith, B., Arneth, A., Jung, M., Reichstein, M., Canadell, J. G., Friedlingstein, P., Jain, A. K., Kato, E., Poulter, B., Sitch, S., Stocker, B. D., Viovy, N., Wang, Y. P., Wiltshire, A., Zaehle, S., and Zeng, N.: The dominant role of semi-arid ecosystems in the trend and variability of the land CO2 sink, Science, 348, 895–899, https://doi.org/10.1126/science.aaa1668, 2015.

Andela, N., Morton, D. C., Giglio, L., Chen, Y., van der Werf, G. R., Kasibhatla, P. S., DeFries, R. S., Collatz, G. J., Hantson, S., Kloster, S., Bachelet, D., Forrest, M., Lasslop, G., Li, F., Mangeon, S., Melton, J. R., Yue, C., and Randerson, J. T.: A human-driven decline in global burned area, Science, 356, 1356–1362, https://doi.org/10.1126/science.aal4108, 2017.

Andrew, R. M.: A comparison of estimates of global carbon dioxide emissions from fossil carbon sources, Earth Syst. Sci. Data, 12, 1437–1465, https://doi.org/10.5194/essd-12-1437-2020, 2020a.

Andrew, R. M.: Timely estimates of India's annual and monthly fossil CO2 emissions, Earth Syst. Sci. Data, 12, 2411–2421, https://doi.org/10.5194/essd-12-2411-2020, 2020b.

Andrew, R. M.: Towards near real-time, monthly fossil CO2 emissions estimates for the European Union with current-year projections, Atmospheric Pollution Research, 12, 101229, https://doi.org/10.1016/j.apr.2021.101229, 2021.

Andrew, R. M.: ~~., & Peters, G. P.:The~~ Global ~~Carbon Project's fossil~~ CO2 emissions ~~dataset (Version 251022~~from cement production (version 260830) [Data set]. Zenodo. https://doi.org/10.5281/~~zenodo.5569234, 2025~~ZENODO.831454, last access: 30 October 2026, 2026.

Andrew, R. M., & Peters, G. P.:The Global Carbon Project's fossil CO2 emissions dataset (version 2026v11) [Data set]. Zenodo. https://doi.org/10.5281/zenodo.5569234, last access: 30 October 2026, 2026.

Aragão, L. E. O. C., Anderson, L. O., Fonseca, M. G., Rosan, T. M., Vedovato, L. B., Wagner, F. H., Silva, C. V. J., Silva Junior, C. H. L., Arai, E., Aguiar, A. P., Barlow, J., Berenguer, E., Deeter, M. N., Domingues, L. G., Gatti, L., Gloor, M., Malhi, Y., Marengo, J. A., Miller, J. B., Phillips, O. L., and Saatchi, S.: 21st Century drought-related fires counteract the decline of Amazon deforestation carbon emissions, Nat Commun, 9, 536, https://doi.org/10.1038/s41467-017-02771-y, 2018.

Archer, D., Eby, M., Brovkin, V., Ridgwell, A., Cao, L., Mikolajewicz, U., Caldeira, K., Matsumoto, K., Munhoven, G., Montenegro, A., and Tokos, K.: Atmospheric Lifetime of Fossil Fuel Carbon Dioxide, Annu. Rev. Earth Planet. Sci., 37, 117–134, https://doi.org/10.1146/annurev.earth.031208.100206, 2009.

Arneth, A., Sitch, S., Pongratz, J., Stocker, B. D., Ciais, P., Poulter, B., Bayer, A. D., Bondeau, A., Calle, L., Chini, L. P., Gasser, T., Fader, M., Friedlingstein, P., Kato, E., Li, W., Lindeskog, M., Nabel, J. E. M. S., Pugh, T. A. M., Robertson, E., Viovy, N., Yue, C., and Zaehle, S.: Historical carbon dioxide emissions caused by land-use changes are possibly larger than assumed, Nature Geosci, 10, 79–84, https://doi.org/10.1038/ngeo2882, 2017.

~~Asaadi, A., Arora, V. K., Melton, J. R., and Bartlett, P.: An improved parameterization of leaf area index (LAI) seasonality in the Canadian Land Surface Scheme (CLASS) and Canadian Terrestrial Ecosystem Model (CTEM) modelling framework, 15, 6885–6907, https://doi.org/10.5194/bg-15-6885-2018, 2018.~~

Aumont, O., Orr, J. C., Monfray, P., Ludwig, W., Amiotte-Suchet, P., and Probst, J.-L.: Riverine-driven interhemispheric transport of carbon, Global Biogeochem. Cycles, 15, 393–405, https://doi.org/10.1029/1999GB001238, 2001.

Aumont, O., Ethé, C., Tagliabue, A., Bopp, L., and Gehlen, M.: PISCES-v2: an ocean biogeochemical model for carbon and ecosystem studies, 8, 2465–2513, https://doi.org/10.5194/gmd-8-2465-2015, 2015.

Babiker, M., G. Berndes, K. Blok, B. Cohen, A. Cowie, O. Geden, V. Ginzburg, A. Leip, P. Smith, M. Sugiyama, F. Yamba, Al Khourdajie, A., Arneth, A., Lima de Azevedo, I. M., Bataille, C., Beerling, D., Bezner Kerr, R., Bradley, J., Buck, H. J., Cabeza, L. F., Calvin, K., Campbell, D., Carnicer Cols, J., Daioglou, V., Harmsen, M., Höglund-Isaksson, L., House, J. I., Keller, D., de Kleijne, K., Kugelberg, S., Makarov, I., Meza, F., Minx, J. C., Morecroft, M., Nabuurs, G. J., Neufeldt, H., Novikova, A., Nugroho, S. B., Oschlies, A., Parmesan, C., Peters, G. P., Poore, J., Portugal-Pereira, J., Postigo, J. C., Pradhan, P., Renforth, P., Rivera-Ferre, M. G., Roe, S., Singh, P. K., Slade, R., Smith, S. M., Tirado von der Pahlen, M. C., and Toribio Ramirez, D.: Cross sectoral perspectives. In:

Formatted: Font: 10 pt

Formatted: Indent: Left: 0.63 cm, Hanging: 0.63 cm

Formatted: Space Before: 0 pt, After: 8 pt

Formatted: Font: 9 pt

Formatted: Space Before: 0 pt, After: 8 pt

Formatted: Space Before: 0 pt, After: 8 pt

Climate Change 2022: Mitigation of Climate Change. Contribution of Working Group III to the Sixth Assessment Report of the Intergovernmental Panel on Climate Change [P.R. Shukla, J. Skea, R. Slade, A. Al Khourdajie, R. van Diemen, D. McCollum, M. Pathak, S. Some, P. Vyas, R. Fradera, M. Belkacemi, A. Hasija, G. Lisboa, S. Luz, J. Malley, (eds.)]. Cambridge University Press, Cambridge, UK and New York, NY, USA. doi: 10.1017/9781009157926.014, 2022.

Baccini, A., Walker, W., Carvalho, L., Farina, M., Sulla-Menashe, D., and Houghton, R. A.: Tropical forests are a net carbon source based on aboveground measurements of gain and loss, Science, 358, 230–234, https://doi.org/10.1126/science.aam5962, 2017.

Bakker, D. C. E., Pfeil, B., Landa, C. S., Metzl, N., O'Brien, K. M., Olsen, A., Smith, K., Cosca, C., Harasawa, S., Jones, S. D., Nakaoka, S., Nojiri, Y., Schuster, U., Steinhoff, T., Sweeney, C., Takahashi, T., Tilbrook, B., Wada, C., Wanninkhof, R., Alin, S. R., Balestrini, C. F., Barbero, L., Bates, N. R., Bianchi, A. A., Bonou, F., Boutin, J., Bozec, Y., Burger, E. F., Cai, W.-J., Castle, R. D., Chen, L., Chierici, M., Currie, K., Evans, W., Featherstone, C., Feely, R. A., Fransson, A., Goyet, C., Greenwood, N., Gregor, L., Hankin, S., Hardman-Mountford, N. J., Harlay, J., Hauck, J., Hoppema, M., Humphreys, M. P., Hunt, C. W., Huss, B., Ibánhez, J. S. P., Johannessen, T., Keeling, R., Kitidis, V., Körtzinger, A., Kozyr, A., Krasakopoulou, E., Kuwata, A., Landschützer, P., Lauvset, S. K., Lefèvre, N., Lo Monaco, C., Manke, A., Mathis, J. T., Merlivat, L., Millero, F. J., Monteiro, P. M. S., Munro, D. R., Murata, A., Newberger, T., Omar, A. M., Ono, T., Paterson, K., Pearce, D., Pierrot, D., Robbins, L. L., Saito, S., Salisbury, J., Schlitzer, R., Schneider, B., Schweitzer, R., Sieger, R., Skjelvan, I., Sullivan, K. F., Sutherland, S. C., Sutton, A. J., Tadokoro, K., Telszewski, M., Tuma, M., van Heuven, S. M. A. C., Vandemark, D., Ward, B., Watson, A. J., and Xu, S.: A multi-decade record of high-quality CO2 data in version 3 of the Surface Ocean CO2 Atlas (SOCAT), Earth Syst. Sci. Data, 8, 383–413, https://doi.org/10.5194/essd-8-383-2016, 2016.

Bakker, D. C. E., Alin, S. R., ~~Aramaki, T., Barbero, L.,~~ Bates, N. R., Ehmen, T., Gkritzalis, T., Jones, S. D., Kamb, L., Kozyr, A., Lauvset, S. K., Macovei, V. A., Metzl, N., ~~Munro, D. R.,~~ Nakaoka, S.-i., O'Brien, K. M., Olsen, A., Pierrot, D., Poelmans, S., Steinhoff, T., ~~Sullivan, K. F.,~~ Sutton, A. J., Sweeney, C., Takao, S., Telszewski, M., Theetaert, H., Tilbrook, B., Wada, C., Wanninkhof, R., Akl, J., Aramaki, T., Arbilla, L. A., Ávila, R. A., Baier, B. C., ~~Azetsu-Scott, K~~Barbero, L., Battisti, R., Beatty, C. M., Becker, ~~M~~H., Benoit-Cattin, A., Berghoff, C. F., Bittig, H. C., Bonin, J. A~~., Bott, R.~~, Bozzano, R., Burger, E. F., ~~Brunetti, F~~Cai, W.-J., Cantoni, C., Castelli, G., Castro, A., Chambers, D. P., Chierici, M., ~~Corbo, A.,~~ Cronin, M., Cubiella, A. H., Curbelo, D., Curless, S. E., ~~Cross, J. N., Currie, K. I., Dentico, C., Emerson, S.~~ Czyz, C., Diverrès, D., Dougherty, S., ~~R.,~~ Enochs, I., Enright, M. P., Enyo, K., ~~Ericson, Y.,~~ Evans, W., ~~Fay, A. R.,~~ Feely, R. A., Flohr, A., Fragiacomo, E., Frangoulis, C., Fransson, A., Gehrung, M., ~~Giani, M.,~~ Glockzin, M., González, A. G., González-Dávila, M., González-Santana, D., Hales, B., Hamnca, S., ~~Holodkov, N~~Hartman, S. E., Hermes, R., Herndon, J., Hoppema, M., ~~Ibánhez, J. S.~~ Howard, E., Huertas, E., Kerr, R., Kristensen, T. O., Landschützer, P., ~~Kadono, K.,~~ Lee, C., ~~Kamb, L., Kralj,~~ M., ~~Kristensin, T. O., Laudicella, V. A~~Lee, H., Lefèvre, N., Leseurre, C., Lo Monaco, C., Luchetta, A., Maenner Jones, S. M., ~~Maenza, R. A~~Manalang, D., McAuliffe, A. M., Mdokwana, B. W., Monacci, N. M., Monteiro, P. M. S., Morell, J. M., ~~M., Musielewicz, S~~Munro, D. R., Neill, C., Newberger, T., ~~Nojiri, Y., Ohman, M~~Nickford, S., Nillson, E., Noakes, S., Noh, J.-H., Noisel, C., O'Brien, C., ~~., D., Ólafsdóttir, S. R.,~~ Olivier, L., Omar, A., ~~Osborne, J~~Orselli, I., Padin, A., Pena, L. D., Pensieri, S., ~~Petersen, W., Plueddemann, A. J~~Pryterch, J., Rehder, G., ~~Roden, N. P.,~~ Rutgersson, A., Sabine, C. L., Sallée, J.-B., Sanders, R., Santana-Casiano, J. M., Sarpe, D., Schirnik, C., Schlitzer, R., ~~Send, U~~Shadwick, E., Skjelvan, I., ~~Sutherland, S., C.,~~ T'Jampens, M., Tamsitt, V., Toledo Aboy, A. E., Tovar-Sanchez, A., ~~Telszewski, M., Theetaert, H., Tilbrook, B., Trull, T.,~~ Tsanwani, M., Van de Velde, S., Van ~~Heuven, S. M. A. C~~Ooijen, E., Vandemark, D., Veccia, M. H., Voynova, Y. G~~C., Weller, R. A~~., Williams, N. L., and Xu, Y.: Surface Ocean CO2 Atlas Database Version ~~2025 (SOCATv2025~~2026 (SOCATv2026) (NCEI Accession ~~0304549~~0315110), NOAA National Centers for Environmental Information, ~~Dataset, https://doi.org/10.25921/648f-fv35, 2025a~~ [data set], https://doi.org/10.25921/8dba-fr90, 2026a.

Bakker, D. C. E., Alin, S. R., ~~Aramaki, T., Barbero, L.,~~ Bates, N. R., Ehmen, T., Gkritzalis, T., Jones, S. D., Kamb, L., Kozyr, A., Lauvset, S. K., Macovei, V. A., Metzl, N., ~~Munro, D. R.,~~ Nakaoka, S.-i., O'Brien, K. M., Olsen, A., Pierrot, D., Poelmans, S., Steinhoff, T., ~~Sullivan, K. F.,~~ Sutton, A. J., Sweeney, C., Takao, S., Telszewski, M., Theetaert, H., Tilbrook, B., Wada, C., and Wanninkhof, R~~.~~.: SOCAT version ~~2025: Open~~2026: High-quality synthesis products for ocean CO2 ~~data submissions stabilise~~sink quantification, https://socat.info/index.php/posters/, Poster published on ~~05~~16/06/~~2025~~2026. Last access ~~23~~30 October ~~2025, 2025b.~~2026, 2026b

Ballantyne, A. P., Alden, C. B., Miller, J. B., Tans, P. P., and White, J. W. C.: Increase in observed net carbon dioxide uptake by land and oceans during the past 50 years, Nature, 488, 70–72, https://doi.org/10.1038/nature11299, 2012.

Formatted: Space Before: 0 pt, After: 8 pt

Ballantyne, A. P., Andres, R., Houghton, R., Stocker, B. D., Wanninkhof, R., Anderegg, W., Cooper, L. A., DeGrandpre, M., Tans, P. P., Miller, J. B., Alden, C., and White, J. W. C.: Audit of the global carbon budget: estimate errors and their impact on uptake uncertainty, Biogeosciences, 12, 2565–2584, https://doi.org/10.5194/bg-12-2565-2015, 2015.

Bar-On, Y. M.,Li, X., O'Sullivan, M., Wigneron, J-P., Sitch, S., Ciais, P., Frankenberg, C., Fischer, W. W.: Recent gains in global terrestrial carbon stocks are mostly stored in nonliving pools, Science 387, 1291–1295, 2025.

Bastos, A., Hartung, K., Nützel, T. B., Nabel, J. E. M. S., Houghton, R. A., and Pongratz, J.: Comparison of uncertainties in land-use change fluxes from bookkeeping model parameterisation, 12, 745–762, https://doi.org/10.5194/esd-12-745-2021, 2021.

Battle, M. O., Raynor, R., Kesler, S., and Keeling, R.: Technical Note: The impact of industrial activity on the amount of atmospheric O2, Atmospheric Chem. Phys. Discuss., 1–17, https://doi.org/10.5194/acp-2022-765, 2023.

Behncke, J., Ilyina, T., Chegini, F., and Landschützer, P.: Improved air-sea CO2 flux estimates from sailboat measurements, Sci. Adv., 12, eadz1502, https://doi.org/10.1126/sciadv.adz1502, 2026.

Bellenger, H., Bopp, L., Ethé, C., Ho, D., Duvel, J. P., Flavoni, S., Guez, L., Kataoka, T., Perrot, X., Parc, L., and Watanabe, M.: Sensitivity of the Global Ocean Carbon Sink to the Ocean Skin in a Climate Model, J. Geophys. Res. Oceans, 128, e2022JC019479, https://doi.org/10.1029/2022JC019479, 2023.

Bennington, V., Gloege, L., and McKinley, G. A.: Variability in the Global Ocean Carbon Sink From 1959 to 2020 by Correcting Models with Observations, Geophys. Res. Lett., 49, e2022GL098632, https://doi.org/10.1029/2022GL098632, 2022.

Bernardello, R., Sicardi, V., Lapin, V., Ortega, P., Ruprich-Robert, Y., Tourigny, E. and Ferrer, E.: Ocean biogeochemical reconstructions to estimate historical ocean CO 2 uptake. Earth System Dynamics, 15(5), pp.1255-1275, https://doi.org/10.5194/esd-15-1255-2024, 2024.

~~Berthet, S., Séférian, R., Bricaud, C., Chevallier, M., Voldoire, A., and Ethé, C.: Evaluation of an Online Grid-Coarsening Algorithm in a Global Eddy-Admitting Ocean Biogeochemical Model, J. Adv. Model Earth Sy., 11, 1759–1783, https://doi.org/10.1029/2019MS001644, 2019.~~

Bethke, I., Wang, Y., Counillon, F., Keenlyside, N., Kimmritz, M., Fransner, F., Samuelsen, A., Langehaug, H., Svendsen, L., Chiu, P.-G., Passos, L., Bentsen, M., Guo, C., Gupta, A., Tjiputra, J., Kirkevåg, A., Olivié, D., Seland, Ø., Solsvik Vågane, J., Fan, Y., and Eldevik, T.: NorCPM1 and its contribution to CMIP6 DCPP, Geosci. Model Dev., 14, 7073–7116~~, https://doi.org/10.5194/gmd-14-7073-2021,~~, https://doi.org/10.5194/gmd-14-7073-2021, 2021.

Betts, R. A., Jones, C. D., Knight, J. R., Keeling, R. F., and Kennedy, J. J.: El Niño and a record CO2 rise, Nat. Clim. Change, 6, 806–810, https://doi.org/10.1038/nclimate3063, 2016.

Bilbao, R., Wild, S., Ortega, P., Acosta-Navarro, J., Arsouze, T., Bretonnière, P.A., Caron, L.P., Castrillo, M., Cruz-García, R., Cvijanovic, I. and Doblas-Reyes, F.J.: Assessment of a full-field initialised decadal climate prediction system with the CMIP6 version of EC-Earth. Earth System Dynamics Discussions, 2020, pp.1-30, https://doi.org/10.5194/esd-12-173-2021, ~~2020~~2021.

Bloom, A. A. and Williams, M.: Constraining ecosystem carbon dynamics in a data-limited world: integrating ecological "common sense" in a model–data fusion framework, Biogeosciences, 12, 1299–1315, https://doi.org/10.5194/bg-12-1299-2015, 2015.

Bloom, A. A., Exbrayat, J.-F., van der Velde, I. R., Feng, L., and Williams, M.: The decadal state of the terrestrial carbon cycle: Global retrievals of terrestrial carbon allocation, pools, and residence times, Proc. Natl. Acad. Sci., 113, 1285–1290, https://doi.org/10.1073/pnas.1515160113, 2016.

Boer, G. J., Smith, D. M., Cassou, C., Doblas-Reyes, F., Danabasoglu, G., Kirtman, B., Kushnir, Y., Kimoto, M., Meehl, G. A., Msadek, R., Mueller, W. A., Taylor, K. E., Zwiers, F., Rixen, M., Ruprich-Robert, Y., and Eade, R.: The Decadal Climate Prediction Project (DCPP) contribution to CMIP6, Geosci. Model Dev., 9, 3751–3777, https://doi.org/10.5194/gmd-9-3751-2016, 2016.

Boucher, O., Servonnat, J., Albright, A. L., Aumont, O., Balkanski, Y., Bastrikov, V., Bekki, S., Bonnet, R., Bony, S., Bopp, L., Braconnot, P., Brockmann, P., Cadule, P., Caubel, A., Cheruy, F., Codron, F., Cozic, A., Cugnet, D., D'Andrea, F., Davini, P., de Lavergne, C., Denvil, S., Deshayes, J., Devilliers, M., Ducharne, A., Dufresne, J.-L., Dupont, E., Éthé, C., Fairhead, L., Falletti, L., Flavoni, S., Foujols, M.-A., Gardoll, S., Gastineau, G., Ghattas, J., Grandpeix, J.-Y., Guenet, B., Guez, E., Lionel, Guilyardi, E., Guimberteau, M., Hauglustaine, D., Hourdin, F.,

Formatted: Space Before: 0 pt, After: 8 pt

Formatted: Space Before: 0 pt, After: 8 pt

Idelkadi, A., Joussaume, S., Kageyama, M., Khodri, M., Krinner, G., Lebas, N., Levavasseur, G., Lévy, C., Li, L., Lott, F., Lurton, T., Luyssaert, S., Madec, G., Madeleine, J.-B., Maignan, F., Marchand, M., Marti, O., Mellul, L., Meurdesoif, Y., Mignot, J., Musat, I., Ottlé, C., Peylin, P., Planton, Y., Polcher, J., Rio, C., Rochetin, N., Rousset, C., Sepulchre, P., Sima, A., Swingedouw, D., Thiéblemont, R., Traore, A. K., Vancoppenolle, M., Vial, J., Vialard, J., Viovy, N., and Vuichard, N.: Presentation and Evaluation of the IPSL-CM6A-LR Climate Model, J. Adv. Model. Earth Syst., 12, e2019MS002010, https://doi.org/10.1029/2019MS002010, 2020.

Bourgeois, T., Goris, N., Schwinger, J., and Tjiputra, J. F.: Stratification constrains future heat and carbon uptake in the Southern Ocean between 30°S and 55°S, Nat. Commun., 13, 340, https://doi.org/10.1038/s41467-022-27979-5, 2022.

Bourgoin, C., Beuchle, R., Branco, A., Carreiras, J., Ceccherini, G., Oom, D., San-Miguel-Ayanz, J., and Sedano, F.: Extensive fire-driven degradation in 2024 marks worst Amazon forest disturbance in over 2 decades, Biogeosciences, 22, 5247–5256, https://doi.org/10.5194/bg-22-5247-2025, 2025.

Bray, E.: 2017 Minerals Yearbook: Aluminum [Advance Release], Tech. rep., U.S. Geological Survey, https://d9-wret.s3-us-west-2.amazonaws.com/assets/palladium/production/atoms/files/myb1-2017-alumi.pdf, 2020.

Brienen, R. J. W., Caldwell, L., Duchesne, L., Voelker, S., Barichivich, J., Baliva, M., Ceccantini, G., Di Filippo, A., Helama, S., Locosselli, G. M., Lopez, L., Piovesan, G., Schöngart, J., Villalba, R., and Gloor, E.: Forest carbon sink neutralized by pervasive growth-lifespan trade-offs, Nat. Commun., 11, 4241, https://doi.org/10.1038/s41467-020-17966-z, 2020.

Brienen, R. J. W., Phillips, O. L., Feldpausch, T. R., Gloor, E., Baker, T. R., Lloyd, J., Lopez-Gonzalez, G., Monteagudo-Mendoza, A., Malhi, Y., Lewis, S. L., Vásquez Martinez, R., Alexiades, M., Álvarez Dávila, E., Alvarez-Loayza, P., Andrade, A., Aragão, L. E. O. C., Araujo-Murakami, A., Arets, E. J. M. M., Arroyo, L., Aymard C., G. A., Bánki, O. S., Baraloto, C., Barroso, J., Bonal, D., Boot, R. G. A., Camargo, J. L. C., Castilho, C. V., Chama, V., Chao, K. J., Chave, J., Comiskey, J. A., Cornejo Valverde, F., da Costa, L., de Oliveira, E. A., Di Fiore, A., Erwin, T. L., Fauset, S., Forsthofer, M., Galbraith, D. R., Grahame, E. S., Groot, N., Hérault, B., Higuchi, N., Honorio Coronado, E. N., Keeling, H., Killeen, T. J., Laurance, W. F., Laurance, S., Licona, J., Magnussen, W. E., Marimon, B. S., Marimon-Junior, B. H., Mendoza, C., Neill, D. A., Nogueira, E. M., Núñez, P., Pallqui Camacho, N. C., Parada, A., Pardo-Molina, G., Peacock, J., Peña-Claros, M., Pickavance, G. C., Pitman, N. C. A., Poorter, L., Prieto, A., Quesada, C. A., Ramírez, F., Ramírez-Angulo, H., Restrepo, Z., Roopsind, A., Rudas, A., Salomão, R. P., Schwarz, M., Silva, N., Silva-Espejo, J. E., Silveira, M., Stropp, J., Talbot, J., ter Steege, H., Teran-Aguilar, J., Terborgh, J., Thomas-Caesar, R., Toledo, M., Torello-Raventos, M., Umetsu, R. K., van der Heijden, G. M. F., van der Hout, P., Guimarães Vieira, I. C., Vieira, S. A., Vilanova, E., Vos, V. A., and Zagt, R. J.: Long-term decline of the Amazon carbon sink, 519, 344–348, https://doi.org/10.1038/nature14283, 2015.

~~Bronselaer, B., Winton, M., Russell, J., Sabine, C. L., and Khatiwala, S.: Agreement of CMIP5 Simulated and Observed Ocean Anthropogenic CO2 Uptake, Geophys. Res. Lett., 44, 12,298-12,305, https://doi.org/10.1002/2017GL074435, 2017.~~

Bruno, M. and Joos, F.: Terrestrial carbon storage during the past 200 years: A Monte Carlo Analysis of CO 2 data from ice core and atmospheric measurements, Global Biogeochem. Cycles, 11, 111–124, https://doi.org/10.1029/96GB03611, 1997.

Burrows, S. M., Maltrud, M., Yang, X., Zhu, Q., Jeffery, N., Shi, X., Ricciuto, D., Wang, S., Bisht, G., Tang, J., Wolfe, J., Harrop, B. E., Singh, B., Brent, L., Baldwin, S., Zhou, T., Cameron-Smith, P., Keen, N., Collier, N., Xu, M., Hunke, E. C., Elliott, S. M., Turner, A. K., Li, H., Wang, H., Golaz, J.-C., Bond-Lamberty, B., Hoffman, F. M., Riley, W. J., Thornton, P. E., Calvin, K., and Leung, L. R.: The DOE E3SM v1.1 Biogeochemistry Configuration: Description and Simulated Ecosystem-Climate Responses to Historical Changes in Forcing, J. Adv. Model. Earth Syst., 12, e2019MS001766, https://doi.org/10.1029/2019MS001766, 2020.

Bunsen, F., Nissen, C., and Hauck, J.: The Impact of Recent Climate Change on the Global Ocean Carbon Sink. Geophysical Research Letters, 51(4), e2023GL107030, https://doi.org/10.1029/2023GL107030, 2024.

Burton, C., Betts, R., Cardoso, M., Feldpausch, T. R., Harper, A., Jones, C. D., Kelley, D. I., Robertson, E., and Wiltshire, A.: Representation of fire, land-use change and vegetation dynamics in the Joint UK Land Environment Simulator vn4.9 (JULES), Geosci. Model Dev., 12, 179–193, https://doi.org/10.5194/gmd-12-179-2019, 2019.

Burton, C., Lampe, S., Kelley, D. I., Thiery, W., Hantson, S., Christidis, N., Gudmundsson, L., Forrest, M., Burke, E., Chang, J., Huang, H., Ito, A., Kou-Giesbrecht, S., Lasslop, G., Li, W., Nieradzik, L., Li, F., Chen, Y., Randerson, J., Reyer, C. P. O., and Mengel, M.: Global burned area increasingly explained by climate change, Nature Climate Change, https://doi.org/10.1038/s41558-024-02140-w, 2024.

Formatted: Space Before: 0 pt, After: 8 pt

Burton, C., Di Giuseppe, F., Jones, M. W., Kelley, D. I., Barbosa, M. L. F., McNorton, J., Potts, R., Segura-Garcia, C., Abatzoglou, J. T., Alin Rosu, I., Andela, N., Anderson, L. O., Archibald, S., Brambleby, E., Chuvieco, E., Ciavarella, A., Clarke, H., De La Barrera, F., Di Bella, C. M., Di Tomaso, E., Dintwe, K., Doherty, T. S., Donovan, V. M., Eden, J. M., Fernandes, P. M., Fiedler, L., Giglio, L., Haas, O., Hamilton, D., Hantson, S., Harris, S., Hartley, A. J., Keeping, T. R., Kolden, C. A., Kouassi, J.-L., Kukavskaya, E., Lampe, S., Liu, Z., Mataveli, G., Meier, S., Oom, D., Parrington, M., Qu, Y., Resco De Dios, V., Ruffault, J., Sadegh, M., Santín, C., Sedano, F., Shuman, J. K., Silva, P. S., Spuler, F. R., Steinmann, C. B., Tanpipat, V., Torres-Vazquez, M. Á., Turco, M., Van Der Werf, G. R., Van Wees, D., Veraverbeke, S., Wessel, J. B., and Zheng, B.: State of Wildfires 2025–2026, https://doi.org/10.5194/essd-2026-587, 3 August 2026., 2026.

Bushinsky, S. M., Landschützer, P., Rödenbeck, C., Gray, A. R., Baker, D., Mazloff, M. R., Resplandy, L., Johnson, K. S., and Sarmiento, J. L.: Reassessing Southern Ocean Air-Sea CO 2 Flux Estimates With the Addition of Biogeochemical Float Observations, Global Biogeochem. Cycles, 33, 1370–1388, https://doi.org/10.1029/2019GB006176, 2019.

Byrne, B., Liu, J., Bowman, K.W., Pascolini-Campbell, M., Chatterjee, A., Pandey, S., Miyazaki, K., van der Werf, G.R., Wunch, D., Wennberg, P.O., Roehl, C.M., and Sinha, S.: Carbon emissions from the 2023 Canadian wildfires. Nature, 633, 835–839, https://doi.org/10.1038/s41586-024-07878-z, 2024.

Canadell, J. G., Le Quere, C., Raupach, M. R., Field, C. B., Buitenhuis, E. T., Ciais, P., Conway, T. J., Gillett, N. P., Houghton, R. A., and Marland, G.: Contributions to accelerating atmospheric CO2 growth from economic activity, carbon intensity, and efficiency of natural sinks, Proceedings of the National Academy of Sciences, 104, 18866–18870, https://doi.org/10.1073/pnas.0702737104, 2007.

Canadell, J. G., Monteiro, P. M. S., Costa, M. H., Cotrim da Cunha, L., Cox, P. M., Eliseev, A. V., Henson, S., Ishii, M., Jaccard, S., Koven, C., Lohila, A., Patra, P. K., Piao, S., Rogelj, J., Syampungani, S., Zaehle, S., and Zickfeld, K.: Global Carbon and other Biogeochemical Cycles and Feedbacks. In: Climate Change 2021: The Physical Science Basis. Contribution of Working Group I to the Sixth Assessment Report of the Intergovernmental Panel on Climate Change [Masson-Delmotte, V., P. Zhai, A. Pirani, S. L. Connors, C. Péan, S. Berger, N. Caud, Y. Chen, L. Goldfarb, M. I. Gomis, M. Huang, K. Leitzell, E. Lonnoy, J.B.R. Matthews, T. K. Maycock, T. Waterfield, O. Yelekçi, R. Yu and B. Zhou (eds.)]. Cambridge University Press, Cambridge, United Kingdom and New York, NY, USA, pp. 673–816, https://doi.org/10.1017/9781009157896.007., 2021.

Cao, Z., Myers, R. J., Lupton, R. C., Duan, H., Sacchi, R., Zhou, N., Reed Miller, T., Cullen, J. M., Ge, Q., and Liu, G.: The sponge effect and carbon emission mitigation potentials of the global cement cycle, Nat Commun, 11, 3777, https://doi.org/10.1038/s41467-020-17583-w, 2020.

Carbon Monitor: Year in Review: Global carbon emissions and decarbonization in ~~2024~~2025, available at: ~~https://carbonmonitor.org/~~https://carbonmonitor.org/ , last access: ~~23~~30 October ~~2025, 2025~~2026, 2026.

~~Centro Nacional de Monitoramento e Alertas de Desastres Naturais (CEMADEN): Monitoramento de secas e impactos no Brasil - Agosto 2024, available at: https://www.gov.br/cemaden/pt-br/assuntos/monitoramento/monitoramento-de-seca-para-o-brasil/monitoramento-de-secas-e-impactos-no-brasil-agosto-2024, last access: 23 October 2025.~~

~~Céspedes, J., Sylvester, J. M., Pérez-Marulanda, L., Paz-Garcia, P., Reymondin, L., Khodadadi, M., Tello, J. J., and Castro-Nunez, A.: Has global deforestation accelerated due to the COVID-19 pandemic?, J. For. Res., 34, 1153–1165, https://doi.org/10.1007/s11676-022-01561-7, 2023.~~

~~Chandra, N., Patra, P. K., Niwa, Y., Ito, A., Iida, Y., Goto, D., Morimoto, S., Kondo, M., Takigawa, M., Hajima, T., and Watanabe, M.: Estimated regional CO2 flux and uncertainty based on an ensemble of atmospheric CO2 inversions, Atmospheric Chem. Phys., 22, 9215–9243, https://doi.org/10.5194/acp-22-9215-2022, 2022.~~

~~Chatfield, C.: The Holt-Winters Forecasting Procedure, J. Roy. Stat. Soc. C., 27, 264–279, https://doi.org/10.2307/2347162, 1978.~~

Chau, T. T. T., Gehlen, M., and Chevallier, F.: A seamless ensemble-based reconstruction of surface ocean pCO2 and air–sea CO2 fluxes over the global coastal and open oceans, Biogeosciences, 19, 1087–1109, https://doi.org/10.5194/bg-19-1087-2022, 2022.

Chau, T.-T., Gehlen, M., Metzl, N., and Chevallier, F.: CMEMS-LSCE: a global, 0.25°, monthly reconstruction of the surface ocean carbonate system, Earth Syst. Sci. Data, 16, 121–160, https://doi.org/10.5194/essd-16-121-2024, 2024.

Formatted: Space Before: 0 pt, After: 8 pt

Formatted: Font: Cambria Math

Formatted: Space Before: 0 pt, After: 8 pt

Chen, Y., Morton, D.C., Andela, N. Giglio, L., Van Der Werf, G. R., and Randerson, J. T.: A pan-tropical cascade of fire driven by El Niño/Southern Oscillation. *Nature Clim Change* **7**, 906–911. https://doi.org/10.1038/s41558-017-0014-8, 2017.

Chen, Y., Hall, J., Van Wees, D., Andela, N., Hantson, S., Giglio, L., Van Der Werf, G. R., Morton, D. C., and Randerson, J. T.: Multi-decadal trends and variability in burned area from the fifth version of the Global Fire Emissions Database (GFED5), Earth Syst. Sci. Data, 15, 5227–5259, https://doi.org/10.5194/essd-15-5227-2023, 2023.

Chen, Y., Morton, D. C., and Randerson, J. T.: Remote sensing for wildfire monitoring: Insights into burned area, emissions, and fire dynamics, One Earth, 7, 1022–1028, https://doi.org/10.1016/j.oneear.2024.05.014, 2024.

Chen, Y., Van Der Werf, G. R., Mu, M., Van Wees, D., Hall, J. V., Giglio, L., Vernooij, R., Morton, D. C., Xu, L., Liu, T., Scholten, R. C., Coffield, S. R., Follette-Cook, M. B., Ott, L., and Randerson, J. T.: Tracking recent extremes and interannual variability of global fire emissions using a near-real-time extension to the Global Fire Emissions Database, Earth Syst. Sci. Data, 18, 7535–7555, https://doi.org/10.5194/essd-18-7535-2026, 2026.

Chevallier, F., Fisher, M., Peylin, P., Serrar, S., Bousquet, P., Bréon, F.-M., Chédin, A., and Ciais, P.: Inferring CO 2 sources and sinks from satellite observations: Method and application to TOVS data, J. Geophys. Res., 110, D24309, https://doi.org/10.1029/2005JD006390, 2005.

Chevallier, F., Martinez, A., Lloret, Z., Takache, S., and Cozic, A.: Offline Atmospheric Transport on a Global Mesh of Hexagons, JGR Atmospheres, 130, e2025JD043579, https://doi.org/10.1029/2025JD043579, 2025.

Ciais, P., Sabine, C., Bala, G., Bopp, L., Brovkin, V., Canadell, J. G., Chhabra, A., DeFries, R., Galloway, J., Heimann, M., Jones, C., Le Quéré, C., Myneni, R., Piao, S., Thornton, P., Willem, J., Friedlingstein, P., and Munhoven, G.: Carbon and Other Biogeochemical Cycles, in Climate Change 2013: The Physical Science Basis, Contribution of Working Group I to the Fifth Assessment Report of the Intergovernmental Panel on Climate Change, edited by: Intergovernmental Panel on Climate Change, Cambridge University Press, Cambridge, United Kingdom and New York, NY, USA, https://doi.org/10.1017/CBO9781107415324.015, 2013.

Ciais, P., Tan, J., Wang, X., Roedenbeck, C., Chevallier, F., Piao, S.-L., Moriarty, R., Broquet, G., Le Quéré, C., Canadell, J. G., Peng, S., Poulter, B., Liu, Z., and Tans, P.: Five decades of northern land carbon uptake revealed by the interhemispheric CO2 gradient, Nature, 568, 221–225, https://doi.org/10.1038/s41586-019-1078-6, 2019.

Ciais, P., Bastos, A., Chevallier, F., Lauerwald, R., Poulter, B., Canadell, P., Hugelius, G., Jackson, R. B., Jain, A., Jones, M., Kondo, M., Luijkx, I. T., Patra, P. K., Peters, W., Pongratz, J., Petrescu, A. M. R., Piao, S., Qiu, C., Von Randow, C., Regnier, P., Saunois, M., Scholes, R., Shvidenko, A., Tian, H., Yang, H., Wang, X., and Zheng, B.: Definitions and methods to estimate regional land carbon fluxes for the second phase of the REgional Carbon Cycle Assessment and Processes Project (RECCAP-2), Geosci. Model Dev., 15, 1289–1316, https://doi.org/10.5194/gmd-15-1289-2022, 2022.

Ciais, P., Ke, P., Yao, Y., Sitch, S., Li, W., Xu, Y., Du, X., Gui, X., Bastos, A., Zaehle, S., Poulter, B., Colligan, T., van der Woude, A. M., Peters, W., Liu, Z., Jin, Z., Tian, X., Wang, Y., Liu, J., Pandey, S., O'Dell, C., Bian, J., Zhou, C., Miller, J., Lan, X., Goncalves De Souza, J., O'Sullivan, M., Friedlingstein, P., van der Werf, G. R., Peters, G. P., and Chevallier, F.: Low latency global carbon budget indicates reduced land carbon sink in the year 2024, National Science Review, Volume 13, Issue 2, January 2026, nwaf594, https://doi.org/10.1093/nsr/nwaf594.

Collier, N., Hoffman, F. M., Lawrence, D. M., Keppel-Aleks, G., Koven, C. D., Riley, W. J., Mu, M., and Randerson, J. T.: The International Land Model Benchmarking (ILAMB) System: Design, Theory, and Implementation, J. Adv. Model. Earth Syst., 10, 2731–2754, https://doi.org/10.1029/2018MS001354, 2018.

Conchedda, G. and Tubiello, F. N.: Drainage of organic soils and GHG emissions: Validation with country data, Biosphere – Biogeosciences, https://doi.org/10.5194/essd-2020-202, 2020.

Cox, P. M., Pearson, D., Booth, B. B., Friedlingstein, P., Huntingford, C., Jones, C. D., and Luke, C. M.: Sensitivity of tropical carbon to climate change constrained by carbon dioxide variability, Nature, 494, 341–344, https://doi.org/10.1038/nature11882, 2013.

Crisp, D., Dolman, H., Tanhua, T., McKinley, G. A., Hauck, J., Bastos, A., Sitch, S., Eggleston, S., and Aich, V.: How Well Do We Understand the Land-Ocean-Atmosphere Carbon Cycle?, Reviews of Geophysics, 60, e2021RG000736, https://doi.org/10.1029/2021RG000736, 2022.

Formatted: Space Before: 0 pt, After: 8 pt

Formatted: Space Before: 0 pt, After: 8 pt

Formatted: Space Before: 0 pt, After: 8 pt

Formatted: Font: Cambria Math

Formatted: Space Before: 0 pt, After: 8 pt

Danek, C. and Hauck, J.: Contrasting high-latitude mixed layer depth trends in Earth System Models and data products and their impact on temporal pCO2 variability, Clim Dyn, 64, 211, https://doi.org/10.1007/s00382-026-08109-z, 2026.

De Kauwe, M. G., Medlyn, B. E., Zaehle, S., Walker, A. P., Dietze, M. C., Wang, Y.-P., Luo, Y., Jain, A. K., El-Masri, B., Hickler, T., Wårlind, D., Weng, E., Parton, W. J., Thornton, P. E., Wang, S., Prentice, I. C., Asao, S., Smith, B., McCarthy, H. R., Iversen, C. M., Hanson, P. J., Warren, J. M., Oren, R., and Norby, R. J.: Where does the carbon go? A model–data intercomparison of vegetation carbon allocation and turnover processes at two temperate forest free-air CO2 enrichment sites, New Phytol., 203, 883–899, https://doi.org/10.1111/nph.12847, 2014.

Decharme, B., Delire, C., Minvielle, M., Colin, J., Vergnes, J.-P., Alias, A., Saint-Martin, D., Séférian, R., Sénési, S., and Voldoire, A.: Recent Changes in the ISBA-CTRIP Land Surface System for Use in the CNRM-CM6 Climate Model and in Global Off-Line Hydrological Applications, Journal of Advances in Modeling Earth Systems, 11, 1207–1252, https://doi.org/10.1029/2018MS001545, 2019.

Delire, C., Séférian, R., Decharme, B., Alkama, R., Calvet, J.-C., Carrer, D., Gibelin, A.-L., Joetzjer, E., Morel, X., Rocher, M., and Tzanos, D.: The Global Land Carbon Cycle Simulated With ISBA-CTRIP: Improvements Over the Last Decade, J. Adv. Model. Earth Syst., 12, e2019MS001886, https://doi.org/10.1029/2019MS001886, 2020.

Denman, K. L., Brasseur, G., Chidthaisong, A., Ciais, P., Cox, P. M., Dickinson, R. E., Hauglustaine, D., Heinze, C., Holland, E., Jacob, D., Lohmann, U., Ramachandran, S., Leite da Silva Dias, P., Wofsy, S. C., and Zhang, X.: Couplings Between Changes in the Climate System and Biogeochemistry, in: Climate Change 2007: The Physical Science Basis. Contribution of Working Group I to the Fourth Assessment Report of the Intergovernmental Panel on Climate Change, edited by: Solomon, S., Qin, D., Manning, M., Marquis, M., Averyt, K., Tignor, M. M. B., Miller, H. L., and Chen, Z. L., Cambridge University Press, Cambridge, UK and New York, USA, 499–587, ISBN: 9780521705967, 2007.

Denvil-Sommer, A., Gehlen, M., and Vrac, M.: Observation system simulation experiments in the Atlantic Ocean for enhanced surface ocean pCO2 reconstructions, Ocean Sci., 17, 1011–1030, https://doi.org/10.5194/os-17-1011-2021, 2021.

DeVries, T., Holzer, M., and Primeau, F.: Recent increase in oceanic carbon uptake driven by weaker upper-ocean overturning, Nature, 542, 215–218, https://doi.org/10.1038/nature21068, 2017.

DeVries, T.: The oceanic anthropogenic CO 2 sink: Storage, air-sea fluxes, and transports over the industrial era, Global Biogeochem. Cycles, 28, 631–647, https://doi.org/10.1002/2013GB004739, 2014.

DeVries, T., Quéré, C. L., Andrews, O., Berthet, S., Hauck, J., Ilyina, T., Landschützer, P., Lenton, A., Lima, I. D., Nowicki, M., Schwinger, J., and Séférian, R.: Decadal trends in the ocean carbon sink, PNAS, 116, 11646–11651, https://doi.org/10.1073/pnas.1900371116, 2019.

DeVries, T.: Atmospheric CO2 and Sea Surface Temperature Variability Cannot Explain Recent Decadal Variability of the Ocean CO2 Sink, Geophysical Research Letters, 49, e2021GL096018, ~~https://doi.org/10.1029/2021GL096018,~~ https://doi.org/10.1029/2021GL096018, 2022.

DeVries, T., Yamamoto, K., Wanninkhof, R., Gruber, N., Hauck, J., Müller, J. D., Bopp, L., Carroll, D., Carter, B., Chau, T.-T.-T., Doney, S. C., Gehlen, M., Gloege, L., Gregor, L., Henson, S., Kim, J. H., Iida, Y., Ilyina, T., Landschützer, P., Le Quéré, C., Munro, D., Nissen, C., Patara, L., Pérez, F. F., Resplandy, L., Rodgers, K. B., Schwinger, J., Séférian, R., Sicardi, V., Terhaar, J., Triñanes, J., Tsujino, H., Watson, A., Yasunaka, S., and Zeng, J.: Magnitude, trends, and variability of the global ocean carbon sink from 1985-2018, Glob. Biogeochem. Cycles, n/a, e2023GB007780, https://doi.org/10.1029/2023GB007780, 2023.

Döscher, R., Acosta, M., Alessandri, A., Anthoni, P., Arneth, A., Arsouze, T., Bergmann, T., Bernadello, R., Bousetta, S., Caron, L.P. and Carver, G.: The EC-earth3 Earth system model for the climate model intercomparison project 6. Geoscientific Model Development Discussions, 2021, pp.1-90, https://doi.org/10.5194/gmd-15-2973-2022, 2021.

Doney, S. C., Lima, I., Feely, R. A., Glover, D. M., Lindsay, K., Mahowald, N., Moore, J. K., and Wanninkhof, R.: Mechanisms governing interannual variability in upper-ocean inorganic carbon system and air–sea CO2 fluxes: Physical climate and atmospheric dust, Deep Sea Research Part II: Topical Studies in Oceanography, 56, 640–655, https://doi.org/10.1016/j.dsr2.2008.12.006, 2009.

Formatted: Space Before: 0 pt, After: 8 pt

Formatted: Space Before: 0 pt, After: 8 pt

Dong, Y., Bakker, D. C. E., Bell, T. G., Huang, B., Landschützer, P., Liss, P. S., and Yang, M.: Update on the Temperature Corrections of Global Air-Sea CO2 Flux Estimates, Glob. Biogeochem. Cycles, 36, e2022GB007360, https://doi.org/10.1029/2022GB007360, 2022.

Dong, Y., Bakker, D. C. E., Bell, T. G., Yang, M., Landschützer, P., Hauck, J., Rödenbeck, C., Kitidis, V., Bushinsky, S. M., and Liss, P. S. (2024).: Direct observational evidence of strong CO2 uptake in the Southern Ocean. Science Advances., Sci. Adv., 10(30), eadn5781, https://doi.org/10.1126/sciadv.adn5781, 2024a.

Dong, Y., Bakker, D. C. E., and Landschützer, P.: Accuracy of ocean CO2 uptake estimates at a risk by a reduction in the data collection, Geophys. Res. Lett., Geophysical Research Letters, 51, e2024GL108502, https://doi.org/10.1029/2024GL108502, 2024b.

Dorgeist, L., Schwingshackl, C., Bultan, S., and Pongratz, J.: A consistent budgeting of terrestrial carbon fluxes. Nature Communications, 15(1), 7426, https://doi.org/10.1038/s41467-024-51126-x, 2024.

Dou, X., Wang, Y., Ciais, P., Chevallier, F., Davis, S. J., Crippa, M., Janssens-Maenhout, G., Guizzardi, D., Solazzo, E., Yan, F., Huo, D., Zheng, B., Zhu, B., Cui, D., Ke, P., Sun, T., Wang, H., Zhang, Q., Gentine, P., Deng, Z., and Liu, Z.: Near-real-time global gridded daily CO2 emissions, The Innovation, 3, 100182, https://doi.org/10.1016/j.xinn.2021.100182, 2022.

Eckes-Shephard, A. H., Argles, A. P. K., Brzeziecki, B., Cox, P. M., De Kauwe, M. G., Esquivel-Muelbert, A., Fisher, R. A., Hurtt, G. C., Knauer, J., Koven, C. D., Lehtonen, A., Luyssaert, S., Marqués, L., Ma, L., Marie, G., Moore, J. R., Needham, J. F., Olin, S., Peltoniemi, M., Piltz, K., Sato, H., Sitch, S., Stocker, B. D., Weng, E., Zuleta, D., and Pugh, T. A. M. Pugh: Demography, dynamics and data: building confidence for simulating changes in the world's forests, New Phytologist, doi: 10.1111/nph.70643, 2025.

Edwards, M., Geden, O., Gidden, M., Lamb, W. F., Minx, J., Nemet, G. F., Smith, S., Bellamy, R., Brutschin, E., Anadon, L. D., Fuss, S., Grassi, G., Injy Johnstone, Lebling, K., Lunstrum, A., Müller-Hansen, F., Portugal-Pereira, J., Probst, B. Edson, J. B., Jampana, V., Weller, R. S., and Vaughan, N.: The State of Carbon Dioxide Removal - 3rd Edition (2026), https://doi.org/10.17605/OSF.IO/ZRD65, 2026.

A., Bigorre, S. P., Plueddemann, A. J., Fairall, C. W., Miller, S. D., Mahrt, L., Vickers, D., and Hersbach, H.: On the Exchange of Momentum over the Open Ocean, J. Phys. Oceanogr., 43, 1589–1610, https://doi.org/10.1175/JPO-D-12-0173.1, 2013.

EIA: Short-Term Energy Outlook: March 2026. U.S. Energy Information Administration [Data set]. Available at: http://www.eia.gov/forecasts/steo/outlook.cfm, last access: 23 March 2026, 20232026.

Embury, O., Merchant, C.J., Good, S.A., Rayner, N.A., Høyer, J.L., Atkinson, C., Block, T.,Alerskans, E., Pearson, K.J., Worsfold, M. and McCarroll, N. and Donlon, C.: Satellite-based time-series of sea-surface temperature since 1980 for climate applications. Scientific Data, 11(1), 326, https://doi.org/10.1038/s41597-024-03147-w, 2024.

Erb, K.-H., Kastner, T., Luyssaert, S., Houghton, R. A., Kuemmerle, T., Olofsson, P., and Haberl, H.: Bias in the attribution of forest carbon sinks, Nature Clim Change, 3, 854–856, https://doi.org/10.1038/nclimate2004, 2013.

Erb, K.-H., Kastner, T., Plutzar, C., Bais, A. L. S., Carvalhais, N., Fetzel, T., Gingrich, S., Haberl, H., Lauk, C., Niedertscheider, M., Pongratz, J., Thurner, M., and Luyssaert, S.: Unexpectedly large impact of forest management and grazing on global vegetation biomass, Nature, 553, 73–76, https://doi.org/10.1038/nature25138, 2018.

Erb, M. and Marland G.: Global, Regional, and National Fossil-Fuel CO2 Emisisons: 1751-2022 CDIAC-FF, Research Institute for Environment, Energy, and Economics, Appalachian State University. https://rieee.appstate.edu/projects-programs/cdiac/, last access: 23 October 2025, 2025, G.: Global carbon dioxide emissions from 1750 to 2022: the CDIAC-FF annual product, Carbon Res., 5, 65, https://doi.org/10.1007/s44246-026-00304-1, 2026a.

Erb, M. and Marland, G.: Global, Regional, and National Fossil-Fuel CO2 Emissions: 1751-2023 CDIAC-FF, Research Institute for Environment, Energy, and Economics, Appalachian State University, https://rieee.appstate.edu/projects-programs/cdiac/ (last access: 30 October 2026), 2026b.

Eskander, S. M. S. U. and Fankhauser, S.: Reduction in greenhouse gas emissions from national climate legislation, Nat. Clim. Chang., 10, 750–756, https://doi.org/10.1038/s41558-020-0831-z, 2020.

Etheridge, D. M., Steele, L. P., Langenfelds, R. L., Francey, R. J., Barnola, J.-M., and Morgan, V. I.: Natural and anthropogenic changes in atmospheric CO 2 over the last 1000 years from air in Antarctic ice and firn, J. Geophys. Res., 101, 4115–4128, https://doi.org/10.1029/95JD03410, 1996.

Formatted: Space Before: 0 pt, After: 8 pt

Formatted: Space Before: 0 pt, After: 8 pt

Formatted: Space Before: 0 pt, After: 8 pt

Formatted: Space Before: 0 pt, After: 8 pt

Fan, Y., Miguez-Macho, G., Jobbágy, E. G., Jackson, R. B., and Otero-Casal, C.: Hydrologic regulation of plant rooting depth, Proc. Natl. Acad. Sci. ~~FAO, Food and Agriculture Organization of the United Nations (FAO): Impact of the Ukraine-Russia conflict on global food security and related matters under the mandate of the Food and Agriculture Organization of the United Nations (FAO), Hundred and Seventieth Session of the Council, https://www.fao.org/3/nj164en/nj164en.pdf, last access: 23 October 2025, 2023.~~

~~FAO: FAOSTAT Emissions from drained organic soils. Available at http://www.fao.org/faostat/en/#data/GV, last access: 23 October 2025, 2025a.~~

~~FAO: Forest emissions and removals – Global, regional and country trends 1990–2025.FAOSTAT Analytical Briefs, No. 114. Rome., available at: https://doi.org/10.4060/cd7163en, last access: 23 October 2025, 2025b.~~ U.S.A., 114, 10572–10577, https://doi.org/10.1073/pnas.1712381114, 2017.

FAO: Land statistics 2001–2023 – Global, regional and country trends. FAOSTAT Analytical Briefs, No.107. Rome, available at: https://doi.org/10.4060/cd5765en, last access: ~~23~~30 October 2026, 2025~~, 2025e~~.

FAO: FAOSTAT Emissions from drained organic soils. Available at http://www.fao.org/faostat/en/#data/GV, last access: 30 October 2026, 2026a.

FAO: FAOSTAT Land Use. Available at http://www.fao.org/faostat/en/#data/RL, last access: 30 October 2026, 2026b.

FAO: FAOSTAT Emissions totals database, available at~~:~~ https://faostat.fao.org/internal/en/#data/GT, ~~FAO, Rome, ,~~ last access: ~~23~~14 October ~~2025, 2025d~~2026, FAO2026c.

Fay, A. R., Gregor, L., Landschützer, P., McKinley, G. A., Gruber, N., Gehlen, M., Iida, Y., Laruelle, G. G., Rödenbeck, C., Roobaert, A., and Zeng, J.: SeaFlux: harmonization of air–sea CO2 fluxes from surface pCO2 data products using a standardized approach, Earth System Science Data, 13, 4693–4710, https://doi.org/10.5194/essd-13-4693-2021, 2021.

Fay, A. R., McKinley, G. A., Lovenduski, N. S., Eddebbar, Y., Levy, M. N., Long, M. C., Olivarez, H. C., and Rustagi, R. R.: Immediate and Long-Lasting Impacts of the Mt. Pinatubo Eruption on Ocean Oxygen and Carbon Inventories. Global Biogeochemical Cycles, 37(2). https://doi.org/10.1029/2022gb007513, 2023.

Fay, A. R., Carroll, D., McKinley, G. A., Menemenlis, D., and Zhang, H.: Scale-Dependent Drivers of Air-Sea CO2 Flux Variability, Geophysical Research Letters, 51, e2024GL111911, https://doi.org/10.1029/2024GL111911, 2024.

~~Fay, A. R., Heimdal, T. H., Acquaviva, V., Shaum, A. P., and McKinley, G. A.: Sensitivity of Ocean Carbon Sink Estimates to Rare Observations, Geophysical Research Letters, 52, e2025GL117961, https://doi.org/10.1029/2025GL117961, 2025.~~

Felzer, B. S.: Carbon, nitrogen, and water response to climate and land use changes in Pennsylvania during the 20th and 21st centuries, Ecological Modelling, 240, 49–63~~, https://doi.org/10.1016/j.ecolmodel.2012.05.003.,~~ https://doi.org/10.1016/j.ecolmodel.2012.05.003, 2012.

Felzer, B. S. and Jiang, M.: Effect of Land Use and Land Cover Change in Context of Growth Enhancements in the United States Since 1700: Net Source or Sink?, JGR Biogeosciences, 123, 3439–3457~~,~~ ~~https://doi.org/10.1029/2017JG004378.,~~ https://doi.org/10.1029/2017JG004378, 2018.

Felzer, B. S., Cronin, T. W., Melillo, J. M., Kicklighter, D. W., and Schlosser, C. A.: Importance of carbon-nitrogen interactions and ozone on ecosystem hydrology during the 21st century, J. Geophys. Res., 114, 2008JG000826~~, https://doi.org/10.1029/2008JG000826.,~~ https://doi.org/10.1029/2008JG000826, 2009.

Felzer, B. S., Cronin, T. W., Melillo, J. M., Kicklighter, D. W., Schlosser, C. A., and Dangal, S. R. S.: Nitrogen effect on carbon-water coupling in forests, grasslands, and shrublands in the arid western United States, J. Geophys. Res., 116, G03023~~, https://doi.org/10.1029/2010JG001621.,~~ https://doi.org/10.1029/2010JG001621, 2011.

~~Feng, L., Palmer, P. I., Bösch, H., and Dance, S.: Estimating surface CO2 fluxes from space-borne CO2 dry air mole fraction observations using an ensemble Kalman Filter, Atmospheric Chem. Phys., 9, 2619–2633, https://doi.org/10.5194/acp-9-2619-2009, 2009.~~

Feng, L., Palmer, P. I., Parker, R. J., Deutscher, N. M., Feist, D. G., Kivi, R., Morino, I., and Sussmann, R.: Estimates of European uptake of CO2 inferred from GOSAT XCO2 retrievals: sensitivity to measurement bias inside and outside Europe, Atmos. Chem. Phys., 16, 1289–1302, https://doi.org/10.5194/acp-16-1289-2016, 2016.

Formatted: Space Before: 0 pt, After: 8 pt

Formatted: Space Before: 0 pt, After: 8 pt, Border: Top: (No border), Bottom: (No border), Left: (No border), Right: (No border), Between : (No border)

Formatted: Space Before: 0 pt, After: 8 pt

Formatted: Font: Cambria Math

Formatted: Font: Cambria Math

Formatted: Space Before: 0 pt, After: 8 pt

Formatted: Font: Cambria Math

Formatted: Space Before: 0 pt, After: 8 pt

Fernández-Blanco, R., Rodríguez-Gómez, N., Pozo, D., Costescu, A., and Bolado-Lavín, R.: Natural gas consumption estimation in the European Union, Energy Reports, 11, 558–566, https://doi.org/10.1016/j.egyr.2023.12.011, 2024.

Fisher, R. A., Muszala, S., Verteinstein, M., Lawrence, P., Xu, C., McDowell, N. G., Knox, R. G., Koven, C., Holm, J., Rogers, B. M., Spessa, A., Lawrence, D., and Bonan, G.: Taking off the training wheels: the properties of a dynamic vegetation model without climate envelopes, CLM4.5(ED), Geosci. Model Dev., 8, 3593–3619, https://doi.org/10.5194/gmd-8-3593-2015, 2015.

Flanagan, D.: 2017 Minerals Yearbook: Copper [Advance Release], Tech. rep., U.S. Geological Survey, https://pubs.usgs.gov/myb/vol1/2017/myb1-2017-copper.pdf, 2021.

Ford, D. J., Blannin, J., Watts, J., Watson, A. J., Landschützer, P., Jersild, A., and Shutler, J. D.: A Comprehensive Analysis of Air-Sea CO2 Flux Uncertainties Constructed From Surface Ocean Data Products, Global Biogeochemical Cycles, 38, e2024GB008188, https://doi.org/10.1029/2024GB008188, 2024.

Ford, D.J., Shutler, J.D., Blanco-Sacristán, J. et al. Enhanced ocean CO2 uptake due to near-surface temperature gradients. Nat. Geosci. 17, 1135–1140 . https://doi.org/10.1038/s41561-024-01570-7,https://doi.org/10.1038/s41561-024-01570-7, 2024a

Ford, D. J., Shutler, J. D., Holding, T., Sims, R. P., Ashton, I., Woolf, D. K., Goddijn-Murphy, L., Bakker, D. C. E., Sabine, C., Merchant, C. J., Embury, O., Dong, Y., and Wanninkhof, R.: Recalculating the Surface Ocean CO2 Atlas (SOCAT) to a sea surface temperature climate data record, Sci Data, 13, 1329, https://doi.org/10.1038/s41597-026-07532-5, 2026a.

Ford, D. J., Shutler, J. D., Ashton, I., Sims, R. Ford, D. J., Shutler, J. D., Ashton, I., Sims, R. P., and Holding, T.: Recalculated (depth and temperature consistent) surface ocean CO_2 atlas (SOCAT) version 20252026 (v0-1),) [Data set], Zenodo, https://doi.org/10.5281/ZENODO.15656803, 2025 20757579, 2026b.

Forkel, M., Carvalhais, N., Rödenbeck, C., Keeling, R., Heimann, M., Thonicke, K., Zaehle, S., and Reichstein, M.: Enhanced seasonal CO2 exchange caused by amplified plant productivity in northern ecosystems, Science, 351, 696–699, https://doi.org/10.1126/science.aac4971, 2016.

Forster, P. M., Smith, C., Walsh, T., Lamb, W. F., Lamboll, R., Cassou, C., Hauser, M., Hausfather, Z., Lee, J.-Y., Palmer, M. D., Von Schuckmann, K., Slangen, A. B. A., Szopa, S., Trewin, B., Yun, J., Gillett, N. P., Jenkins, S., Matthews, H. D., Raghavan, K., Ribes, A., Rogelj, J., Rosen, D., Zhang, X., Allen, M., Aleluia Reis, L., Andrew, R. M., Betts, R. A., Borger, A., Broersma, J. A., Burgess, S. N., Cheng, L., Friedlingstein, P., Domingues, C. M., Gambarini, M., Gasser, T., Gütschow, J., Ishii, M., Kadow, C., Kennedy, J., Killick, R. E., Krummel, P. B., Liné, A., Monselesan, D. P., Morice, C., Mühle, J., Naik, V., Peters, G. P., Pirani, A., Pongratz, J., Minx, J. C., Rigby, M., Rohde, R., Savita, A., Seneviratne, S. I., Thorne, P., Wells, C., Western, L. M., Van Der Werf, G. R., Wijffels, S. E., Masson-Delmotte, V., and Zhai, P.: Indicators of Global Climate Change 2024: annual update of key indicators of the state of the climate system and human influence, Earth Syst. Sci. Data, 17, 2641–2680, https://doi.org/10.5194/essd-17-2641-2025, https://doi.org/10.5194/essd-17-2641-2025, 2025.

Forster, P. M., Walsh, T., Smith, C., Lamb, W. F., Lamboll, R., Cassou, C., Hauser, M., Hausfather, Z., Lee, J.-Y., Palmer, M. D., Von Schuckmann, K., Slangen, A. B. A., Szopa, S., Trewin, B., Yun, J., Gillett, N. P., Jenkins, S., Matthews, H. D., Raghavan, K., Ribes, A., Rogelj, J., Rosen, D., Zhang, X., Allen, M., Andrew, R. M., Atkinson, C., Betts, R. A., Bombelli, A., Burgess, S. N., Cheng, L., Claxton, H. E., Friedlingstein, P., Frölicher, T. L., Domingues, C. M., Gasser, T., Gregory, C. H., Hoesly, R. M., Huppmann, D., Ishii, M., Kadow, C., Karwat, A., Kennedy, J., Killick, R. E., Kovilakam, M. V. M., Krummel, P. B., Lan, X., Lamarque, J.-F., Liné, A., Martín-Míguez, B., Monselesan, D. P., Morice, C., Mühle, J., Mussak, P., Peters, G. P., Pirani, A., Pongratz, J., Rigby, M., Rohde, R., Savita, A., Seneviratne, S. I., Smith, S. J., Taha, G., Tassone, C., Thorne, P., Wells, C., Western, L. M., Van Der Werf, G. R., Wijffels, S. E., Zecchetto, M., Zhong, J., Zhang, X.-Y., Masson-Delmotte, V., and Zhai, P.: Indicators of Global Climate Change 2025: annual update of key indicators of the state of the climate system and human influence, Earth Syst. Sci. Data, 18, 3889–3933, https://doi.org/10.5194/essd-18-3889-2026, 2026.

Friedlingstein, P., Houghton, R. A., Marland, G., Hackler, J., Boden, T. A., Conway, T. J., Canadell, J. G., Raupach, M. R., Ciais, P., and Le Quéré, C.: Update on CO2 emissions, Nature Geosci, 3, 811–812, https://doi.org/10.1038/ngeo1022, 2010.

Friedlingstein, P., Andrew, R. M., Rogelj, J., Peters, G. P., Canadell, J. G., Knutti, R., Luderer, G., Raupach, M. R., Schaeffer, M., van Vuuren, D. P., and Le Quéré, C.: Persistent growth of CO2 emissions and implications for reaching climate targets, Nature Geosci, 7, 709–715, https://doi.org/10.1038/ngeo2248, 2014.

Formatted: Space Before: 0 pt, After: 8 pt

Formatted: Font: Cambria Math

Formatted: Space Before: 0 pt, After: 8 pt

Formatted: Space Before: 0 pt, After: 8 pt

Formatted: Space Before: 0 pt, After: 8 pt

Friedlingstein, P., Jones, M. W., O'Sullivan, M., Andrew, R. M., Hauck, J., Peters, G. P., Peters, W., Pongratz, J., Sitch, S., Le Quéré, C., Bakker, D. C. E., Canadell, J. G., Ciais, P., Jackson, R. B., Anthoni, P., Barbero, L., Bastos, A., Bastrikov, V., Becker, M., Bopp, L., Buitenhuis, E., Chandra, N., Chevallier, F., Chini, L. P., Currie, K. I., Feely, R. A., Gehlen, M., Gilfillan, D., Gkritzalis, T., Goll, D. S., Gruber, N., Gutekunst, S., Harris, I., Haverd, V., Houghton, R. A., Hurtt, G., Ilyina, T., Jain, A. K., Joetzjer, E., Kaplan, J. O., Kato, E., Klein Goldewijk, K., Korsbakken, J. I., Landschützer, P., Lauvset, S. K., Lefèvre, N., Lenton, A., Lienert, S., Lombardozzi, D., Marland, G., McGuire, P. C., Melton, J. R., Metzl, N., Munro, D. R., Nabel, J. E. M. S., Nakaoka, S.-I., Neill, C., Omar, A. M., Ono, T., Peregon, A., Pierrot, D., Poulter, B., Rehder, G., Resplandy, L., Robertson, E., Rödenbeck, C., Séférian, R., Schwinger, J., Smith, N., Tans, P. P., Tian, H., Tilbrook, B., Tubiello, F. N., van der Werf, G. R., Wiltshire, A. J., and Zaehle, S.: Global Carbon Budget 2019, Earth Syst. Sci. Data, 11, 1783–1838, https://doi.org/10.5194/essd-11-1783-2019, 2019.

Friedlingstein, P., O'Sullivan, M., Jones, M. W., Andrew, R. M., Hauck, J., Olsen, A., Peters, G. P., Peters, W., Pongratz, J., Sitch, S., Le Quéré, C., Canadell, J. G., Ciais, P., Jackson, R. B., Alin, S., Aragão, L. E. O. C., Arneth, A., Arora, V., Bates, N. R., Becker, M., Benoit-Cattin, A., Bittig, H. C., Bopp, L., Bultan, S., Chandra, N., Chevallier, F., Chini, L. P., Evans, W., Florentie, L., Forster, P. M., Gasser, T., Gehlen, M., Gilfillan, D., Gkritzalis, T., Gregor, L., Gruber, N., Harris, I., Hartung, K., Haverd, V., Houghton, R. A., Ilyina, T., Jain, A. K., Joetzjer, E., Kadono, K., Kato, E., Kitidis, V., Korsbakken, J. I., Landschützer, P., Lefèvre, N., Lenton, A., Lienert, S., Liu, Z., Lombardozzi, D., Marland, G., Metzl, N., Munro, D. R., Nabel, J. E. M. S., Nakaoka, S.-I., Niwa, Y., O'Brien, K., Ono, T., Palmer, P. I., Pierrot, D., Poulter, B., Resplandy, L., Robertson, E., Rödenbeck, C., Schwinger, J., Séférian, R., Skjelvan, I., Smith, A. J. P., Sutton, A. J., Tanhua, T., Tans, P. P., Tian, H., Tilbrook, B., van der Werf, G., Vuichard, N., Walker, A. P., Wanninkhof, R., Watson, A. J., Willis, D., Wiltshire, A. J., Yuan, W., Yue, X., and Zaehle, S.: Global Carbon Budget 2020, Earth Syst. Sci. Data, 12, 3269–3340, https://doi.org/10.5194/essd-12-3269-2020, 2020.

Friedlingstein, P., Jones, M. W., O'Sullivan, M., Andrew, R. M., Bakker, D. C. E., Hauck, J., Le Quéré, C., Peters, G. P., Peters, W., Pongratz, J., Sitch, S., Canadell, J. G., Ciais, P., Jackson, R. B., Alin, S. R., Anthoni, P., Bates, N. R., Becker, M., Bellouin, N., Bopp, L., Chau, T. T. T., Chevallier, F., Chini, L. P., Cronin, M., Currie, K. I., Decharme, B., Djeutchouang, L. M., Dou, X., Evans, W., Feely, R. A., Feng, L., Gasser, T., Gilfillan, D., Gkritzalis, T., Grassi, G., Gregor, L., Gruber, N., Gürses, Ö., Harris, I., Houghton, R. A., Hurtt, G. C., Iida, Y., Ilyina, T., Luijkx, I. T., Jain, A., Jones, S. D., Kato, E., Kennedy, D., Klein Goldewijk, K., Knauer, J., Korsbakken, J. I., Körtzinger, A., Landschützer, P., Lauvset, S. K., Lefèvre, N., Lienert, S., Liu, J., Marland, G., McGuire, P. C., Melton, J. R., Munro, D. R., Nabel, J. E. M. S., Nakaoka, S.-I., Niwa, Y., Ono, T., Pierrot, D., Poulter, B., Rehder, G., Resplandy, L., Robertson, E., Rödenbeck, C., Rosan, T. M., Schwinger, J., Schwingshackl, C., Séférian, R., Sutton, A. J., Sweeney, C., Tanhua, T., Tans, P. P., Tian, H., Tilbrook, B., Tubiello, F., van der Werf, G. R., Vuichard, N., Wada, C., Wanninkhof, R., Watson, A. J., Willis, D., Wiltshire, A. J., Yuan, W., Yue, C., Yue, X., Zaehle, S., and Zeng, J.: Global Carbon Budget 2021, Earth Syst. Sci. Data, 14, 1917–2005, https://doi.org/10.5194/essd-14-1917-2022, 2022a.

Friedlingstein, P., O'Sullivan, M., Jones, M. W., Andrew, R. M., Gregor, L., Hauck, J., Le Quéré, C., Luijkx, I. T., Olsen, A., Peters, G. P., Peters, W., Pongratz, J., Schwingshackl, C., Sitch, S., Canadell, J. G., Ciais, P., Jackson, R. B., Alin, S. R., Alkama, R., Arneth, A., Arora, V. K., Bates, N. R., Becker, M., Bellouin, N., Bittig, H. C., Bopp, L., Chevallier, F., Chini, L. P., Cronin, M., Evans, W., Falk, S., Feely, R. A., Gasser, T., Gehlen, M., Gkritzalis, T., Gloege, L., Grassi, G., Gruber, N., Gürses, Ö., Harris, I., Hefner, M., Houghton, R. A., Hurtt, G. C., Iida, Y., Ilyina, T., Jain, A. K., Jersild, A., Kadono, K., Kato, E., Kennedy, D., Klein Goldewijk, K., Knauer, J., Korsbakken, J. I., Landschützer, P., Lefèvre, N., Lindsay, K., Liu, J., Liu, Z., Marland, G., Mayot, N., McGrath, M. J., Metzl, N., Monacci, N. M., Munro, D. R., Nakaoka, S., Niwa, Y., O'Brien, K., Ono, T., Palmer, P. I., Pan, N., Pierrot, D., Pocock, K., Poulter, B., Resplandy, L., Robertson, E., Rödenbeck, C., Rodriguez, C., Rosan, T. M., Schwinger, J., Séférian, R., Shutler, J. D., Skjelvan, I., Steinhoff, T., Sun, Q., Sutton, A. J., Sweeney, C., Takao, S., Tanhua, T., Tans, P. P., Tian, X., Tian, H., Tilbrook, B., Tsujino, H., Tubiello, F., van der Werf, G. R., Walker, A. P., Wanninkhof, R., Whitehead, C., Willstrand Wranne, A., Wright, R., Yuan, W., Yue, C., Yue, X., Zaehle, S., Zeng, J., and Zheng, B.: Global Carbon Budget 2022, Earth Syst. Sci. Data, 14, 4811–4900, https://doi.org/10.5194/essd-14-4811-2022, 2022b.

Friedlingstein, P., O'Sullivan, M., Jones, M. W., Andrew, R. M., Bakker, D. C. E., Hauck, J., Landschützer, P., Le Quéré, C., Luijkx, I. T., Peters, G. P., Peters, W., Pongratz, J., Schwingshackl, C., Sitch, S., Canadell, J. G., Ciais, P., Jackson, R. B., Alin, S. R., Anthoni, P., Barbero, L., Bates, N. R., Becker, M., Bellouin, N., Decharme, B., Bopp, L., Brasika, I. B. M., Cadule, P., Chamberlain, M. A., Chandra, N., Chau, T.-T.-T., Chevallier, F., Chini, L. P., Cronin, M., Dou, X., Enyo, K., Evans, W., Falk, S., Feely, R. A., Feng, L., Ford, D. J., Gasser, T., Ghattas, J., Gkritzalis, T., Grassi, G., Gregor, L., Gruber, N., Gürses, Ö., Harris, I., Hefner, M., Heinke, J., Houghton, R. A., Hurtt, G. C., Iida, Y., Ilyina, T., Jacobson, A. R., Jain, A. K., Jarníková, T., Jersild, A., Jiang, F., Jin, Z., Joos, F., Kato, E., Keeling, R. F., Kennedy, D., Klein Goldewijk, K., Knauer, J., Korsbakken, J. I., Körtzinger, A., Lan, X., Lefèvre, N., Li, H., Liu, J., Liu, Z., Ma, L., Marland, G., Mayot, N., McGuire, P. C., McKinley, G. A., Meyer, G.,

Morgan, E. J., Munro, D. R., Nakaoka, S., Niwa, Y., O'Brien, K. M., Olsen, A., Omar, A. M., Ono, T., Paulsen, M., Pierrot, D., Pocock, K., Poulter, B., Powis, C. M., Rehder, G., Resplandy, L., Robertson, E., Rödenbeck, C., Rosan, T. M., Schwinger, J., Séférian, R., Smallman, T. L., Smith, S. M., Sospedra-Alfonso, R., Sun, Q., Sutton, A. J., Sweeney, C., Takao, S., Tans, P. P., Tian, H., Tilbrook, B., Tsujino, H., Tubiello, F., van der Werf, G. R., van Ooijen, E., Wanninkhof, R., Watanabe, M., Wimart-Rousseau, C., Yang, D., Yang, X., Yuan, W., Yue, X., Zaehle, S., Zeng, J., and Zheng, B.: Global Carbon Budget 2023, Earth Syst. Sci. Data, 15, 5301–5369, https://doi.org/10.5194/essd-15-5301-2023, 2023.

Friedlingstein, P., O'Sullivan, M., Jones, M. W., Andrew, R. M., Hauck, J., Landschützer, P., Le Quéré, C., Li, H., Luijkx, I. T., Olsen, A., Peters, G. P., Peters, W., Pongratz, J., Schwingshackl, C., Sitch, S., Canadell, J. G., Ciais, P., Jackson, R. B., Alin, S. R., Arneth, A., Arora, V., Bates, N. R., Becker, M., Bellouin, N., Berghoff, C. F., Bittig, H. C., Bopp, L., Cadule, P., Campbell, K., Chamberlain, M. A., Chandra, N., Chevallier, F., Chini, L. P., Colligan, T., Decayeux, J., Djeutchouang, L. M., Dou, X., Duran Rojas, C., Enyo, K., Evans, W., Fay, A. R., Feely, R. A., Ford, D. J., Foster, A., Gasser, T., Gehlen, M., Gkritzalis, T., Grassi, G., Gregor, L., Gruber, N., Gürses, Ö., Harris, I., Hefner, M., Heinke, J., Hurtt, G. C., Iida, Y., Ilyina, T., Jacobson, A. R., Jain, A. K., Jarníková, T., Jersild, A., Jiang, F., Jin, Z., Kato, E., Keeling, R. F., Klein Goldewijk, K., Knauer, J., Korsbakken, J. I., Lan, X., Lauvset, S. K., Lefèvre, N., Liu, Z., Liu, J., Ma, L., Maksyutov, S., Marland, G., Mayot, N., McGuire, P. C., Metzl, N., Monacci, N. M., Morgan, E. J., Nakaoka, S.-I., Neill, C., Niwa, Y., Nützel, T., Olivier, L., Ono, T., Palmer, P. I., Pierrot, D., Qin, Z., Resplandy, L., Roobaert, A., Rosan, T. M., Rödenbeck, C., Schwinger, J., Smallman, T. L., Smith, S. M., Sospedra-Alfonso, R., Steinhoff, T., Sun, Q., Sutton, A. J., Séférian, R., Takao, S., Tatebe, H., Tian, H., Tilbrook, B., Torres, O., Tourigny, E., Tsujino, H., Tubiello, F., van der Werf, G., Wanninkhof, R., Wang, X., Yang, D., Yang, X., Yu, Z., Yuan, W., Yue, X., Zaehle, S., Zeng, N., and Zeng, J.: Global Carbon Budget 2024, Earth Syst. Sci. Data, 17, 965–1039~~, https://doi.org/10.5194/essd-17-965-2025~~,, https://doi.org/10.5194/essd-17-965-2025, 2025a.

Friedlingstein, P. ,Le Quéré, C., O'Sullivan, M., Hauck, J., Landschützer, P., Luijkx, I.T., Li, H., van der Woude, A., Schwingshackl, C., Pongratz, P., Regnier, P., Andrew, R.M., Bakker, D.C.E., Canadell, J.G., Ciais, P., Gasser, T., Jones, M.W., Lan, X., Morgan, E., Olsen, A., Peters, G.P., Peters, W., Sitch, S., and Tian, H.: Emerging climate impact on carbon sinks in a consolidated carbon budget, Nature, https://doi.org/10.1038/s41586-025-09802-5, 2025b.

Friedlingstein, P., O'Sullivan, M., Jones, M. W., Andrew, R. M., Bakker, D. C. E., Hauck, J., Landschützer, P., Le Quéré, C., Li, H., Luijkx, I. T., Peters, G. P., Peters, W., Pongratz, J., Schwingshackl, C., Sitch, S., Canadell, J. G., Ciais, P., Aas, K., Alin, S. R., Anthoni, P., Barbero, L., Bates, N. R., Bellouin, N., Benoit-Cattin, A., Berghoff, C. F., Bernardello, R., Bopp, L., Brasika, I. B. M., Chamberlain, M. A., Chandra, N., Chevallier, F., Chini, L. P., Collier, N. O., Colligan, T. H., Cronin, M., Djeutchouang, L. M., Dou, X., Enright, M. P., Enyo, K., Erb, M., Evans, W., Feely, R. A., Feng, L., Ford, D. J., Foster, A., Fransner, F., Gasser, T., Gehlen, M., Gkritzalis, T., Goncalves De Souza, J., Grassi, G., Gregor, L., Gruber, N., Guenet, B., Gürses, Ö., Harrington, K., Harris, I., Heinke, J., Hurtt, G. C., Iida, Y., Ilyina, T., Ito, A., Jacobson, A. R., Jain, A. K., Jarníková, T., Jersild, A., Jiang, F., Jones, S. D., Kato, E., Keeling, R. F., Klein Goldewijk, K., Knauer, J., Kong, Y., Korsbakken, J. I., Koven, C., Kunimitsu, T., Lan, X., Liu, J., Liu, Z., Liu, Z., Lo Monaco, C., Ma, L., Marland, G., McGuire, P. C., McKinley, G. A., Melton, J. R., Monacci, N., Monier, E., Morgan, E. J., Munro, D. R., Müller, J. D., Nakaoka, S.-I., Nayagam, L. R., Niwa, Y., Nutzel, T., Olsen, A., Omar, A. M., Pan, N., Pandey, S., Pierrot, D., Qin, Z., Regnier, P., Rehder, G., Resplandy, L., Roobaert, A., Rosan, T. M., Rödenbeck, C., Schwinger, J., Skjelvan, I., Smallman, T. L., Spada, V., Sreeush, M. G., Sun, Q., Sutton, A. J., Sweeney, C., Swingedouw, D., Séférian, R., Takao, S., Tatebe, H., Tian, H., Tian, X., Tilbrook, B., Tsujino, H., Tubiello, F., ~~van~~Van Ooijen, E., ~~van der~~Van Der Werf, G. R., ~~van de~~Van De Velde, S. J., Walker, A. P., Wanninkhof, R., Yang, X., Yuan, W., Yue, X., and Zeng, J~~.: Supplemental data of the~~.: Global Carbon Budget 2025, ~~ICOS-ERIC Carbon Portal~~Earth Syst. Sci. Data, 18, 3211–3288, https://doi.org/10.~~18160/GCP-2025, 2025c~~5194/essd-18-3211-2026, 2026a.

Friedlingstein, P., O'Sullivan, M., Andrew, R. M., Hauck, J., Jones, M. W., Landschützer, P., Le Quéré, C., Li, H., Luijkx, I. T., Olsen, A., Peters, G. P., Peters, W., Pongratz, J., Schwingshackl, C., Sitch, S., Canadell, J. G., Ciais, P., Aas, K., Alin, S. R., Arora, V., Bates, N. R., Bedard, K., Martin Belda, D., Bellouin, N., Benoit-Cattin, A., Berghoff, C. F., Berthet, S., Bopp, L., Brasika, I. B. M., Burke, E., Casse, L., Chamberlain, M. A., Chevallier, F., Chini, L. P., Cronin, M., Curless, S. E., DeVries, T., Ehmen, T., Enright, M. P., Enyo, K., Erb, M., Evans, W., Fay, A. R., Felzer, B., Ford, D. J., Foster, A., Fransner, F., Fransson, A., Friedman, A., Gasser, T., Gehlen, M., Gkritzalis, T., Grassi, G., Gregor, L., Gruber, N., Gürses, Ö., Hao, W., Harrington, K., Heinke, J., Hurtt, G. C., Ilyina, T., Ito, A., Jacobson, A. R., Jain, A. K., Janardanan, R. R., Jarníková, T., Jersild, A., Jiang, F., Jin, Z., Kamb, L., Kato, E., Keeling, R. F., Klein Goldewijk, K., Knauer, J., Korsbakken, J. I., Kunimitsu, T., Lan, X., Lapin, V., Lauvset, S. K., Le Chevère, S., Lee, W.-S., Liao, E., Liu, J., Liu, Z., Luyssaert, S., Ma, L., Maity, S., Marland, G., McGuire, P. C., Metzl, N., Mignot, J., Monacci, N. M., Morgan, E. J., Müller, J. D., Munro, D. R., Muramatsu, M., Nakaoka, S.-I., Neill, C., Nützel, T., Olivier, L., Osborn, T., Padín, X. A., Palmer, P. I., Pandey, S., Pierrot, D., Poulter, B., Qin, Z., Qiu, Y., Rehder, G., Resplandy, L., Rödenbeck, C., Roobaert, A., Rosan, T. M.,

Rossi, S., Schwinger, J., Seeberg, G., Séférian, R., Shadwick, E. H., Skjelvan, I., Slominska-Durdasiak, K., Smallman, T. L., Sreeush, M. G., Sun, Q., Sutton, A. J., Sweeney, C., Takao, S., Tatebe, H., Terhaar, J., Tian, H., Tilbrook, B., Toyoda, T., Triñanes, J. A., Tubiello, F., van der Werf, G. R., van der Woude, A. M., van de Velde, S. J., Walker, A. P., Wanninkhof, R., Yang, X., Yuan, W., Yue, X., Zeng, J., Zheng, N., and Zheng, B.: Supplemental data of the Global Carbon Budget 2026, ICOS-ERIC Carbon Portal [data set], https://doi.org/10.18160/GCP-2026, 2026b.

Fu, W., Moore, J. K., Primeau, F., Collier, N., Ogunro, O. O., Hoffman, F. M., and Randerson, J. T.: Evaluation of Ocean Biogeochemistry and Carbon Cycling in CMIP Earth System Models With the International Ocean Model Benchmarking (IOMB) Software System, JGR Oceans, 127, e2022JC018965, https://doi.org/10.1029/2022JC018965, 2022.

Ganzenmüller, R., Bultan, S., Winkler, K., Fuchs, R., Zabel, F., and Pongratz, J.: Land-use change emissions based on high-resolution activity data substantially lower than previously estimated, Environ. Res. Lett., 17, 064050, https://doi.org/10.1088/1748-9326/ac70d8, 2022.

Gasser, T., Crepin, L., Quilcaille, Y., Houghton, R. A., Ciais, P., and Obersteiner, M.: Historical CO2 emissions from land use and land cover change and their uncertainty, Biogeosciences, 17, 4075–4101, https://doi.org/10.5194/bg-17-4075-2020, 2020.

Gaubert, B., Stephens, B. B., Basu, S., Chevallier, F., Deng, F., Kort, E. A., Patra, P. K., Peters, W., Rödenbeck, C., Saeki, T., Schimel, D., Van der Laan-Luijkx, I., Wofsy, S., and Yin, Y.: Global atmospheric CO2 inverse models converging on neutral tropical land exchange, but disagreeing on fossil fuel and atmospheric growth rate, Biogeosciences, 16, 117–134, https://doi.org/10.5194/bg-16-117-2019, 2019.

Gauthier, C. B., Melton, J. R., Meyer, G., Raj Deepak, S. N., and Sonnentag, O.: Parameter Optimization for Global Soil Carbon Simulations: Not a Simple Problem, J Adv Model Earth Syst, 17, e2024MS004577~~,~~ ~~https://doi.org/10.1029/2024MS004577,~~, https://doi.org/10.1029/2024MS004577, 2025.

GCP: The Global Carbon Budget 2007, available at: http://www.globalcarbonproject.org/carbonbudget/archive.htm, last access: ~~23~~30 October ~~2025, 2007~~2026, 2008.

Giglio, L., Schroeder, W., and Justice, C. O.: The collection 6 MODIS active fire detection algorithm and fire products, Remote Sensing of Environment, 178, 31–41, https://doi.org/10.1016/j.rse.2016.02.054, 2016.

Giglio, L., Boschetti, L., Roy, D. P., Humber, M. L., and Justice, C. O.: The Collection 6 MODIS burned area mapping algorithm and product, Remote Sensing of Environment, 217, 72–85, https://doi.org/10.1016/j.rse.2018.08.005, 2018.

Gitz V, Ciais P. Amplifying effects of land-use change on future atmospheric CO2 levels. Global Biogeochemical Cycles. ~~https://doi.org/10.1029/2002GB001963,~~https://doi.org/10.1029/2002GB001963, 2003.

Gloege, L., McKinley, G. A., Landschützer, P., Fay, A. R., Frölicher, T. L., Fyfe, J. C., Ilyina, T., Jones, S., Lovenduski, N. S., Rodgers, K. B., Schlunegger, S., and Takano, Y.: Quantifying Errors in Observationally Based Estimates of Ocean Carbon Sink Variability, Global Biogeochem. Cy., 35, e2020GB006788, https://doi.org/10.1029/2020GB006788, 2021.

Gloege, L., Yan, M., Zheng, T., and McKinley, G. A.: Improved Quantification of Ocean Carbon Uptake by Using Machine Learning to Merge Global Models and pCO2 Data, J. Adv. Model. Earth Syst., 14, e2021MS002620, https://doi.org/10.1029/2021MS002620, 2022.

~~Golar, G., Malik, A., Muis, H., Herman, A., Nurudin, N., and Lukman, L.: The social-economic impact of COVID-19 pandemic: implications for potential forest degradation, Heliyon, 6, e05354, https://doi.org/10.1016/j.heliyon.2020.e05354, 2020.~~

Goris, N., Tjiputra, J. F., Olsen, A., Schwinger, J., Lauvset, S. K., and Jeansson, E.: Constraining Projection-Based Estimates of the Future North Atlantic Carbon Uptake, J. Clim., 31, 3959–3978, https://doi.org/10.1175/JCLI-D-17-0564.1, 2018.

Grassi, G., House, J., Kurz, W. A., Cescatti, A., Houghton, R. A., Peters, G. P., Sanz, M. J., Viñas, R. A., Alkama, R., Arneth, A., Bondeau, A., Dentener, F., Fader, M., Federici, S., Friedlingstein, P., Jain, A. K., Kato, E., Koven, C. D., Lee, D., Nabel, J. E. M. S., Nassikas, A. A., Perugini, L., Rossi, S., Sitch, S., Viovy, N., Wiltshire, A., and Zaehle, S.: Reconciling global-model estimates and country reporting of anthropogenic forest CO2 sinks, Nature Clim Change, 8, 914–920, https://doi.org/10.1038/s41558-018-0283-x, 2018.

Formatted: Space Before: 0 pt, After: 8 pt

Formatted: Font: Cambria Math

Formatted: Space Before: 0 pt, After: 8 pt

Formatted: Space Before: 0 pt, After: 8 pt

Grassi, G., Stehfest, E., Rogelj, J., van Vuuren, D., Cescatti, A., House, J., Nabuurs, G.-J., Rossi, S., Alkama, R., Viñas, R. A., Calvin, K., Ceccherini, G., Federici, S., Fujimori, S., Gusti, M., Hasegawa, T., Havlik, P., Humpenöder, F., Korosuo, A., Perugini, L., Tubiello, F. N., and Popp, A.: Critical adjustment of land mitigation pathways for assessing countries' climate progress, Nat. Clim. Chang., 11, 425–434, https://doi.org/10.1038/s41558-021-01033-6, 2021.

Grassi, G., Schwingshackl, C., Gasser, T., Houghton, R. A., Sitch, S., Canadell, J. G., Cescatti, A., Ciais, P., Federici, S., Friedlingstein, P., Kurz, W. A., Sanz Sanchez, M. J., Abad Viñas, R., Alkama, R., Bultan, S., Ceccherini, G., Falk, S., Kato, E., Kennedy, D., Knauer, J., Korosuo, A., Melo, J., McGrath, M. J., Nabel, J. E. M. S., Poulter, B., Romanovskaya, A. A., Rossi, S., Tian, H., Walker, A. P., Yuan, W., Yue, X., and Pongratz, J.: Harmonising the land-use flux estimates of global models and national inventories for 2000–2020, Earth Syst. Sci. Data, 15, 1093–1114, https://doi.org/10.5194/essd-15-1093-2023, 2023.

Grassi, G., Peters, G. P., Canadell, J. G., Cescatti, A., Federici, S., Gidden, M. J., Harris, N., Herold, M., Krug, T., O'Sullivan, M., Pongratz, J., Sanz, M. J., Schwingshackl, C., and Van Vuuren, D.: Improving land-use emission estimates under the Paris Agreement, Nat Sustain, 8, 579–581~~, https://doi.org/10.1038/s41893-025-01565-1,~~ https://doi.org/10.1038/s41893-025-01565-1, 2025.

Graven, H. D., Keeling, R. F., Piper, S. C., Patra, P. K., Stephens, B. B., Wofsy, S. C., Welp, L. R., Sweeney, C., Tans, P. P., Kelley, J. J., Daube, B. C., Kort, E. A., Santoni, G. W., and Bent, J. D.: Enhanced Seasonal Exchange of CO2 by Northern Ecosystems Since 1960, Science, 341, 1085–1089, https://doi.org/10.1126/science.1239207, 2013.

Gregor, L., Lebehot, A. D., Kok, S., and Scheel Monteiro, P. M.: A comparative assessment of the uncertainties of global surface ocean CO2 estimates using a machine-learning ensemble (CSIR-ML6 version 2019a)–have we hit the wall?. Geoscientific Model Development, 12(12), 5113-5136, https://doi.org/10.5194/gmd-12-5113-2019, 2019.

Gregor, L. and Gruber, N.: OceanSODA-ETHZ: a global gridded data set of the surface ocean carbonate system for seasonal to decadal studies of ocean acidification, Earth System Science Data, 13, 777–808, https://doi.org/10.5194/essd-13-777-2021, 2021.

Gregor, L., Shutler, J., and Gruber, N.: High-resolution variability of the ocean carbon sink. Global Biogeochemical Cycles, 38(8), e2024GB008127, https://doi.org/10.1029/2024GB008127, 2024.

Gruber, N., Gloor, M., Mikaloff Fletcher, S. E., Doney, S. C., Dutkiewicz, S., Follows, M. J., Gerber, M., Jacobson, A. R., Joos, F., Lindsay, K., Menemenlis, D., Mouchet, A., Müller, S. A., Sarmiento, J. L., and Takahashi, T.: Oceanic sources, sinks, and transport of atmospheric CO2, Global Biogeochemical Cycles, 23, GB1005, https://doi.org/10.1029/2008GB003349, 2009.

Gruber, N., Bakker, D. C. E., DeVries, T., Gregor, L., Hauck, J., Landschützer, P., McKinley, G. A., and Müller, J. D.: Trends and variability in the ocean carbon sink, Nat. Rev. Earth Environ., 4, 119–134, https://doi.org/10.1038/s43017-022-00381-x, 2023.

Gruber, N., Clement, D., Carter, B. R., Feely, R. A., van Heuven, S., Hoppema, M., Ishii, M., Key, R. M., Kozyr, A., Lauvset, S. K., Lo Monaco, C., Mathis, J. T., Murata, A., Olsen, A., Perez, F. F., Sabine, C. L., Tanhua, T., and Wanninkhof, R.: The oceanic sink for anthropogenic CO2 from 1994 to 2007, 363, 1193–1199, https://doi.org/10.1126/science.aau5153, 2019.

Guan, D., Liu, Z., Geng, Y., Lindner, S., and Hubacek, K.: The gigatonne gap in China's carbon dioxide inventories, Nature Clim Change, 2, 672–675, https://doi.org/10.1038/nclimate1560, 2012.

Gulev, S. K., Thorne, P. W., Ahn, J., Dentener, F. J., Domingues, C. M., Gerland, S., Gong, D. S., Kaufman, S., Nnamchi, H. C., Quaas, J., Rivera, J. A., Sathyendranath, S., Smith, S. L., Trewin, B., von Shuckmann, K., and Vose, R. S.: Changing State of the Climate System. In: Climate Change 2021: The Physical Science Basis. Contribution of Working Group I to the Sixth Assessment Report of the Intergovernmental Panel on Climate Change [Masson-Delmotte, V., Zhai, P., Pirani, A., Connors, S. L., Péan, C., Berger, S., Caud, N., Chen, Y., Goldfarb, L., Gomis, M. I., Huang, M., Leitzell, K., Lonnoy, E., Matthews, J.B.R., Maycock, T.K., Waterfield, T., Yelekçi, O., Yu, R. and Zhou, B. (eds.)]. Cambridge University Press, Cambridge, United Kingdom and New York, NY, USA, pp. 287–422, https://doi.org/10.1017/9781009157896.004, 2021.

~~Guo, R., Wang, J., Bing, L., Tong, D., Ciais, P., Davis, S. J., Andrew, R. M., Xi, F., and Liu, Z.: Global CO2 uptake by cement from 1930 to 2019, 13, 1791–1805, https://doi.org/10.5194/essd-13-1791-2021, 2021.~~

Formatted: Space Before: 0 pt, After: 8 pt

Formatted: Font: Cambria Math

Formatted: Space Before: 0 pt, After: 8 pt

Formatted: Space Before: 0 pt, After: 8 pt

Gürses, Ö., Oziel, L., Karakuş, O., Sidorenko, D., Völker, C., Ye, Y., Zeising, M., Butzin, M., and Hauck, J.: Ocean biogeochemistry in the coupled ocean–sea ice–biogeochemistry model FESOM2.1–REcoM3, Geosci. Model Dev., 16, 4883–4936, https://doi.org/10.5194/gmd-16-4883-2023, 2023.

Gütschow, J., Jeffery, M. L., Gieseke, R., Gebel, R., Stevens, D., Krapp, M., and Rocha, M.: The PRIMAP-hist national historical emissions time series, 8, 571–603, https://doi.org/10.5194/essd-8-571-2016, 2016.

Gütschow, J~~., Busch, D~~. and Pflüger, M.: The PRIMAP-hist national historical emissions time series (1750-~~2023~~2025) v2.~~6, Zenodo~~8 (v2.8) [Data set], Zenodo, https://doi.org/10.5281/~~zenodo.13752654, 2023.~~ ZENODO.22876287, 2026.

Hall, B. D., Crotwell, A. M., Kitzis, D. R., Mefford, T., Miller, B. R., Schibig, M. F., and Tans, P. P.: Revision of the World Meteorological Organization Global Atmosphere Watch (WMO/GAW) CO2 calibration scale, 14, 3015–3032, https://doi.org/10.5194/amt-14-3015-2021, 2021.

Hansis, E., Davis, S. J., and Pongratz, J.: Relevance of methodological choices for accounting of land use change carbon fluxes, Global Biogeochem. Cycles, 29, 1230–1246, https://doi.org/10.1002/2014GB004997, 2015.

Hauck, J., Nissen, C., Landschützer, P., Rödenbeck, C., Bushinsky, S., and Olsen, A.: Sparse observations induce large biases in estimates of the global ocean CO2 sink: an ocean model subsampling experiment, Philos. Trans. R. Soc. Math. Phys. Eng. Sci., 381, 20220063, https://doi.org/10.1098/rsta.2022.0063, 2023a.

Hauck, J., Gregor, L., Nissen, C., Patara, L., Hague, M., Mongwe, P., Bushinsky, S., Doney, S. C., Gruber, N., Le Quéré, C., Manizza, M., Mazloff, M., Monteiro, P. M. S., and Terhaar, J.: The Southern Ocean Carbon Cycle 1985–2018: Mean, Seasonal Cycle, Trends, and Storage. Global Biogeochemical Cycles, 37(11), e2023GB007848, https://doi.org/10.1029/2023GB007848, 2023b.

Hauck, J., Zeising, M., Le Quéré, C., Gruber, N., Bakker, D. C. E., Bopp, L., Chau, T. T. T., Gürses, Ö., Ilyina, T., Landschützer, P., Lenton, A., Resplandy, L., Rödenbeck, C., Schwinger, J., and Séférian, R.: Consistency and Challenges in the Ocean Carbon Sink Estimate for the Global Carbon Budget, Front. Mar. Sci., 7, 571720, https://doi.org/10.3389/fmars.2020.571720, 2020.

Hauck, J., Landschützer, P., Le Chevere, S., Roobaert, A., Berthet, S., Bopp, Laurent ., Chamberlain, M., DeVries, T., Fay, A., Ford, D. J., Gehlen, M., Gregor, L., Gruber, N., Gürses, Ö., Ilyina, T., Jarnikova, T., Jersild, A., Liao, E., Muramatsu, M., Resplandy, L., Rödenbeck, C., Schwinger, J., Takahiro, T., Triñanes, J., Zeng, J.: Global Carbon Budget Ocean - Models and data sets for the ocean sink estimate in the Global Carbon Budget 2026 [Dataset]. Zenodo. https://doi.org/10.5281/zenodo.23723209, 2026.

Haverd, V., Smith, B., Nieradzik, L., Briggs, P. R., Woodgate, W., Trudinger, C. M., Canadell, J. G., and Cuntz, M.: A new version of the CABLE land surface model (Subversion revision r4601) incorporating land use and land cover change, woody vegetation demography, and a novel optimisation-based approach to plant coordination of photosynthesis, Geosci. Model Dev., 11, 2995–3026, https://doi.org/10.5194/gmd-11-2995-2018, 2018.

Heimdal, T. H., McKinley, G. A., Sutton, A. J., Fay, A. R., and Gloege, L.: Assessing improvements in global ocean p CO2 machine learning reconstructions with Southern Ocean autonomous sampling, Biogeosciences, 21, 2159–2176, https://doi.org/10.5194/bg-21-2159-2024, 2024.

Heinke, J., Rolinski, S., and Müller, C.: Modelling the role of livestock grazing in C and N cycling in grasslands with LPJmL5.0-grazing, Geosci. Model Dev., 16, 2455–2475, https://doi.org/10.5194/gmd-16-2455-2023, 2023.

Heinke, J., Schaphoff, S., Wirth, S. B., and Müller, C.: Revised nitrogen balance for plant photosynthesis and growth in the dynamic global vegetation, hydrology and agriculture model LPJmL (5.10), https://doi.org/10.5194/egusphere-2026-4549, 28 September 2026., 2026.

Hersbach, H., Bell, B., Berrisford, P., Hirahara, S., Horányi, A., Muñoz-Sabater, J., Nicolas, J., Peubey, C., Radu, R., Schepers, D., Simmons, A., Soci, C., Abdalla, S., Abellan, X., Balsamo, G., Bechtold, P., Biavati, G., Bidlot, J., Bonavita, M., Chiara, G., Dahlgren, P., Dee, D., Diamantakis, M., Dragani, R., Flemming, J., Forbes, R., Fuentes, M., Geer, A., Haimberger, L., Healy, S., Hogan, R. J., Hólm, E., Janisková, M., Keeley, S., Laloyaux, P., Lopez, P., Lupu, C., Radnoti, G., Rosnay, P., Rozum, I., Vamborg, F., Villaume, S., and Thépaut, J.: The ERA5 global reanalysis, Q.J.R. Meteorol. Soc., 146, 1999–2049, https://doi.org/10.1002/qj.3803, 2020.

Hickler, T., Smith, B., Prentice, I. C., Mjöfors, K., Miller, P., Arneth, A., and Sykes, M. T.: CO2 fertilization in temperate FACE experiments not representative of boreal and tropical forests, Glob. Change Biol., 14, 1531–1542, https://doi.org/10.1111/j.1365-2486.2008.01598.x, 2008.

Formatted: Space Before: 0 pt, After: 8 pt

Hoesly, R., Smith, S. J., Ahsan, H., Prime, N., O'Rourke, P., Crippa, M., Klimont, Z., Guizzardi, D., Feng, L., Harkins, C., M., Smith, S. J., Feng, L., MCDONALD, B., and Wang, S.: CEDS v_2025_03_18 Aggregate Data (v_2025_03_18) [Data set], Zenodo, https://doi.org/10.5281/ZENODO.15059443, 2025. Klimont, Z., Janssens-Maenhout, G., Pitkanen, T., Seibert, J. J., Vu, L., Andres, R. J., Bolt, R. M., Bond, T. C., Dawidowski, L., Kholod, N., Kurokawa, J., Li, M., Liu, L., Lu, Z., Moura, M. C. P., O'Rourke, P. R., and Zhang, Q.: Historical (1750–2014) anthropogenic emissions of reactive gases and aerosols from the Community Emissions Data System (CEDS), Geosci. Model Dev., 11, 369–408, https://doi.org/10.5194/gmd-11-369-2018, 2018.

Hoesly, R., Smith, S. J., Prime, N., Ahsan, H., Suchyta, H., O'Rourke, P., Crippa, M., Klimont, Z., Guizzardi, D., Behrendt, J., Feng, L., Hollitzer, H. A. L., Patara, L., Terhaar, J., and Oschlies, A.: Competing effects of wind and buoyancy forcing on ocean oxygen trends in recent decades, Nat Commun, 15, 9264, https://doi.org/10.1038/s41467-024-53557-y, 2024.

Holzer, M., DeVries, T., and De Lavergne, C.: Diffusion controls the ventilation of a Pacific Shadow Zone above abyssal overturning, Nat Commun, 12, 4348, https://doi.org/10.1038/s41467-021-24648-x, 2021.

Harkins, C., McDonald, B., Mott, A., McDuffie, A., Nicholson, M. and Wang, S.: CEDS v_2024_07_08 Release Emission Data, Zenodo [Data set], https://doi.org/10.5281/zenodo.12803196, 2024.

Hong, C., Burney, J. A., Pongratz, J., Nabel, J. E. M. S., Mueller, N. D., Jackson, R. B., and Davis, S. J.: Global and regional drivers of land-use emissions in 1961–2017, Nature, 589, 554–561, https://doi.org/10.1038/s41586-020-03138-y, 2021.

Holding, T., Ashton, I. G., Shutler, J. D., Land, P. E., Nightingale, P. D., Rees, A. P., Brown, I., Piolle, J.-F., Kock, A., Bange, H. W., Woolf, D. K., Goddijn-Murphy, L., Pereira, R., Paul, F., Girard-Ardhuin, F., Chapron, B., Rehder, G., Ardhuin, F., and Donlon, C. J.: The FluxEngine air–sea gas flux toolbox: simplified interface and extensions for in situ analyses and multiple sparingly soluble gases, Ocean Sci., 15, 1707–1728, https://doi.org/10.5194/os-15-1707-2019, 2019.

Hoppe, J., Hinder, B., Rafaty, R., Patt, A., and Grubb, M.: Three Decades of Climate Mitigation Policy: What Has It Delivered?, Annu. Rev. Environ. Resour., 48, 615–650, https://doi.org/10.1146/annurev-environ-112321-103821, https://doi.org/10.1146/annurev-environ-112321-103821, 2023.

Houghton, R. A. and Castanho, A.: Annual emissions of carbon from land use, land-use change, and forestry from 1850 to 2020, Earth Syst. Sci. Data, 15, 2025–2054, https://doi.org/10.5194/essd-15-2025-2023, 2023.

Houghton, R. A., House, J. I., Pongratz, J., van der Werf, G. R., DeFries, R. S., Hansen, M. C., Le Quéré, C., and Ramankutty, N.: Carbon emissions from land use and land-cover change, Biogeosciences, 9, 5125–5142, https://doi.org/10.5194/bg-9-5125-2012, 2012.

Houghton, R. A. and Nassikas, A. A.: Global and regional fluxes of carbon from land use and land cover change 1850-2015: Carbon Emissions From Land Use, Global Biogeochem. Cycles, 31, 456–472, https://doi.org/10.1002/2016GB005546, 2017.

Huang, B., Thorne, P. W., Banzon, V. F., Boyer, T., Chepurin, G., Lawrimore, J. H., Menne, M. J., Smith, T. M., Vose, R. S., and Zhang, H.-M.: NOAA Extended Reconstructed Sea Surface Temperature (ERSST), Version 5, National Centers for Environmental Information [data set], https://doi.org/10.7289/V5T72FNM, 2017.

Hubau, W., Lewis, S.L., Phillips, O.L., Affum-Baffoe, K., Beeckman, H., Cuní-Sanchez, A., Daniels, A.K., Ewango, C.E.N., Fauset, S., Mukinzi, J.M., Sheil, D., Sonké, B., Sullivan, M.J.P., Sunderland, T.C.H., Taedoumg, H., Thomas, S.C., White, L.J.T., Abernethy, K.A., Adu-Bredu, S., Amani, C.A., Baker, T.R., Banin, L.F., Baya, F., Begne, S.K., Bennett, A.C., Benedet, F., Bitariho, R., Bocko, Y.E., Boeckx, P., Boundja, P., Brienen, R.J.W., Brncic, T., Chezeaux, E., Chuyong, G.B., Clark, C.J., Collins, M., Comiskey, J.A., Coomes, D.A., Dargie, G.C., de Haulleville, T., Kamdem, M.N.D., Doucet, J.-L., Esquivel-Muelbert, A., Feldpausch, T.R., Fofanah, A., Foli, E.G., Gilpin, M., Gloor, E., Gonmadje, C., Gourlet-Fleury, S., Hall, J.S., Hamilton, A.C., Harris, D.J., Hart, T.B., Hockemba, M.B.N., Hladik, A., Ifo, S.A., Jeffery, K.J., Jucker, T., Yakusu, E.K., Kearsley, E., Kenfack, D., Koch, A., Leal, M.E., Levesley, A., Lindsell, J.A., Lisingo, J., Lopez-Gonzalez, G., Lovett, J.C., Makana, J.-R., Malhi, Y., Marshall, A.R., Martin, J., Martin, E.H., Mbayu, F.M., Medjibe, V.P., Mihindou, V., Mitchard, E.T.A., Moore, S., Munishi, P.K.T., Bengone, N.N., Ojo, L., Ondo, F.E., Peh, K.S.-H., Pickavance, G.C., Poulsen, A.D., Poulsen, J.R., Qie, L., Reitsma, J., Rovero, F., Swaine, M.D., Talbot, J., Taplin, J., Taylor, D.M., Thomas, D.W., Toirambe, B., Mukendi, J.T., Tuagben, D., Umunay, P.M., van der Heijden, G.M.F., Verbeeck, H., Vleminckx, J., Willcock, S., Wöll, H., Woods, J.T., Zemagho, L.: Asynchronous carbon sink saturation in African and Amazonian tropical forests, Nature, 579, 80–87, https://doi.org/10.1038/s41586-020-2035-0, 2020.

Huguenin, M. F., Humphrey, V., Holmes, R. M., and England, M. H.: Drivers and distribution of global ocean heat uptake over the last half century, Nat Commun, 13, 4921, https://doi.org/10.1038/s41467-022-32540-5, 2022.Humphrey, V., Zscheischler, J., Ciais, P., Gudmundsson, L., Sitch, S., and Seneviratne, S. I.: Sensitivity of

Formatted: Space Before: 0 pt, After: 8 pt

Formatted: Space Before: 0 pt, After: 8 pt

Formatted: Space Before: 0 pt, After: 8 pt

Formatted: Space Before: 0 pt, After: 8 pt

atmospheric CO2 growth rate to observed changes in terrestrial water storage, Nature, 560, 628–631, https://doi.org/10.1038/s41586-018-0424-4, 2018.

Humphrey, V., Berg, A., Ciais, P., Gentine, P., Jung, M., Reichstein, M., Seneviratne, S. I., and Frankenberg, C.: Soil moisture–atmosphere feedback dominates land carbon uptake variability, Nature, 592, 65–69, https://doi.org/10.1038/s41586-021-03325-5, 2021.

Huntzinger, D. N., Michalak, A. M., Schwalm, C., Ciais, P., King, A. W., Fang, Y., Schaefer, K., Wei, Y., Cook, R. B., Fisher, J. B., Hayes, D., Huang, M., Ito, A., Jain, A. K., Lei, H., Lu, C., Maignan, F., Mao, J., Parazoo, N., Peng, S., Poulter, B., Ricciuto, D., Shi, X., Tian, H., Wang, W., Zeng, N., and Zhao, F.: Uncertainty in the response of terrestrial carbon sink to environmental drivers undermines carbon-climate feedback predictions, Sci Rep, 7, 4765, https://doi.org/10.1038/s41598-017-03818-2, 2017.

Iida, Y., Takatani, Y., Kojima, A., and Ishii, M.: Global trends of ocean CO2 sink and ocean acidification: an observation-based reconstruction of surface ocean inorganic carbon variables, J Oceanogr, 77, 323–358, https://doi.org/10.1007/s10872-020-00571-5, 2021.

Ilyina, T., Li, H., Spring, A., Müller, W. A., Bopp, L., Chikamoto, M. O., Danabasoglu, G., Dobrynin, M., Dunne, J., Fransner, F., Friedlingstein, P., Lee, W., Lovenduski, N. S., Merryfield, W. j., Mignot, J., Park, J. y., Séférian, R., Sospedra-Alfonso, R., Watanabe, M., and Yeager, S.: Predictable Variations of the Carbon Sinks and Atmospheric CO2 Growth in a Multi-Model Framework, Geophys. Res. Lett., 48, e2020GL090695, https://doi.org/10.1029/2020GL090695, 2021.

IMF: International Monetary Fund: World Economic Outlook, available at: http://www.imf.org, last access: ~~23~~30 October ~~2025, 2025~~2026, 2026.

Inoue, M., Morino, I., Uchino, O., Nakatsuru, T., Yoshida, Y., Yokota, T., Wunch, D., Wennberg, P., O., Roehl, C. M., Griffith, D. W. T., Velazco, V. A., Deutscher, N. M., Warneke, T., Notholt, J., Robinson, J., Sherlock, V., Hase, F., Blumenstock, T., Rettinger, M., Sussmann, R., Kyrö, E., Kivi, R., Shiomi, K., Kawakami, S., De Mazière, M., Arnold, S. G., Feist, D. G., Barrow, E. A., Barney, J., Dubey, M., Schneider, M., Iraci, L. T., Podolske, J. R., Hillyard, P. W., Machida, T., Sawa, Y., Tsuboi, K., Matsueda, H., Sweeney, C., Tans, P. P., Andrews, A. E., Biraud, S. C., Fukuyama, Y., Pittman, J. V., ~~Instituto Nacional de Pesquisas Espaciais (INPE): Portal TerraBrasilis, available at: http://terrabrasilis.dpi.inpe.br/en/home-page/, last access: 23 October 2025.~~
Kort, E. A., and Tanaka, T.: Bias corrections of GOSAT SWIR XCO₂ and XCH₄ with TCCON data andtheir evaluation using aircraft measurement data, Atmos. Meas. Tech., 9, 3491–3512, https://doi.org/10.5194/amt-9-3491-2016, 2016.

Ito, A.: Disequilibrium of terrestrial ecosystem CO2 budget caused by disturbance-induced emissions and non-CO2 carbon export flows: a global model assessment, Earth Syst. Dynam., 10, 685–709~~, https://doi.org/10.5194/esd-10-685-2019.~~, https://doi.org/10.5194/esd-10-685-2019, 2019.

Ito, A. and Inatomi, M.: Use of a process-based model for assessing the methane budgets of global terrestrial ecosystems and evaluation of uncertainty, 9, 759–773, https://doi.org/10.5194/bg-9-759-2012, 2012.

Jackson, R. B., Canadell, J. G., Le Quéré, C., Andrew, R. M., Korsbakken, J. I., Peters, G. P., and Nakicenovic, N.: Reaching peak emissions, Nature Clim Change, 6, 7–10, https://doi.org/10.1038/nclimate2892, 2016.

Jackson, R. B., Le Quéré, C., Andrew, R. M., Canadell, J. G., Korsbakken, J. I., Liu, Z., Peters, G. P., and Zheng, B.: Global energy growth is outpacing decarbonization, Environ. Res. Lett., 13, 120401, https://doi.org/10.1088/1748-9326/aaf303, 2018.

Jackson, R. B., Friedlingstein, P., Andrew, R. M., Canadell, J. G., Le Quéré, C., and Peters, G. P.: Persistent fossil fuel growth threatens the Paris Agreement and planetary health, Environ. Res. Lett., 14, 121001, https://doi.org/10.1088/1748-9326/ab57b3, 2019.

Jackson, R. B., Friedlingstein, P., Quéré, C. L., Abernethy, S., Andrew, R. M., Canadell, J. G., Ciais, P., Davis, S. J., Deng, Z., Liu, Z., Korsbakken, J. I., and Peters, G. P.: Global fossil carbon emissions rebound near pre-COVID-19 levels, Environ. Res. Lett., 17, 031001, https://doi.org/10.1088/1748-9326/ac55b6, 2022.

Jacobson, A. R., Schuldt, K. N., Miller, J. B., ~~Tans, P.,~~ Pera, A., Kaushik, A., Andrews, A., ~~Miller, J. B.,~~ ~~Oda, T.,~~ Basu, S., Triñanes, J., Landschützer, P., Mund, J., Weir, B., Ott, L., Aalto, T., Aaltonen, H., Abshire, J. B., Aikin, K., ~~Aoki, S~~Allen, G., Andrade, M., Apadula, F., Arnold, S., Baier, B., Bakwin, P., Bartyzel, J., Bentz, G., Bergamaschi, P., Beyersdorf, A., Biermann, T., Biraud, S. C., Blanc, P.-E., Boenisch, H., Bowling, D., Brailsford, G., Brand, W. A., Brunner, D., Bui, T. P. V., ~~A~~Burban, B., Bäni, L., Calzolari, F., Chang, C. S., Chen, G., Chen, H., Chmura, L., St. Clair, J. M., Clark, S., Climadat, S., Della Coletta, J., Colomb, A., Commane, R., Condori, L.,

Formatted: Space Before: 0 pt, After: 8 pt

Conen, F., Conil, S., Couret, C., ~~Cox, A.,~~ Cristofanelli, P., Cuevas, E., Curcoll, R., Daube, B., Davis, K. J., De Mazière, M., de Souza, R. A. F., De Wekker, S., ~~Della Coletta~~Dean-Day, J. M., Delmotte, M., Di Iorio, T., di Sarra, A. G., Dickerson, R., DiGangi, E., DiGangi, J. P., ~~di Sarra, A. G., Dlugokencky,~~ Elsasser, M~~E.,~~ Elkins, J. ~~W.~~., Emmenegger, L., Fang, S., Fischer, M. L., Forster, G., France, J., Frumau, A., Fuente-Lastra, M., Galkowski, M., Gatti, L. V., Gehrlein, T., Gerbig, C., Gheusi, F., Gloor, E., ~~Gomez-Trueba, V.,~~ Goto, D., Griffis, T., Hammer, S., Hanisco, T. F., Hanson, C., Hashimoto, S., Haszpra, L., Hatakka, J., Heimann, M., Heliasz, M., Heltai, D., Henne, S., Hensen, A., Hermans, C., Hermansen, O., Higgs, J., Hintsa, E., Hoheisel, A., Holst, J., Iraci, L. T., Ivakhov, V., Jaffe, D. A., Joly, L., Jordan, A., Joubert, W., Kang, H.-Y., Karion, A., Kawa, S. R., Kazan, V., Keeling, R. F., Ishijima, K., Keronen, P., Kim, J., Klausen, J., Kneuer, T., Ko, M.-Y., Kolari, P., Komínková, K., Kort, E., Kozlova, E., Krummel, P., Kubistin, D., Kulawik, S. S., Kumps, N., Labuschagne, C., Lam, D. H. Y., Lan, X., Langenfelds, R. L., Lanza, A., Larmanou, E., Laurent, O., ~~Laurila, T.,~~ Lauvaux, T., Lavric, J., Law, B. E., Lee, ~~J~~C.-H., Lee, ~~O. S. M~~J., Lehner, I., Lehtinen, K., Leppert, R., Leskinen, A., Leuenberger, M., Leung, W. H., Levin, I., Levula, J., Lin, J., Lindauer, M., Lindroth, A., Loh, Z., Lopez, M., Lueker, T. J., Luijkx, I. T., Lunder, C. R., Machida, T., Mammarella, I., Manca, G., Manning, A., Manning, A., Marek, M. ~~V.,~~ V., Marklund, P., Marrero, J. E., Martin, D., Martin, M. Y., Martins, G. A., Matsueda, H., McAuliffe, A., McKain, K., Meijer, H., Meinhardt, F., Merchant, L., Metzger, J.-M., Mihalopoulos, N., Miles, N. L., Miller, C. E., Mitchell, L., Mölder, M., Müller-Williams, J., Monteiro, V., Montzka, S., ~~Moore, F.,~~ Moossen, H., Moreno, C., Morgan, E., Morgui, J.-A., Morimoto, S., ~~Müller-Williams, J~~Mukai, H., Munger, J. W., Munro, D., Mutuku, M., Lund Myhre, C. ~~L.~~, Nakaoka, S.-I., Necki, J., Newberger, T., Newman, S., Nichol, S., Nisbet, E., Niwa, Y., Njiru, D. M., Noe, S. M., Nojiri, Y., Obersteiner, F., O'Doherty, S., Paplawsky, B., Parworth, C. L., Peischl, J., Peltola, O., Peters, W., Philippon, C., Piacentino, S., Pichon, J.-M., Pickers, P., Piper, S., Pitt, J., Plass-Dülmer, C., Platt, S. M., Prinzivalli, S., Ramonet, M., Ramos, R., Ren, X., Reyes-Sanchez, E., Richardson, S. J., Rigouleau, L.-J., Riris, H., Rivas, P. ~~P~~P., Rothe, M., Roulet, Y.-A., Ryerson, T., ~~Saito, K~~Ryoo, J.-M., Sargent, M., Sasakawa, M., Scheeren, B., Schmidt, M., Schuck, T., Schumacher, M., Seibel, J., Seifert, T., Sha, M. K., Shepson, P., Shin, D., Shook, M., Sloop, C. ~~D., Smith, P., Stanley, K~~D., Smale, D., Spain, G., Stavert, A., Steger, D., Steinbacher, M., Stephens, B., Sweeney, C., Sørensen, L. L., Taipale, R., Takatsuji, S., Tans, P., Terao, Y., Thoning, K., Timas, H., Torn, M., ~~Tørseth, K.,~~ Trisolino, P., Tørseth, K., Turnbull, J., van den Bulk, P., ~~van Dinther, D.,~~ Vermeulen, A., Viner, B., Vitkova, G., Walker, S., Watson, A., Weiss, R., Weyrauch, D., Wofsy, S. C., Wolter, S., Worsey, J., Worthy, D., Xueref-Remy, I., Yates, E. L., Young, D., Yver-Kwok, C., Zaehle, S., Zahn, A., ~~and~~Zellweger, C., Zimnoch, M.: CarbonTracker ~~CT2022, NOAA GML~~CT2026 [Data set], NOAA, https://doi.org/10.25925/~~Z1GJ-3254, 2023a~~hqp0-rk68, 2026.

~~Jacobson, A. R., Schuldt, K. N., Tans, P., Andrews, A., Miller, J. B., Oda, T., Basu, S., Mund, J., Weir, B., Ott, L., Aalto, T., Abshire, J. B., Aikin, K., Aoki, S., Apadula, F., Arnold, S., Baier, B., Bartyzel, J., Beyersdorf, A., Biermann, T., Biraud, S. C., Boenisch, H., Brailsford, G., Brand, W. A., Chen, G., Chen, H., Chmura, L., Clark, S., Colomb, A., Commane, R., Conil, S., Couret, C., Cox, A., Cristofanelli, P., Cuevas, E., Curcoll, R., Daube, B., Davis, K. J., De Wekker, S., Della Coletta, J., Delmotte, M., DiGangi, E., DiGangi, J. P., di Sarra, A. G., Dlugokencky, E., Elkins, J. W., Emmenegger, L., Fang, S., Fischer, M. L., Forster, G., Frumau, A., Galkowski, M., Gatti, L. V., Gehrlein, T., Gerbig, C., Gheusi, F., Gloor, E., Gomez-Trueba, V., Goto, D., Griffis, T., Hammer, S., Hanson, C., Haszpra, L., Hatakka, J., Heimann, M., Heliasz, M., Hensen, A., Hermansen, O., Hintsa, E., Holst, J., Ivakhov, V., Jaffe, D. A., Jordan, A., Joubert, W., Karion, A., Kawa, S. R., Kazan, V., Keeling, R. F., Keronen, P., Kneuer, T., Kolari, P., Komínková, K., Kort, E., Kozlova, E., Krummel, P., Kubistin, D., Labuschagne, C., Lam, D. H. Y., Lan, X., Langenfelds, R. L., Laurent, O., Laurila, T., Lauvaux, T., Lavric, J., Law, B. E., Lee, J., Lee, O. S. M., Lehner, I., Lehtinen, K., Leppert, R., Leskinen, A., Leuenberger, M., Levin, I., Levula, J., Lin, J., Lindauer, M., Loh, Z., Lopez, M., Luijkx, I. T., Lunder, C. R., Machida, T., Mammarella, I., Manca, G., Manning, A., Manning, A., Marek, M. V., Martin, M. Y., Matsueda, H., McKain, K., Meijer, H., Meinhardt, F., Merchant, L., Mihalopoulos, N., Miles, N. L., Miller, C. E., Mitchell, L., Mölder, M., Montzka, S., Moore, F., Moossen, H., Morgan, E., Morgui, J.-A., Morimoto, S., Müller-Williams, J., Munger, J. W., Munro, D., Myhre, C. L., Nakaoka, S. I., Necki, J., Newman, S., Nichol, S., Niwa, Y., Obersteiner, F., O'Doherty, S., Paplawsky, B., Peischl, J., Peltola, O., Piacentino, S., Pichon, J.-M., Pickers, P., Piper, S., Pitt, J., Plass-Dülmer, C., Platt, S. M., Prinzivalli, S., Ramonet, M., Ramos, R., Reyes-Sanchez, E., Richardson, S. J., Riris, H., Rivas, P. P., Ryerson, T., Saito, K., Sargent, M., Sasakawa, M., Scheeren, B., Schuck, T., Schumacher, M., Seifert, T., Sha, M. K., Shepson, P., Shook, M., Sloop, C. D., Smith, P., Stanley, K., Steinbacher, M., Stephens, B., Sweeney, C., Thoning, K., Timas, H., Torn, M., Tørseth, K., Trisolino, P., Turnbull, J., van den Bulk, P., van Dinther, D., Vermeulen, A., Viner, B., Vitkova, G., Walker, S., Watson, A., Wofsy, S. C., Worsey, J., Worthy, D., Young, D., Zachle, S., Zahn, A., and Zimnoch, M.: CarbonTracker CT-NRT.v2023-3, NOAA GML [Data set], https://doi.org/10.25925/7TAF-J322, 2023b.~~

Jain, A. K., Meiyappan, P., Song, Y., and House, J. I.: CO2 emissions from land-use change affected more by nitrogen cycle, than by the choice of land-cover data, Global Change Biology, 19, 2893–2906~~,~~ ~~https://doi.org/10.1111/gcb.12207,~~ https://doi.org/10.1111/gcb.12207, 2013.

~~Jain, P., Barber, Q. E., Taylor, S., W., Whitman, E., Castellanos Acuna, D., Boulanger, Y., Chavardès, R. D., Chen, J., Englefield, P., Flannigan, M., Girardin, M. P., Hanes, C. C., Little, J., Morrison, K., Skakun, R. S., Thompson,~~

Formatted: Space Before: 0 pt, After: 8 pt

~~D. K., Wang, X., Parisien, M.-A.: Drivers and Impacts of the Record-Breaking 2023 Wildfire Season in Canada. Nature Communications, 15(1), p.6764, https://doi.org/10.1038/s41467-024-51154-7, 2024.~~

Janssens-Maenhout, G., Crippa, M., Guizzardi, D., Muntean, M., Schaaf, E., Dentener, F., Bergamaschi, P., Pagliari, V., Olivier, J. G. J., Peters, J. A. H. W., van Aardenne, J. A., Monni, S., Doering, U., Petrescu, A. M. R., Solazzo, E., and Oreggioni, G. D.: EDGAR v4.3.2 Global Atlas of the three major greenhouse gas emissions for the period 1970–2012, Earth Syst. Sci. Data, 11, 959–1002, https://doi.org/10.5194/essd-11-959-2019, 2019.

~~Jean-Michel, L., Eric, G., Romain, B.-B., Gilles, G., Angélique, M., Marie, D., Clément, B.,~~ ~~Mathieu, H., Olivier, L. G., Charly, R., Tony, C., Charles-Emmanuel, T., Florent, G., Giovanni, R., Mounir, B., Yann, D., and Pierre-Yves, L. T.: The Copernicus Global 1/12° Oceanic and Sea Ice GLORYS12 Reanalysis, Front. Earth Sci., 9, 2021.~~

~~Jiang, F., Ju, W., He, W.,~~ ~~Wu, M., Wang, H., Wang, J., Jia, M., Feng, S., Zhang, L., and Chen, J. M.: A 10-year global monthly averaged terrestrial net ecosystem exchange dataset inferred from the ACOS GOSAT v9 XCO2 retrievals (GCAS2021), Earth Syst. Sci. Data, 14, 3013–3037, https://doi.org/10.5194/essd-14-3013-2022, 2022.~~

Jiang, F., Wang, H., Chen, J. M., Ju, W., Tian, X., Feng, S., Li, G., Chen, Z., Zhang, S., Lu, X., Liu, J., Wang, H., Wang, J., He, W., and Wu, M.: Regional CO2 fluxes from 2010 to 2015 inferred from GOSAT XCO2 retrievals using a new version of the Global Carbon Assimilation System, Atmospheric Chem. Phys., 21, 1963–1985, https://doi.org/10.5194/acp-21-1963-2021, 2021.

Jin, Y., Keeling, R. F., Stephens, B. B., Long, M. C., Patra, P. K., Rödenbeck, C., Morgan, E. J., Kort, E. A., and Sweeney, C.: Improved atmospheric constraints on Southern Ocean CO 2 exchange. Proceedings of the National Academy of Sciences, 121(6), e2309333121, https://doi.org/10.1073/pnas.2309333121, 2024.

Jin, Z., Wang, T., Zhang, H., Wang, Y., Ding, J., and Tian, X.: Constraint of satellite CO2 retrieval on the global carbon cycle from a Chinese atmospheric inversion system, Sci. China Earth Sci., 66, 609–618, https://doi.org/10.1007/s11430-022-1036-7, 2023.

Joos, F. and Spahni, R.: Rates of change in natural and anthropogenic radiative forcing over the past 20,000 years, Proceedings of the National Academy of Sciences, 105, 1425–1430, https://doi.org/10.1073/pnas.0707386105, 2008.

Jones, ~~C. D., Hickman, J. E.,~~ ~~Rumbold, S. T., Walton, J., Lamboll, R. D., Skeie, R. B., Fiedler, S., Forster, P. M., Rogelj, J., Abe, M., Botzet, M., Calvin, K.,~~ ~~Cassou, C.,~~ ~~Cole, J. N. S., Davini, P., Deushi, M., Dix, M., Fyfe, J. C.,~~ ~~Gillett, N. P., Ilyina, T., Kawamiya, M., Kelley, M., Kharin, S., Koshiro, T., Li, H., Mackallah, C., Müller, W. A., Nabat, P., van Noije, T., Nolan, P., Ohgaito, R., Olivié, D., Oshima, N., Parodi, J., Reerink, T. J., Ren, L., Romanou, A., Séférian, R., Tang, Y., Timmreck, C., Tjiputra, J., Tourigny, E., Tsigaridis, K., Wang, H., Wu, M., Wyser, K., Yang, S., Yang,~~ ~~Y.,~~ ~~and Ziehn, T.: The Climate Response to Emissions Reductions Due to COVID-19: Initial Results From CovidMIP, Geophys.~~ ~~Res. Lett.,~~ ~~48, e2020GL091883, https://doi.org/10.1029/2020GL091883, 2021a.~~

~~Jones,~~ M. W., Abatzoglou, J. T., Veraverbeke, S., Andela, N., Lasslop, G., Forkel, M., Smith, A. J. P., Burton, C., Betts, R. A., van der Werf, G. R., Sitch, S., Canadell, J. G., Santín, C., Kolden, C., Doerr, S. H., and Le Quéré, C.: Global and Regional Trends and Drivers of Fire Under Climate Change, Rev. Geophys., 60, e2020RG000726, https://doi.org/10.1029/2020RG000726, 2022.

Jones, M. W., Andrew, R. M., Peters, G. P., Janssens-Maenhout, G., De-Gol, A. J., Ciais, P., Patra, P. K., Chevallier, F., and Le Quéré, C.: Gridded fossil CO2 emissions and related O2 combustion consistent with national inventories 1959–2018, Sci Data, 8, 2, https://doi.org/10.1038/s41597-020-00779-6, ~~2021b~~2021.

Jones, M. W., Andrew, R. M., Peters, G. P., Janssens-Maenhout, G., De-Gol, A. J., Dou, X., Liu, Z., Pickers, P., Ciais, P., Patra, P. K., Chevallier, F., and Le Quéré, C.: Gridded fossil CO2 emissions and related O2 combustion consistent with national inventories, Zenodo [Data set], https://doi.org/10.5281/zenodo.17467681, 2025.

Jones, M. W., Kelley, D. I., Burton, C. A., Di Giuseppe, F., Barbosa, M. L. F., Brambleby, E., Hartley, A. J., Lombardi, A., Mataveli, G., McNorton, J. R., Spuler, F. R., Wessel, J. B., Abatzoglou, J. T., Anderson, L. O., Andela, N., Archibald, S., Armenteras, D., Burke, E., Carmenta, R., Chuvieco, E., Clarke, H., Doerr, S. H., Fernandes, P. M., Giglio, L., Hamilton, D. S., Hantson, S., Harris, S., Jain, P., Kolden, C. A., Kurvits, T., Lampe, S., Meier, S., New, S., Parrington, M., Perron, M. M. G., Qu, Y., Ribeiro, N. S., Saharjo, B. H., San-Miguel-Ayanz, J., Shuman, J. K., Tanpipat, V., van der Werf, G. R., Veraverbeke, S., and Xanthopoulos, G.: State of Wildfires 2023–2024, Earth System Science Data, 16, 3601–3685, https://doi.org/10.5194/essd-16-3601-2024, ~~2024b~~2024a.

Jones, M.W., Veraverbeke, S., Andela, N., Doerr, S.H., Kolden, C., Mataveli, G., Pettinari, M.L., Le Quéré, C., Rosan, T.M., van der Werf, G.R. and van Wees, D.: Global rise in forest fire emissions linked to climate change in the extratropics. Science, 386(6719), p.eadl5889, ~~2024c~~2024b.

Formatted: Space Before: 0 pt, After: 8 pt

Formatted: Space Before: 0 pt, After: 8 pt

Formatted: Space Before: 0 pt, After: 8 pt

Jung, M., Reichstein, M., Schwalm, C. R., Huntingford, C., Sitch, S., Ahlström, A., Arneth, A., Camps-Valls, G., Ciais, P., Friedlingstein, P., Gans, F., Ichii, K., Jain, A. K., Kato, E., Papale, D., Poulter, B., Raduly, B., Rödenbeck, C., Tramontana, G., Viovy, N., Wang, Y.-P., Weber, U., Zaehle, S., and Zeng, N.: Compensatory water effects link yearly global land CO2 sink changes to temperature, Nature, 541, 516–520, https://doi.org/10.1038/nature20780, 2017.

Kaiser, J. W., Heil, A., Andreae, M. O., Benedetti, A., Chubarova, N., Jones, L., Morcrette, J.-J., Razinger, M., Schultz, M. G., Suttie, M., and van der Werf, G. R.: Biomass burning emissions estimated with a global fire assimilation system based on observed fire radiative power, Biogeosciences, 9, 527–554, https://doi.org/10.5194/bg-9-527-2012, 2012.

Kato, E., Kinoshita, T., Ito, A., Kawamiya, M., and Yamagata, Y.: Evaluation of spatially explicit emission scenario of land-use change and biomass burning using a process-based biogeochemical model, J. Land Use Sci., 8, 104–122, https://doi.org/10.1080/1747423X.2011.628705, 2013.

~~Kawasaki, T., Hasumi, H., and Tanaka, Y.: Role of tide-induced vertical mixing in the deep Pacific Ocean circulation, J. Oceanogr., 77, 173–184, https://doi.org/10.1007/s10872-020-00584-0, 2021.~~

~~Ke, P., Ciais, P., Sitch, S., Li, W., Bastos, A., Liu, Z., Xu, Y., Gui, X., Bian, J., Goll, D. S., Xi, Y., Li, W., O'Sullivan, M., Goncalves de Souza, J., Friedlingstein, P., Chevallier, F.: Low latency carbon budget analysis reveals a large decline of the land carbon sink in 2023. National Science Review, p.nwae367, https://doi.org/10.1093/nsr/nwae367, 2024.~~

Keeley, J. E. and Pausas, J. G.: Distinguishing disturbance from perturbations in fire-prone ecosystems, Int. J. Wildland Fire, 28, 282–287, https://doi.org/10.1071/WF18203, 2019.

Keeling, C. D., Bacastow, R. B., Bainbridge, A. E., Ekdahl, C. A., Guenther, P. R., Waterman, L. S., and Chin, J. F. S.: Atmospheric carbon dioxide variations at Mauna Loa Observatory, Hawaii, Tellus A., 28, 538–551, https://doi.org/10.1111/j.2153-3490.1976.tb00701.x, 1976.

Keeling R.F.: Development of an Interferometric Oxygen Analyzer for Precise Measurement of the Atmospheric O2 Mole Fraction, PhD thesis, Harvard University, Cambridge, Massachusetts, available at: https://bluemoon.ucsd.edu/publications/ralph/34_PhDthesis.pdf, last access: ~~23~~30 October ~~2025~~2026, 1988.

Keeling, R. F., Manning, A. C., Paplawsky, W. J., and Cox, A. C.: On the long-term stability of reference gases for atmospheric O2/N2 and CO2 measurements, Tellus B Chem. Phys. Meteorol., 59, 3–14, https://doi.org/10.1111/j.1600-0889.2006.00196.x, 2007.

Keeling, R. F. and Manning, A. C.: 5.15 - Studies of Recent Changes in Atmospheric O2 Content, in: Treatise on Geochemistry (Second Edition), edited by: Holland, H. D. and Turekian, K. K., Elsevier, Oxford, 385–404, https://doi.org/10.1016/B978-0-08-095975-7.00420-4, 2014.

Kelley, D. I., Burton, C., Di Giuseppe, F., Jones, M. W., Barbosa, M. L. F., Brambleby, E., McNorton, J. R., Liu, Z., Bradley, A. S. I., Blackford, K., Burke, E., Ciavarella, A., Di Tomaso, E., Eden, J., Ferreira, I. J. M., Fiedler, L., Hartley, A. J., Keeping, T. R., Lampe, S., Lombardi, A., Mataveli, G., Qu, Y., Silva, P. S., Spuler, F. R., Steinmann, C. B., Torres-Vázquez, M. Á., Veiga, R., Van Wees, D., Wessel, J. B., Wright, E., Bilbao, B., Bourbonnais, M., Gao, C., Di Bella, C. M., Dintwe, K., Donovan, V. M., Harris, S., Kukavskaya, E. A., N'Dri, A. B., Santín, C., Selaya, G., Sjöström, J., Abatzoglou, J. T., Andela, N., Carmenta, R., Chuvieco, E., Giglio, L., Hamilton, D. S., Hantson, S., Meier, S., Parrington, M., Sadegh, M., San-Miguel-Ayanz, J., Sedano, F., Turco, M., Van Der Werf, G. R., Veraverbeke, S., Anderson, L. O., Clarke, H., Fernandes, P. M., and Kolden, C. A.: State of Wildfires 2024–2025, Earth Syst. Sci. Data, 17, 5377–5488~~, https://doi.org/10.5194/essd-17-5377-2025,~~ https://doi.org/10.5194/essd-17-5377-2025, 2025.

Keppler, L. and Landschützer, P.: Regional Wind Variability Modulates the Southern Ocean Carbon Sink, Sci Rep, 9, 7384, https://doi.org/10.1038/s41598-019-43826-y, 2019.

Keppler, L., Landschützer, P., Lauvset, S. K., and Gruber, N.: Recent Trends and Variability in the Oceanic Storage of Dissolved Inorganic Carbon, Global Biogeochemical Cycles, 37, e2022GB007677, https://doi.org/10.1029/2022GB007677, 2023.

Kharin, V. V., Boer, G. J., Merryfield, W. J., Scinocca, J. F., and Lee, W. -S.: Statistical adjustment of decadal predictions in a changing climate, Geophysical Research Letters, 39, 2012GL052647, https://doi.org/10.1029/2012GL052647, 2012.

Khatiwala, S., Primeau, F., and Hall, T.: Reconstruction of the history of anthropogenic CO2 concentrations in the ocean, Nature, 462, 346–349, https://doi.org/10.1038/nature08526, 2009.

Formatted: Space Before: 0 pt, After: 8 pt

Formatted: Font: Cambria Math

Formatted: Space Before: 0 pt, After: 8 pt

Khatiwala, S., Tanhua, T., Mikaloff Fletcher, S., Gerber, M., Doney, S. C., Graven, H. D., Gruber, N., McKinley, G. A., Murata, A., Ríos, A. F., and Sabine, C. L.: Global ocean storage of anthropogenic carbon, Biogeosciences, 10, 2169–2191, https://doi.org/10.5194/bg-10-2169-2013, 2013.

Kong, Y., Zheng, B., Zhang, Q., and He, K.: Global and regional carbon budget for 2015–2020 inferred from OCO-2 based on an ensemble Kalman filter coupled with GEOS-Chem, Atmospheric Chem. Phys., 22, 10769–10788, https://doi.org/10.5194/acp-22-10769-2022, 2022.

Kou-Giesbrecht, S. and Arora, V. K.: Representing the Dynamic Response of Vegetation to Nitrogen Limitation via Biological Nitrogen Fixation in the CLASSIC Land Model, Global Biogeochemical Cycles, 36, e2022GB007341~~, https://doi.org/10.1029/2022GB007341.~~, https://doi.org/10.1029/2022GB007341, 2022.

Korsbakken, J. I., Peters, G. P., and Andrew, R. M.: Uncertainties around reductions in China's coal use and CO2 emissions, Nature Clim Change, 6, 687–690, https://doi.org/10.1038/nclimate2963, 2016.

Koven, C. D., Knox, R. G., Fisher, R. A., Chambers, J. Q., Christoffersen, B. O., Davies, S. J., Detto, M., Dietze, M. C., Faybishenko, B., Holm, J., Huang, M., Kovenock, M., Kueppers, L. M., Lemieux, G., Massoud, E., McDowell, N. G., Muller-Landau, H. C., Needham, J. F., Norby, R. J., Powell, T., Rogers, A., Serbin, S. P., Shuman, J. K., Swann, A. L. S., Varadharajan, C., Walker, A. P., Wright, S. J., and Xu, C.: Benchmarking and parameter sensitivity of physiological and vegetation dynamics using the Functionally Assembled Terrestrial Ecosystem Simulator (FATES) at Barro Colorado Island, Panama, Biogeosciences, 17, 3017–3044~~,~~ ~~https://doi.org/10.5194/bg-17-3017-2020.~~, https://doi.org/10.5194/bg-17-3017-2020, 2020.

~~Krinner, G.,~~ Krol, M., Houweling~~Vieovy, N.,~~ ~~de Noblet-Ducoudré, N., Ogée, J., Polcher, J., Friedlingstein, P., Ciais, P., Sitch~~, S., Bregman, B., van den Broek, M., Segers, A., van Velthoven, P., Peters, W., Dentener, F., and ~~Prentice, I. C.: A dynamic~~Bergamaschi, P.: The two-way nested global ~~vegetation~~chemistry-transport zoom model ~~for studies of the coupled atmosphere-biosphere system: DVGM for coupled climate studies, Global Biogeochem. Cycles, 19, GB1015~~TM5: algorithm and applications, Atmospheric Chemistry and Physics, 5, 417–432, https://doi.org/10.~~1029/2003GB002199, ~~5194/acp-5-417-~~2005, 2005.

Kunimitsu, T. and Andrew, R. M.: Monthly-updated territorial fossil CO2 emissions estimates for Japan [Accepted], Earth System Science Data Discussions, https://doi.org/10.5194/essd-2026-417, 2026.

Lacroix, F., Ilyina, T., and Hartmann, J.: Oceanic CO2 outgassing and biological production hotspots induced by pre-industrial river loads of nutrients and carbon in a global modeling approach, Biogeosciences, 17, 55–88, https://doi.org/10.5194/bg-17-55-2020, 2020.

Lacroix, F., Ilyina, T., Mathis, M., Laruelle, G. G., and Regnier, P.: Historical increases in land-derived nutrient inputs may alleviate effects of a changing physical climate on the oceanic carbon cycle, Glob Change Biol, 27, 5491–5513, https://doi.org/10.1111/gcb.15822, 2021.

Lamboll, R. D., Nicholls, Z. R. J., Smith, C. J., Kikstra, J. S., Byers, E., and Rogelj, J.: Assessing the size and uncertainty of remaining carbon budgets, Nat. Clim. Change, https://doi.org/10.1038/s41558-023-01848-5, 2023.

~~Lamboll, R. D., Jones, C. D., Skeie, R. B., Fiedler, S., Samset, B. H., Gillett, N. P., Rogelj, J., Forster, P. M., 2021: Modifying emissions scenario projections to account for the effects of COVID-19: protocol for CovidMIP, Geosci. Model Dev., 14, 3683–3695, https://doi.org/10.5194/gmd-14-3683-2021, 2021.~~

Lan, X., Tans, P. and Thoning, K.: NOAA Greenhouse Gas Marine Boundary Layer Reference - CO2 [Data set]. NOAA Global Monitoring Laboratory, https://doi.org/10.15138/DVNP-F961, 2024.Lan, X., Tans, P. and K.W. Thoning: Trends in globally-averaged CO2 determined from NOAA Global Monitoring Laboratory measurements (Version 2026-09) [Data set], NOAA, https://doi.org/10.15138/9N0H-ZH07, 2026.

~~Lan, X., Tans, P. and Thoning, K. W.: Trends in globally-averaged CO2 determined from NOAA Global Monitoring Laboratory measurements, https://doi.org/10.15138/9N0H-ZH07, 2025.~~

Landschützer, P., Gruber, N., Haumann, F. A., Rödenbeck, C., Bakker, D. C. E., van Heuven, S., Hoppema, M., Metzl, N., Sweeney, C., Takahashi, T., Tilbrook, B., and Wanninkhof, R.: The reinvigoration of the Southern Ocean carbon sink, Science, 349, 1221–1224, https://doi.org/10.1126/science.aab2620, 2015.

Landschützer, P., Gruber, N., and Bakker, D. C. E.: Decadal variations and trends of the global ocean carbon sink: decadal air-sea CO2 flux variability, Global Biogeochem. Cycles, 30, 1396–1417, https://doi.org/10.1002/2015GB005359, 2016.

Lapola, D. M., Pinho, P., Barlow, J., Aragão, L. E. O. C., Berenguer, E., Carmenta, R., Liddy, H. M., Seixas, H., Silva, C. V. J., Silva-Junior, C. H. L., Alencar, A. A. C., Anderson, L. O., Armenteras, D., Brovkin, V., Calders, K., Chambers, J., Chini, L., Costa, M. H., Faria, B. L., Fearnside, P. M., Ferreira, J., Gatti, L., Gutierrez-Velez, V.

Formatted: Font: Cambria Math

Formatted: Space Before: 0 pt, After: 8 pt

Formatted: Font: Cambria Math

Formatted: Space Before: 0 pt, After: 8 pt

Formatted: Space Before: 0 pt, After: 8 pt

H., Han, Z., Hibbard, K., Koven, C., Lawrence, P., Pongratz, J., Portela, B. T. T., Rounsevell, M., Ruane, A. C., Schaldach, R., da Silva, S. S., von Randow, C., Walker, W. S.: The drivers and impacts of Amazon forest degradation. Science, 379(6630), p.eabp8622, https://doi.org/10.1126/science.abp8622, 2023.

Law, R. M., Ziehn, T., Matear, R. J., Lenton, A., Chamberlain, M. A., Stevens, L. E., Wang, Y.-P., Srbinovsky, J., Bi, D., Yan, H., and Vohralik, P. F.: The carbon cycle in the Australian Community Climate and Earth System Simulator (ACCESS-ESM1) – Part 1: Model description and pre-industrial simulation, Geosci. Model Dev., 10, 2567–2590, https://doi.org/10.5194/gmd-10-2567-2017, 2017.

Laughner, J. L., Roche, S., Kiel, M., Toon, G. C., Wunch, D., Baier, B. C., Biraud, S., Chen, H., Kivi, R., Laemmel, T., McKain, K., Quéhé, P.-Y., Rousogenous, C., Stephens, B. B., Walker, K., and Wennberg, P. O.: A new algorithm to generate a priori trace gas profiles for the GGG2020 retrieval algorithm, Atmos. Meas. Tech., 16, 1121–1146, ~~https://doi.org/10.5194/amt-16-1121-2023,~~ https://doi.org/10.5194/amt-16-1121-2023, 2023.

Lauvset, S. K., Lange, N., Tanhua, T., Bittig, H. C., Olsen, A., Kozyr, A., Álvarez, M., Azetsu-Scott, K., Brown, P. J., Carter, B. R., Cotrim Da Cunha, L., Hoppema, M., Humphreys, M. P., Ishii, M., Jeansson, E., Murata, A., Müller, J. D., Pérez, F. F., Schirnick, C., Steinfeldt, R., Suzuki, T., Ulfsbo, A., Velo, A., Woosley, R. J., and Key, R. M.: The annual update GLODAPv2.2023: the global interior ocean biogeochemical data product, Earth Syst. Sci. Data, 16, 2047–2072, https://doi.org/10.5194/essd-16-2047-2024, 2024.

Lawrence, D. M., Fisher, R. A., Koven, C. D., Oleson, K. W., Swenson, S. C., Bonan, G., Collier, N., Ghimire, B., van Kampenhout, L., Kennedy, D., Kluzek, E., Lawrence, P. J., Li, F., Li, H., Lombardozzi, D., Riley, W. J., Sacks, W. J., Shi, M., Vertenstein, M., Wieder, W. R., Xu, C., Ali, A. A., Badger, A. M., Bisht, G., van den Broeke, M., Brunke, M. A., Burns, S. P., Buzan, J., Clark, M., Craig, A., Dahlin, K., Drewniak, B., Fisher, J. B., Flanner, M., Fox, A. M., Gentine, P., Hoffman, F., Keppel-Aleks, G., Knox, R., Kumar, S., Lenaerts, J., Leung, L. R., Lipscomb, W. H., Lu, Y., Pandey, A., Pelletier, J. D., Perket, J., Randerson, J. T., Ricciuto, D. M., Sanderson, B. M., Slater, A., Subin, Z. M., Tang, J., Thomas, R. Q., Val Martin, M., and Zeng, X.: The Community Land Model Version 5: Description of New Features, Benchmarking, and Impact of Forcing Uncertainty, J. Adv. Model Earth, Sy., 11, 4245–4287, https://doi.org/10.1029/2018MS001583, 2019.

Le Quéré, C., Rödenbeck, C., Buitenhuis, E. T., Conway, T. J., Langenfelds, R., Gomez, A., Labuschagne, C., Ramonet, M., Nakazawa, T., Metzl, N., Gillett, N., and Heimann, M.: Saturation of the Southern Ocean CO2 Sink Due to Recent Climate Change, Science, 316, 1735–1738, https://doi.org/10.1126/science.1136188, 2007.

Le Quéré, C., Raupach, M. R., Canadell, J. G., Marland, G., Bopp, L., Ciais, P., Conway, T. J., Doney, S. C., Feely, R. A., Foster, P., Friedlingstein, P., Gurney, K., Houghton, R. A., House, J. I., Huntingford, C., Levy, P. E., Lomas, M. R., Majkut, J., Metzl, N., Ometto, J. P., Peters, G. P., Prentice, I. C., Randerson, J. T., Running, S. W., Sarmiento, J. L., Schuster, U., Sitch, S., Takahashi, T., Viovy, N., van der Werf, G. R., and Woodward, F. I.: Trends in the sources and sinks of carbon dioxide, Nature Geosci, 2, 831–836, https://doi.org/10.1038/ngeo689, 2009.

Le Quéré, C., Takahashi, T., Buitenhuis, E. T., Rödenbeck, C., and Sutherland, S. C.: Impact of climate change and variability on the global oceanic sink of CO2, Global Biogeochemical Cycles, 24, https://doi.org/10.1029/2009GB003599, 2010.

Le Quéré, C., Andres, R. J., Boden, T., Conway, T., Houghton, R. A., House, J. I., Marland, G., Peters, G. P., van der Werf, G. R., Ahlström, A., Andrew, R. M., Bopp, L., Canadell, J. G., Ciais, P., Doney, S. C., Enright, C., Friedlingstein, P., Huntingford, C., Jain, A. K., Jourdain, C., Kato, E., Keeling, R. F., Klein Goldewijk, K., Levis, S., Levy, P., Lomas, M., Poulter, B., Raupach, M. R., Schwinger, J., Sitch, S., Stocker, B. D., Viovy, N., Zaehle, S., and Zeng, N.: The global carbon budget 1959–2011, Earth Syst. Sci. Data, 5, 165–185, https://doi.org/10.5194/essd-5-165-2013, 2013.

Le Quéré, C., Peters, G. P., Andres, R. J., Andrew, R. M., Boden, T. A., Ciais, P., Friedlingstein, P., Houghton, R. A., Marland, G., Moriarty, R., Sitch, S., Tans, P., Arneth, A., Arvanitis, A., Bakker, D. C. E., Bopp, L., Canadell, J. G., Chini, L. P., Doney, S. C., Harper, A., Harris, I., House, J. I., Jain, A. K., Jones, S. D., Kato, E., Keeling, R. F., Klein Goldewijk, K., Körtzinger, A., Koven, C., Lefèvre, N., Maignan, F., Omar, A., Ono, T., Park, G.-H., Pfeil, B., Poulter, B., Raupach, M. R., Regnier, P., Rödenbeck, C., Saito, S., Schwinger, J., Segschneider, J., Stocker, B. D., Takahashi, T., Tilbrook, B., van Heuven, S., Viovy, N., Wanninkhof, R., Wiltshire, A., and Zaehle, S.: Global carbon budget 2013, Earth Syst. Sci. Data, 6, 235–263, https://doi.org/10.5194/essd-6-235-2014, 2014.

Le Quéré, C., Moriarty, R., Andrew, R. M., Peters, G. P., Ciais, P., Friedlingstein, P., Jones, S. D., Sitch, S., Tans, P., Arneth, A., Boden, T. A., Bopp, L., Bozec, Y., Canadell, J. G., Chini, L. P., Chevallier, F., Cosca, C. E., Harris, I., Hoppema, M., Houghton, R. A., House, J. I., Jain, A. K., Johannessen, T., Kato, E., Keeling, R. F., Kitidis, V., Klein Goldewijk, K., Koven, C., Landa, C. S., Landschützer, P., Lenton, A., Lima, I. D., Marland, G., Mathis, J. T.,

Formatted: Space Before: 0 pt, After: 8 pt

Metzl, N., Nojiri, Y., Olsen, A., Ono, T., Peng, S., Peters, W., Pfeil, B., Poulter, B., Raupach, M. R., Regnier, P., Rödenbeck, C., Saito, S., Salisbury, J. E., Schuster, U., Schwinger, J., Séférian, R., Segschneider, J., Steinhoff, T., Stocker, B. D., Sutton, A. J., Takahashi, T., Tilbrook, B., van der Werf, G. R., Viovy, N., Wang, Y.-P., Wanninkhof, R., Wiltshire, A., and Zeng, N.: Global carbon budget 2014, Earth Syst. Sci. Data, 7, 47–85, https://doi.org/10.5194/essd-7-47-2015, 2015a.

Le Quéré, C., Moriarty, R., Andrew, R. M., Canadell, J. G., Sitch, S., Korsbakken, J. I., Friedlingstein, P., Peters, G. P., Andres, R. J., Boden, T. A., Houghton, R. A., House, J. I., Keeling, R. F., Tans, P., Arneth, A., Bakker, D. C. E., Barbero, L., Bopp, L., Chang, J., Chevallier, F., Chini, L. P., Ciais, P., Fader, M., Feely, R. A., Gkritzalis, T., Harris, I., Hauck, J., Ilyina, T., Jain, A. K., Kato, E., Kitidis, V., Klein Goldewijk, K., Koven, C., Landschützer, P., Lauvset, S. K., Lefèvre, N., Lenton, A., Lima, I. D., Metzl, N., Millero, F., Munro, D. R., Murata, A., Nabel, J. E. M. S., Nakaoka, S., Nojiri, Y., O'Brien, K., Olsen, A., Ono, T., Pérez, F. F., Pfeil, B., Pierrot, D., Poulter, B., Rehder, G., Rödenbeck, C., Saito, S., Schuster, U., Schwinger, J., Séférian, R., Steinhoff, T., Stocker, B. D., Sutton, A. J., Takahashi, T., Tilbrook, B., van der Laan-Luijkx, I. T., van der Werf, G. R., van Heuven, S., Vandemark, D., Viovy, N., Wiltshire, A., Zaehle, S., and Zeng, N.: Global Carbon Budget 2015, Earth Syst. Sci. Data, 7, 349–396, https://doi.org/10.5194/essd-7-349-2015, 2015b.

Le Quéré, C., Andrew, R. M., Canadell, J. G., Sitch, S., Korsbakken, J. I., Peters, G. P., Manning, A. C., Boden, T. A., Tans, P. P., Houghton, R. A., Keeling, R. F., Alin, S., Andrews, O. D., Anthoni, P., Barbero, L., Bopp, L., Chevallier, F., Chini, L. P., Ciais, P., Currie, K., Delire, C., Doney, S. C., Friedlingstein, P., Gkritzalis, T., Harris, I., Hauck, J., Haverd, V., Hoppema, M., Klein Goldewijk, K., Jain, A. K., Kato, E., Körtzinger, A., Landschützer, P., Lefèvre, N., Lenton, A., Lienert, S., Lombardozzi, D., Melton, J. R., Metzl, N., Millero, F., Monteiro, P. M. S., Munro, D. R., Nabel, J. E. M. S., Nakaoka, S., O'Brien, K., Olsen, A., Omar, A. M., Ono, T., Pierrot, D., Poulter, B., Rödenbeck, C., Salisbury, J., Schuster, U., Schwinger, J., Séférian, R., Skjelvan, I., Stocker, B. D., Sutton, A. J., Takahashi, T., Tian, H., Tilbrook, B., van der Laan-Luijkx, I. T., van der Werf, G. R., Viovy, N., Walker, A. P., Wiltshire, A. J., and Zaehle, S.: Global Carbon Budget 2016, Earth Syst. Sci. Data, 8, 605–649, https://doi.org/10.5194/essd-8-605-2016, 2016.

Le Quéré, C., Andrew, R. M., Friedlingstein, P., Sitch, S., Pongratz, J., Manning, A. C., Korsbakken, J. I., Peters, G. P., Canadell, J. G., Jackson, R. B., Boden, T. A., Tans, P. P., Andrews, O. D., Arora, V. K., Bakker, D. C. E., Barbero, L., Becker, M., Betts, R. A., Bopp, L., Chevallier, F., Chini, L. P., Ciais, P., Cosca, C. E., Cross, J., Currie, K., Gasser, T., Harris, I., Hauck, J., Haverd, V., Houghton, R. A., Hunt, C. W., Hurtt, G., Ilyina, T., Jain, A. K., Kato, E., Kautz, M., Keeling, R. F., Klein Goldewijk, K., Körtzinger, A., Landschützer, P., Lefèvre, N., Lenton, A., Lienert, S., Lima, I., Lombardozzi, D., Metzl, N., Millero, F., Monteiro, P. M. S., Munro, D. R., Nabel, J. E. M. S., Nakaoka, S., Nojiri, Y., Padin, X. A., Peregon, A., Pfeil, B., Pierrot, D., Poulter, B., Rehder, G., Reimer, J., Rödenbeck, C., Schwinger, J., Séférian, R., Skjelvan, I., Stocker, B. D., Tian, H., Tilbrook, B., Tubiello, F. N., van der Laan-Luijkx, I. T., van der Werf, G. R., van Heuven, S., Viovy, N., Vuichard, N., Walker, A. P., Watson, A. J., Wiltshire, A. J., Zaehle, S., and Zhu, D.: Global Carbon Budget 2017, Earth Syst. Sci. Data, 10, 405–448, https://doi.org/10.5194/essd-10-405-2018, 2018a.

Le Quéré, C., Andrew, R. M., Friedlingstein, P., Sitch, S., Hauck, J., Pongratz, J., Pickers, P. A., Korsbakken, J. I., Peters, G. P., Canadell, J. G., Arneth, A., Arora, V. K., Barbero, L., Bastos, A., Bopp, L., Chevallier, F., Chini, L. P., Ciais, P., Doney, S. C., Gkritzalis, T., Goll, D. S., Harris, I., Haverd, V., Hoffman, F. M., Hoppema, M., Houghton, R. A., Hurtt, G., Ilyina, T., Jain, A. K., Johannessen, T., Jones, C. D., Kato, E., Keeling, R. F., Klein Goldewijk, K., Landschützer, P., Lefèvre, N., Lienert, S., Liu, Z., Lombardozzi, D., Metzl, N., Munro, D. R., Nabel, J. E. M. S., Nakaoka, S., Neill, C., Olsen, A., Ono, T., Patra, P., Peregon, A., Peters, W., Peylin, P., Pfeil, B., Pierrot, D., Poulter, B., Rehder, G., Resplandy, L., Robertson, E., Rocher, M., Rödenbeck, C., Schuster, U., Schwinger, J., Séférian, R., Skjelvan, I., Steinhoff, T., Sutton, A., Tans, P. P., Tian, H., Tilbrook, B., Tubiello, F. N., van der Laan-Luijkx, I. T., van der Werf, G. R., Viovy, N., Walker, A. P., Wiltshire, A. J., Wright, R., Zaehle, S., and Zheng, B.: Global Carbon Budget 2018, Earth Syst. Sci. Data, 10, 2141–2194, https://doi.org/10.5194/essd-10-2141-2018, 2018b.

Le Quéré, C., Korsbakken, J. I., Wilson, C., Tosun, J., Andrew, R., Andres, R. J., Canadell, J. G., Jordan, A., Peters, G. P., and van Vuuren, D. P.: Drivers of declining CO2 emissions in 18 developed economies, Nat. Clim. Chang., 9, 213–217, https://doi.org/10.1038/s41558-019-0419-7, 2019.

Le Quéré, C., Peters, G. P., Friedlingstein, P., Andrew, R. M., Canadell, J. G., Davis, S. J., Jackson, R. B., and Jones, M. W.: Fossil CO2 emissions in the post-COVID-19 era, Nat. Clim. Chang., 11, 197–199, https://doi.org/10.1038/s41558-021-01001-0, 2021.

Le Quéré, C., Andrew, R.M., Candela, J.G., Friedlingstein, P, Jackson, R.B, & Peters, G.P.: A further acceleration of clean energy is needed for global CO_2 emissions to peak and decline. *Nature Climate Change* https://dx.doi.org/10.1038/s41558-026-02821-8, 2026.

Levitus, S., Antonov, J. I., Boyer, T. P., Baranova, O. K., Garcia, H. E., Locarnini, R. A., Mishonov, A. V., Reagan, J. R., Seidov, D., Yarosh, E. S., and Zweng, M. M.: World ocean heat content and thermosteric sea level change (0–2000 m), 1955–2010, Geophys. Res. Lett., 39, https://doi.org/10.1029/2012GL051106, 2012.

Li, H., Ilyina, T., Müller, W. A., and Sienz, F.: Decadal predictions of the North Atlantic CO2 uptake, Nat. Commun., 7, 11076, https://doi.org/10.1038/ncomms11076, 2016.

Li, H., Ilyina, T., Müller, W. A., and Landschützer, P.: Predicting the variable ocean carbon sink, Sci. Adv., 5, eaav6471, https://doi.org/10.1126/sciadv.aav6471, 2019.

Li, H., Ilyina, T., Loughran, T., Spring, A., and Pongratz, J.: Reconstructions and predictions of the global carbon budget with an emission-driven Earth system model, Earth Syst. Dyn., 14, 101–119, https://doi.org/10.5194/esd-14-101-2023, 2023.

Li, W., Ciais, P., Peng, S., Yue, C., Wang, Y., Thurner, M., Saatchi, S. S., Arneth, A., Avitabile, V., Carvalhais, N., Harper, A. B., Kato, E., Koven, C., Liu, Y. Y., Nabel, J. E. M. S., Pan, Y., Pongratz, J., Poulter, B., Pugh, T. A. M., Santoro, M., Sitch, S., Stocker, B. D., Viovy, N., Wiltshire, A., Yousefpour, R., and Zaehle, S.: Land-use and land-cover change carbon emissions between 1901 and 2012 constrained by biomass observations, Biogeosciences, 14, 5053–5067, https://doi.org/10.5194/bg-14-5053-2017, 2017.

~~Liao, E., Resplandy, L., Liu, J., and Bowman, K. W.: Amplification of the Ocean Carbon Sink During El Niños: Role of Poleward Ekman Transport and Influence on Atmospheric CO2, Global Biogeochem. Cy., 34, e2020GB006574, https://doi.org/10.1029/2020GB006574, 2020.~~
Li, H., Ilyina, T., Dunkl, I., Brune, S., Müller, W. A., Bernardello, R., Bethke, I., Bopp, L., Fransner, F., Friedlingstein, P., Lapin, V., Merryfield, W. J., Mignot, J., O'Sullivan, M., Sospedra-Alfonso, R., Swingedouw, D., Tatebe, H., Tjiputra, J., Torres, O., and Tourigny, E.: Multimodel Reconstructions and Predictions of the CO2 Fluxes and Atmospheric CO2 Variations, Bulletin of the American Meteorological Society, 107, E1352–E1369, https://doi.org/10.1175/BAMS-D-25-0139.1, 2026.

Lienert, S. and Joos, F.: A Bayesian ensemble data assimilation to constrain model parameters and land-use carbon emissions, Biogeosciences, 15, 2909–2930, https://doi.org/10.5194/bg-15-2909-2018, 2018.

Liu, J., Baskaran, L., Bowman, K., Schimel, D., Bloom, A. A., Parazoo, N. C., Oda, T., Carroll, D., Menemenlis, D., Joiner, J., Commane, R., Daube, B., Gatti, L. V., McKain, K., Miller, J., Stephens, B. B., Sweeney, C., and Wofsy, S.: Carbon Monitoring System Flux Net Biosphere Exchange 2020 (CMS-Flux NBE 2020), 13, 299–330, https://doi.org/10.5194/essd-13-299-2021, 2021.

Liu, Z., Guan, D., Wei, W., Davis, S. J., Ciais, P., Bai, J., Peng, S., Zhang, Q., Hubacek, K., Marland, G., Andres, R. J., Crawford-Brown, D., Lin, J., Zhao, H., Hong, C., Boden, T. A., Feng, K., Peters, G. P., Xi, F., Liu, J., Li, Y., Zhao, Y., Zeng, N., and He, K.: Reduced carbon emission estimates from fossil fuel combustion and cement production in China, Nature, 524, 335–338, https://doi.org/10.1038/nature14677, 2015.

Liu, Z., Zeng, N., Liu, Y., Kalnay, E., Asrar, G., Wu, B., Cai, Q., Liu, D., and Han, P.: Improving the joint estimation of CO2 and surface carbon fluxes using a constrained ensemble Kalman filter in COLA (v1.0), Geosci. Model Dev., 15, 5511–5528, https://doi.org/10.5194/gmd-15-5511-2022, 2022.

Liu, Z., Ciais, P., Deng, Z., Lei, R., Davis, S. J., Feng, S., Zheng, B., Cui, D., Dou, X., Zhu, B., Guo, R., Ke, P., Sun, T., Lu, C., He, P., Wang, Y., Yue, X., Wang, Y., Lei, Y., Zhou, H., Cai, Z., Wu, Y., Guo, R., Han, T., Xue, J., Boucher, O., Boucher, E., Chevallier, F., Tanaka, K., Wei, Y., Zhong, H., Kang, C., Zhang, N., Chen, B., Xi, F., Liu, M., Bréon, F.-M., Lu, Y., Zhang, Q., Guan, D., Gong, P., Kammen, D. M., He, K., and Schellnhuber, H. J.: Near-real-time monitoring of global CO2 emissions reveals the effects of the COVID-19 pandemic, Nat Commun, 11, 5172~~, https://doi.org/10.1038/s41467-020-18922-7~~,~~, https://doi.org/10.1038/s41467-020-18922-7, 2020a.

Liu, Z., Ciais, P., Deng, Z., Davis, S. J., Zheng, B., Wang, Y., Cui, D., Zhu, B., Dou, X., Ke, P., Sun, T., Guo, R., Zhong, H., Boucher, O., Bréon, F.-M., Lu, C., Guo, R., Xue, J., Boucher, E., Tanaka, K., and Chevallier, F.: Carbon Monitor, a near-real-time daily dataset of global CO2 emission from fossil fuel and cement production, Sci Data, 7, 392~~, https://doi.org/10.1038/s41597-020-00708-7~~,~~, https://doi.org/10.1038/s41597-020-00708-7, 2020b.

~~Long, M. C., Stephens, B. B., McKain, K., Sweeney, C., Keeling, R. F., Kort, E. A., Morgan, E. J., Bent, J. D., Chandra, N., Chevallier, F., Commane, R., Daube, B. C., Krummel, P. B., Loh, Z., Luijkx, I. T., Munro, D., Patra, P., Peters, W., Ramonet, M., Rödenbeck, C., Stavert, A., Tans, P., Wofsy, S. C.: Strong Southern Ocean carbon uptake evident in airborne observations. Science, 374(6572), 1275–1280, https://doi.org/10.1126/science.abi4355, 2021.~~

Formatted: Space Before: 0 pt, After: 8 pt

Formatted: Space Before: 0 pt, After: 8 pt

Lovenduski, N. S., Bonan, G. B., Yeager, S. G., Lindsay, K., and Lombardozzi, D. L.: High predictability of terrestrial carbon fluxes from an initialized decadal prediction system, Environ. Res. Lett., 14, 124074, https://doi.org/10.1088/1748-9326/ab5c55, 2019a.

Lovenduski, N. S., Yeager, S. G., Lindsay, K., and Long, M. C.: Predicting near-term variability in ocean carbon uptake, Earth Syst. Dyn., 10, 45–57, https://doi.org/10.5194/esd-10-45-2019, 2019b.

Lutz, F., Herzfeld, T., Heinke, J., Rolinski, S., Schaphoff, S., von Bloh, W., Stoorvogel, J. J., and Müller, C.: Simulating the effect of tillage practices with the global ecosystem model LPJmL (version 5.0-tillage), Geosci. Model Dev., 12, 2419–2440, https://doi.org/10.5194/gmd-12-2419-2019, 2019.

Ma, L., Hurtt, G., Ott, L., Sahajpal, R., Fisk, J., Lamb, R., Tang, H., Flanagan, S., Chini, L., Chatterjee, A., and Sullivan, J.: Global evaluation of the Ecosystem Demography model (ED v3.0), Geosci. Model Dev., 15, 1971–1994, https://doi.org/10.5194/gmd-15-1971-2022, 2022.

Ma, L., Hurtt, G., Tang, H., Hao, D., Ciais, P., Pan, Y., Sitch, S., Friedlingstein, P., ~~Magi, B.~~Dubayah, R., Nunes, M. H., and Wei, X.: Widespread carbon accumulation in mature forests remains underestimated by satellite observations, Nat Ecol Evol, 10, 1864–1872, https://doi.org/10.1038/s41559-026-03151-w, 2026.

Madec, G., Bell, M., Blaker, A., Bricaud, C., Bruciaferri, D., Castrillo, M., Calvert, D., Chanut, J., Clementi, E., Coward, A., Epicoco, I., Éthé, C., Ganderton, J., Harle, J., Hutchinson, K., Iovino, D., Lea, D., Lovato, T., Martin, M., Martin, N., Mele, F., Martins, D., Masson, S., Mathiot, P., Mele, F., Mocavero, S., Müller, S., Nurser, A. J. G., Paronuzzi, S., Peltier, M., Person, R., Rousset, C., Rynders, S., Samson, G., Téchené, S., Vancoppenolle, M., Wilson, C. (2023). NEMO Ocean Engine Reference Manual. In Scientific Notes of IPSL Climate Modelling Center (Version v4.2). Zenodo. https://doi.org/10.5281/zenodo.8167700, 2023.Magi, B. I., Rabin, S., Shevliakova, E., and Pacala, S.: Separating agricultural and non-agricultural fire seasonality at regional scales, Biogeosciences, 9, 3003–3012, https://doi.org/10.5194/bg-9-3003-2012, 2012.

Maity, S., Niwa, Y., Saeki, T., Someya, Y., and Yoshida, Y.: Drivers of 2023–2024 Atmospheric CO2 Growth: Role of Northern Mid-to-High Latitude Land Carbon Cycle, Geophysical Research Letters, 53, e2026GL122221, https://doi.org/10.1029/2026GL122221, 2026.

Maksyutov, S., Oda, T., Saito, M., Janardanan, R., Belikov, D., Kaiser, J. W., Zhuravlev, R., Ganshin, A., Valsala, V. K., Andrews, A., Chmura, L., Dlugokencky, E., Haszpra, L., Langenfelds, R. L., Machida, T., Nakazawa, T., Ramonet, M., Sweeney, C., and Worthy, D.: Technical note: A high-resolution inverse modelling technique for estimating surface CO2 fluxes based on the NIES-TM–FLEXPART coupled transport model and its adjoint, Atmos. Chem. Phys., 21, 1245–1266, https://doi.org/10.5194/acp-21-1245-2021, 2021.

Masarie, K. A. and Tans, P. P.: Extension and integration of atmospheric carbon dioxide data into a globally consistent measurement record, J. Geophys. Res., 100, 11593, https://doi.org/10.1029/95JD00859, 1995.

~~Mataveli, G., Jones, M.W., Carmenta, R., Sanchez, A., Dutra, D.J., Chaves, M., de Oliveira, G., Anderson, L.O. and Aragão, L.E.: Deforestation falls but rise of wildfires continues degrading Brazilian Amazon forests. Global Change Biology, 30(2), p.e17202, https://doi.org/10.1111/gcb.17202, 2024.~~

Mather, A. S.: The transition from deforestation to reforestation in Europe, in: Agricultural technologies and tropical deforestation (eds. Angelsen, A.; Kaimowitz, D.), CABI in association with centre for international Forestry Research, 35–52, 2001.

Matsumoto, K., Sarmiento, J. L., Key, R. M., Aumont, O., Bullister, J. L., Caldeira, K., Campin, J. -M., Doney, S. C., Drange, H., Dutay, J. -C., Follows, M., Gao, Y., Gnanadesikan, A., Gruber, N., Ishida, A., Joos, F., Lindsay, K., Maier-Reimer, E., Marshall, J. C., Matear, R. J., Monfray, P., Mouchet, A., Najjar, R., Plattner, G. -K., Schlitzer, R., Slater, R., Swathi, P. S., Totterdell, I. J., Weirig, M. -F., Yamanaka, Y., Yool, A., and Orr, J. C.: Evaluation of ocean carbon cycle models with data-based metrics, Geophysical Research Letters, 31, 2003GL018970, https://doi.org/10.1029/2003GL018970, 2004.

Mauritsen, T., Bader, J., Becker, T., Behrens, J., Bittner, M., Brokopf, R., Brovkin, V., Claussen, M., Crueger, T., Esch, M., Fast, I., Fiedler, S., Fläschner, D., Gayler, V., Giorgetta, M., Goll, D. S., Haak, H., Hagemann, S., Hedemann, C., Hohenegger, C., Ilyina, T., Jahns, T., Jimenéz-de-la-Cuesta, D., Jungclaus, J., Kleinen, T., Kloster, S., Kracher, D., Kinne, S., Kleberg, D., Lasslop, G., Kornblueh, L., Marotzke, J., Matei, D., Meraner, K., Mikolajewicz, U., Modali, K., Möbis, B., Müller, W. A., Nabel, J. E. M. S., Nam, C. C. W., Notz, D., Nyawira, S.-S., Paulsen, H., Peters, K., Pincus, R., Pohlmann, H., Pongratz, J., Popp, M., Raddatz, T. J., Rast, S., Redler, R., Reick, C. H., Rohrschneider, T., Schemann, V., Schmidt, H., Schnur, R., Schulzweida, U., Six, K. D., Stein, L., Stemmler, I., Stevens, B., von Storch, J.-S., Tian, F., Voigt, A., Vrese, P., Wieners, K.-H., Wilkenskjeld, S., Winkler, A., and Roeckner, E.: Developments in the MPI-M Earth System Model version 1.2 (MPI-ESM1.2) and

Formatted: Space Before: 0 pt, After: 8 pt

Formatted: Space Before: 0 pt, After: 8 pt

Formatted: Space Before: 0 pt, After: 8 pt

Formatted: Space Before: 0 pt, After: 8 pt

Formatted: Space Before: 0 pt, After: 8 pt

Its Response to Increasing CO2, J. Adv. Model Earth Sy., 11, 998–1038, https://doi.org/10.1029/2018MS001400, 2019.

Mayot, N., Buitenhuis, E. T., Wright, R. M., Hauck, J., Bakker, D. C. E., and Le Quéré, C.: Constraining the trend in the ocean CO2 sink during 2000–2022. Nat Commun 15, 8429, https://doi.org/10.1038/s41467-024-52641-7, 2024.

McGrath, M. J., Luyssaert, S., Meyfroidt, P., Kaplan, J. O., Bürgi, M., Chen, Y., Erb, K., Gimmi, U., McInerney, D., Naudts, K., Otto, J., Pasztor, F., Ryder, J., Schelhaas, M.-J., and Valade, A.: Reconstructing European forest management from 1600 to 2010, 12, 4291–4316, https://doi.org/10.5194/bg-12-4291-2015, 2015.

McGuire, A. D., Sitch, S., Clein, J. S., Dargaville, R., Esser, G., Foley, J., Heimann, M., Joos, F., Kaplan, J., Kicklighter, D. W., Meier, R. A., Melillo, J. M., Moore, B., Prentice, I. C., Ramankutty, N., Reichenau, T., Schloss, A., Tian, H., Williams, L. J., and Wittenberg, U.: Carbon balance of the terrestrial biosphere in the Twentieth Century: Analyses of CO2 , climate and land use effects with four process-based ecosystem models, Global Biogeochemical Cycles, 15, 183–206, https://doi.org/10.1029/2000GB001298, 2001.

McKinley, G. A., Fay, A. R., Eddebbar, Y. A., Gloege, L., and Lovenduski, N. S.: External Forcing Explains Recent Decadal Variability of the Ocean Carbon Sink, AGU Advances, 1, e2019AV000149, https://doi.org/10.1029/2019AV000149, 2020.

McKinley, G. A., Fay, A. R., Lovenduski, N. S., and Pilcher, D. J.: Natural Variability and Anthropogenic Trends in the Ocean Carbon Sink, Annu. Rev. Mar. Sci., 9, 125–150, https://doi.org/10.1146/annurev-marine-010816-060529, 2017.

McKinley, G. A., Fay, A., Heimdal, T. H., Moseley, L., and Shaum, A.: How well do global ocean approaches constrain local fCO2?, Environ. Res. Lett., 21, 134011, https://doi.org/10.1088/1748-9326/ae803e, 2026.

Meiyappan, P., Jain, A. K., and House, J. I.: Increased influence of nitrogen limitation on CO 2 emissions from future land use and land use change, Global Biogeochem. Cycles, 29, 1524–1548, https://doi.org/10.1002/2015GB005086, 2015.

Melo, J., Rossi, S., Achard, F., Alkama, R., Canadell, J. G., Federici, S., Friedlingstein, P., Gibbs, D., Harris, N., Heinrich, V., O'Sullivan, M., Peters, G., Pongratz, J., Rose, M., Roman-Cuesta, R., Sanz Sanchez, M. J., Schwingshackl, C., Sitch, S., and Grassi, G.: The LULUCF Data Hub: translating global land use emissions estimates into the national GHG inventory framework (Version ~~3.0, 2025 NGHGI release) (3.0), https://doi.org/10.5281/ZENODO.17140775, 2025~~4.0.0, 2026 NGHGI release) (4.0.0) [Dataset], Zenodo. https://doi.org/10.5281/ZENODO.17140775, 2026.

Melton, J. R., Arora, V. K., Wisernig-Cojoc, E., Seiler, C., Fortier, M., Chan, E., and Teckentrup, L.: CLASSIC v1.0: the open-source community successor to the Canadian Land Surface Scheme (CLASS) and the Canadian Terrestrial Ecosystem Model (CTEM) – Part 1: Model framework and site-level performance, Geosci. Model Dev., 13, 2825–2850, https://doi.org/10.5194/gmd-13-2825-2020, 2020.

Mercado, L. M., Bellouin, N., Sitch, S., Boucher, O., Huntingford, C., Wild, M., and Cox, P. M.: Impact of changes in diffuse radiation on the global land carbon sink, Nature, 458, 1014–1017, https://doi.org/10.1038/nature07949, 2009.

~~Merchant, C. J., Embury, O., Bulgin, C. E., Block, T., Corlett, G. K., Fiedler, E., Good, S. A., Mittaz, J., Rayner, N. A., Berry, D., Eastwood, S., Taylor, M., Tsushima, Y., Waterfall, A., Wilson, R., and Donlon, C.: Satellite-based time-series of sea-surface temperature since 1981 for climate applications, Sci. Data, 6, 223, https://doi.org/10.1038/s41597-019-0236-x, 2019.~~

Moorcroft, P. R., Hurtt, G. C., and Pacala, S. W.: A Method for Scaling Vegetation Dynamics: The Ecosystem Demography Model (ed), Ecol. Monogr., 71, 557–586, https://doi.org/10.1890/0012-9615(2001)071[0557:AMFSVD]2.0.CO;2, 2001.

Mouillot, F., Schultz, M. G., Yue, C., Cadule, P., Tansey, K., Ciais, P., and Chuvieco, E.: Ten years of global burned area products from spaceborne remote sensing—A review: Analysis of user needs and recommendations for future developments, International Journal of Applied Earth Observation and Geoinformation, 26, 64–79, https://doi.org/10.1016/j.jag.2013.05.014, 2014.

Müller, J. D., Gruber, N., Carter, B., Feely, R., Ishii, M., Lange, N., Lauvset, S. K., Murata, A., Olsen, A., Pérez, F. F., Sabine, C., Tanhua, T., Wanninkhof, R., and Zhu, D.: Decadal Trends in the Oceanic Storage of Anthropogenic Carbon From 1994 to 2014, AGU Adv., 4, e2023AV000875, https://doi.org/10.1029/2023AV000875, 2023.

Formatted: Space Before: 0 pt, After: 8 pt

Formatted: Space Before: 0 pt, After: 8 pt

Formatted: Space Before: 0 pt, After: 8 pt

Formatted: Space Before: 0 pt, After: 8 pt

Müller, J. D., Gruber, N., Schneuwly, A., Bakker, D. C. E., Gehlen, M., Gregor, L., Hauck, J., Landschützer, P., and McKinley, G. A.: Unexpected decline in the ocean carbon sink under record-high sea surface temperatures in 2023, Nat. Clim. Chang., 15, 978–985, https://doi.org/10.1038/s41558-025-02380-4, 2025.

Müller, J. and Joos, F.: Committed and projected future changes in global peatlands – continued transient model simulations since the Last Glacial Maximum, Biogeosciences, 18, 3657–3687, https://doi.org/10.5194/bg-18-3657-2021, 2021.

Naudts, K., Ryder, J., McGrath, M. J., Otto, J., Chen, Y., Valade, A., Bellasen, V., Berhongaray, G., Bönisch, G., Campioli, M., Ghattas, J., De Groote, T., Haverd, V., Kattge, J., MacBean, N., Maignan, F., Merilä, P., Penuelas, J., Peylin, P., Pinty, B., Pretzsch, H., Schulze, E. D., Solyga, D., Vuichard, N., Yan, Y., and Luyssaert, S.: A vertically discretised canopy description for ORCHIDEE (SVN r2290) and the modifications to the energy, water and carbon fluxes, Geosci. Model Dev., ~~Nayagam, L., Maksyutov, S., Oda, T., Janardanan, R., Trisolino, P., Zeng J., Kaiser, J.W. and Matsunaga, T.: A top-down estimation of subnational CO2 budget using a global high-resolution inverse model with data from regional surface networks,~~8, 2035–2065, https://doi.org/10.5194/gmd-8-2035-2015, 2015.

Naus, S., Peters, W., Hooghiem, J., van der Woude, A., Luijkx, I., Rödenbeck, C., Chevallier, F., Martinez, A., Niwa, Y., Maity, S., Jacobson, A.R., Liu, J., Bowman, K., Yun, J., Bloom, A., Jin, Z., Tian, X., Piao, S., Wang, Y., Zhang, H., Wang, T., Liu, Z., Zeng, N., Jiang, F., Feng, L., Palmer, P., Maksyutov, S., Nayagam, L., Janardanan, R., Kong, Y., Zheng, B. Qiu, Y "Global gridded CO2 fluxes and simulated mole fractions from the sixteen inverse models in the Global Carbon Budget 2026" DOI:10.18160/99Y6-6994, 2026.

~~Environ. Res. Lett., 19, 0140312024, https://doi.org/10.1088/1748-9326/ad0f74, 2024.~~
NCEP: National Centers for Environmental Prediction. ONI Index. Cold & Warm Episodes by Season [Data set], NOAA, available at: https://www.cpc.ncep.noaa.gov/products/analysis_monitoring/ensostuff/ONI_v5.php, last access: ~~23~~30 October ~~2025, 2025~~2026, 2026.

Nayagam, L., Maksyutov, S., Janardanan, R., Oda, T., Tiwari, Y. K., Sreenivas, G., Datye, A., Jain, C. D., Ratnam, M. V., Sinha, V., Hakkim, H., Terao, Y., Naja, M., Ahmed, Md. K., Mukai, H., Zeng, J., Kaiser, J. W., Someya, Y., Yoshida, Y., and Matsunaga, T.: Indian Land Carbon Sink Estimated from Surface and GOSAT Observations, Remote Sensing, 17, 450~~, https://doi.org/10.3390/rs17030450.~~, https://doi.org/10.3390/rs17030450, 2025.

Nevison, C.D., Mahowald, N.M., Doney, S.C., Lima, I.D. and Cassar, N.:. Impact of variable air-sea O 2 and CO 2 fluxes on atmospheric potential oxygen (APO) and land-ocean carbon sink partitioning. Biogeosciences, 5(3), pp.875-889, https://doi.org/10.5194/bg-5-875-2008, 2008.

Niu, ~~G.-Y., Yang, Z.-L., Mitchell, K. E., Chen, F., Ek, M. B., Barlage, M., Kumar, A., Manning, K., Niyogi, D., Rosero, E., Tewari, M., and Xia, Y.: The community Noah land surface model with multiparameterization options (Noah-MP): 1. Model description and evaluation with local-scale measurements, J. Geophys. Res. Atmospheres, 116, https://doi.org/10.1029/2010JD015139, 2011~~L., Wu, S., Andrew, R. M., Shao, Z., Wang, J., and Xi, F.: Global and national CO2 uptake by cement carbonation from 1928 to 2024, Earth Syst. Sci. Data, 17, 2231–2247, https://doi.org/10.5194/essd-17-2231-2025, 2025.

Niwa, Y., Ishijima, K., Ito, A., and Iida, Y.: Toward a long-term atmospheric CO2 inversion for elucidating natural carbon fluxes: technical notes of NISMON-CO2 v2021.1, Prog. Earth Planet Sci., 9, 42, https://doi.org/10.1186/s40645-022-00502-6, 2022.

Niwa, Y., Fujii, Y., Sawa, Y., Iida, Y., Ito, A., Satoh, M., Imasu, R., Tsuboi, K., Matsueda, H., and Saigusa, N.: A 4D-Var inversion system based on the icosahedral grid model (NICAM-TM 4D-Var v1.0) – Part 2: Optimization scheme and identical twin experiment of atmospheric CO₂ inversion, Geosci. Model Dev., 10, 2201–2219~~, https://doi.org/10.5194/gmd-10-2201-2017,~~, https://doi.org/10.5194/gmd-10-2201-2017, 2017.

~~Niwa, Y., Langenfelds, R., Krummel, P., Loh, Zoe, Worthy, Doug, Hatakka, Juha, Aalto, Tuula, Ramonet, Michel, Delmotte, Marc, Schmidt, Martina, Gheusi, Francois, Mihalopoulos, N., Morgui, J.A., Andrews, Arlyn, Dlugokencky, Ed, Lee, John, Sweeney, Colm, Thoning, Kirk, Tans, Pieter, De Wekker, Stephan, Fischer, Marc L., Jaffe, Dan, McKain, Kathryn, Viner, Brian, Miller, John B., Karion, Anna, Miller, Charles, Sloop, Christopher D., Saito, Kazuyuki, Aoki, Shuji, Morimoto, Shinji, Goto, Daisuke, Steinbacher, Martin, Myhre, Cathrine Lund, Hermanssen, Ove, Stephens, Britton, Keeling, Ralph, Afshar, Sara, Paplawsky, Bill, Cox, Adam, Walker, Stephen, Schuldt, Kenneth, Mukai, Hitoshi, Machida, Toshinobu, Sasakawa, Motoki, Nomura, Shohei, Ito, Akihiko, Iida, Yosuke, and Jones, Matthew W.: Long-term global CO2 fluxes estimated by NICAM-based Inverse Simulation for Monitoring CO2 (NISMON-CO2) (ver.2022.1), National Institute for Environmental Studies Japan [Data set], https://doi.org/10.17595/20201127.001, 2020.~~

Formatted: Space Before: 0 pt, After: 8 pt

Norby, R.J.: Forest productivity response to elevated CO2 in free-air CO2 enrichment experiments: the 23 percent solution, revisited, New Phytologist, ~~https://doi.org/10.1111/nph.70162,~~https://doi.org/10.1111/nph.70162, 2025.

Obermeier, W. A., Nabel, J. E. M. S., Loughran, T., Hartung, K., Bastos, A., Havermann, F., Anthoni, P., Arneth, A., Goll, D. S., Lienert, S., Lombardozzi, D., Luyssaert, S., McGuire, P. C., Melton, J. R., Poulter, B., Sitch, S., Sullivan, M. O., Tian, H., Walker, A. P., Wiltshire, A. J., Zaehle, S., and Pongratz, J.: Modelled land use and land cover change emissions – a spatio-temporal comparison of different approaches, 12, 635–670, https://doi.org/10.5194/esd-12-635-2021, 2021.

Obermeier, W. A., Schwingshackl, C., Ganzenmüller, R., Grassi, G., Heinrich, V., Luijkx, I. T., Bastos, A., Ciais, P., Sitch, S., and Pongratz, J.: Differences and uncertainties in land-use CO2 flux estimates, Nat Rev Earth Environ, https://doi.org/10.1038/s43017-025-00730-6, 2025.

Obli-Laryea, G. and Tubiello, F.: FAO net Forest Emissions/removals 1990-2025 [Dataset], Zenodo. https://doi.org/10.5281/ZENODO.21489542, 2026.

O'Dell, C. W., Eldering, A., Wennberg, P. O., Crisp, D., Gunson, M. R., Fisher, B., Frankenberg, C., Kiel, M., Lindqvist, H., Mandrake, L., Merrelli, A., Natraj, V., Nelson, R. R., Osterman, G. B., Payne, V. H., Taylor, T. E., Wunch, D., Drouin, B. J., Oyafuso, F., Chang, A., McDuffie, J., Smyth, M., Baker, D. F., Basu, S., Chevallier, F., Crowell, S. M. R., Feng, L., Palmer, P. I., Dubey, M., García, O. E., Griffith, D. W. T., Hase, F., Iraci, L. T., Kivi, R., Morino, I., Notholt, J., Ohyama, H., Petri, C., Roehl, C. M., Sha, M. K., Strong, K., Sussmann, R., Te, Y., Uchino, O., and Velazco, V. A.: Improved retrievals of carbon dioxide from Orbiting Carbon Observatory-2 with the version 8 ACOS algorithm, Atmos. Meas. Tech., 11, 6539–6576~~, https://doi.org/10.5194/amt-11-6539-2018,~~ https://doi.org/10.5194/amt-11-6539-2018, 2018.

~~O'Rourke, P. R., Smith, S. J., Mott, A., Ahsan, H., McDuffie, E. E., Crippa, M., Klimont, Z., McDonald, B., Wang, S., Nicholson, M. B., Feng, L., and Hoesly, R. M.: CEDS v_2021_04_21 Release Emission Data, Zenodo [Data set], https://doi.org/10.5281/zenodo.4741285, 2021.~~

O'Sullivan, M., Zhang, Y., Bellouin, N., Harris, I., Mercado, L. M., Sitch, S., Ciais, P., and Friedlingstein, P.: Aerosol–light interactions reduce the carbon budget imbalance, Environ. Res. Lett., 16, 124072, https://doi.org/10.1088/1748-9326/ac3b77, 2021.

O'Sullivan, M., Friedlingstein, P., Sitch, S., Anthoni, P., Arneth, A., Arora, V. K., Bastrikov, V., Delire, C., Goll, D. S., Jain, A., Kato, E., Kennedy, D., Knauer, J., Lienert, S., Lombardozzi, D., McGuire, P. C., Melton, J. R., Nabel, J. E. M. S., Pongratz, J., Poulter, B., Séférian, R., Tian, H., Vuichard, N., Walker, A. P., Yuan, W., Yue, X., and Zaehle, S.: Process-oriented analysis of dominant sources of uncertainty in the land carbon sink, Nat. Commun., 13, 4781, https://doi.org/10.1038/s41467-022-32416-8, 2022.

O'Sullivan, M., Spracklen, D. V., Batterman, S. A., Arnold, S. R., Gloor, M., and Buermann, W.: Have Synergies Between Nitrogen Deposition and Atmospheric CO2 Driven the Recent Enhancement of the Terrestrial Carbon Sink?, Glob. Biogeochem. Cycles, 33, 163–180, https://doi.org/10.1029/2018GB005922, 2019.

O'Sullivan, M., Sitch, S., Friedlingstein, P., Luijkx, I. T., Peters, W., Rosan, T. M., Arneth, A., Arora, V. K., Chandra, N., Chevallier, F., Ciais, P., Falk, S., Feng, L., Gasser, T., Houghton, R. A., Jain, A. K., Kato, E., Kennedy, D., Knauer, J., McGrath, M. J., Niwa, Y., Palmer, P. I., Patra, P. K., Pongratz, J., Poulter, B., Rödenbeck, C., Schwingshackl, C., Sun, Q., Tian, H., Walker, A. P., Yang, D., Yuan, W., Yue, X., and Zaehle, S.: The key role of forest disturbance in reconciling estimates of the northern carbon sink. Commun Earth Environ 5, 705, ~~https://doi.org/10.1038/s43247-024-01827-4,~~https://doi.org/10.1038/s43247-024-01827-4, 2024.

~~O'Sullivan~~O'Sullivan, M., Friedlingstein, P., Sitch, S., Pongratz, J., Schwingshackl, C., Gasser, T., Ciais, P., Arora, V., Kato, E., Knauer, J., Monier, E., Nützel, T., Sun, Q., Yuan~~,~~, W., Yue, X., and Zaehle, S.: An improved approach to estimate the natural land carbon sink, ~~27 July 2025, PREPRINT (Version 1) available at Research Square [https://doi.org/10.21203/rs.3.rs-7207206/v1], 2025~~npj Clim Atmos Sci, 9, 29, https://doi.org/10.1038/s41612-025-01302-7, 2026a.

O'Sullivan, M., Sitch, S., Friedlingstein, P., Smallman, T. L., Knauer, J., Arora, V., Foster, A., Aas, K., Tian, H., Ma, L., Yang, X., Felzer, B., Yuan, W., Yue, X., Jain, A. K., Nutzel, T., Burke, E., Belda, D., Poulter, B., Heinke, J., Sun, Q., Luyssaert, S., Slominska-Durdasiak, K., Walker, A., Kato, E., Ito, A., Séférian, R.: TRENDY Land Model Output for the Global Carbon Budget 2026 [Dataset]. Zenodo. https://doi.org/10.5281/zenodo.23561904, 2026b.

Palmer, P. I., Feng, L., Baker, D., Chevallier, F., Bösch, H., and Somkuti, P.: Net carbon emissions from African biosphere dominate pan-tropical atmospheric CO2 signal, Nat Commun, 10, 3344, https://doi.org/10.1038/s41467-019-11097-w, 2019.

Formatted: Space Before: 0 pt, After: 8 pt

Formatted: Space Before: 0 pt, After: 8 pt

Formatted: Space Before: 0 pt, After: 8 pt

Formatted: Space Before: 0 pt, After: 8 pt

Pan, Y., Birdsey, R. A., Fang, J., Houghton, R., Kauppi, P. E., Kurz, W. A., Phillips, O. L., Shvidenko, A., Lewis, S. L., Canadell, J. G., Ciais, P., Jackson, R. B., Pacala, S. W., McGuire, A. D., Piao, S., Rautiainen, A., Sitch, S., and Hayes, D.: A Large and Persistent Carbon Sink in the World's Forests, Science, 333, 988–993, https://doi.org/10.1126/science.1201609, 2011.

Pandey, S., Miller, J. B., Basu, S., Liu, J., Weir, B., Byrne, B., Chevallier, F., Bowman, K. W., Liu, Z., Deng, F., O'Dell, C. W., and Chatterjee, A.: Toward Low-Latency Estimation of Atmospheric CO2 Growth Rates Using Satellite Observations: Evaluating Sampling Errors of Satellite and In Situ Observing Approaches, AGU Advances, 5, e2023AV001145~~, https://doi.org/10.1029/2023AV001145.~~, https://doi.org/10.1029/2023AV001145, 2024.

Pandey, S., Chevallier, F., Rödenbeck, C., Byrne, B., Chatterjee, A., Liu, J., and Frankenberg, C.: Reduction in Earth's carbon budget imbalance, Nat Commun, 16, 6818~~, https://doi.org/10.1038/s41467-025-61588-2.~~, https://doi.org/10.1038/s41467-025-61588-2, 2025.

~~Patra, P. K., Takigawa, M., Watanabe, S., Chandra, N.,~~ Patara, L., Rieck, J. K., Hauck, J., Ödalen, M., Oschlies, A., and Gürses, Ö.: Stronger Southern Ocean Anthropogenic Carbon Uptake in Eddying Ocean Simulations, Journal of Climate, 39, 2017–2037, https://doi.org/10.1175/JCLI-D-25-0198.1, 2026.

~~Ishijima, K., and Yamashita, Y.: Improved Chemical Tracer Simulation by MIROC4.0-based Atmospheric Chemistry-Transport Model (MIROC4-ACTM), SOLA, 14, 91–96, https://doi.org/10.2151/sola.2018-016, 2018.~~

Pendrill, F., Persson, U. M., Godar, J., Kastner, T., Moran, D., Schmidt, S., and Wood, R.: Agricultural and forestry trade drives large share of tropical deforestation emissions, Global Environmental Change, 56, 1–10, https://doi.org/10.1016/j.gloenvcha.2019.03.002, 2019.

Pérez, F. F., Becker, M., Goris, N., Gehlen, M., López-Mozos, M., Tjiputra, J., Olsen, A., Müller, J. D., Huertas, I. E., Chau, T. T. T., Cainzos, V., Velo, A., Benard, G., Hauck, J., Gruber, N., and Wanninkhof, R.: An Assessment of CO 2 Storage and Sea-Air Fluxes for the Atlantic Ocean and Mediterranean Sea Between 1985 and 2018. Global Biogeochemical Cycles, 38(4), e2023GB007862, https://doi.org/10.1029/2023GB007862, 2024.

Peters, G. P., Minx, J. C., Weber, C. L., and Edenhofer, O.: Growth in emission transfers via international trade from 1990 to 2008, Proceedings of the National Academy of Sciences, 108, 8903–8908, https://doi.org/10.1073/pnas.1006388108, ~~2011a~~2011.

Peters, G. P., Marland, G., Le Quéré, C., Boden, T., Canadell, J. G., and Raupach, M. R.: Rapid growth in CO2 emissions after the 2008–2009 global financial crisis, Nature Clim Change, 2, 2–4, https://doi.org/10.1038/nclimate1332, 2012a.

Peters, G. P., Andrew, R. M., Boden, T., Canadell, J. G., Ciais, P., Le Quéré, C., Marland, G., Raupach, M. R., and Wilson, C.: The challenge to keep global warming below 2 °C, Nature Clim Change, 3, 4–6, https://doi.org/10.1038/nclimate1783, 2013.

Peters, G. P., Le Quéré, C., Andrew, R. M., Canadell, J. G., Friedlingstein, P., Ilyina, T., Jackson, R. B., Joos, F., Korsbakken, J. I., McKinley, G. A., Sitch, S., and Tans, P.: Towards real-time verification of CO2 emissions, Nature Clim Change, 7, 848–850, https://doi.org/10.1038/s41558-017-0013-9, 2017a.

Peters, G. P., Andrew, R. M., Canadell, J. G., Fuss, S., Jackson, R. B., Korsbakken, J. I., Le Quéré, C. and Nakicenovic, N.: Key indicators to track current progress and future ambition of the Paris Agreement, 7, 118–122, https://doi.org/10.1038/nclimate3202, 2017b.

Peters, G. P., Andrew, R. M., Canadell, J. G., Friedlingstein, P., Jackson, R. B., Korsbakken, J. I., Le Quéré, C., and Peregon, A.: Carbon dioxide emissions continue to grow amidst slowly emerging climate policies, Nat. Clim. Chang., 10, 3–6, https://doi.org/10.1038/s41558-019-0659-6, 2020.

~~Peters, W., Miller, J. B., Whitaker, J., Denning, A. S., Hirsch, A., Krol, M. C., Zupanski, D., Bruhwiler, L., and Tans, P. P.: An ensemble data assimilation system to estimate CO2 surface fluxes from atmospheric trace gas observations, J. Geophys. Res. Atmospheres, 110, https://doi.org/10.1029/2005JD006157, 2005.~~

Petrescu, A. M. R., Peters, G. P., Janssens-Maenhout, G., Ciais, P., Tubiello, F. N., Grassi, G., Nabuurs, G.-J., Leip, A., Carmona-Garcia, G., Winiwarter, W., Höglund-Isaksson, L., Günther, D., Solazzo, E., Kiesow, A., Bastos, A., Pongratz, J., Nabel, J. E. M. S., Conchedda, G., Pilli, R., Andrew, R. M., Schelhaas, M.-J., and Dolman, A. J.: European anthropogenic AFOLU greenhouse gas emissions: a review and benchmark data, Earth Syst. Sci. Data, 12, 961–1001, https://doi.org/10.5194/essd-12-961-2020, 2020.

Pfeil, B., Olsen, A., Bakker, D. C. E., Hankin, S., Koyuk, H., Kozyr, A., Malczyk, J., Manke, A., Metzl, N., Sabine, C. L., Akl, J., Alin, S. R., Bates, N., Bellerby, R. G. J., Borges, A., Boutin, J., Brown, P. J., Cai, W.-J., Chavez, F.

Formatted: Font: Cambria Math

Formatted: Space Before: 0 pt, After: 8 pt

Formatted: Font: Cambria Math

Formatted: Font: Cambria Math

Formatted: Space Before: 0 pt, After: 8 pt

P., Chen, A., Cosca, C., Fassbender, A. J., Feely, R. A., González-Dávila, M., Goyet, C., Hales, B., Hardman-Mountford, N., Heinze, C., Hood, M., Hoppema, M., Hunt, C. W., Hydes, D., Ishii, M., Johannessen, T., Jones, S. D., Key, R. M., Körtzinger, A., Landschützer, P., Lauvset, S. K., Lefèvre, N., Lenton, A., Lourantou, A., Merlivat, L., Midorikawa, T., Mintrop, L., Miyazaki, C., Murata, A., Nakadate, A., Nakano, Y., Nakaoka, S., Nojiri, Y., Omar, A. M., Padin, X. A., Park, G.-H., Paterson, K., Perez, F. F., Pierrot, D., Poisson, A., Ríos, A. F., Santana-Casiano, J. M., Salisbury, J., Sarma, V. V. S. S., Schlitzer, R., Schneider, B., Schuster, U., Sieger, R., Skjelvan, I., Steinhoff, T., Suzuki, T., Takahashi, T., Tedesco, K., Telszewski, M., Thomas, H., Tilbrook, B., Tjiputra, J., Vandemark, D., Veness, T., Wanninkhof, R., Watson, A. J., Weiss, R., Wong, C. S., and Yoshikawa-Inoue, H.: A uniform, quality controlled Surface Ocean CO2 Atlas (SOCAT), Earth Syst. Sci. Data, 5, 125–143, https://doi.org/10.5194/essd-5-125-2013, 2013.

Piao, S., Ciais, P., Friedlingstein, P., de Noblet-Ducoudré, N., Cadule, P., Viovy, N., and Wang, T.: Spatiotemporal patterns of terrestrial carbon cycle during the 20th century, Global Biogeochem. Cy., 23, GB4026, https://doi.org/10.1029/2008GB003339, 2009.

Piao, S., Huang, M., Liu, Z., Wang, X., Ciais, P., Canadell, J. G., Wang, K., Bastos, A., Friedlingstein, P., Houghton, R. A., Le Quéré, C., Liu, Y., Myneni, R. B., Peng, S., Pongratz, J., Sitch, S., Yan, T., Wang, Y., Zhu, Z., Wu, D., and Wang, T.: Lower land-use emissions responsible for increased net land carbon sink during the slow warming period, Nature Geosci, 11, 739–743, https://doi.org/10.1038/s41561-018-0204-7, 2018.

Planchat, A., Bopp, L., and Kwiatkowski, L.: A fresh look at the pre-industrial air–sea carbon flux using the alkalinity budget, Biogeosciences, 22, 6017–6055, https://doi.org/10.5194/bg-22-6017-2025, 2025.

Pongratz, J., Reick, C.H., Raddatz, T. and Claussen, M.: Effects of anthropogenic land cover change on the carbon cycle of the last millennium. Global Biogeochemical Cycles, 23(4), doi:10.1029/2009GB003488, 2009.

Pongratz, J., Reick, C. H., Houghton, R. A., and House, J. I.: Terminology as a key uncertainty in net land use and land cover change carbon flux estimates, Earth Syst. Dynam., 5, 177–195, https://doi.org/10.5194/esd-5-177-2014, 2014.

~~Pongratz, J., Smith, S. M., Schwingshackl, C., Dayathilake, L., Gasser, T., Grassi, G. and Pilli, R.: Chapter 7: Current levels of CDR. in The State of Carbon Dioxide Removal 2024 – 2nd Edition, https://doi.org/10.17605/OSF.IO/ZXSKB, 2024.~~

Poulter, B., Bastos, A., Canadell, J., Ciais, P., Gruber, N., Hauck, J., Jackson, R., Ishii, M., Müller, J., Patra, P., and Tian, H.: Inventorying Earth's Land and Ocean Greenhouse Gases, Eos, 103, https://doi.org/10.1029/2022EO179084, 2022.

Poulter, B., Frank, D. C., Hodson, E. L., and Zimmermann, N. E.: Impacts of land cover and climate data selection on understanding terrestrial carbon dynamics and the CO2 airborne fraction, Biogeosciences, 8, 2027–2036, https://doi.org/10.5194/bg-8-2027-2011, 2011.

~~Poulter, B., Freeborn, P. H., Jolly, W. M., and Varner, J. M.: COVID-19 lockdowns drive decline in active fires in southeastern United States, PNAS, 118, e2105666118, https://doi.org/10.1073/pnas.2105666118, 2021.~~

Powis, C. M., Smith, S. M., Minx, J. C., and Gasser, T.: Quantifying global carbon dioxide removal deployment, Environ. Res. Lett., 18, 024022, https://doi.org/10.1088/1748-9326/acb450, 2023.

Prentice, I. C., Farquhar, G. D., Fasham, M. J. R., Goulden, M. L., Heimann, M., Jaramillo, V. J., Kheshgi, H. S., Le Quéré, C., Scholes, R. J., and Wallace, D. W. R.: The Carbon Cycle and Atmospheric Carbon Dioxide, in Climate Change 2001: The Scientific Basis. Contribution of Working Group I to the Third Assessment Report of the Intergovernmental Panel on Climate Change, edited by: Houghton, J. T., Ding, Y., Griggs, D. J., Noguer, M., van der Linden, P. J., Dai, X., Maskell, K., and Johnson, C. A., Cambridge University Press, Cambridge, United Kingdom and New York, NY, USA, 183–237, ISBN: 978-0521014953, 2001.

Price, J. T. and Warren, R.: Literature Review of the Potential of "Blue Carbon" Activities to Reduce Emissions, available at: https://avoid-net-uk.cc.ic.ac.uk/wp-content/uploads/delightful-downloads/2016/03/Literature-review-of-the-potential-of-blue-carbon-activities-to-reduce-emissions-AVOID2-WPE2.pdf, last access: ~~23~~30 October ~~2025~~2026, 2016.

Qin, Y., Xiao, X., Wigneron, J.-P., Ciais, P., Brandt, M., Fan, L., Li, X., Crowell, S., Wu, X., Doughty, R., Zhang, Y., Liu, F., Sitch, S., and Moore, B.: Carbon loss from forest degradation exceeds that from deforestation in the Brazilian Amazon, Nat. Clim. Chang., 11, 442–448, https://doi.org/10.1038/s41558-021-01026-5, 2021.

Formatted: Space Before: 0 pt, After: 8 pt

Formatted: Space Before: 0 pt, After: 8 pt

Formatted: Space Before: 0 pt, After: 8 pt

Qin, Z., Zhu, Y., Canadell, J.G., Chen, M., Li, T., Mishra, U. and Yuan, W.: Global spatially explicit carbon emissions from land-use change over the past six decades (1961–2020). One Earth, 7(5), pp.835-847, https://doi.org/10.1016/j.oneear.2024.04.002, 2024.

Qiu, C., Ciais, P., Zhu, D., Guenet, B., Peng, S., Petrescu, A. M. R., Lauerwald, R., Makowski, D., Gallego-Sala, A. V., Charman, D. J., and Brewer, S. C.: Large historical carbon emissions from cultivated northern peatlands, Sci. Adv., 7, eabf1332, https://doi.org/10.1126/sciadv.abf1332, 2021.

Randerson, J. T., Chen, Y., van der Werf, G. R., Rogers, B. M., and Morton, D. C.: Global burned area and biomass burning emissions from small fires: BURNED AREA FROM SMALL FIRES, J. Geophys. Res. Biogeosciences, 117, n/a-n/a, https://doi.org/10.1029/2012JG002128, 2012.

Randerson, J. T., Li, Y., Fu, W., Primeau, F., Kim, J. E., Mu, M., Hoffman, F. M., Trugman, A. T., Yang, L., Wu, C., Wang, J. A., Anderegg, W. R. L., Baccini, A., Friedl, M. A., Saatchi, S. S., Denning, A. S., and Goulden, M. L.: The weak land carbon sink hypothesis, Sci. Adv., 11, eadr5489, https://doi.org/10.1126/sciadv.adr5489, 2025.

Raupach, M. R., Marland, G., Ciais, P., Le Quere, C., Canadell, J. G., Klepper, G., and Field, C. B.: Global and regional drivers of accelerating CO2 emissions, Proceedings of the National Academy of Sciences, 104, 10288–10293, https://doi.org/10.1073/pnas.0700609104, 2007.

Regnier, P., Resplandy, L., Najjar, R. G., and Ciais, P.: The land-to-ocean loops of the global carbon cycle, Nature, 603, 401–410, https://doi.org/10.1038/s41586-021-04339-9, 2022.

Reick, C. H., Gayler, V., Goll, D., Hagemann, S., Heidkamp, M., Nabel, J. E. M. S., Raddatz, T., Roeckner, E., Schnur, R., 110 and Wilkenskjeld, S.: JSBACH 3 – The land component of the MPI Earth System Model: documentation of version 3.2, available at: https://doi.org/10.17617/2.3279802, 2021.

Remaud, M., Chevallier, F., Cozic, A., Lin, X., and Bousquet, P.: On the impact of recent developments of the LMDz atmospheric general circulation model on the simulation of CO2 transport, 11, 4489, https://doi.org/10.5194/gmd-11-4489-2018, 2018.

Resplandy, L., Keeling, R. F., ~~Rödenbeck, C., Stephens, B. B., Khatiwala, S., Rodgers, K. B., Long, M. C., Bopp, L., and Tans, P. P.: Revision of global carbon fluxes based on a reassessment of oceanic and riverine carbon transport, Nature Geosci, 11, 504–509, https://doi.org/10.1038/s41561-018-0151-3, 2018. Resplandy, L., Keeling, R. F.,~~ Eddebbar, Y., Brooks, M., Wang, R., Bopp, L., Long, M. C., Dunne, J. P., Koeve, W., and Oschlies, A.: Quantification of ocean heat uptake from changes in atmospheric O2 and CO2 composition, Scientific Reports, 9, 20244, https://doi.org/10.1038/s41598-019-56490-z, 2019.

Rödenbeck, C., ~~Houweling, S., Gloor, M., and Heimann, M.: CO2 flux history 1982–2001 inferred from atmospheric data using a global inversion of atmospheric transport, Atmos Chem Phys, 3, 1919–1964, 2003. Rödenbeck, C.,~~ Bakker, D. C. E., Metzl, N., Olsen, A., Sabine, C., Cassar, N., Reum, F., Keeling, R. F., and Heimann, M.: Interannual sea–air CO2 flux variability from an observation-driven ocean mixed-layer scheme, 11, 4599–4613, https://doi.org/10.5194/bg-11-4599-2014, 2014.

Rödenbeck, C., Zaehle, S., Keeling, R., and Heimann, M.: History of El Niño impacts on the global carbon cycle 1957–2017: a quantification from atmospheric CO2 data, 373, 20170303, https://doi.org/10.1098/rstb.2017.0303, 2018.

Rödenbeck, C., DeVries, T., Hauck, J., Le Quéré, C., and Keeling, R. F.: Data-based estimates of interannual sea–air CO2 flux variations 1957–2020 and their relation to environmental drivers, Biogeosciences, 19, 2627–2652, https://doi.org/10.5194/bg-19-2627-2022, 2022.

Roobaert, A., Ford, D. J., Sreeush, M. G., McKinley, G. A., Hauck, J., Fay, A. R., Heimdal, T. H., Gruber, N., Bopp, L., Chevallier, F., Djeutchouang, L. M., Gehlen, M., Gregor, L., Iida, Y., Jersild, A., Rödenbeck, C., Rogerson, J., Schwinger, J., Shaum, C. A., Tsujino, H., Watson, A., ~~Rosan, T. M.,~~ Zeng, J., Shutler, J. D., and Landschützer, P.: Reconciling ocean carbon uptake estimates: a multi-model assessment of surface ocean CO2 reconstruction skill within the SOCOMv2 initiative, https://doi.org/10.22541/essoar.15003624/v1, 20 May 2026., 2026.

~~Klein Goldewijk, K., Ganzenmüller, R., O'Sullivan, M., Pongratz, J., Mercado, L. M., Aragao, L. E. O. C., Heinrich, V., Randow, C. V., Wiltshire, A., Tubiello, F. N., Bastos, A., Friedlingstein, P., and Sitch, S.: A multi-data assessment of land use and land cover emissions from Brazil during 2000–2019, Environ. Res. Lett., 16, 074004, https://doi.org/10.1088/1748-9326/ac08e3, 2021.~~

Formatted: Space Before: 0 pt, After: 8 pt

Formatted: Space Before: 0 pt, After: 8 pt

Rosan, T. M., Sitch, S., O'Sullivan, M., Basso, L. S., Wilson, C., Silva, C., Gloor, E., Fawcett, D., Heinrich, V., Souza, J. G. and Bezerra, F.G.S.: Synthesis of the land carbon fluxes of the Amazon region between 2010 and 2020. Communications Earth & Environment, 5(1), p.46. ~~https://doi.org/10.1038/s43247-024-01205-0,~~https://doi.org/10.1038/s43247-024-01205-0, 2024.

~~Sakamoto, K., H. Nakano, S. Urakawa, T. Toyoda, Y. Kawakami, H. Tsujino, G. Yamanaka, 2023: Reference manual for the Meteorological Research Institute Community Ocean Model version 5 (MRI.COMv5), Technical Reports of the Meteorological Research Institute, No.87, https://doi.org/10.11483/mritechrepo.87.~~

Sarma, V. V. S. S., Sridevi, B., Metzl, N., Patra, P. K., Lachkar, Z., Chakraborty, K., Goyet, C., Levy, M., Mehari, M., and Chandra, N.: Air-Sea Fluxes of CO2 in the Indian Ocean Between 1985 and 2018: A Synthesis Based on Observation-Based Surface CO2, Hindcast and Atmospheric Inversion Models, Glob. Biogeochem. Cycles, 37, e2023GB007694, https://doi.org/10.1029/2023GB007694, 2023.

Schaphoff, S., von Bloh, W., Rammig, A., Thonicke, K., Biemans, H., Forkel, M., Gerten, D., Heinke, J., Jägermeyr, J., Knauer, J., Langerwisch, F., Lucht, W., Müller, C., Rolinski, S., and Waha, K.: LPJmL4 – a dynamic global vegetation model with managed land – Part 1: Model description, Geosci. Model Dev., 11, 1343–1375, https://doi.org/10.5194/gmd-11-1343-2018, 2018.

Schimel, D., Alves, D., Enting, I. G., Heimann, M., Joos, F., Raynaud, D., Wigley, T., Prater, M., Derwent, R., Ehhalt, D., Fraser, P., Sanhueza, E., Zhou, X., Jonas, P., Charlson, R., Rodhe, H., Sadasivan, S., Shine, K. P., Fouquart, Y., Ramaswamy, V., Solomon, S., Srinivasan, J., Albritton, D., Derwent, R., Isaksen, I., Lal, M., and Wuebbles, D.: Radiative Forcing of Climate Change, in: Climate Change 1995: The Science of Climate Change, Contribution of Working Group I to the Second Assessment Report of the Intergovernmental Panel on Climate Change [Houghton, J. T., Meira Rilho, L. G., Callander, B. A., Harris, N., Kattenberg, A., and Maskell, K. (eds.)], Cambridge University Press, Cambridge, United Kingdom and New York, NY, USA, ISBN: 978-0521559621, 1995.

Schimel, D., Stephens, B. B., and Fisher, J. B.: Effect of increasing CO 2 on the terrestrial carbon cycle, Proc Natl Acad Sci USA, 112, 436–441, https://doi.org/10.1073/pnas.1407302112, 2015.

Schuh, A. E., Jacobson, A. R., Basu, S., Weir, B., Baker, D., Bowman, K., Chevallier, F., Crowell, S., Davis, K. J., Deng, F., Denning, S., Feng, L., Jones, D., Liu, J., and Palmer, P. I.: Quantifying the Impact of Atmospheric Transport Uncertainty on CO 2 Surface Flux Estimates, Global Biogeochem. Cycles, 33, 484–500, https://doi.org/10.1029/2018GB006086, 2019.

Schuldt, K. N., Mund, J., Aalto, T., Abshire, J. B., Aikin, K., Allen, G., Andrade, M., Andrews, A., Apadula, F., Arnold, S., Baier, B., Bakwin, P., Bartyzel, J., Bentz, G., Bergamaschi, P., Beyersdorf, A., Biermann, T., Biraud, S. C., Blanc, P.-E., Boenisch, H., Bowling, D., Brailsford, G., Brand, W. A., Brunner, D., Bui, T. P., Burban, B., Bäni, L., Calzolari, F., Chang, C. S., Chen, H., Chen, G., Chmura, L., Clark, S., Climadat, S., Colomb, A., Commane, R., Condori, L., Conen, F., Conil, S., Couret, C., Cristofanelli, P., Cuevas, E., Curcoll, R., Daube, B., Davis, K. J., De Mazière, M., De Wekker, S., Dean-Day, J. M., Della Coletta, J., Delmotte, M., Di Iorio, T., DiGangi, E., DiGangi, J. P., Dickerson, R., Elsasser, M., Emmenegger, L., Fang, S., Forster, G., France, J., Frumau, A., Fuente-Lastra, M., Galkowski, M., Gatti, L. V., Gehrlein, T., Gerbig, C., Gheusi, F., Gloor, E., Goto, D., Griffis, T., Hammer, S., Hanisco, T. F., Hanson, C., Haszpra, L., Hatakka, J., Heimann, M., Heliasz, M., Heltai, D., Henne, S., Hensen, A., Hermans, C., Hermansen, O., Hintsa, E., Hoheisel, A., Holst, J., Iraci, L. T., Ivakhov, V., Jaffe, D. A., Jordan, A., Joubert, W., Kang, H.-Y., Karion, A., Kawa, S. R., Kazan, V., Keeling, R. F., Keronen, P., Kim, J., Klausen, J., Kneuer, T., Ko, M.-Y., Kolari, P., Kominkova, K., Kort, E., Kozlova, E., Krummel, P. B., Kubistin, D., Kulawik, S. S., Kumps, N., Labuschagne, C., Lam, D. H., Lan, X., Langenfelds, R. L., Lanza, A., Laurent, O., Laurila, T., Lauvaux, T., Lavric, J., Law, B. E., Lee, C.-H., Lee, J., Lehner, I., Lehtinen, K., Leppert, R., Leskinen, A., Leuenberger, M., Leung, W. H., Levin, I., Levula, J., Lin, J., Lindauer, M., Lindroth, A., Loh, Z. M., Lopez, M., Lunder, C. R., Löfvenius, M. O., Machida, T., Mammarella, I., Manca, G., Manning, A., Manning, A., Marek, M. V., Marklund, P., Marrero, J. E., Martin, M. Y., Martin, D., Martins, G. A., Matsueda, H., McKain, K., Meijer, H., Meinhardt, F., Merchant, L., Metzger, J.-M., Mihalopoulos, N., Miles, N. L., Miller, C. E., Miller, J. B., Mitchell, L., Monteiro, V., Montzka, S., Moossen, H., Moreno, C., Morgan, E., Morgui, J.-A., Morimoto, S., Munger, J. W., Munro, D., Mutuku, M., Myhre, C. L., Mölder, M., Müller-Williams, J., Nakaoka, S.-I., Necki, J., Newman, S., Nichol, S., Nisbet, E., Niwa, Y., Njiru, D. M., Noe, S. M., Nojiri, Y., O'Doherty, S., Obersteiner, F., Paplawsky, B., Parworth, C. L., Peischl, J., Peltola, O., Peters, W., Philippon, C., Piacentino, S., Pichon, J. M., Pickers, P., Piper, S., Pitt, J., Plass-Dülmer, C., Platt, S. M., Prinzivalli, S., Ramonet, M., Ramos, R., Ren, X., Reyes-Sanchez, E., Richardson, S. J., Rigouleau, L.-J., Riris, H., Rivas, P. P., Rothe, M., Roulet, Y.-A., Ryerson, T., Ryoo, J.-M., Sargent, M., Sasakawa, M., Schaefer, H., Scheeren, B., Schmidt, M., Schuck, T., Schumacher, M., Seibel, J., Seifert, T., Sha, M. K., Shepson, P., Shin, D., Shook, M., Sloop, C. D., Smale, D., Smith, P. D., Spain, G., St. Clair, J. M., Steger, D., Steinbacher, M., Stephens, B., Sweeney, C., Sørensen, L. L., Taipale, R., Takatsuji, S., Tans, P., Thoning, K., Timas, H., Torn, M., Trisolino, P., Turnbull, J., Vermeulen, A., Viner, B., Vitkova, G.,

Formatted: Space Before: 0 pt, After: 8 pt

Formatted: Space Before: 0 pt, After: 8 pt

Walker, S., Watson, A., Weiss, R., Weyrauch, D., Wofsy, S. C., Worsey, J., Worthy, D., Xueref-Remy, I., Yates, E. L., Young, D., Yver-Kwok, C., Zaehle, S., Zahn, A., Zellweger, C., Zimnoch, M., de Souza, R. A., di Sarra, A. G., van Dinther, D., van den Bulk, P.: Multi-laboratory compilation of atmospheric carbon dioxide data for the period 1957-2023; obspack_co2_1_GLOBALVIEWplus_v10.1_2024-11-13~~, https://doi.org/10.25925/20241101.~~, https://doi.org/10.25925/20241101, 2024.

Schuldt, K. N., Jacobson, A. R., Aalto, T., Aaltonen, H., Andrews, A., Apadula, F., Arnold, S., Bakwin, P., Bartyzel, J., Bergamaschi, P., Biermann, T., Biraud, S. C., Blanc, P.-E., Brunner, D., Bäni, L., Calzolari, F., Chen, H., Chmura, L., Colomb, A., Condori, L., Conen, F., Conil, S., Couret, C., Cristofanelli, P., Cuevas, E., De Mazière, M., De Wekker, S., Della Coletta, J., Delmotte, M., Di Iorio, T., Elsasser, M., Emmenegger, L., Forster, G., Frumau, A., Fuente-Lastra, M., Galkowski, M., Gheusi, F., Hammer, S., Haszpra, L., Hatakka, J., Heliasz, M., Heltai, D., Henne, S., Hensen, A., Hermans, C., Hermansen, O., Hoheisel, A., Holst, J., Jaffe, D. A., Karion, A., Kazan, V., Keronen, P., Kneuer, T., Kolari, P., Kominkova, K., Krummel, P. B., Kubistin, D., Kumps, N., Lan, X., Langenfelds, R. L., Lanza, A., Laurent, O., Lee, J., Lehner, I., Lehtinen, K., Leskinen, A., Leuenberger, M., Levin, I., Levula, J., Lindauer, M., Lindroth, A., Loh, Z. M., Lopez, M., Lunder, C. R., Löfvenius, M. O., Mammarella, I., Manca, G., Manning, A., Manning, A., Marek, M. V., Marklund, P., McKain, K., Meijer, H., Meinhardt, F., Metzger, J.-M., Miller, J. B., Miller, C. E., Myhre, C. L., Mölder, M., Müller-Williams, J., Necki, J., Noe, S. M., O'Doherty, S., Peltola, O., Philippon, C., Piacentino, S., Pichon, J. M., Pickers, P., Pitt, J., Plass-Dülmer, C., Platt, S. M., Ramonet, M., Ramos, R., Reyes-Sanchez, E., Rigouleau, L.-J., Rivas, P. P., Roulet, Y.-A., Scheeren, B., Schmidt, M., Schumacher, M., Sha, M. K., Sloop, C. D., Smith, P. D., Steger, D., Steinbacher, M., Sweeney, C., Sørensen, L. L., Taipale, R., Tans, P., Thoning, K., Trisolino, P., Vermeulen, A., Viner, B., Vitkova, G., Weyrauch, D., Worthy, D., Xueref-Remy, I., Young, D., Yver-Kwok, C., Zimnoch, M., di Sarra, A. G., van den Bulk, P.: Multi-laboratory compilation of atmospheric carbon dioxide data for the year 2024; obspack_co2_1_NRT_v10.1_2025-02-07~~, https://doi.org/10.25925/20250101.~~, https://doi.org/10.25925/20250101, 2025.

Schwinger, J., Goris, N., Tjiputra, J. F., Kriest, I., Bentsen, M., Bethke, I., Ilicak, M., Assmann, K. M., and Heinze, C.: Evaluation of NorESM-OC (versions 1 and 1.2), the ocean carbon-cycle stand-alone configuration of the Norwegian Earth System Model (NorESM1), Geosci. Model Dev., 9, 2589–2622, https://doi.org/10.5194/gmd-9-2589-2016, 2016.

Schwingshackl, C., Obermeier, W. A., Bultan, S., Grassi, G., Canadell, J. G., Friedlingstein, P., Gasser, T., Houghton, R. A., Kurz, W. A., Sitch, S., and Pongratz, J.: Differences in land-based mitigation estimates reconciled by separating natural and land-use CO2 fluxes at the country level, One Earth, 5, 1367–1376, https://doi.org/10.1016/j.oneear.2022.11.009, 2022.

Schwingshackl, C., Gasser, T., Qin, Z., Seeberg, G., Fu, Z., & Pongratz, J. (2026). Land-use change CO2 emissions (ELUC) data for the Global Carbon Budget 2026 (Version 1.0) [Data set]. Zenodo. https://doi.org/10.5281/zenodo.23528902, 2026.

Séférian, R., Nabat, P., Michou, M., Saint-Martin, D., Voldoire, A., Colin, J., Decharme, B., Delire, C., Berthet, S., Chevallier, M., Sénési, S., Franchisteguy, L., Vial, J., Mallet, M., Joetzjer, E., Geoffroy, O., Guérémy, J.-F., Moine, M.-P., Msadek, R., Ribes, A., Rocher, M., Roehrig, R., Salas-y-Mélia, D., Sanchez, E., Terray, L., Valcke, S., Waldman, R., Aumont, O., Bopp, L., Deshayes, J., Éthé, C., and Madec, G.: Evaluation of CNRM Earth System Model, CNRM-ESM2-1: Role of Earth System Processes in Present-Day and Future Climate, Journal of Advances in Modeling Earth Systems, 11, 4182–4227, https://doi.org/10.1029/2019MS001791, 2019.

Seiler, C., Melton, J. R., Arora, V. K., Sitch, S., Friedlingstein, P., Anthoni, P., Goll, D., Jain, A. K., Joetzjer, E., Lienert, S., Lombardozzi, D., Luyssaert, S., Nabel, J. E. M. S., Tian, H., Vuichard, N., Walker, A. P., Yuan, W., and Zaehle, S.: Are Terrestrial Biosphere Models Fit for Simulating the Global Land Carbon Sink?, J. Adv. Model. Earth Syst., 14, e2021MS002946, https://doi.org/10.1029/2021MS002946, 2022.

Sellar, A. A., Jones, C. G., Mulcahy, J. P., Tang, Y., Yool, A., Wiltshire, A., O'Connor, F. M., Stringer, M., Hill, R., Palmieri, J., Woodward, S., Mora, L., Kuhlbrodt, T., Rumbold, S. T., Kelley, D. I., Ellis, R., Johnson, C. E., Walton, J., Abraham, N. L., Andrews, M. B., Andrews, T., Archibald, A. T., Berthou, S., Burke, E., Blockley, E., Carslaw, K., Dalvi, M., Edwards, J., Folberth, G. A., Gedney, N., Griffiths, P. T., Harper, A. B., Hendry, M. A., Hewitt, A. J., Johnson, B., Jones, A., Jones, C. D., Keeble, J., Liddicoat, S., Morgenstern, O., Parker, R. J., Predoi, V., Robertson, E., Siahaan, A., Smith, R. S., Swaminathan, R., Woodhouse, M. T., Zeng, G., and Zerroukat, M.: UKESM1: Description and Evaluation of the U.K. Earth System Model, J. Adv. Model. Earth Syst., 11, 4513–4558, https://doi.org/10.1029/2019MS001739, 2019.

~~Ship and Bunker, 2026. Bunker demand change, Q3 2025, at key global bunkering locations. Available at: https://shipandbunker.com/bi/bunker-volumes, last access: 23 March 2026.~~

Formatted: Space Before: 0 pt, After: 8 pt

Formatted: Font: 9 pt

Shu, S., Jain, A. K., Koven, C. D., and Mishra, U.: Estimation of Permafrost SOC Stock and Turnover Time Using a Land Surface Model With Vertical Heterogeneity of Permafrost Soils, Global Biogeochem. Cy., 34, e2020GB006585, https://doi.org/10.1029/2020GB006585, 2020.

~~Shutler, J. D., Land, P. E., Piolle, J.-F., Woolf, D. K., Goddijn-Murphy, L., Paul, F., Girard-Ardhuin, F., Chapron, B., and Donlon, C. J.: FluxEngine: A Flexible Processing System for Calculating Atmosphere–Ocean Carbon Dioxide Gas Fluxes and Climatologies, J. Atmospheric Ocean. Technol., 33, 741–756, https://doi.org/10.1175/JTECH-D-14-00204.1, 2016.~~

~~Silva Junior, C.H., Anderson, L.O., Silva, A.L., Almeida, C.T., Dalagnol, R., Pletsch, M.A., Penha, T.V., Paloschi, R.A. and Aragão, L.E.: Fire responses to the 2010 and 2015/2016 Amazonian droughts. Frontiers in Earth Science, 7, p.97, https://doi.org/10.3389/feart.2019.00097, 2019.~~

~~-~~Sitch, S., V. Brovkin, W. von Bloh, D. Van Vuuren, B. Eickhout, and Ganopolski, A.: Impacts of future land cover on atmospheric CO2 and climate. Global Biogeochemical Cycles, 19, GB2013. doi:10.1029/2004GB002311, 2005.

Sitch, S., ~~Huntingford, C., Gedney, N., Levy, P. E., Lomas, M., Piao, S. L., Betts, R., Ciais, P., Cox, P., Friedlingstein, P., Jones, C. D., Prentice, I. C., and Woodward, F. I.: Evaluation of the terrestrial carbon cycle, future plant geography and climate-carbon cycle feedbacks using five Dynamic Global Vegetation Models (DGVMs). Uncertainty In Land Carbon Cycle Feedbacks, Glob. Change Biol., 14, 2015–2039, https://doi.org/10.1111/j.1365-2486.2008.01626.x, 2008.~~

~~Sitch, S.,~~ O'Sullivan, M., Robertson, E., Friedlingstein, P., Albergel, C., Anthoni, P., Arneth, A., Arora, V. K., Bastos, A., Bastrikov, V., Bellouin, N., Canadell, J. G., Chini, L., Ciais, P., Falk, S., Harris, I., Hurtt, G., Ito, A., Jain, A. K., Jones, M. W., Joos, F., Kato, E., Kennedy, D., Klein Goldewijk, K., Kluzek, E., Knauer, J., Lawrence, P. J., Lombardozzi, D., Melton, J. R., Nabel, J. E. M. S., Pan, N., Peylin, P., Pongratz, J., Poulter, B., Rosan, T. M., Sun, Q., Tian, H., Walker, A. P., Weber, U., Yuan, W., Yue, X., Zaehle, S.: Trends and Drivers of Terrestrial Sources and Sinks of Carbon Dioxide: An Overview of the TRENDY Project, Global Biogeochemical Cycles, 38(7), e2024GB008102, https://doi.org/10.1029/2024GB008102, 2024.

Smallman, T. L., Milodowski, D. T., Neto, E. S., Koren, G., Ometto, J., and Williams, M.: Parameter uncertainty dominates C-cycle forecast errors over most of Brazil for the 21st century, Earth Syst. Dyn., 12, 1191–1237, https://doi.org/10.5194/esd-12-1191-2021, 2021.

Smith, B., Wårlind, D., Arneth, A., Hickler, T., Leadley, P., Siltberg, J., and Zaehle, S.: Implications of incorporating N cycling and N limitations on primary production in an individual-based dynamic vegetation model, Biogeosciences, 11, 2027–2054, https://doi.org/10.5194/bg-11-2027-2014, 2014.

Smith, S~~.~~., Grassi~~-M., Geden, O., Gidden, M. J., Lamb, W.~~ F., ~~Nemet~~, G~~.~~ F., Minx, J.~~,~~ Harrington, K., Schwingshackl, C., ~~Buck, H., Burke, J., Cox, E., Edwards, M.~~ Pilli, R., ~~Fuss~~Gupta, S., ~~Johnstone, I., Müller-Hansen, F., Pongratz, J., Probst, B.~~ S., Roe, S., Schenuit, F., Schulte, I., and ~~Vaughan, N. E.~~Rink, A.: Chapter 7: Current levels of CDR, The State of Carbon Dioxide Removal ~~2024 - 2nd~~ 3rd Edition~~, http://dx.~~ (2026), https://doi.org/10.17605/OSF.IO/~~F85QJ, 2024~~VH7U6, 2026.

Sospedra-Alfonso, R., Merryfield, W. J., Boer, G. J., Kharin, V. V., Lee, W.-S., Seiler, C., and Christian, J. R.: Decadal climate predictions with the Canadian Earth System Model version 5 (CanESM5), Geosci. Model Dev., 14, 6863–6891, https://doi.org/10.5194/gmd-14-6863-2021, 2021.

Steele, L. P., Dlugokencky, E. J., Lang, P. M., Tans, P. P., Martin, R. C., and Masarie, K. A.: Slowing down of the global accumulation of atmospheric methane during the 1980s, Nature 358, 313–316, https://doi.org/10.1038/358313a0, 1992.

Stephens, B. B., Gurney, K. R., Tans, P. P., Sweeney, C., Peters, W., Bruhwiler, L., Ciais, P., Ramonet, M., Bousquet, P., Nakazawa, T., Aoki, S., Machida, T., Inoue, G., Vinnichenko, N., Lloyd, J., Jordan, A., Heimann, M., Shibistova, O., Langenfelds, R. L., Steele, L. P., Francey, R. J., and Denning, A. S.: Weak Northern and Strong Tropical Land Carbon Uptake from Vertical Profiles of Atmospheric CO2, Science, 316, 1732–1735, https://doi.org/10.1126/science.1137004, 2007.

Stephens, B. B., Keeling, R. F., Heimann, M., Six, K. D., Murnane, R., and Caldeira, K.: Testing global ocean carbon cycle models using measurements of atmospheric O2 and CO2 concentration, Glob. Biogeochem. Cycles, 12, 213–230, https://doi.org/10.1029/97GB03500, 1998.

Stephens, B. B., Jin, Y., Sweeney, C., McKain, K., Gaubert, B., Baker, D. F., Basu, S., Bertolacci, M., Chevallier, F., Commane, R., Crowell, S., Deng, F., Johnson, M. S., Keeling, R. F., Liu, J., Liu, Z., Maity, S., Morgan, E. J., Patra, P., Philip, S., Wofsy, S. C., and Zammit-Mangion, A.: Improved latitudinal carbon budgets from global

Formatted: Font: 9 pt

Formatted: Space Before: 0 pt, After: 8 pt

Formatted: Space Before: 0 pt, After: 8 pt

Formatted: Space Before: 0 pt, After: 8 pt

airborne surveys, Proc. Natl. Acad. Sci. U.S.A., 123, e2523984123, https://doi.org/10.1073/pnas.2523984123, 2026.

Stock, C. A., Dunne, J. P., Luo, J. Y., Ross, A. C., Van Oostende, N., Zadeh, N., Cordero, T. J., Liu, X., and Teng, Y.: Photoacclimation and Photoadaptation Sensitivity in a Global Ocean Ecosystem Model, J Adv Model Earth Syst, 17, e2024MS004701, https://doi.org/10.1029/2024MS004701, https://doi.org/10.1029/2024MS004701, 2025.

Stocker, T., Qin, D., and Platner, G.-K.: Climate Change 2013: The Physical Science Basis. Contribution of Working Group I to the Fifth Assessment Report of the Intergovernmental Panel on Climate Change [Intergovernmental Panel on Climate Change (eds.)], Cambridge University Press, Cambridge, ISBN: 9789291691388, 2013.

Su, W., Wang, B., Chen, H., Zhu, L., Zheng, X., and Chen, S. X.: A new global carbon flux estimation methodology by assimilation of both in situ and satellite CO2 observations, npj Clim Atmos Sci, 7, 287, https://doi.org/10.1038/s41612-024-00824-w, 2024.

Swart, N. C., Cole, J. N. S., Kharin, V. V., Lazare, M., Scinocca, J. F., Gillett, N. P., Anstey, J., Arora, V., Christian, J. R., Hanna, S., Jiao, Y., Lee, W. G., Majaess, F., Saenko, O. A., Seiler, C., Seinen, C., Shao, A., Sigmond, M., Solheim, L., von Salzen, K., Yang, D., and Winter, B.: The Canadian Earth System Model version 5 (CanESM5.0.3), Geosci. Model Dev., 12, 4823–4873, https://doi.org/10.5194/gmd-12-4823-2019, 2019.

SX Coal: Monthly coal consumption estimates, http://www.sxcoal.com/, last access: 23 October 2025, 2022.

Takahashi, T., Sutherland, S. C., Wanninkhof, R., Sweeney, C., Feely, R. A., Chipman, D. W., Hales, B., Friederich, G., Chavez, F., Sabine, C., Watson, A., Bakker, D. C. E., Schuster, U., Metzl, N., Yoshikawa-Inoue, H., Ishii, M., Midorikawa, T., Nojiri, Y., Körtzinger, A., Steinhoff, T., Hoppema, M., Olafsson, J., Arnarson, T. S., Tilbrook, B., Johannessen, T., Olsen, A., Bellerby, R., Wong, C. S., Delille, B., Bates, N. R., and de Baar, H. J. W.: Climatological mean and decadal change in surface ocean pCO2, and net sea–air CO2 flux over the global oceans, Deep Sea Research Part II: Topical Studies in Oceanography, 56, 554–577, https://doi.org/10.1016/j.dsr2.2008.12.009, 2009.

Takano, Y., Ilyina, T., Tjiputra, J., Eddebbar, Y. A., Berthet, S., Bopp, L., Buitenhuis, E., Butenschön, M., Christian, J. R., Dunne, J. P., Gröger, M., Hayashida, H., Hieronymus, J., Koenigk, T., Krasting, J. P., Long, M. C., Lovato, T., Nakano, H., Palmieri, J., Schwinger, J., Séférian, R., Suntharalingam, P., Tatebe, H., Tsujino, H., Urakawa, S., Watanabe, M., and Yool, A.: Simulations of ocean deoxygenation in the historical era: insights from forced and coupled models, Front. Mar. Sci., 10, 1139917, https://doi.org/10.3389/fmars.2023.1139917, 2023.

Taylor, T. E., O'Dell, C. W., Chang, A., Chatterjee, A., Cheng, C., Dang, L., et al.: The OCO-2 and OCO-3 ACOS version 11 XCO2 data products: A benchmark record for space-based global carbon cycle research. Earth and Space Science, 13, e2026EA005360. https://doi.org/10.1029/2026EA005360, 2026.

Terhaar, J., Frölicher, T. L., and Joos, F.: Southern Ocean anthropogenic carbon sink constrained by sea surface salinity, Sci. Adv., 7, eabd5964, https://doi.org/10.1126/sciadv.abd5964, 2021.

Terhaar, J., Frölicher, T. L., and Joos, F.: Observation-constrained estimates of the global ocean carbon sink from Earth system models, Biogeosciences, 19, 4431–4457, https://doi.org/10.5194/bg-19-4431-2022, 2022.

Terhaar, J.: Drivers of decadal trends in the ocean carbon sink in the past, present, and future in Earth system models, Biogeosciences, 21, 3903–3926, https://doi.org/10.5194/bg-21-3903-2024, 2024.

Terhaar, J., Goris, N., Müller, J. D., DeVries, T., Gruber, N., Hauck, J., Perez, F. F., and Séférian, R.: Assessment of Global Ocean Biogeochemistry Models for Ocean Carbon Sink Estimates in RECCAP2 and Recommendations for Future Studies. Journal of Advances in Modeling Earth Systems, 16(3), e2023MS003840, https://doi.org/10.1029/2023MS003840, 2024.

Terhaar, J.: Composite model-based estimate of the ocean carbon sink from 1959 to 2022, Biogeosciences, 22, 1631–1649, https://doi.org/10.5194/bg-22-1631-2025, 2025.

Tian, H., Xu, X., Lu, C., Liu, M., Ren, W., Chen, G., Melillo, J., and Liu, J.: Net exchanges of CO2, CH4, and N2O between China's terrestrial ecosystems and the atmosphere and their contributions to global climate warming, J. Geophys. Res. Biogeosciences, 116, G02011, https://doi.org/10.1029/2010JG001393, 2011.

Tian, H., Chen, G., Lu, C., Xu, X., Hayes, D. J., Ren, W., PanThum, T., Caldararu, S., Huntzinger, D. NEngel, J., Kern, M., Pallandt, M., Schnur, R., Yu, L., and WofsyZaehle, S. C.: North American.: A new model of the coupled carbon, nitrogen, and phosphorus cycles in the terrestrial CO2 uptake largely offset by CH4 and N2O emissions:

Formatted: Space Before: 0 pt, After: 8 pt

Formatted: Space Before: 0 pt, After: 8 pt

Formatted: Space Before: 0 pt, After: 8 pt

Formatted: Space Before: 0 pt, After: 8 pt

Formatted: Space Before: 0 pt, After: 8 pt

Formatted: Space Before: 0 pt, After: 8 pt

toward a full accounting of the greenhouse gas budget, Climatic Change, 129, 413–426biosphere (QUINCY v1.0; revision 1996), Geosci. Model Dev., 12, 4781–4802, https://doi.org/10.1007/s10584-014-1072-9, 20155194/gmd-12-4781-2019, 2019.

Tjiputra, J. F., Schwinger, J., Bentsen, M., Morée, A. L., Gao, S., Bethke, I., Heinze, C., Goris, N., Gupta, A., He, Y.-C., Olivié, D., Seland, Ø., and Schulz, M.: Ocean biogeochemistry in the Norwegian Earth System Model version 2 (NorESM2), Geosci. Model Dev., 13, 2393–2431, https://doi.org/10.5194/gmd-13-2393-2020, https://doi.org/10.5194/gmd-13-2393-2020, 2020.

Torres, R., Waldman, R., Madec, G., De Lavergne, C., Séférian, R., and Mak, J.: An Energetically and Observationally Constrained Mesoscale Parameterization for Ocean Climate Models, J Adv Model Earth Syst, 17, e2025MS005394, https://doi.org/10.1029/2025MS005394, 2025.

Tsujino, H., Nakano, H., Sakamoto, K., Urakawa, L. S., Toyama, K., Kosugi, N., Kitamura, Y., Ishii, M., Nishikawa, S., Nishikawa, H., Sugiyama, T., and Ishikawa, Y.: Impact of increased horizontal resolutionIncreased Horizontal Resolution of an ocean modelOcean Model on carbon circulationCarbon Circulation in the North Pacific Ocean. Journal of Advances in Modeling, J Adv Model Earth SystemsSyst, 16, e2023MS003720, https://doi.org/10.1029/2023MS003720, 2024.

Tubiello, F. N., Conchedda, G., Wanner, N., Federici, S., Rossi, S., and Grassi, G.: Carbon emissions and removals from forests: new estimates, 1990–2020, Earth Syst. Sci. Data, 13, 1681–1691, https://doi.org/10.5194/essd-13-1681-2021, 2021.
Tubiello, F., Pekkarinen, A., Branthomme, A., Piccoli, M., Obli-Laryea, G., Piccoli, M., Ramadan, N., and Conchedda, G.: New FAOSTATCondor, R. D., Wanner, N., Brivio, R., Jonsson, Ö., Conchedda, G., and Pekkarinen, A.: FAO estimates of net forest emissions and removals estimates:, 1990–2025, Earth Syst. Sci. Data Discussions, 18, 6799–6813, https://doi.org/10.5194/essd-2025-635, 2025 18-6799-2026, 2026.

Tuck, C.: 2022 Mineral Commodity Summary: Iron Ore, Tech. rep., U.S. Geological Survey, https://pubs.usgs.gov/periodicals/mcs2022/mcs2022-iron-ore.pdf, 2022.

UNFCCC: Synthesis report for the technical assessment component of the first global stocktake, available at: https://unfccc.int/documents/461466, last access: 2330 October 20252026, 2022.

Van Den Berg, A.-W., Hooghiem, J. J. D., Van Der Woude, A. M., Rijsdijk, P., Vernooij, R., Botía, S., Van Der Werf, G. R., Miller, J. B., Luijkx, I. T., Krol, M. C., and Peters, W.: Fire carbon emission constraints from space-based carbon monoxide retrievals during the 2019 intense burning season in Brazil, Atmos. Chem. Vale, M. M., Berenguer, E., Argollo de Menezes, M., Viveiros de Castro, E. B., Pugliese de Siqueira, L., and Portela, R. de C. Q.: The COVID-19 pandemic as an opportunity to weaken environmental protection in Brazil, Biological Conservation, 255, 108994, https://doi.org/10.1016/j.biocon.2021.108994, 2021.
Phys., 26, 13929–13958, https://doi.org/10.5194/acp-26-13929-2026, 2026.

van der Laan-Luijkx, I. T., van der Velde, I. R., van der Veen, E., Tsuruta, A., Stanislawska, K., Babenhauserheide, A., Zhang, H. F., Liu, Y., He, W., Chen, H., Masarie, K. A., Krol, M. C., and Peters, W.: The CarbonTracker Data Assimilation Shell (CTDAS) v1.0: implementation and global carbon balance 2001–2015, Geosci. Model Dev., 10, 2785–2800, https://doi.org/10.5194/gmd-10-2785-2017, 2017.

van der Velde, I. R., van der Werf, G. R., Houweling, S., Maasakkers, J. D., Borsdorff, T., Landgraf, J., Tol, P., van Kempen, T. A., van Hees, R., Hoogeveen, R., Veefkind, J. P., and Aben, I.: Vast CO2 release from Australian fires in 2019–2020 constrained by satellite, Nature, 597, 366–369, https://doi.org/10.1038/s41586-021-03712-y, 2021.

van der Werf, G. R., Randerson, J. T., Giglio, L., Collatz, G. J., Mu, M., Kasibhatla, P. S., Morton, D. C., DeFries, R. S., Jin, Y., and van Leeuwen, T. T.: Global fire emissions and the contribution of deforestation, savanna, forest, agricultural, and peat fires (1997–2009), Atmospheric Chem. Phys., 10, 11707–11735, https://doi.org/10.5194/acp-10-11707-2010, 2010.

van der Werf, G. R., Randerson, J. T., Giglio, L., van Leeuwen, T. T., Chen, Y., Rogers, B. M., Mu, M., van Marle, M. J. E., Morton, D. C., Collatz, G. J., Yokelson, R. J., and Kasibhatla, P. S.: Global fire emissions estimates during 1997–2016, Earth Syst. Sci. Data, 9, 697–720, https://doi.org/10.5194/essd-9-697-2017, 2017.

van der Werf, G. R., Randerson, J. T., Van Wees, D., Chen, Y., Giglio, L., Hall, J., Vernooij, R., Mu, M., Binte Shahid, S., Barsanti, K. C., Yokelson, R., and Morton, D. C.: Landscape fire emissions from the 5th version of the Global Fire Emissions Database (GFED5), Sci Data, 12, 1870, https://doi.org/10.1038/s41597-025-06127-w, 2025.

Formatted: Space Before: 0 pt, After: 8 pt

Formatted: Space Before: 0 pt, After: 8 pt

Formatted: Space Before: 0 pt, After: 8 pt

van Wees, D., van der Werf, G. R., Randerson, J. T., Andela, N., Chen, Y., and Morton, D. C.: The role of fire in global forest loss dynamics, Glob. Change Biol., 27, 2377–2391, https://doi.org/10.1111/gcb.15591, 2021.

von Bloh, W., Schaphoff, S., Müller, C., Rolinski, S., Waha, K., and Zaehle, S.: Implementing the nitrogen cycle into the dynamic global vegetation, hydrology, and crop growth model LPJmL (version 5.0), Geosci. Model Dev., 11, 2789–2812, https://doi.org/10.5194/gmd-11-2789-2018, 2018.

Vaittinada Ayar, P., Bopp, L., Christian, J. R., Ilyina, T., Krasting, J. P., Séférian, R., Tsujino, H., Watanabe, M., Yool, A., and Tjiputra, J.: Contrasting projections of the ENSO-driven CO2 flux variability in the equatorial Pacific under high-warming scenario, Earth Syst. Dynam., 13, 1097–1118, https://doi.org/10.5194/esd-13-1097-2022, 2022.

Vuichard, N., Messina, P., Luyssaert, S., Guenet, B., Zaehle, S., Ghattas, J., Bastrikov, V., and Peylin, P.: Accounting for carbon and nitrogen interactions in the global terrestrial ecosystem model ORCHIDEE (trunk version, rev 4999): multi-scale evaluation of gross primary production, Geosci. Model Dev., 12, 4751–4779, https://doi.org/10.5194/gmd-12-4751-2019, 2019.

Walker, A. P., Quaife, T., Bodegom, P. M., De Kauwe, M. G., Keenan, T. F., Joiner, J., Lomas, M. R., MacBean, N., Xu, C., Yang, X., and Woodward, F. I.: The impact of alternative trait-scaling hypotheses for the maximum photosynthetic carboxylation rate (V cmax) on global gross primary production, New Phytol., 215, 1370–1386, https://doi.org/10.1111/nph.14623, 2017.

Walker, A. P., De Kauwe, M. G., Bastos, A., Belmecheri, S., Georgiou, K., Keeling, R. F., McMahon, S. M., Medlyn, B. E., Moore, D. J. P., Norby, R. J., Zaehle, S., Anderson-Teixeira, K. J., Battipaglia, G., Brienen, R. J. W., Cabugao, K. G., Cailleret, M., Campbell, E., Canadell, J. G., Ciais, P., Craig, M. E., Ellsworth, D. S., Farquhar, G. D., Fatichi, S., Fisher, J. B., Frank, D. C., Graven, H., Gu, L., Haverd, V., Heilman, K., Heimann, M., Hungate, B. A., Iversen, C. M., Joos, F., Jiang, M., Keenan, T. F., Knauer, J., Körner, C., Leshyk, V. O., Leuzinger, S., Liu, Y., MacBean, N., Malhi, Y., McVicar, T. R., Penuelas, J., Pongratz, J., Powell, A. S., Riutta, T., Sabot, M. E. B., Schleucher, J., Sitch, S., Smith, W. K., Sulman, B., Taylor, B., Terrer, C., Torn, M. S., Treseder, K. K., Trugman, A. T., Trumbore, S. E., van Mantgem, P. J., Voelker, S. L., Whelan, M. E., and Zuidema, P. A.: Integrating the evidence for a terrestrial carbon sink caused by increasing atmospheric CO2, New Phytol., 229, 2413–2445, https://doi.org/10.1111/nph.16866, 2021.

Walker, A. P., Obermeier, W. A., Pongratz, J., Friedlingstein, P., Koven, C. D., Schwingshackl, C., Sitch, S., and O'Sullivan, M.: Harmonizing direct and indirect anthropogenic land carbon fluxes indicates a substantial missing sink in the global carbon budget since the early 20th century, Plants People Planet, 7, 1123–1136, https://doi.org/10.1002/ppp3.10619, 2025.

Wanninkhof, R., Triñanes, J., Pierrot, D., Munro, D. R., Sweeney, C., and Fay, A. R.: Trends in Sea-Air CO2 Fluxes and Sensitivities to Atmospheric Forcing Using an Extremely Randomized Trees Machine Learning Approach, Global Biogeochemical Cycles, 39, e2024GB008315, https://doi.org/10.1029/2024GB008315, 2025.

Watanabe, M., Tatebe, H., Koyama, H., Hajima, T., Watanabe, M., and Kawamiya, M.: Importance of El Niño reproducibility for reconstructing historical CO2 flux variations in the equatorial Pacific, Ocean Sci., 16, 1431–1442, https://doi.org/10.5194/os-16-1431-2020, 2020.

Watson, A. J., Schuster, U., Shutler, J. D., Holding, T., Ashton, I. G. C., Landschützer, P., Woolf, D. K., and Goddijn-Murphy, L.: Revised estimates of ocean-atmosphere CO2 flux are consistent with ocean carbon inventory, Nat Commun, 11, 4422, https://doi.org/10.1038/s41467-020-18203-3, 2020.

Watson, R. T., Rohde, H., Oeschger, H., and Siegenthaler, U.: Greenhouse Gases and Aerosols, in: Climate Change: The IPCC Scientific Assessment. Intergovernmental Panel on Climate Change (IPCC), edited by: Houghton, J. T., Jenkins, G. J., and Ephraums, J. J., Cambridge University Press, Cambridge, ISBN: 978-0521403603, 1990.

Wenzel, S., Cox, P. M., Eyring, V., and Friedlingstein, P.: Projected land photosynthesis constrained by changes in the seasonal cycle of atmospheric CO2, Nature, 538, 499–501, https://doi.org/10.1038/nature19772, 2016.

Wilkenskjeld, S., Kloster, S., Pongratz, J., Raddatz, T., and Reick, C. H.: Comparing the influence of net and gross anthropogenic land-use and land-cover changes on the carbon cycle in the MPI-ESM, Biogeosciences, 11, 4817–4828, https://doi.org/10.5194/bg-11-4817-2014, 2014.

Willey, D. A., Fine, R. A., Sonnerup, R. E., Bullister, J. L., Smethie, W. M., and Warner, M. J.: Global oceanic chlorofluorocarbon inventory, Geophysical Research Letters, 31, 2003GL018816, https://doi.org/10.1029/2003GL018816, 2004.

Formatted: Space Before: 0 pt, After: 8 pt

Formatted: Font: Cambria Math

Formatted: Space Before: 0 pt, After: 8 pt

Wiltshire, A. J., Burke, E. J., Chadburn, S. E., Jones, C. D., Cox, P. M., Davies-Barnard, T., Friedlingstein, P., Harper, A. B., Liddicoat, S., Sitch, S., and Zaehle, S.: JULES-CN: a coupled terrestrial carbon–nitrogen scheme (JULES vn5.1), 14, 2161–2186, https://doi.org/10.5194/gmd-14-2161-2021, 2021.

~~Winkler, K., Yang, H., Ganzenmüller, R., Fuchs, R., Ceccherini, G., Duveiller, G., Grassi, G., Pongratz, J., Bastos, A., Shvidenko, A., Araza, A., Herold, M., Wigneron, J.-P., and Ciais, P.: Changes in land use and management led to a decline in Eastern Europe's terrestrial carbon sink, Commun. Earth Environ., 4, 1–14, https://doi.org/10.1038/s43247-023-00893-4, 2023.~~

Woodward, F. I. and Lomas, M. R.: Vegetation dynamics – simulating responses to climatic change, Biol. Rev., 79, 643–670, https://doi.org/10.1017/S1464793103006419, 2004.

Wooster, M. J., Roberts, G. J., Giglio, L., Roy, D. P., Freeborn, P. H., Boschetti, L., Justice, C., Ichoku, C., Schroeder, W., Davies, D., Smith, A. M. S., Setzer, A., Csiszar, I., Strydom, T., Frost, P., Zhang, T., Xu, W., De Jong, M. C., Johnston, J. M., Ellison, L., Vadrevu, K., Sparks, A. M., Nguyen, H., McCarty, J., Tanpipat, V., Schmidt, C., and San-Miguel-Ayanz, J.: Satellite remote sensing of active fires: History and current status, applications and future requirements, Remote Sensing of Environment, 267, 112694, https://doi.org/10.1016/j.rse.2021.112694, 2021.

Wright, R. M., Le Quéré, C., Buitenhuis, E., Pitois, S., and Gibbons, M. J.: Role of jellyfish in the plankton ecosystem revealed using a global ocean biogeochemical model, 18, 1291–1320, https://doi.org/10.5194/bg-18-1291-2021, 2021.

Wunch, D., Wennberg, P. O., Osterman, G., Fisher, B., Naylor, B., Roehl, C. M., O'Dell, C., Mandrake, L., Viatte, C., Kiel, M., Griffith, D. W. T., Deutscher, N. M., Velazco, V. A., Notholt, J., Warneke, T., Petri, C., De Maziere, M., Sha, M. K., Sussmann, R., Rettinger, M., Pollard, D., Robinson, J., Morino, I., Uchino, O., Hase, F., Blumenstock, T., Feist, D. G., Arnold, S. G., Strong, K., Mendonca, J., Kivi, R., Heikkinen, P., Iraci, L., Podolske, J., Hillyard, P. W., Kawakami, S., Dubey, M. K., Parker, H. A., Sepulveda, E., García, O. E., Te, Y., Jeseck, P., Gunson, M. R., Crisp, D., and Eldering, A.: Comparisons of the Orbiting Carbon Observatory-2 (OCO-2) X CO2 measurements with TCCON, Atmos. Meas. Tech., 10, 2209–2238~~, https://doi.org/10.5194/amt-10-2209-2017,~~ https://doi.org/10.5194/amt-10-2209-2017, 2017.

~~Wunder, S., Kaimowitz, D., Jensen, S., and Feder, S.: Coronavirus, macroeconomy, and forests: What likely impacts?, For. Policy Econ., 131, 102536, https://doi.org/10.1016/j.forpol.2021.102536, 2021.~~

~~Xi, F., Davis, S. J., Ciais, P., Crawford-Brown, D., Guan, D., Pade, C., Shi, T., Syddall, M., Lv, J., Ji, L., Bing, L., Wang, J., Wei, W., Yang, K.-H., Lagerblad, B., Galan, I., Andrade, C., Zhang, Y., and Liu, Z.: Substantial global carbon uptake by cement carbonation, Nature Geosci, 9, 880–883, https://doi.org/10.1038/ngeo2840, 2016.~~

~~Xia, J., Chen, Y., Liang, S., Liu, D., and Yuan, W.: Global simulations of carbon allocation coefficients for deciduous vegetation types, Tellus B, 67, 28016, https://doi.org/10.3402/tellusb.v67.28016, 2015.~~

Xia, X., Ren, P., Wang, X., Liu, D., Chen, X., Dan, L., He, B., He, H., Ju, W., Liang, M., Lu, X., Peng, J., Qin, Z., Xia, J., Zheng, B., Wei, J., Yue, X., Yu, G., Piao, S., and Yuan, W.: The carbon budget of China: 1980–2021, Science Bulletin, 69, 114–124~~, https://doi.org/10.1016/j.scib.2023.11.016,~~ https://doi.org/10.1016/j.scib.2023.11.016, 2024.

~~Yang, D., Liu, Y., Feng, L., Wang, J., Yao, L., Cai, Z., Zhu, S., Lu, N., and Lyu, D.: The First Global Carbon Dioxide Flux Map Derived from TanSat Measurements, Adv. Atmospheric Sci., 38, 1433–1443, https://doi.org/10.1007/s00376-021-1179-7, 2021.~~

Xiao, R., Prentice, D., Sarkar, M., Kumar, A., Rosner, F., Neithalath, N., La Plante, E., Bauchy, M., and Sant, G.: Ambient concrete carbonation is a trivial contributor in mitigating carbon dioxide emissions from cement production, Commun. Sustain., 1, 118, https://doi.org/10.1038/s44458-026-00116-9, 2026.Yang, X., Thornton, P., Ricciuto, D., Wang, Y., and Hoffman, F.: Global evaluation of terrestrial biogeochemistry in the Energy Exascale Earth System Model (E3SM) and the role of the phosphorus cycle in the historical terrestrial carbon balance, Biogeosciences, 20, 2813–2836, https://doi.org/10.5194/bg-20-2813-2023, 2023.

Yao, Y., Joetzjer, E., Ciais, P., Viovy, N., Cresto Aleina, F., Chave, J., Sack, L., Bartlett, M., Meir, P., Fisher, R., and Luyssaert, S.: Forest fluxes and mortality response to drought: model description (ORCHIDEE-CAN-NHA r7236) and evaluation at the Caxiuanã drought experiment, Geosci. Model Dev., 15, 7809–7833, https://doi.org/10.5194/gmd-15-7809-2022, 2022.

Yao, Y., Ciais, P., Viovy, N., Joetzjer, E. and Chave, J.: How drought events during the last century have impacted biomass carbon in Amazonian rainforests. Global Change Biology, 29(3), pp.747-762, https://doi.org/10.1111/gcb.16504, 2023.

Formatted: Space Before: 0 pt, After: 8 pt

Formatted: Space Before: 0 pt, After: 8 pt

Formatted: Space Before: 0 pt, After: 8 pt

Formatted: Space Before: 0 pt, After: 8 pt

Formatted: Space Before: 0 pt, After: 8 pt

You, Y., Tian, H., Pan, S., Shi, H., Bian, Z., Gurgel, A., Huang, Y., Kicklighter, D., Liang, X.-Z., Lu, C., Melillo, J., Miao, R., Pan, N., Reilly, J., Ren, W., Xu, R., Yang, J., Yu, Q., and Zhang, J.: Incorporating dynamic crop growth processes and management practices into a terrestrial biosphere model for simulating crop production in the United States: Toward a unified modeling framework, Agricultural and Forest Meteorology, 325, 109144, https://doi.org/10.1016/j.agrformet.2022.109144, 2022.

Yu, Z., Ciais, P., Piao, S., Houghton, R. A., Lu, C., Tian, H., Agathokleous, E., Kattel, G. R., Sitch, S., Goll, D., Yue, X., Walker, A., Friedlingstein, P., Jain, A. K., Liu, S., and Zhou, G.: Forest expansion dominates China's land carbon sink since 1980, Nat. Commun., 13, 5374, https://doi.org/10.1038/s41467-022-32961-2, 2022.

Yue, X. and Unger, N.: The Yale Interactive terrestrial Biosphere model version 1.0: description, evaluation and implementation into NASA GISS ModelE2, Geosci. Model Dev., 8, 2399–2417, https://doi.org/10.5194/gmd-8-2399-2015, 2015.

Yue, X., Zhou, H., Tian, C., Ma, Y., Hu, Y., Gong, C., Zheng, H., and Liao, H.: Development and evaluation of the interactive Model for Air Pollution and Land Ecosystems (iMAPLE) version 1.0, Geosci. Model Dev., 17, 4621–4642, https://doi.org/10.5194/gmd-17-4621-2024, 2024.

Yuan, W., Liu, D., Dong, W., Liu, S., Zhou, G., Yu, G., Zhao, T., Feng, J., Ma, Z., Chen, J., Chen, Y., Chen, S., Han, S., Huang, J., Li, L., Liu, H., Liu, S., Ma, M., Wang, Y., Xia, J., Xu, W., Zhang, Q., Zhao, X., and Zhao, L.: Multiyear precipitation reduction strongly decreases carbon uptake over northern China, J. Geophys. Res. Biogeo., 119, 881–896, https://doi.org/10.1002/2014JG002608, 2014.

Yue, C., Ciais, P., Zhu, D., Wang, T., Peng, S. S., and Piao, S. L.: How have past fire disturbances contributed to the current carbon balance of boreal ecosystems?, Biogeosciences, 13, 675–690, https://doi.org/10.5194/bg-13-675-2016, 2016.

Zaehle, S. and Friend, A. D.: Carbon and nitrogen cycle dynamics in the O-CN land surface model: 1. Model description, site-scale evaluation, and sensitivity to parameter estimates: Site-scale evaluation of a C-N model, Global Biogeochem. Cycles, 24, GB1005, https://doi.org/10.1029/2009GB003521, 2010.

Zaehle, S., Ciais, P., Friend, A. D., and Prieur, V.: Carbon benefits of anthropogenic reactive nitrogen offset by nitrous oxide emissions, Nature Geosci, 4, 601–605, https://doi.org/10.1038/ngeo1207, 2011.

Zaehle, S., Medlyn, B. E., De Kauwe, M. G., Walker, A. P., Dietze, M. C., Hickler, T., Luo, Y., Wang, Y.-P., El-Masri, B., Thornton, P., Jain, A., Wang, S., Warlind, D., Weng, E., Parton, W., Iversen, C. M., Gallet-Budynek, A., McCarthy, H., Finzi, A., Hanson, P. J., Prentice, I. C., Oren, R., and Norby, R. J.: Evaluation of 11 terrestrial carbon–nitrogen cycle models against observations from two temperate Free-Air CO2 Enrichment studies, New Phytol., 202, 803–822, https://doi.org/10.1111/nph.12697, 2014.

Zeng, J., Iida, Y., Matsunaga, T., and Shirai, T.: Surface ocean CO2 concentration and air-sea flux estimate by machine learning with modelled variable trends, Front. Mar. Sci., 9, https://doi.org/10.3389/fmars.2022.989233, 2022.

Zhang, X., Liao, E., Lu, W., Wu, Z., Wang, G., Zhu, X., and Liang, S.: A surface ocean p CO2 product with improved representation of interannual variability using a vision transformer-based model, Earth Syst. Sci. Data, 17, 6071–6095, https://doi.org/10.5194/essd-17-6071-2025, 2025.

Zheng, B., Ciais, P., Chevallier, F., Chuvieco, E., Chen, Y., and Yang, H.: Increasing forest fire emissions despite the decline in global burned area, Sci. Adv., 7, eabh2646, https://doi.org/10.1126/sciadv.abh2646, 2021.

Zhu, Y., Xia, X., Canadell, J. G., Piao, S., Lu, X., Mishra, U., Wang, X., Yuan, W., and Qin, Z.: China's carbon sinks from land-use change underestimated, Nat. Clim. Chang., 15, 428–435, https://doi.org/10.1038/s41558-025-02296-z, 2025.

Zou, Y., Wang, Y., Ke, Z., Tian, H., Yang, J., and Liu, Y.: Development of a REgion-Specific Ecosystem Feedback Fire (RESFire) Model in the Community Earth System Model, J. Adv. Model. Earth Syst., 11, 417–445, https://doi.org/10.1029/2018MS001368, 2019.

Zscheischler, J., Mahecha, M. D., Avitabile, V., Calle, L., Carvalhais, N., Ciais, P., Gans, F., Gruber, N., Hartmann, J., Herold, M., Ichii, K., Jung, M., Landschützer, P., Laruelle, G. G., Lauerwald, R., Papale, D., Peylin, P., Poulter, B., Ray, D., Regnier, P., Rödenbeck, C., Roman-Cuesta, R. M., Schwalm, C., Tramontana, G., Tyukavina, A., Valentini, R., van der Werf, G., West, T. O., Wolf, J. E., and Reichstein, M.: Reviews and syntheses: An empirical spatiotemporal description of the global surface–atmosphere carbon fluxes: opportunities and data limitations, Biogeosciences, 14, 3685–3703, https://doi.org/10.5194/bg-14-3685-2017, 2017.

Formatted: Space Before: 0 pt, After: 8 pt

Formatted: Space Before: 0 pt, After: 8 pt

Formatted: Space Before: 0 pt, After: 8 pt

Formatted: Space Before: 0 pt, After: 8 pt

Formatted: Font: Cambria Math

5134

5135 **Tables**

5136

5137 **Table 1.** Factors used to convert carbon in various units (by convention, Unit 1 = Unit 2 × conversion).

Unit 1	Unit 2	Conversion	Source
GtC (gigatonnes of carbon)	ppm (parts per million) (a)	2.124 (b)	Ballantyne et al. (2012)
GtC (gigatonnes of carbon)	PgC (petagrams of carbon)	1	SI unit conversion
GtCO2 (gigatonnes of carbon dioxide)	GtC (gigatonnes of carbon)	3.664	44.01/12.011 in mass equivalent
(a) Measurements of atmospheric CO_2 concentration have units of dry-air mole fraction. 'ppm' is an abbreviation for micromole/mol, dry air.			
(b) The use of a factor of 2.124 assumes that all the atmosphere is well mixed within one year. In reality, only the troposphere is well mixed and the growth rate of CO_2 concentration in the less well-mixed stratosphere is not measured by sites from the NOAA network. Using a factor of 2.124 makes the approximation that the growth rate of CO_2 concentration in the stratosphere equals that of the troposphere on a yearly basis.			

Formatted Table

5138

Table 2. How to cite the individual components of the global carbon budget presented here.

Component	Primary reference
Global and national fossil CO_2 emissions (EFOS), total and by fuel type	This paper and Andrew and Peters (~~2025~~)2026)
~~National territorial fossil CO_2 emissions (EFOS)~~	~~Erb and Marland (2025), UNFCCC (2022)~~
National consumption-based fossil CO_2 emissions (EFOS) by country (consumption)	Peters et al. (2011~~2011a~~) updated as described in this paper
Net land-use change flux (ELUC)	This paper and Schwingshackl et al. (2026); ~~(~~see also Table 4 for individual model references~~).~~
Growth rate in atmospheric CO_2 concentration (GATM)	Lan et al. ~~(2025)~~(2026), Pandey et al (2024)
Atmospheric inversions	This paper and Naus et al (2026); see also Table 4 for individual model references
Ocean ~~and land~~ CO_2 sinks (SOCEAN~~ and SLAND~~)	This paper and Hauck et al (2026); see also~~(see~~ Table 4 for individual model and data products references~~).~~
Land CO_2 sinks (SLAND)	This paper and O'Sullivan et al (2026a); see also Table 4 for individual model references

Formatted Table
Formatted: Not Superscript/ Subscript
Formatted: Not Superscript/ Subscript
Formatted Table
Formatted: Not Superscript/ Subscript
Formatted: Not Superscript/ Subscript
Formatted Table

Table 3. Main methodological changes in the global carbon budget this year (~~GCB2025~~GCB2026). Empty cells mean there were no methodological changes introduced that year. Table S10 lists methodological changes from the first global carbon budget publication up to ~~2024~~2025.

Fossil fuel emissions		LUC emissions	Reservoirs			Other cha
Global	Country (territorial)		Atmosphere	Ocean	Land	
	Canada: Added emissions from historical (1923-1989) lime production USA: Switched to NIR published by Center for Global Sustainability at the University of Maryland Argentina: Added pre-1950 oil trade~~Projection available for Japan for the first time~~	Component 'other transitions' split into contributions from clearing and (re-)growth of shrub and herbaceous vegetation and from transitions between cropland, pasture, and urban areas. Update in land-use data (HYDE3.6). Update to GFED5 for fire emissions.~~Bookkeeping estimates derived from models that estimate ELUC based on transient carbon densities responding to environmental changes (BLUE, OSCAR, LUCE).~~	Satellite-based growth rate (GRESO) now uses combined GOSAT and OCO-2 retrievals from 2010 onward.~~Include an assessment of satellite-derived growth rates~~	Updated ocean uncertainty estimate. Accounting for pre-industrial (natural steady state) carbon fluxes in fCO2-products and inversions to determine SOCEAN regionally.~~Adjustments applied for known underestimation of GOBMs and cool surface skin effect in fCO2 product. Suspension of 19 ocean data sets from SOCAT.~~	Include the δL~~RSS~~ adjustment. Extended evaluation for DGVMs.	

Formatted: Font: 10 pt

Formatted Table

Formatted: Centered

Formatted Table

Table 4. References for the process models, bookkeeping models, ocean data products, and atmospheric inversions. All models and products are updated with new data to the end of year ~~2024~~2025.

Model/data name	Reference	Change from Global Carbon Budget 2025~~2024~~ (Friedlingstein ~~2025a~~2026a)
Bookkeeping models for land-use change emissions		
BLUE	Hansis et al. (2015)	No change~~Transient C densities used to estimate ELUC~~
OSCAR	Gasser et al. (2020)	No change
LUCE	Qin et al. (2024)	No change~~Transient C densities used to estimate ELUC~~
Dynamic global vegetation models		
CABLE-POP	Haverd et al. (2018)	No change~~corrected N deposition input data, minor parameter changes~~
CLASSIC	Melton et al. (2020), ~~Gauthier et al. (2025),~~ Kou-Giesbrecht and Arora (2022~~)~~). Gauthier et al. (2025)	Compared to TRENDY 2025, exponential distribution of saturated hydraulic conductivity with depth is turned on, and dry surface layer parameterization which reduces soil evaporation is turned off.
CLM-FATES~~CLM6.0~~	Fisher~~Lawrence~~ et al. ~~(2019)~~(2015), Koven et al. (2020)	Updated parameters~~New dust scheme, new BGC fire method, updates to MEGAN for BVOCs, parameter updates, new surface datasets, new N fixation method~~
CLM6.0~~CLM-FATES~~	Lawrence~~Fisher~~ et al. ~~(2015), Koven et al. (2020)~~(2019)	Parameter updates, new wetland scheme~~New model~~
DLEM	Tian et al. (2015), You et al. (2022)	No change
E3SM~~EDv3~~	Yang~~Moorcroft~~ et al.(2023), Burrows~~ (2001), Ma~~ et al~~ (2022)~~.(2020)	No change~~Updated meteorology inputs (i.e. hourly air temperature)~~
EDv3~~ELM~~	Moorcroft~~Yang~~ et al. (2001), Ma~~ (2023), Burrows~~ et al~~ (2020)~~. (2022)	Recalibrated fire submodule~~No change~~
GDSTEM~~ELM-FATES~~	Felzer~~Fisher~~ et al. (2009), Felzer~~(2015), Koven~~ et al. ~~(2020), Needham et al. (2025)~~(2011), Felzer (2012), Felzer and Jiang (2018)	No change~~New model~~
IBIS~~GDSTEM~~	Xia et al., (2024)~~Felzer et al. (2009), Felzer et al. (2011), Felzer (2012), Felzer and Jiang (2018)~~	No change~~New model~~
iMAPLE~~IBIS~~	Yue~~Xia~~ et al.~~,~~ (2024)	No change.
IQ~~iMAPLE~~	Thum~~Yue~~ et al. (~~2024~~)2019)	Include representation of agriculture, pasture and sylviculture (wood harvest), land-use change as well as update to fully consistent treatment of physical processes as in the JSBACH model + representation of skin surface temperature, update of model

Formatted Table

		parametersNo change.
ISAM	Jain et al. (2013), Meiyappan et al. (2015), Shu et al. (2020)	Vertically resolved soil biogeochemistry (carbon and nitrogen) module, following Shu et al. (2020)
ISBA-CTRIP	Delire et al. (2020); Decharme et al. (2019)	no change wrt 2024 contribution
JSBACH	Mauritsen et al. (2019), Reick et al. (2021)	No change
JULES-ES	Wiltshire et al. (2021), Sellar et al. (2019), Burton et al. (2019)	No change.Minor updates to wildfire parameters
LPJ-GUESSEOSIM	PoulterSmith et al. (2014)2011) (d)	Used original implementation of respiration temperature response, with no acclimationWood harvest without the LUH2 secondary mature, young, and non-forest harvest fraction info
LPJ-GUESS-PJmL	Smith et al. (2014)Schaphoff et al. (2018), von Bloh et al. (2018), Lutz et al., (2019), Heinke et al. (2023)	Correction in the Burned Area Fraction estimation method to eliminate land cover adjustment during post-processingSwitch from version 5.7.5 to 5.10.0 incorporating updates to soil temperature scheme, revised N demand and N uptake processes, revised tree phenology, as well as bugfixes and code improvements
LPJmLLPJ-EOSIM	Schaphoff et al. (2018), von Bloh et al. (2018), Lutz et al., (2019), Heinke et al. Poulter et al. (2011) (d)(2023), Heinke et al. (2026)	Updated livestock density inputIncorporation of new respiration temperature responses and leaf respiration acclimation, updated the soil temperature and water scheme to have 8 layers
LPX-Bern	Lienert and Joos (2018)	No change
ORCHIDEEv4 ORCHIDEEv3	NaudtsKrinner et al. (2015(2005), Zaehle and Friend (2010), Vuichard et al. (2019)	Switch from v3.0 to v4.3.1 incorporating new albedo scheme, forest demography, forest management, soil insulation, biogeochemistry of permafrost, vertical discretisation of snow and ice, and updating river routing and model parameters.No change
SDGVM	Woodward and Lomas (2004), Walker et al. (2017)	No changeReverted to version used in Friedlingstein et al. (2022), but retaining the recent bug fix to monthly heterotrophic respiration output
VISIT	Ito and Inatomi (2012), Kato et al. (2013)	Improve wood harvesting process. Revised the LAI accounting processes.No change
VISIT-UT	Ito (2019)	Refinement of carbon mass balance including revision of land-use emissions. Additional parameter calibration.New model
Intermediate complexity land carbon cycle model		
CARDAMOM	Bloom et al. (2016), Smallman et al. (2021)	Linear AGB trend from CCI Biomass (v6) added as additional constraint. Maximum rooting depth prior added (Fan et al., 2017). Extended to 2025Analysis resolution increased from 1 x1 to 0.5x0.5 degree. Estimates of fAPAR from MODIS collection 6.1. New prior constraint on the leaf carbon per unit area parameter (LCA). MODIS burned area forcing was replaced by GFEDv5 burned area estimate

Formatted Table

Global ocean biogeochemistry models		
NEMO-PlankTOM12	Wright et all (2021)	model physics version switch from NEMO3.6 to NEMO5.0, update of biogeochemical tuning to Wright et al (in prep), temperature correction to ERA5 atmospheric forcing~~No change~~
NEMO4.2-PISCES (IPSL)	Aumont et al. (2015)	No change~~No change to the model version, but switch to ERA5 forcing - A,B,C,D simulations have been re-run starting from GCB2024 simulation restart fields from 1940 onwards~~
MICOM-HAMOCC (NorESM1-OCv1.2)	Schwinger et al. (2016)	No change~~No change, model has been re-run to provide monthly CFC/SF_6 outputs~~
MPIOM-HAMOCC6	Lacroix et al. (2021)	No change
NEMO4.2.3~~N EMO3.6~~-PISCESv2-gas (CNRM)	~~Berthet et al. (2019),~~ Séférian et al. (2019~~)~~, Madec et al. (2023)	Ocean model version has been updated from NEMO 3.6 to NEMO 4.2.3 (Madec et al 2023) and an improved mesoscale parameterization (Torres et al, 2025) has been activated. PISCESv2-gas remains unchanged and is described in Séférian et al (2019). Forcings have been switched to ERA5 (instead of JRA55-do). Spin-up (1848-1958) has been re-run with ERA5 based on a 10-years loop (1959-1968). A,B,C,D simulations have been re-run with ERA5, starting from the new ERA5 spin-up (i.e. from 1850 onwards).~~Updated simulations using 1750 preindustrial conditions instead of 1850. No change in model configuration, except nudging of surface ocean fields applied to minimize the change of atm forcing. The methodology used is based on Sanchez-Gomez et al. (2024)~~
FESOM2.7~~1~~-REcoM3	Gürses et al. (2023)	Updated physical model version from FESOM2.1 to 2.7. A third zooplankton group and ballasting routines are added in REcoM. ERA5 is used for spin-up and simulations A, B C, D are started from this spinup.~~Switched to ERA5 forcing - A,B,C,D simulations have been re-run starting from GCB2024 simulation restart fields~~
MOM6-COBALTv3 (Princeton)	Stock et al., (2025)	Updated configuraton of MOM6-COBALTv3 with ~0.5° horizontal resolution (720x576)~~New model configuration MOM6-COBALTv3 with ~1° horizontal resolution (360x210). 1) updated ocean biogeochemical module COBALTv3 with an additional fixed nitrogen removal process - anaerobic ammonium oxidation (anammox); 2) updated air-sea gas exchange scheme - wind-wave-bubble formulation; 3) updated riverine carbon and nutrient inputs following R2OMIP protocol (Lacroix et al., 2024, https://zenodo.org/records/13799103); 4) updated river water discharge files.~~
CESM-ETHZ	Doney et al. (2009)	No change.~~Compared to the 2024 submission, we changed the forcing to ERA5. To this end, a new spinup was performed, extending over 500 years.~~

Formatted: Font: 12 pt, Font color: Auto

MRI-ESM2-4	Tsujino et al. ~~(2024), Sakamoto et al. (2023)~~(2026)	~~Iron circulation is modified according to Moore and Braucher (2008) and iron limitation on primary production is adjusted according to this change.~~ ~~Updated atmospheric CO2 for simulations A and C.~~ ~~The JRA-3Q reanalysis (Kosaka et al. 2024) is used to physically force the model.~~ No change.~~The model is spun up for 1925 years with xCO2=278ppm.~~
ACCESS (CSIRO)	Law et al. (2017)	Minor changes~~No change~~ in model since 2025 submission: reduced the timescale for surface salinity restoring from 60~~GCB2024, but switched~~ to 30 days~~ERA5 forcing~~ and provided SF6 output. Extended the~~extended~~ spinup~~.~~ another 200+ years.
fCO2-products		
VLIZ-SOMFFN	Landschützer et al. (2016)	Time period extended to ~~2024~~2025
Jena-MLS	Rödenbeck et al. (2014) updated to Rödenbeck et al (2022)	Time period extended to ~~2024~~2025; replaced prior based on OCIM by an adjustable trend in the ocean-interior sources/sinks; some small technical corrections
CMEMS-LSCE-FFNNv2	Chau et al. (2022) and Chau et al. (2024)	Time period extended to ~~2024~~2025
UExP-FNN-U	Watson et al. (2020) and Ford et al. (2024)	Updated to recalculated SOCATv2026~~SOCATv2025~~ dataset (Fo al. 2026b~~2025~~). Updated SOM~~salinity dataset~~ to ~~use~~ a probab based~~tiered~~ approach. Adds chlorophyll-a as predictor ~~(descri~~ FNN stage. Updates NOAA-COARE to v3.6.~~Gregor et al. 2024) including ESA CCI SSS (v5.51) and CMEMS GLORYS12V1.~~ Upda time period to 1980 to ~~2024~~2025
NIES-ML3	Zeng et al. (2022)	Time period extended to ~~2024.~~2025.
JMA-MLR	Iida et al. (2021)	Time period extended to 2025~~2024~~. Updated to recalculated SOCATv2026~~SOCATv2025~~ dataset (Ford et al. ~~2025)~~2026b)
OceanSODA-ETHZv2	Gregor et al. (2024)	Time period extended to ~~2024~~2025. High latitude winter chloropyll values set to 0 instead of filling with interpolated values.
LDEO-HPD	Gloege et al. (2022) and Bennington et al. (2022)	Time period extended to ~~2024~~2025
AOML-ET	Wanninkhof et al. (2025)	New product for GCB 2026. The published AOML-ET framework was updated to a hybrid GAM + two-stage Extremely Randomized Trees architecture, trained with SOCATv2026 recalculated fCO2 and extended to 1982-2025.
SJTU-AVIT~~CSIR-ML6~~	Zhang~~Gregor~~ et al. (~~2019~~)2025)	Time period extended to ~~2024~~2025. Method unchanged from et al. (2025).
Ocean interior product		
Ocean inverse	Holzer et al. (2019), DeVries (2022)	New this year

Formatted: Font color: Auto

Formatted: Font color: Auto

Formatted: Font color: Auto

Formatted: Font color: Auto

Formatted: Font color: Auto

Formatted: Font color: Auto

Formatted: Font color: Auto

Formatted Table

model OCIM-48L		
Atmospheric inversions		
~~Jena~~ CarboScope	Rödenbeck et al. (2018) & ~~-~~Stephens et al. (2007).	Slight change in station set. Update~~Numerical flux resolution 2x2. TM3 run on spatial resolution 6x4 (multiple~~ of ~~2x2)~~the prior fluxes and assimilated observations.
CarbonTracker ~~-~~Europe (CTE~~)~~ ~~-~~ insitu)	van der Laan-Luijkx et al. (2017~~)~~), van den Berg et al (2026), Stroo et al (2026)	Changed statevector (split temporal domain), in-situ data only in 2nd step for land-fluxes with 3-day filter. Transport model at 1x1 degrees globally. Data selection expanded to use more sites~~Update of prior fluxes and assimilated observations.~~
CarbonTracker Europe (CTE-satellite)	van der Laan-Luijkx et al. (2017), van den Berg et al (2026), Stroo et al (2026)	Same as above, but with only OCO2 column data in 2nd step with 2x5-day smoother
NISMON-CO2	Niwa et al. (2022), Niwa et al. ~~-~~(2017).	Used climatological mean flux for land, derived from NISMON-CO2_SRF ver.2025.1. Vertical structure switched from 40 terrain following layers to 78 hybrid layers. Meteorological data prepared by NICAM were nudged by UV & T (previously, only UV).~~Update of prior fluxes, specifically changed GFED to GBEI. Update of the meteorological input to JRA-3Q. Including more CO2 observations.~~
CT-NOAA	Jacobson et al. (2026~~2025~~), Byrne et ~~-~~al. (2023), Krol et al. (2005~~), Peiro et al. (2022))~~	Switch to mean of two inversions with different sets of priors. Revision of fossil fuel emissions. New land and wildfire priors. Revised air-sea gas exchange including two ~~and~~ new ~~terrestrial NBE (Jacobson et al., 2025). Unlike previous submissions, CT2025 uses only one set of priors.~~pCO2 prior models. A new Kalman filer time-propagation model. Physical parallelization of the analysis period.
CMS-Flux	Liu et al. (2021)	Update of prior fluxes and assimilated observations.
CAMS-Insitu	Chevallier et al. (2005) and Chevallier et al. (2025)	Update of the prior fluxes and assimilated observations.
CAMS-Satellite	Chevallier et al. (2005) and ~~-~~Chevallier et al. (2025)	Update of the prior fluxes and assimilated ~~-~~observations.
GONGGA	Jin et al. (2024)	Update of the prior fluxes and assimilated ~~-~~observations.

Formatted Table

Formatted Table

Formatted Table

COLA	Liu et al. (2022)	Update of the prior fluxes and assimilated observations.
GCASv2	Jiang et al. (2021) & Emmons et al. (2010)	Update of the prior fluxes and assimilated observations.
UoE	Feng et al. (2016) & Palmer et al. (2019)	Update of the prior fluxes and assimilated observations.
~~MIROC-ACTM~~	~~Chandra et al. (2022) & Patra et al. (2018)~~	~~Update of assimilated observations and prior fluxes, specifically changed to MiCASA and GFED. Update of the meteorological input to JRA-3Q.~~
NTFVAR	Nayagam et al. (2025) & Maksyutov et al. (2021)	Update of prior fluxes and assimilated observations.
THU	Kong et al. (2022)	New this year, after missing out 1 year. Compared to the previous submission: update of prior fluxes and assimilated observations.
NISMON-CO2_GOSAT	Niwa et al. (2022), Niwa et al. (2017~~).~~), Maity et al. (2026)	Used climatological mean flux for land, derived from NISMON-CO2_SRF ver.2025.1. GOSAT NIES ver.0305 retrievals over land assimilated.~~New this year.~~
YanDong	Su et al (2024) & Nassar et al. (2010)	First submission.
Earth System Models		
CanESM5	Swart et al. (2019), Sospedra-Alfonso et al. (2021)	No change
EC-Earth3-CC	Döscher et al. (2021), Bilbao et al. (2021), Bernardello et al. (2024)	No change
IPSL-CM6A-CO2-LR	Boucher et al. (2020)	No change
MIROC-ES2L	Watanabe et al. (2020)	No change
MPI-ESM1-2-LR	Mauritsen et al. (2019), Li et al. (2023)	No change
NorCPM-CC	Tjiputra et al. (2020), Bethke et al. (2021)	No change~~New this year.~~

Formatted Table

Formatted Table

5148

Table 5. Comparison of results from the bookkeeping method and budget residuals with results from the DGVMs, as well as additional estimates from atmospheric oxygen, atmospheric inversions and Earth System Models (ESMs) for different periods, the last decade, and the last year available. All values are in GtC yr^{-1}. The best estimate for ~~GCB2025~~GCB2026 (E_{LUC}) is calculated with the bookkeeping models (1a) and used in the budget Table 7, see Section 2 and Figure 7 for description of the bookkeeping component fluxes. The best estimate for ~~GCB2025~~GCB2026 (S_{LAND}) is calculated with the DGVMs including the ~~RSS correction~~δL adjustment (2b), and used in the budget Table 7. The DGVM uncertainties represent ±1σ of the decadal or annual (for ~~2024~~2025) estimates from the individual DGVMs. For the inverse systems the mean and range of available results is given when the number of systems is less than 10, otherwise the ±1σ is provided. All values are rounded to the nearest 0.1 GtC ~~and therefore columns do not necessarily add to zero~~.

Mean (GtC~~/~~yr~~-1~~)

		1960s	1970s	1980s	1990s	2000s	2010s	~~2015-~~20242016-2025	~~20242~~025
Land-use change emissions (E_{LUC})	Bookkeeping (BK) Net flux (1a)	1.~~9~~8± 0.7	1.7±0 .7	1.~~7~~6± 0.7	1.~~7~~8± 0.7	1.7±0 .7	1.6±0 .7	1.~~4~~3± 0.7	1.~~3~~2± 0.7
	BK - deforestation and clearing of other vegetation (total)	~~1.8 [1.6,~~2 .~~1~~3 [2,2.7]	~~1.8 [1.6,~~2 .~~1~~2 [2,2.5]	2.1.~~7 [1.5,1 .9~~ [2,2.3]	~~1.9 [1.6,~~2 .3 [2.1,2 .5]	2 ~~[1.7,~~ .4 [2.1,2 .6]	~~2~~ ~~[1.6,~~2 .4 [2.1,2 .6]	2.2 [1.9 ~~[1,~~2.5 ~~,2.3~~]	2.1.~~9~~ [1.48, 2.45]
	BK - (re-)growth of forest ~~regrowth~~and other vegetation (total)	-1.1 [- 1.3,- 0.9 ~~[- 1,- 0.7~~8]	-1.1 [- 1.3,- 0.9 ~~[- 1,- 0.8~~]	-1.1 [- 1.3,- 0.9 ~~[- 1,- 0.8~~]	-1.3 [- 1.4,- 1~~,- 0.8~~.1]	-1.4 [-1 ~~[-~~ .6,- 1.~~2,- 0.9~~3]	-1.~~3~~6 [- 1.48,- 1.4]	-1.~~3~~6 [- 1.~~5~~8,- 1.4]	-1.~~3~~6 [- 1.~~6~~7,- 1.4]
	BK - ~~other~~cropland–pasture–urban transitions	0.~~3~~ [0.~~3~~,0 .~~3~~]	0.~~2~~ [0.~~2~~,0 .~~3~~]	0.~~2~~ [0.~~1~~,0 .~~3~~]	0.~~1~~ [0.~~1~~,0 .~~2~~]	0.~~1~~ [0,0.1]	0.~~2~~1 [0.1,0 .~~2~~1]	0.1 [0.~~1~~,0 .1]	0.~~1~~ [0.~~1~~,0 .~~1~~]
	BK - peat drainage & peat fires	0.2 [0.1,0 .2]	0.2 [0.1,0 .2]	0.2 [0.2,0 .~~2~~3]	0.3 [0.~~2~~3, 0.~~3~~4]	0.~~2~~3 [0.2,0 .3]	0.3 [0.3,0 .3]	0.2 [0.2,0 .3]	0.2 [0.2,0 .~~2~~3]
	BK - wood harvest & ~~forest~~other management	0.4 [0.1,0 .6]	0.4 [0.1,0 .6]	0.5 [0.1,0 .~~7~~6]	0.5 [0.1,0 .7]	0.~~5~~4 [0.1,0 .~~7~~6]	0.4 [0.1,0 .7]	0.4 [0.1,0 .7]	0.4 [0.1,0 .7]
	DGVMs-net flux (1b~~)~~[†]	1.~~3~~5± 0.~~5~~4	1.~~2~~3± 0.~~5~~4	1.2±0 .~~5~~4	1.~~2~~3± 0.~~5~~3	1.~~2~~3± 0.~~6~~3	1.~~1~~2± 0.~~6~~3	1±0.~~6~~ 3	0.9±0 .~~5~~3
Terrestrial sink (S_{LAND})	Residual sink from global budget (E_{FOS}+E_{LUC}(1a)-G_{ATM}-S_{OCEAN}) (2a)	1.~~9~~8± 0.8	~~2~~1.9± 0.8	1.7±0 .9	2.~~6~~8± 0.9	~~2.9~~3. 0±0.9	3.3±0 .9	2.~~4~~9± 0.9	~~0.3~~4. 1±1
	DGVMs (2b~~)~~[†+]	1.0~~-9~~ ±0.3	1.~~6~~7± 0.5	1.~~4~~5± 0.~~6~~5	2±0.~~5~~ 4	2.~~2~~3± 0.~~6~~4	2.~~5~~6± 0.~~7~~6	2.~~4~~5± 0.~~8~~7	~~1.9~~3. 6±0.9

Formatted: Font: Times New Roman, Not Bold, Not Italic

Formatted Table

Formatted: Font: Arial Unicode MS

Formatted: Font: Arial Unicode MS

		1960s	1970s	1980s	1990s	2000s	2010s	2015-20242016-2025	20242025
Net land fluxes (S_{LAND}-E_{LUC})	GCB2025GCB2026 Budget (2b-1a)	-0.98±0.8	-0.1±0.9	-0.32±0.9	0.2±0.98	0.56±0.98	0.9±10.9	1.2±1	0.72.4±1.1
	Atmospheric O_2	---	---	---	1.3±0.6	0.9±0.7	1.0±0.8	0.7±0.8	-
	DGVMs-net (2b-1b))[+]	-0.34±0.45	0.4±0.6	0.2±0.5	0.87±0.4	1±0.49±0.3	1.43±0.65	1.45±0.76	1.12.7±0.89
	Inversions[*]	- [-,-]	- [-,-]	[,]0.4 [0.1,0.7] (2)	0.78 [0.6,0.8] (1.2] (3)	1.4 [1.32, 1.6] (34)	1.5 [1.3,2.31.9] (8)	1.35±0.3 (1416)	3±0.2±0.7 (146 (16)
	ESMs	0 [-0.7,0.5]	1.5 [1.2,2]	1.1 [0.5,1.4]	1.8 [1.2,2.4]	1.8 [0.4,2.7]	2 [0.7,3]	2.34 [-0.14, 3.69]	3.5 [0.8 [-21-4.9-3.3]

[†]The mean DGVM estimates for S_{LAND} and E_{LUC} are adjusted by δL (estimated by the bookkeeping models), which represents the interaction between land-use change and changing environmental conditions, excluding the direct land-use change effect. See Section S.4.1 for details.

[+]The mean DGVM estimate of S_{LAND} is further reduced by 0.07 GtC/yr to account for the lateral carbon (LOAC) flux for 2016-2025 and for 2025.

[*]Estimates are adjusted for the pre-industrial influence of river fluxes, for the cement carbonation sink, and adjusted to common E_{FOS} (Sect. 2.7). The ranges given include varying numbers (in parentheses) of inversions in each decade (Table S4)

Formatted Table

Formatted Table

Formatted: Subscript

5160

Table 6: Comparison of results for the ~~un-adjusted~~ ocean sinks from the fCO_2-products~~,~~ (without warm layer/cool skin correction), from global ocean biogeochemistry models (GOBMs), the best estimate for ~~GCB2025~~GCB2026 (adjusted S_{OCEAN}) calculated from fCO_2-products and GOBMs~~)~~ and used in the budget Table 7, as well as additional estimates from ocean interior observation-based changes in the dissolved inorganic carbon (DIC) inventory, atmospheric oxygen, atmospheric inversions and Earth System Models (ESMs) for different periods, the last decade, and the last year available. All values are in GtC yr^{-1}. Uncertainties represent ±1σ of the estimates from the GOBMs and inversions (n>10) and range of ensemble members is given for ensembles with n<10 (~~fCO_2-products,~~ inversions prior to 2015, ocean interior, ESMs). The uncertainty of the ~~GCB2025 budget~~GCB2026 S_{OCEAN} estimate is based on expert judgement (Section 2.5 and Supplement ~~S1 to S4~~S3) and for oxygen it is the standard deviation of a Monte Carlo ensemble (Section 2.8). Note that river flux adjustments were applied to the fCO_2-products and two of the ocean interior estimates to match the definition of S_{OCEAN}, and the ocean interior estimates from Müller et al. (2023) were scaled to the closest full decade in proportion to the atmospheric CO_2 increase (see section 2.5.1 and S3.6).

Mean (GtC~~/~~yr~~-1~~)

Product	1960s	1970s	1980s	1990s	2000s	2010s	~~2015-2024~~2016-2025	~~2024~~2025
~~GCB2025~~GCB2026 Budget	1.3±0.4	1.6±0.4	2~~.1~~±0.4	2.3±0.4	2.~~64~~±0.4	~~3.1~~2.9 ±0.4	3~~.2~~±0.4	3.~~42~~±0.4
fCO_2-products	---	---	---	2.~~34~~ [2,3]	2.~~56~~ [2.~~4,2.9~~3,3]	3.1 [2.~~97~~,3.~~54~~]	3.3 [2.~~98~~,3.9]	3.~~54~~ [2.~~86~~,4.2]
GOBMs	1.1±0.2	1.3±0.~~3~~2	1.~~87~~±0.~~3~~2	2~~.~~±0~~±0.3~~.2	2.2±0.3	2.~~65~~±0.3	2.7±0.3	2.9±0.~~34~~
Atmospheric O_2	---	---	---	2~~.0~~±0.4	2.8±0.4	3.4±0.5	3.5±0.5	-
Inversions	- [-,-]	- [-,-]	~~[,]~~ 1.7 [1.4,2.1] (2)	2.~~4 [~~3 [1.9,2.~~2,2.5]~~ (26] (3)	2.3 [2.1,2~~,~~2~~.~~.5] (4~~]~~ (3~~)~~)	2.9 [2.~~1~~6,3.1] (8)	3.1±0.3 (~~14~~16)	3.3±0.4 (~~14~~16)
Ocean interior	1.1 [-,-]	1.~~3~~4 [-,-]	1.8 [-,-]	2.2 [2.1 ~~[2~~,2.3]	2.4 [2 ~~[1.7~~.3, 2.5]	3.~~3~~0 [2.7,3.4]	~~—~~2.9 [-,-]	~~-~~3.0[-,-]

Formatted Table

Product	1960s	1970s	1980s	1990s	2000s	2010s	~~2015-2024~~2016-2025	~~2024~~2025
ESMs	0.7 [0.1,1.1]	1 [0.4,1.4]	1.5 [0.7,2]	1.~~7~~8 [1.1,2.1]	1.9 [1.5,2.2]	2.4 [2,2.~~7~~8]	2.5 [2.~~2,2.8~~3,3]	2.~~6~~7 [2.~~2~~4-3.1]

Formatted Table

Table 7: Decadal mean in the five components of the anthropogenic CO_2 budget for different periods, and last year available. All values are in GtC yr^{-1}, and uncertainties are reported as ±1σ. Fossil CO_2 emissions include cement carbonation. The table also shows the budget imbalance (B_{IM}), which provides a measure of the discrepancies among the nearly independent estimates. A positive imbalance means the emissions are overestimated and/or the sinks are too small. All values are rounded to the nearest 0.1 GtC and therefore columns do not necessarily add to zero.

Mean (GtC yr⁻¹)

		1960s	1970s	1980s	1990s	2000s	2010s	2015-2024 2016-2025	2024 2025	2025 2026 (Projection)
Total emissions (EFOS + ELUC)	Fossil CO2 emissions (EFOS)*	3±0.2	4.76±0.2	5.4±0.3	6.4±0.3	7.8±0.4	9.5±0.5	9.810 ±0.5	10.35 ±0.5	10.4±0.5
	Land-use change emissions (ELUC)	1.98±0.7	1.7±0.7	1.76±0.7	1.78±0.7	1.7±0.7	1.6±0.7	1.43±0.7	1.32±0.7	1.13±0.7
	Total emissions	4.9±0.7	6.43±0.7	7.1±0.8	8.12±0.8	9.5±0.8	11.12 ±0.8	11.23 ±0.9	11.67 ±0.9	11.57 ±0.9
Partitioning	Growth rate in atmos CO2 (GATM)	1.7±0.07	2.8±0.07	3.4±0.02	3.1±0.02	4±0.02	5.1±0.02	5.64±0.02	7.94.4 ±0.2	4.96±0.28
	Ocean sink (SOCEAN)	1.3±0.4	1.6±0.4	2.1±0.4	2.3±0.4	2.64±0.4	3.12.9 ±0.4	3.2±0.4	3.42±0.4	3.21±0.4
	Terrestrial sink (SLAND)	0.91±0.3	1.67±0.5	1.45±0.65	2±0.54	2.23±0.64	2.56±0.76	2.45±0.87	1.93.6 ±0.9	3.4±1.2

		1960s	1970s	1980s	1990s	2000s	2010s	2015-2024 2016-2025	2024 2025	2025 2026 (Projection)
Budget Imbalance	BIM=EFOS+ELUC-(GATM+SOCEAN+SLAND)	0.98	0.53	0.32	0.78	0.7	0.47	0.4	-1.70.5	

*Fossil emissions excluding the cement carbonation sink amount to 3.1±0.2 GtC/yr^{-1}, 4.7±0.2 GtC/yr^{-1}, 5.5±0.3 GtC/yr^{-1}, 6.4±0.3 GtC/yr^{-1}, 7.9±0.4 GtC/yr^{-1}, and 9.7±0.5 GtC/yr, and 10.1±0.5 GtC/yr for the decades 1960s to 2010s2016-2025 respectively and to 10.6±0.5 GtC /yr^{-1} for 20242025, and 10.56±0.52 GtC/yr^{-1} for 2025.2026.

Formatted Table

Formatted: Not Superscript/ Subscript

Formatted: Not Superscript/ Subscript

Formatted: Not Superscript/ Subscript

Formatted: Not Superscript/ Subscript

Formatted: Not Superscript/ Subscript

Formatted: Not Superscript/ Subscript

Table 8. Cumulative CO_2 for different time periods in gigatonnes of carbon (GtC). Fossil CO_2 emissions include cement carbonation. The budget imbalance (B_{IM}) provides a measure of the discrepancies among the nearly independent estimates. All values are rounded to the nearest 5 GtC and therefore columns do not necessarily add to zero. Uncertainties are reported as follows: E_{FOS} is 5% of cumulative emissions; E_{LUC} ~~prior to~~ pre-1959 is 1σ spread from the DGVMs, E_{LUC} post-1959 is 0.7*number of years (where 0.7 GtC yr^{-1} is the uncertainty on the annual E_{LUC} flux estimate); G_{ATM} uncertainty is held constant at 5 GtC for all time periods; S_{OCEAN} uncertainty is ~~20% of the cumulative sink (20% relates to the annual uncertainty of 0.4 GtC yr^{-1}, which is ~20% of the current ocean sink); and~~calculated as the sum of annual uncertainties, assuming errors are fully correlated through time. Annual uncertainties combine the ensemble spread of GOBMs and fCO_2-products, their mean differences, and systematic uncertainties (see Supplement S3.5); prior to 1959, a relative uncertainty of 30% was applied (see Supplement S.3.1). S_{LAND} is the 1σ spread from the DGVMs estimates.

Mean (GtC yr^{-1})

		1750-~~2024~~2025	1850-~~2014~~2021	1850-~~2024~~2025	~~1960-2024~~1959-2025	1850-~~2025~~2026
Emissions	Fossil CO2 emissions (EFOS)	~~500~~510±25	~~400±20~~470 ±25	~~495~~510±25	~~415~~430±20	~~510~~520±25
	Land-use change emissions (ELUC)	~~280±65~~275 ±55	~~235±55~~240 ±50	~~250±60~~245 ±50	110±45	~~250±60~~245 ±50
	Total emissions	~~780±70~~785 ±60	~~635±60~~710 ±55	~~745±65~~755 ±55	~~525~~545±50	~~755±65~~765 ±55
Partitioning	Growth rate in atmos CO2 (GATM)	~~310~~315±5	~~235~~275±5	~~290~~295±5	~~230~~235±5	~~295~~300±5
	Ocean sink (SOCEAN)	210±~~40~~60	~~170±35~~185 ±50	200±~~40~~55	145±~~30~~40	~~205±40~~200 ±55
	Terrestrial sink (SLAND)	~~190±50~~210 ±45	~~150~~180±40	~~175±50~~190 ±40	~~120~~125±30	~~175±50~~195 ±40
Budget imbalance	BIM=EFOS +ELUC-(GATM+SOCEAN+SLAND)	~~65~~50	~~80~~70	~~80~~70	~~35~~40	~~80~~ 70

Formatted Table

Formatted: Not Superscript/ Subscript

Formatted: Not Superscript/ Subscript

Formatted: Not Superscript/ Subscript

Formatted: Not Superscript/ Subscript

Formatted: Not Superscript/ Subscript

Formatted: Not Superscript/ Subscript

Formatted: Not Superscript/ Subscript

Formatted: Not Superscript/ Subscript

Formatted: Not Superscript/ Subscript

5200
5201
5202
5203

Table 9. Average annual growth rate in fossil CO_2 emissions over the most recent decade (~~2015-2024~~2016-2025) and the previous decade (~~2005-2014~~2006-2015). The data for the World include the cement carbonation sink. IAS are emissions from international aviation and shipping. The rest of the world is defined as World minus China, USA, India, EU27, and IAS.

	World	China	USA	India	EU27	OECD	Non-OECD	IAS	Rest of the Wor
~~2005-2014~~2006-2015	~~2.~~1.9 %	5.~~6.7~~ %	-1.4 %	6.~~4%~~ 3 %	-2.~~2~~3 %	-1.0 %	4.~~6~~1 %	1.~~9%~~ 7 %	1.~~8%~~ 6 %
~~2015-2024~~2016-2025	0.~~8~~9 %	2.~~5~~7 %	-~~1.2~~0.8 %	3.~~6~~5 %	-2.~~5~~9 %	-1.~~5~~4 %	2.1 %	-~~1.4~~0.6 %	0.~~6~~4 %

Formatted: Font: Arial, 11 pt
Formatted: Widow/Orphan control
Formatted: Line spacing: Multiple 1.15 li
Formatted Table
Formatted: Font: Times New Roman, 10 pt
Formatted: Centered, Line spacing: Multiple 1.15 li
Formatted: Font: Times New Roman, 10 pt
Formatted: Centered, Line spacing: Multiple 1.15 li
Formatted: Centered, Line spacing: Multiple 1.15 li
Formatted: Font: Times New Roman, 10 pt
Formatted: Font: Times New Roman, 10 pt
Formatted: Font: Times New Roman, 10 pt
Formatted: Font: Times New Roman, 10 pt
Formatted: Font: Times New Roman, 10 pt
Formatted: Font: Times New Roman, 10 pt
Formatted: Font: Times New Roman, 10 pt
Formatted: Font: Times New Roman, 10 pt
Formatted: Font: Times New Roman, 10 pt
Formatted: Font: Times New Roman, 10 pt
Formatted: Centered, Line spacing: Multiple 1.15 li
Formatted: Centered, Line spacing: Multiple 1.15 li
Formatted: Font: Times New Roman, 10 pt
Formatted: Font: Times New Roman, 10 pt
Formatted: Centered, Line spacing: Multiple 1.15 li
Formatted: Font: Times New Roman, 10 pt
Formatted: Font: Times New Roman, 10 pt
Formatted: Font: Times New Roman, 10 pt
Formatted: Font: Times New Roman, 10 pt
Formatted: Font: Times New Roman, 10 pt
Formatted: Font: Times New Roman, 10 pt
Formatted: Font: Times New Roman, 10 pt
Formatted: Font: Times New Roman, 10 pt
Formatted: Font: Times New Roman, 10 pt
Formatted: Font: Times New Roman, 10 pt

Table 10. Major known sources of uncertainties in each component of the Global Carbon Budget, defined as input data or processes that have a demonstrated effect of at least ±0.3 GtC yr^{-1}.

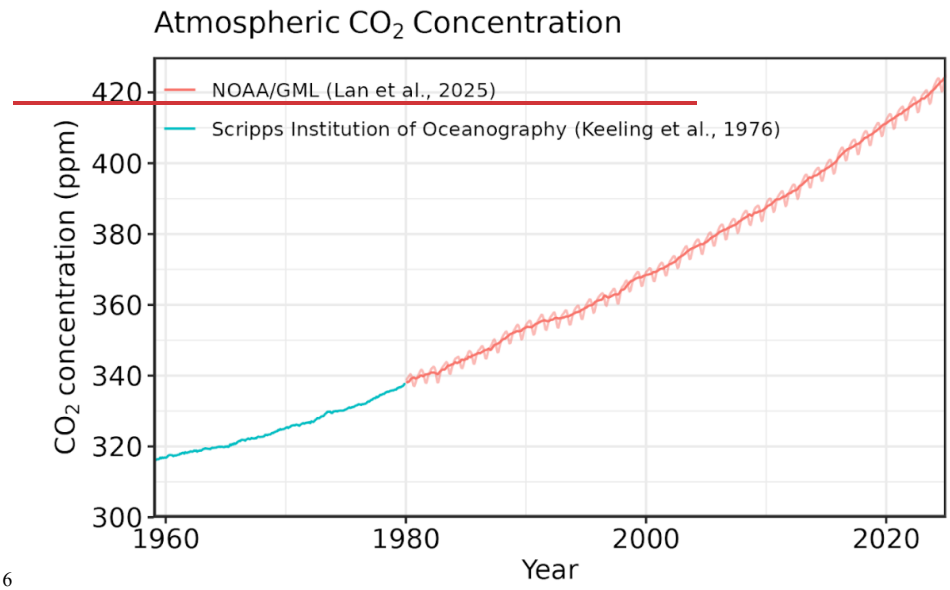
Source of uncertainty	Time scale (years)	Location	Evidence
Fossil CO2 emissions (EFOS; Section 2.1)			
energy statistics	annual to decadal	global, but mainly China & major developing countries	(Korsbakken et al., 2016, Guan et al., 2012)
carbon content of coal	annual to decadal	global, but mainly China & major developing countries	(Liu et al., 2015)
system boundary	annual to decadal	all countries	(Andrew, 2020a)
Net land-use change flux (ELUC; section 2.2)			
land-cover and land-use change statistics	continuous	global; in particular tropics	(Houghton et al., 2012, Gasser et al., 2020, Ganzenmüller et al., 2022, Yu et al. 2022)
sub-grid-scale transitions	annual to decadal	global	(Wilkenskjeld et al., 2014, Bastos et al., 2021)
vegetation biomass	annual to decadal	global; in particular tropics	(Houghton et al., 2012, Bastos et al., 2021)
forest degradation (fire, selective logging)	annual to decadal	tropics; Amazon	(Aragão et al., 2018, Qin et al., 2021, Lapola et al., 2023)
wood and crop harvest	annual to decadal	global; SE Asia	(Arneth et al., 2017, Erb et al., 2018)
peat burning	multi-decadal trend	global	(van der Werf et al., 2010, 2017~~)~~, 2025)

Formatted Table

Atmospheric growth rate (GATM; section 2.4) no demonstrated uncertainties larger than ±0.3 GtC yr-1 . The uncertainties in annual GATM have been estimated as ±0.2 GtC yr-1, although the conversion of the growth rate into a global annual flux assuming instantaneous mixing throughout the atmosphere introduces additional errors (see Section 2.4.2).			
Ocean sink (SOCEAN; section 2.5)			
sparsity in surface fCO2 observations	mean, decadal variability and trend	global, in particular southern hemisphere	(Gloege et al., 2021, Denvil-Sommer et al., 2021, Hauck et al., 2023a; Dong et al., 2024b~~),~~ Roobaert et al 2026)
riverine carbon outgassing and its anthropogenic perturbation	annual to decadal	global, in particular partitioning between Tropics and South	(Aumont et al., 2001, Lacroix et al., 2020, Crisp et al., 2022)
Discrepancy between~~Models underestimate~~ interior ocean anthropogenic carbon storage from models and observation-based estimates	annual to decadal	global	(Friedlingstein et al., 2022a, this study, DeVries et al., 2023, Müller et al., 2023)
near-surface temperature and salinity gradients	mean on all time-scales	global	(Watson et al., 2020, Dong et al., 2022, Bellenger et al., 2023, Dong et al., 2024a~~),~~ Ford et al 2024)
Land sink (SLAND; section 2.6)			
strength of CO2 fertilisation	multi-decadal trend	global	(Wenzel et al., 2016; Walker et al., 2021~~);~~ Norby et al., 2025))
response to variability in temperature and rainfall	annual to decadal	global; in particular tropics	(Cox et al., 2013; Jung et al., 2017; Humphrey et al., 2018; 2021)
nutrient limitation and supply	annual to multi-decadal	global	(Zaehle et al., 2014)
carbon allocation and tissue turnover rates	annual to decadal	global	(De Kauwe et al., 2014; O'Sullivan et al., 2022)

tree mortality	annual	global in particular tropics	(Hubau et al., 2020~~2021~~; Brienen et al., 2020)
response to diffuse radiation	annual	global	(Mercado et al., 2009; O'Sullivan et al., 2021)

Figures



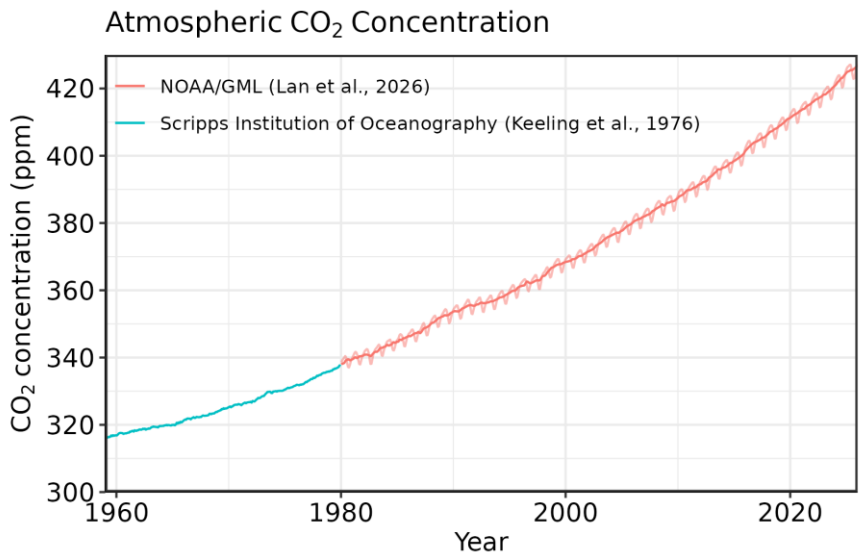
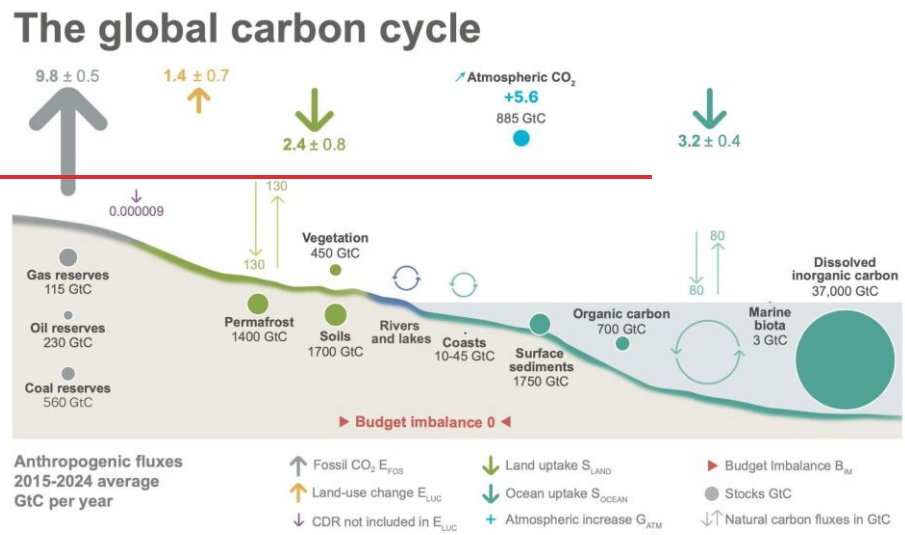
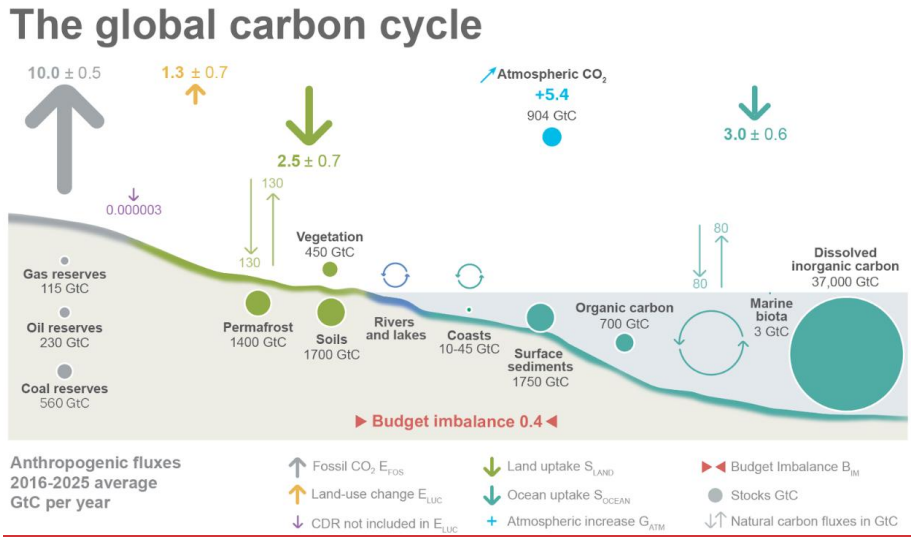


Figure 1. Surface average atmospheric CO_2 concentration (ppm). Since 1980, monthly data are from NOAA/GML (Lan et al., ~~2025~~2026) and are based on an average of direct atmospheric CO_2 measurements from multiple stations in the marine boundary layer (Masarie and Tans, 1995). The 1958-1979 monthly data are from the Scripps Institution of Oceanography, based on an average of direct atmospheric CO_2 measurements from the Mauna Loa and South Pole stations (Keeling et al., 1976). To account for the difference of mean CO_2 and seasonality between the NOAA/GML and the Scripps station networks used here, the Scripps surface average (from two stations) was de-seasonalised and adjusted to match the NOAA/GML surface average (from multiple stations) by adding the mean difference of 0.667 ppm, calculated here from overlapping data during 1980-2012.

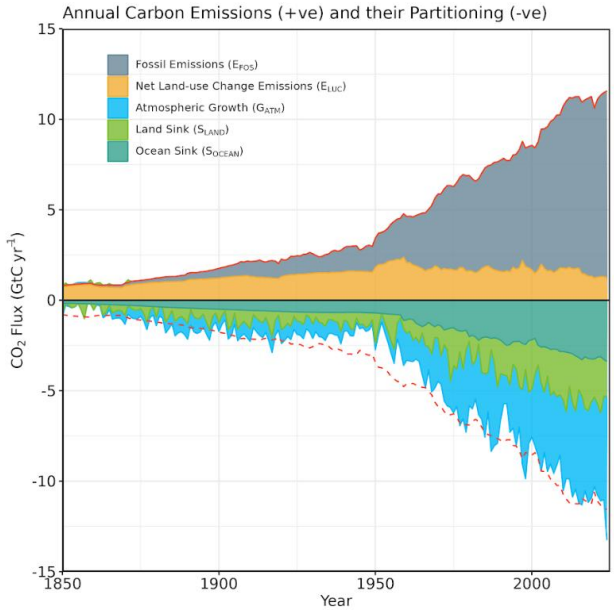

The global carbon cycle
9.8 ± 0.5
1.4 ± 0.7
2.4 ± 0.8
Atmospheric CO2
+5.6
885 GtC
3.2 ± 0.4
0.000009
130
130
Vegetation
450 GtC
80
80
Dissolved inorganic carbon
37,000 GtC
Gas reserves
115 GtC
Oil reserves
230 GtC
Coal reserves
560 GtC
Permafrost
1400 GtC
Soils
1700 GtC
Rivers and lakes
Coasts
10-45 GtC
Surface sediments
1750 GtC
Organic carbon
700 GtC
Marine biota
3 GtC
Budget imbalance 0
Anthropogenic fluxes
2015-2024 average
GtC per year
Fossil CO2 EFOS
Land-use change ELUC
CDR not included in ELUC
Land uptake SLAND
Ocean uptake SOCEAN
Atmospheric increase GATM
Budget Imbalance BIM
Stocks GtC
Natural carbon fluxes in GtC

5227


The global carbon cycle
10.0 ± 0.5
1.3 ± 0.7
2.5 ± 0.7
Atmospheric CO2
+5.4
904 GtC
3.0 ± 0.6
0.000003
130
130
Vegetation
450 GtC
80
80
Dissolved inorganic carbon
37,000 GtC
Gas reserves
115 GtC
Oil reserves
230 GtC
Coal reserves
560 GtC
Permafrost
1400 GtC
Soils
1700 GtC
Rivers and lakes
Coasts
10-45 GtC
Surface sediments
1750 GtC
Organic carbon
700 GtC
Marine biota
3 GtC
Budget imbalance 0.4
Anthropogenic fluxes
2016-2025 average
GtC per year
Fossil CO2 EFOS
Land-use change ELUC
CDR not included in ELUC
Land uptake SLAND
Ocean uptake SOCEAN
Atmospheric increase GATM
Budget Imbalance BIM
Stocks GtC
Natural carbon fluxes in GtC

5228

Figure 2. Schematic representation of the overall perturbation of the global carbon cycle caused by anthropogenic activities, averaged globally for the decade ~~2015-2024~~2016-2025. See legends for the corresponding arrows. Fluxes estimates and their 1 standard deviation uncertainty are as reported in Table 7. The CDR estimate is for the year ~~2024~~2025. The uncertainty in the atmospheric CO_2 growth rate is very small (±0.02 GtC yr^{-1}) and is neglected for the figure. The anthropogenic perturbation occurs on top of an active carbon cycle, with fluxes and stocks represented in the background and taken from Canadell et al. (2021) for all numbers, except for the carbon stocks in coasts which is from a literature review of coastal marine sediments (Price and Warren, 2016). Fluxes are in GtC yr^{-1} and reservoirs in GtC. This figure was produced by Nigel Hawtin.


Annual Carbon Emissions (+ve) and their Partitioning (-ve)
Fossil Emissions (E_{FOS})
Net Land-use Change Emissions (E_{LUC})
Atmospheric Growth (G_{ATM})
Land Sink (S_{LAND})
Ocean Sink (S_{OCEAN})
CO_2 Flux (GtC yr^{-1})
15
10
5
0
-5
-10
-15
1850
1900
1950
2000
Year

5239

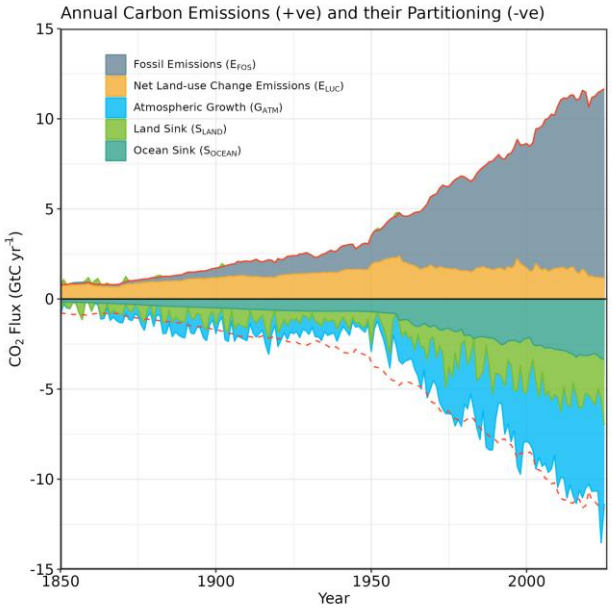
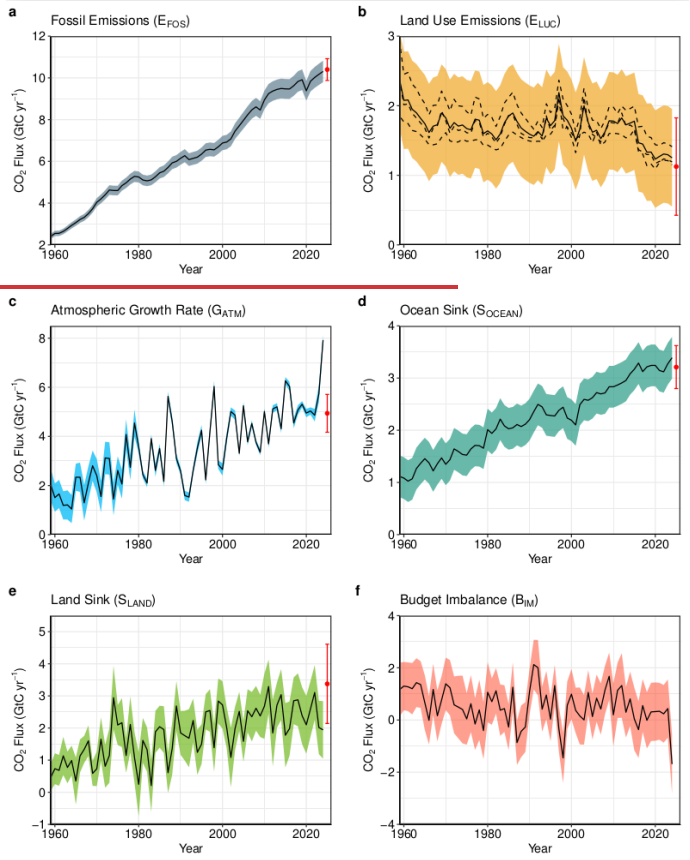


Figure 3. Combined components of the global carbon budget as a function of time, for fossil CO_2 emissions (E_{FOS}, including a small sink from cement carbonation; grey) and emissions from land-use change (E_{LUC}; brown), as well as their partitioning among the atmosphere (G_{ATM}; cyan), ocean (S_{OCEAN}; blue), and land (S_{LAND}; green). The figure shows annual estimates of each flux (in GtC yr^{-1}) since the year 1850. The partitioning is based on nearly independent estimates from observations (for G_{ATM}) and from process model ensembles constrained by data (for S_{OCEAN} and S_{LAND}) and does not exactly add up to the sum of the emissions, resulting in a budget imbalance (B_{IM}) which is represented by the difference between the bottom red line (mirroring total emissions) and the sum of carbon fluxes in the ocean, land, and atmosphere reservoirs. The E_{FOS} estimate is based on a mosaic of different datasets and has an uncertainty of ±5% (±1σ). The E_{LUC} estimate is from three bookkeeping models (Table 4) with uncertainty of ±0.7 GtC yr^{-1}. The G_{ATM} estimates prior to 1959 are from Joos and Spahni (2008) with uncertainties equivalent to about ±0.1-0.15 GtC yr^{-1} and from Lan et al. (~~2025~~2026) since 1959 with uncertainties of about +-0.07 GtC yr^{-1} during 1959-1979 and ±0.02 GtC yr^{-1} since 1980. The S_{OCEAN} estimate prior to 1959 is the average from Khatiwala et al. (2013) and DeVries (2014) with uncertainty of about ±30%. After 1959, it is the average of an ensemble of models (GOBMs) and an ensemble of fCO_2-products (with adjustments and corrections, Table 4) with uncertainties of about ±0.46 GtC yr^{-1}. (see Supplement S.3.5). The S_{LAND} estimate is the average of an ensemble of models (DGVMs) (Table 4) with uncertainties of about ±1 GtC yr^{-1}. See the text for more details of each component and their uncertainties.


a
Fossil Emissions (E_{FOS})
b
Land Use Emissions (E_{LUC})
c
Atmospheric Growth Rate (G_{ATM})
d
Ocean Sink (S_{OCEAN})
e
Land Sink (S_{LAND})
f
Budget Imbalance (B_{IM})
CO_2 Flux (GtC yr^{-1})
Year
1960
1980
2000
2020

5258

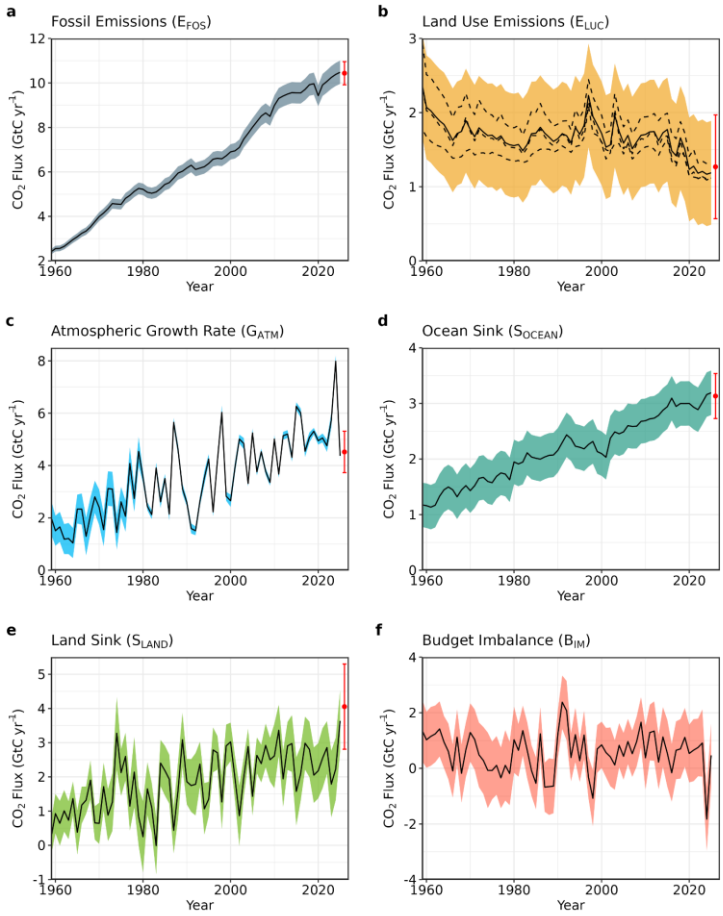
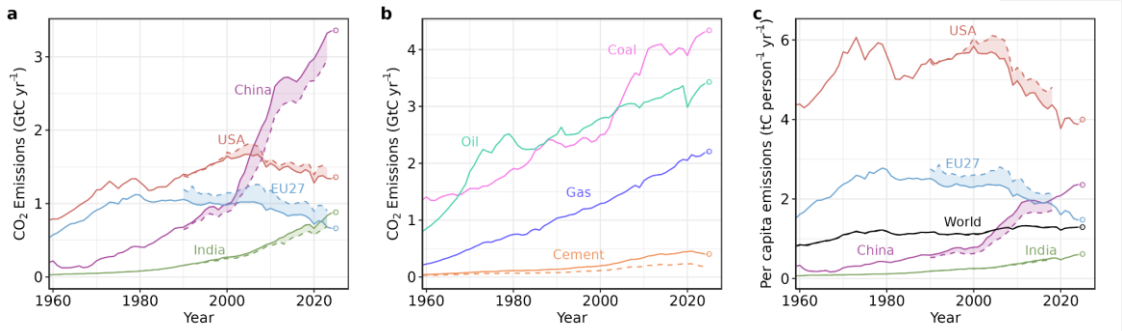


Figure 4. Components of the global carbon budget and their uncertainties as a function of time, presented individually for (a) fossil CO_2, including cement carbonation emissions (E_{FOS}), (b) emissions from land-use change (E_{LUC}), (c) growth rate in atmospheric CO_2 concentration (G_{ATM}), (d) the ocean CO_2 sink (S_{OCEAN}), (e) the land CO_2 sink (S_{LAND}), (f) the budget imbalance (B_{IM}) that is not accounted for by the other terms. Individual estimates from the three bookkeeping models are shown as dashed lines for E_{LUC} in panel (b). Positive values of S_{LAND} and S_{OCEAN} represent a flux from the atmosphere to land or the ocean. All data are in GtC yr^{-1} with the uncertainty bounds representing ±1 standard deviation in shaded colour. Data sources are as in Figure 3. The red dots indicate our projections for the year ~~2025~~2026 and the red error bars the uncertainty in the ~~2025~~2026 projections (see methods).



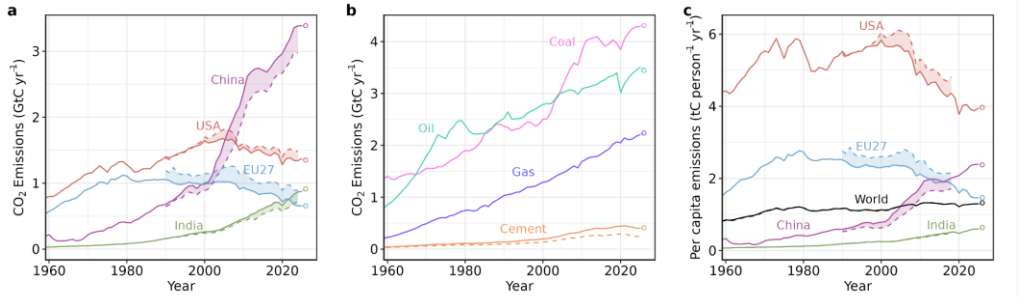


Figure 5. Fossil CO_2 emissions for (a) territorial (solid lines) and consumption (dashed lines) emissions for the top three country emitters (USA, China, India) and for the European Union (EU27), (b) global emissions by fuel type, including coal, oil, gas, and cement, and cement minus cement carbonation (dashed), and (c) per-capita emissions the world and for the large emitters as in panel (a). Territorial emissions are from Andrew & Peters (~~2025~~2026), while consumption-based emissions are updated from Peters et al. (~~2011a~~2011). See Section 2.1 and Supplement S.1 for details of the calculations and data sources.

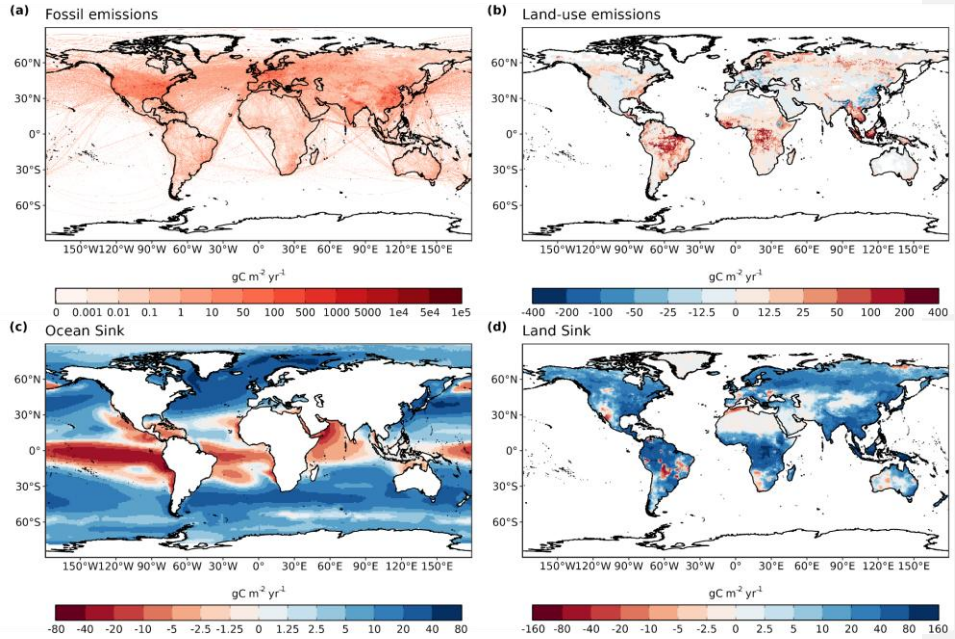
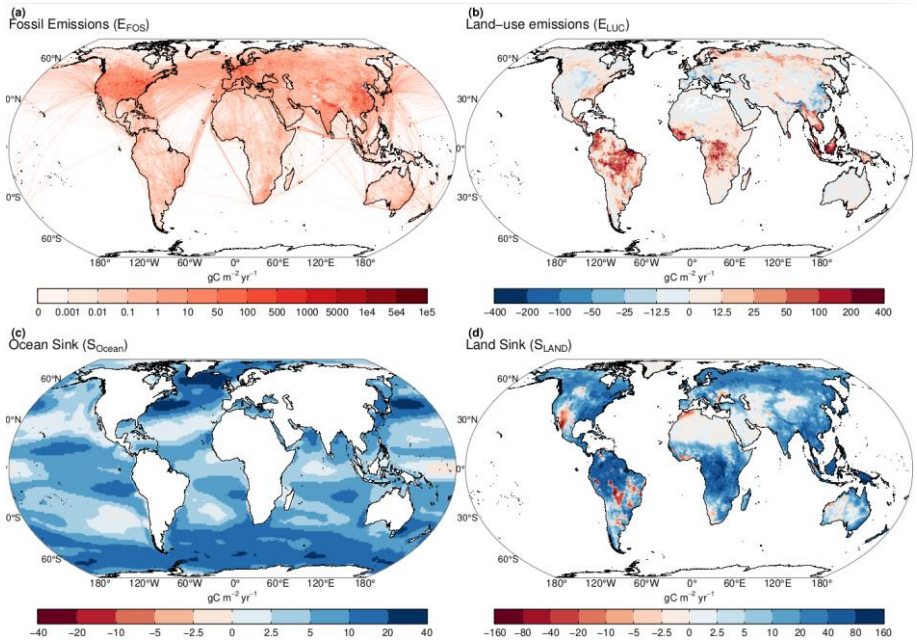
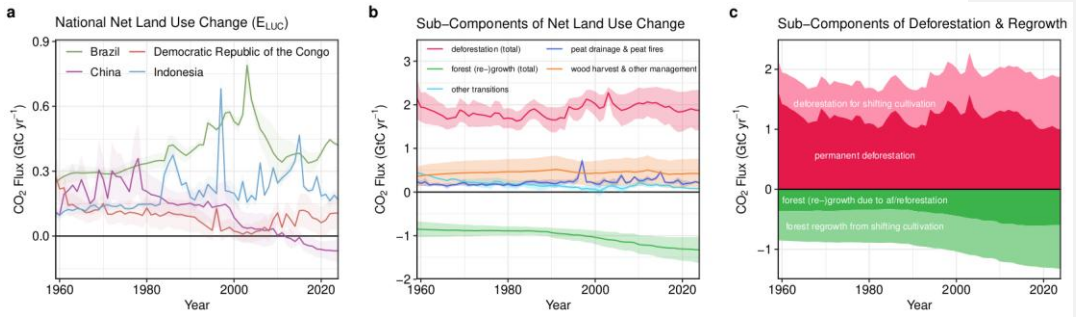


Figure 6. The ~~2015-2024~~2016-2025 decadal mean components of the global carbon budget, presented for (a) fossil CO_2 emissions (E_{FOS}), (b) land-use change emissions (E_{LUC}), (c) the ocean CO_2 sink (S_{OCEAN}), and (d) the land CO_2 sink (S_{LAND}). Positive values for E_{FOS} and E_{LUC} represent a flux to the atmosphere, whereas positive values of S_{OCEAN} and S_{LAND} represent a flux from the atmosphere to the ocean or the land (carbon sink). In all panels, red colours represent a source (flux from the land/ocean to the atmosphere), blue colours represent a sink (flux from the atmosphere into the land/ocean). All units are in gC m^{-2} yr^{-1}. Note the different scales in each panel. E_{FOS} data shown is from GCP-~~GridFEDv2025~~GridFEDv2026.0 and does not include cement carbonation. The E_{LUC} map shows the average E_{LUC} from the three bookkeeping models plus emissions from peat drainage and peat fires. BLUE and LUCE provide spatially explicit estimates at 0.25° resolution. Gridded E_{LUC} estimates for OSCAR are derived by spatially distributing their national data based on the spatial patterns of BLUE gross fluxes in each country (see Schwingshackl et al., 2022~~, for more details about the methodology).~~). S_{OCEAN} ~~data shown~~ is the ~~average of un-adjusted GOBMs and fCO_2 products means, using~~ anthropogenically perturbed atmosphere-ocean flux calculated from the GOBMs simulation A~~, no adjustment for bias and drift applied to the gridded fields (see Section 2.5).~~ minus simulation B. S_{LAND} data shown is the average of the ~~DGVMs for simulation S2, no adjustment for bias and drift applied to the gridded fields (see Section 2.6).~~



DGVM simulations S3-S4+S0+δL, where δL is estimated from the bookkeeping models.



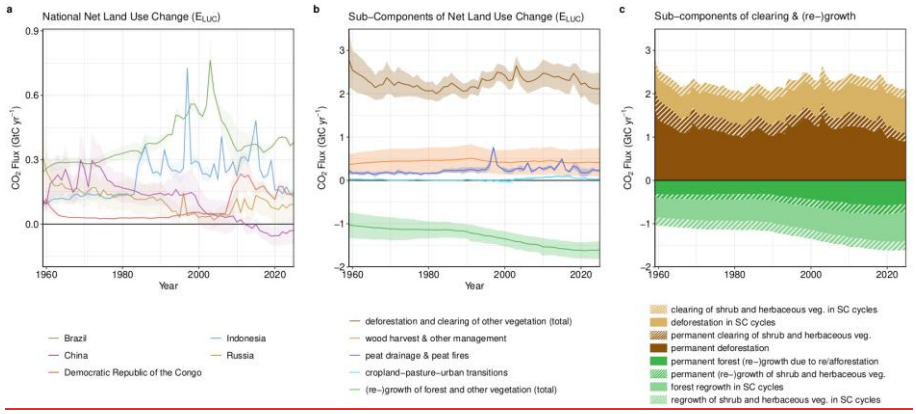
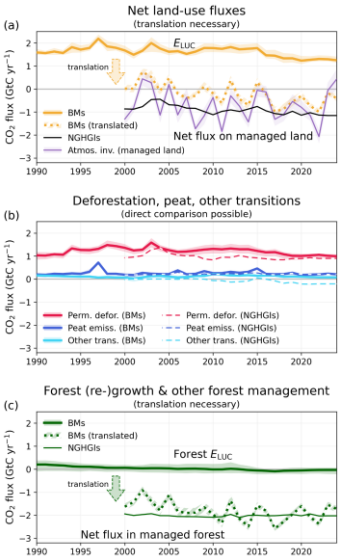


Figure 7. Net CO_2 exchanges between the atmosphere and the terrestrial biosphere related to land–use change. (a) Net CO_2 emissions from land-use change from the ~~four~~five countries with largest cumulative emissions since 1959. Values shown are the average of the three bookkeeping models, with shaded regions as ±1σ uncertainty. (b) Sub-components of E_{LUC}: (i) emissions from deforestation ~~(~~and clearing of other vegetation (total; that is including permanent deforestation and clearing and deforestation and clearing in shifting cultivation cycles), (ii) emissions from peat drainage & peat fires, (iii) removals from ~~forest~~ (re-)growth ~~(~~of forest and other vegetation (total; that is including ~~forest~~permanent (re-)growth ~~due to afforestation and reforestation and forest~~and regrowth in shifting cultivation cycles), (iv) net fluxes from wood harvest and other forest management (comprising slash and product decay following wood harvest, regrowth after wood harvest, and fire suppression), and (v) emissions and removals ~~related to other land-use~~from transitions~~.~~ between cropland, pasture, and urban areas. The sum of the five components is net E_{LUC} shown in Figure 4b. (c) Sub-components of 'deforestation and clearing of other vegetation (total)' and of ~~'forest (~~'(re-)growth of forest and other vegetation (total)'~~: (i) deforestation in~~, where SC denotes shifting cultivation ~~cycles, (ii) permanent deforestation, (iii) forest (re-)growth due to afforestation and/or reforestation, and (iv) forest regrowth in shifting cultivation cycles~~.

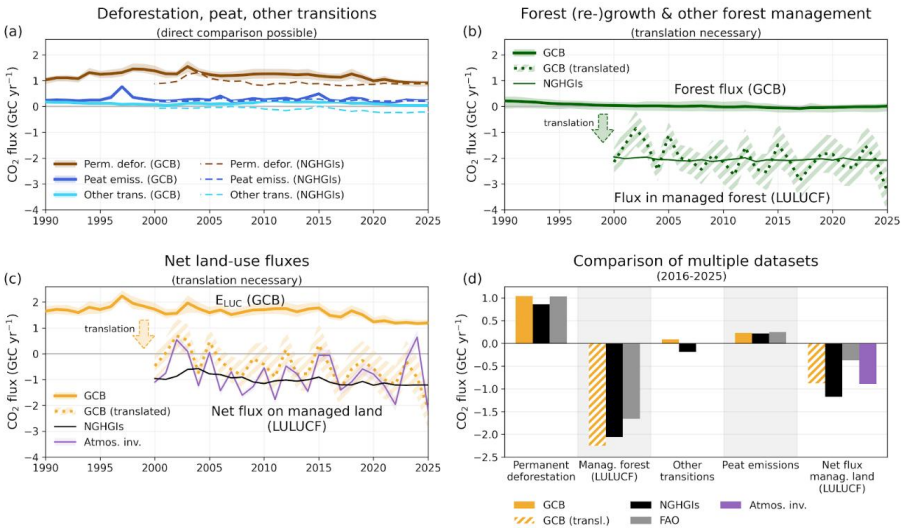
Formatted: Heading 2, Indent: Left: 0.25 cm


Net land-use fluxes
(translation necessary)
(a)
E_{LUC}
translation
BMs
BMs (translated)
NGHGIs
Atmos. inv. (managed land)
Net flux on managed land
CO_2 flux (GtC yr^{-1})
Deforestation, peat, other transitions
(direct comparison possible)
(b)
Perm. defor. (BMs)
Peat emiss. (BMs)
Other trans. (BMs)
Perm. defor. (NGHGIs)
Peat emiss. (NGHGIs)
Other trans. (NGHGIs)
Forest (re-)growth & other forest management
(translation necessary)
(c)
BMs
BMs (translated)
NGHGIs
Forest E_{LUC}
translation
Net flux in managed forest
1990
1995
2000
2005
2010
2015
2020

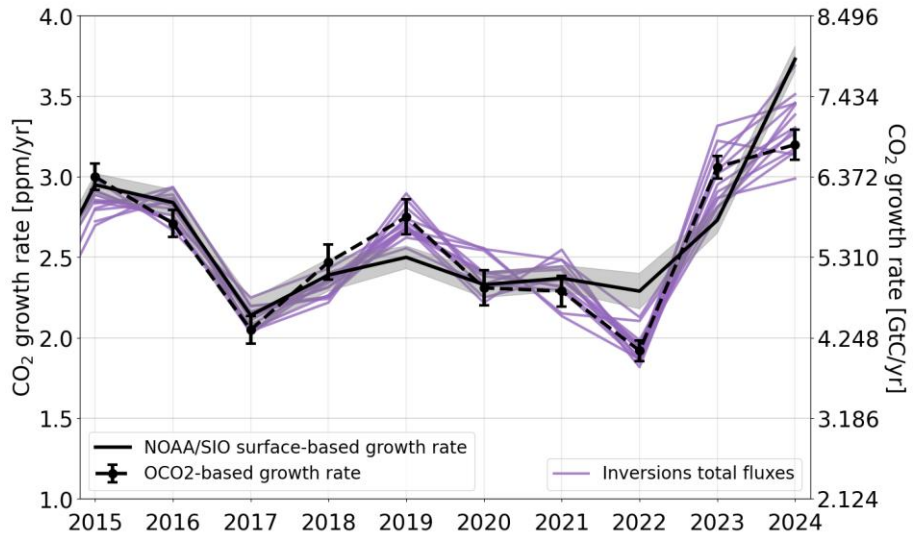
5317

Figure 8. Comparison of GCB land-use CO_2 flux estimates ~~from bookkeeping models (BMs; (~~following the GCB definition of E_{LUC}~~);~~) with national ~~GHG~~greenhouse gas inventories (NGHGIs; following ~~IPCC guidelines and~~ the NGHGI definition of land-use, land-use change, and forestry, LULUCF, thus including all ~~carbon~~CO_2 fluxes on managed land~~);~~) and atmospheric inversion systems (~~considering~~CO_2 fluxes on managed land ~~only);~~) in panels (a) - (c) and additionally with FAO estimates in panel (d). To compare ~~BM~~GCB results with NGHGIs, a translation is necessary for some subcomponents. ~~(a) Net land-use fluxes, for which a translation of BMs is necessary, (b) subcomponents permanent deforestation,~~ (a) 'Permanent deforestation', 'peat drainage & peat ~~fires~~fires', and 'other ~~transitions~~transitions', which can be directly compared ~~and (c) subcomponent forest~~. (b) 'Forest (re-)growth & other forest ~~management~~management', for which a translation is necessary. ~~The lines represent the mean of 3 BMs and 14 atmospheric inversion estimates, respectively; Shaded areas denote the full range across BM estimates and the standard deviation for atmospheric inversions, respectively. The subcomponent forest (re-)growth & other forest management~~ This subcomponent includes removals from permanent forest (re-)growth ~~(permanent),~~ emissions and removals from wood harvest & other forest management, and emissions and removals in shifting cultivation cycles. (c) Net land-use CO_2 fluxes, for which a translation is necessary. The translation of ~~BM~~GCB estimates to NGHGI estimates in (~~a~~b) and (c) is done by adding the natural land sink in managed forests estimated by DGVMs (see Supplement S.2.4) to the ~~BM~~GCB estimates (see also Table S11). Lines show the means of the GCB datasets (three bookkeeping models or three peat drainage datasets plus peat fires, respectively) and of 16 atmospheric inversion estimates, respectively. Shaded areas denote the full range across GCB estimates, the standard deviation for atmospheric inversions, and, for translated estimates, the combined standard deviation (estimated by uncertainty propagation) from bookkeeping model estimates of land-use change fluxes and DGVM estimates of the natural land sink in managed forests. The GCB definition of E_{LUC} and the NGHGI definition of ~~land-use~~LULUCF fluxes are equally valid, each in its own context. ~~For illustrative purposes we only show the translation of BM estimates to the NGHGI definition.~~(d) GCB, NGHGI, FAO, and atmospheric inversion estimates averaged over 2016–2025 (see also Table S11). FAO forest flux estimates include fluxes in both managed and unmanaged forests. The FAO estimate for net flux on managed land (LULUCF) does not include other land-use transitions. NGHGI data are from the LULUCF data hub ~~V3~~V4.1.0 (Melo et al. ~~2025).~~

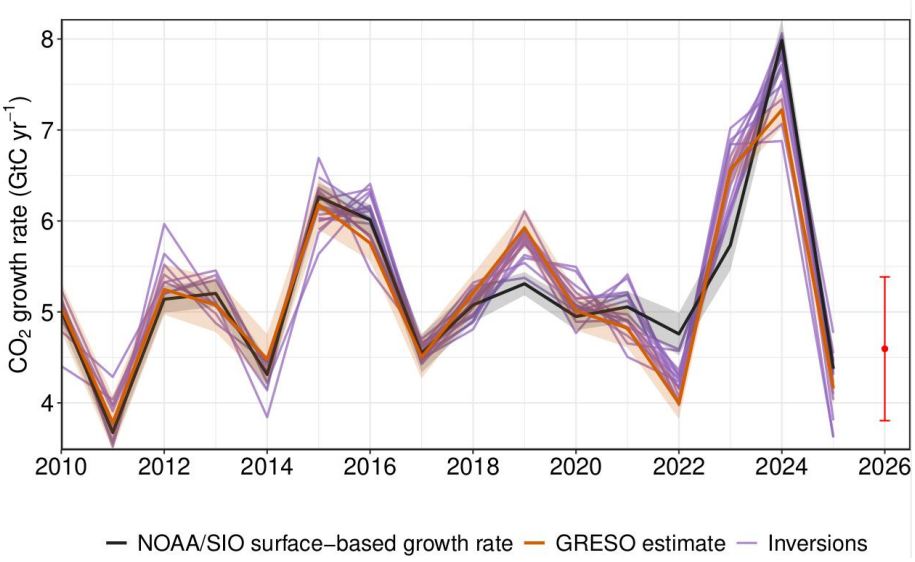
Formatted: Font color: Auto, Not Highlight



2026) and FAO data are from Tubiello et al. (2026) and FAOSTAT (FAO, 2026c).


4.0
3.5
3.0
2.5
2.0
1.5
1.0
8.496
7.434
6.372
5.310
4.248
3.186
2.124
CO2 growth rate [ppm/yr]
CO2 growth rate [GtC/yr]
NOAA/SIO surface-based growth rate
OCO2-based growth rate
Inversions total fluxes
2015
2016
2017
2018
2019
2020
2021
2022
2023
2024

5346


8
7
6
5
4
CO2 growth rate (GtC yr−1)
2010
2012
2014
2016
2018
2020
2022
2024
2026
NOAA/SIO surface−based growth rate
GRESO estimate
Inversions

5347

Figure 9: Annual atmospheric CO_2 growth rates based on observations from the surface network (by NOAA (National Oceanic and Atmospheric Administration) and SIO (Scripps Institution of Oceanography~~),~~)), as well as using the Growth Rate from Satellite Observations (GRESO) approach using OCO-2 (from 2015 onwards) and GOSAT based XCO_2 observations ~~in ppm yr^{-1}~~(from 2010 onwards) with uncertainties. To obtain G_{ATM}, the ~~surface~~ observation-based growth ~~rate~~rates in units of ppm yr^{-1} ~~is~~are converted to units of GtC yr^{-1} by multiplying by a conversion factor (CF) of 2.124 GtC per ppm, assuming ~~instantaneous mixing~~the observations to represent the annual mean mass change of CO_2 throughout the atmosphere. The purple lines are the atmospheric growth rates (in GtC yr^{-1}) calculated as the sum of the fluxes derived by the atmospheric inversions. ~~Note that the right hand axis shows the growth rate in GtC yr^{-1}, with intervals of the conversion factor.~~ The G_{ATM} projection for 2026 is shown in red.

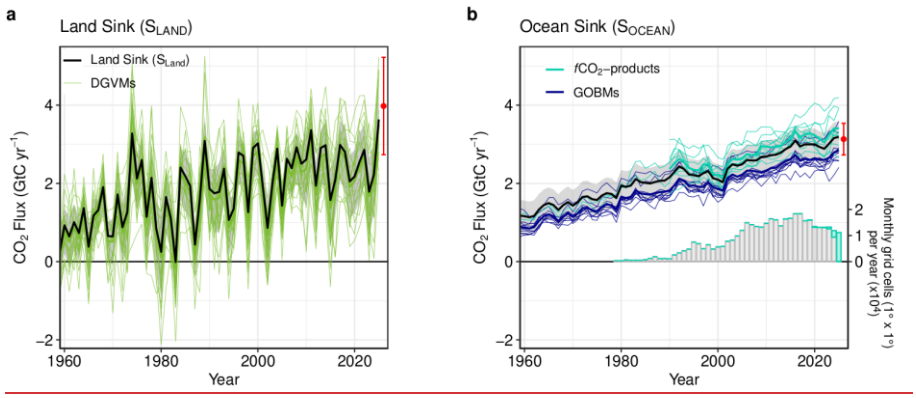
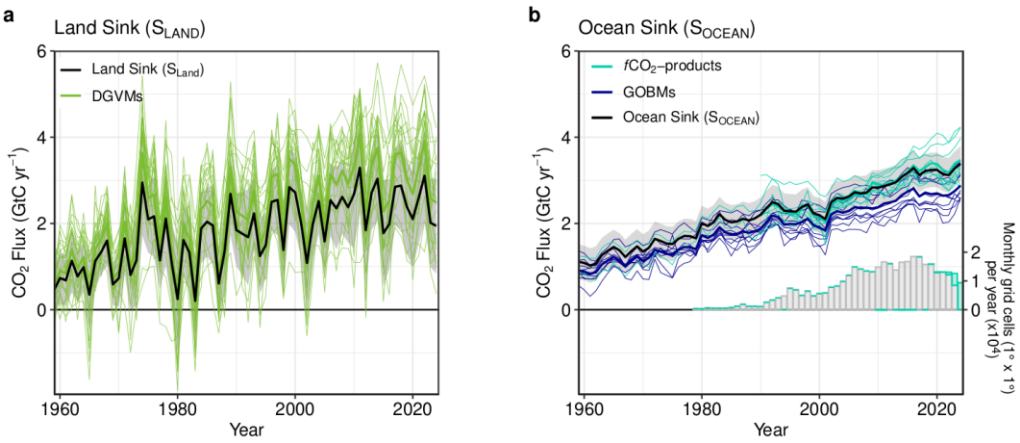
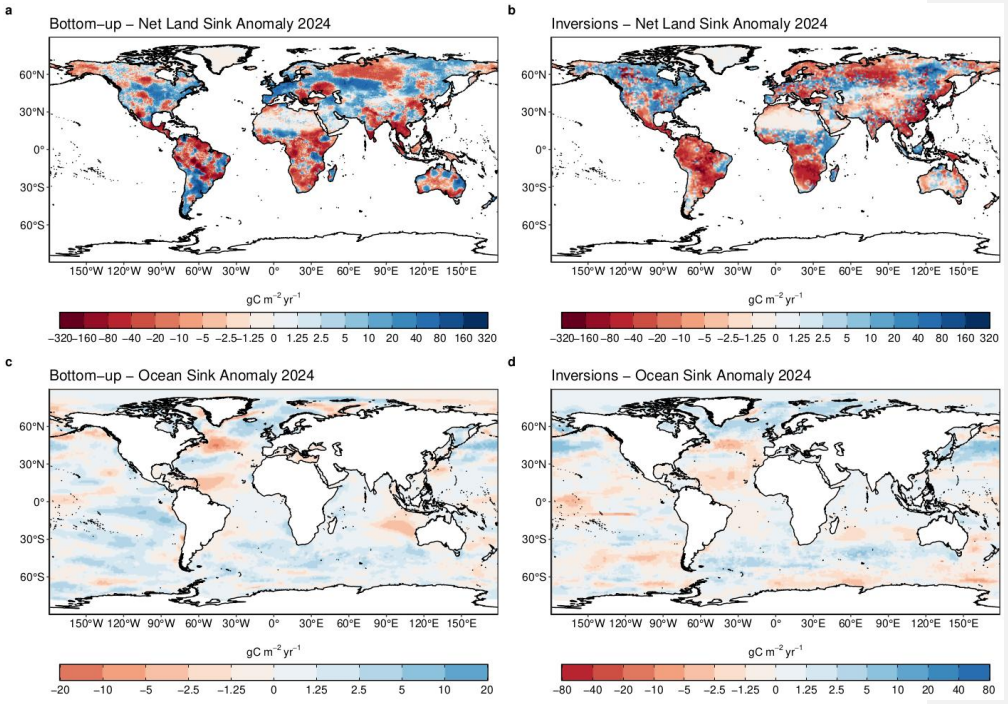


Figure 10. (a) The land CO_2 sink (S_{LAND}) estimated by individual DGVMs (thin green lines). The DGVM multi-model mean is shown as the thick green line. The S_{LAND} budget estimate (black with ±1σ uncertainty), is the DGVM multi-model mean adjusted for the ~~RSS bias (i.e. reduced by 19%).~~δL bias. For years 2015-2025, S_{LAND} is also adjusted for LOAC. The S_{LAND} projection for 2026 is shown in red. (b) Comparison of the anthropogenic atmosphere-ocean CO_2 flux showing the budget values of S_{OCEAN} (black; with the uncertainty in grey shading), individual ocean models (royal blue), and the ocean fCO_2-products (cyan). ~~Adjustments~~Corrections were applied to S_{OCEAN} (black) for the ~~known underestimation in GOBMs and the~~ warm layer/cool skin effect for fCO_2-products. Individual model lines as well as ~~GOBM and~~ fCO_2-product ensemble means (thick cyan ~~and royal blue lines~~line) do not include ~~these adjustments~~this correction, with the exception of ~~23~~ fCO_2-products (~~UExP-FNN-U~~UoEX-UEPFFNU, AOML-ET and JMA-MLR) that include temperature corrections as part of their air-sea CO_2 flux calculation (see section 2.5). Two fCO_2-products (Jena-MLS, LDEO-HPD) extend back to 1959. All fCO_2-products were adjusted for the pre-industrial ocean source of CO_2 from river input to the ocean, by subtracting a source of 0.65 GtC yr^{-1} to make them comparable to S_{OCEAN} (see Section 2.5). The bar-plot in the lower right illustrates the number of monthly gridded values in the SOCAT ~~v2025~~v2026 dataset (Bakker et al., ~~2025a~~2026a). Grey bars indicate the number of grid cells in SOCAT ~~v2024~~v2025, and coloured bars indicate the newly added grid cells in ~~v2025.~~


a
Land Sink (S_{LAND})
Land Sink (S_{Land})
DGVMs
CO_2 Flux (GtC yr^{-1})
Year
b
Ocean Sink (S_{OCEAN})
fCO_2–products
GOBMs
Ocean Sink (S_{OCEAN})
CO_2 Flux (GtC yr^{-1})
Monthly grid cells (1° x 1°) per year (x10^4)
Year

3375 v2026.


a
Bottom–up – Net Land Sink Anomaly 2024
b
Inversions – Net Land Sink Anomaly 2024
c
Bottom–up – Ocean Sink Anomaly 2024
d
Inversions – Ocean Sink Anomaly 2024
60°N
30°N
0°
30°S
60°S
150°W 120°W 90°W 60°W 30°W 0° 30°E 60°E 90°E 120°E 150°E
gC m⁻² yr⁻¹
−320 −160 −80 −40 −20 −10 −5 −2.5 −1.25 0 1.25 2.5 5 10 20 40 80 160 320
−20 −10 −5 −2.5 −1.25 0 1.25 2.5 5 10 20
−80 −40 −20 −10 −5 −2.5 −1.25 0 1.25 2.5 5 10 20 40 80

5376

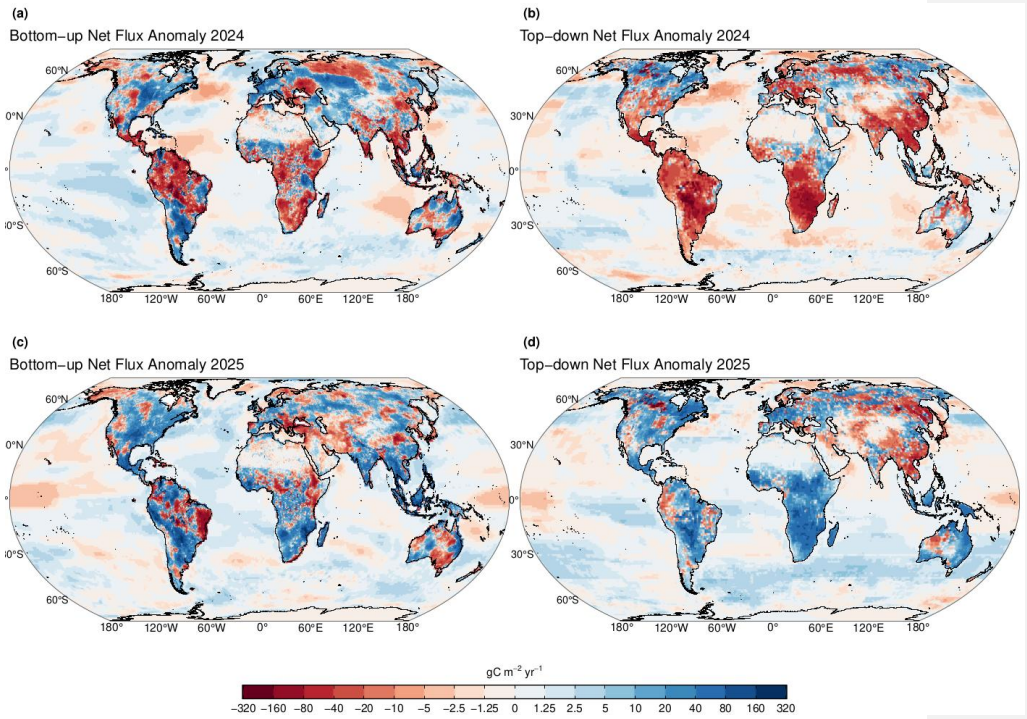
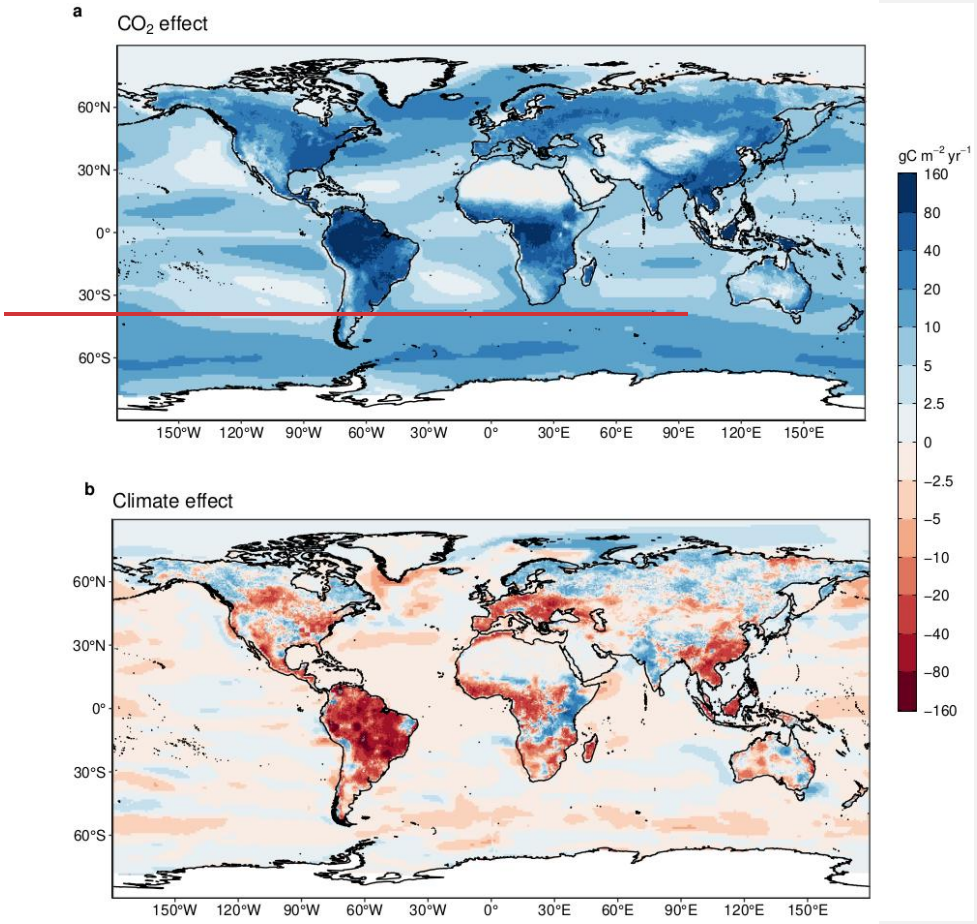


Figure 11. Anomalies in net land and ocean ~~sinks~~fluxes for 2024~~. Maps show the 2024 fluxes~~ and 2025 relative to the ~~2015-2024~~2016-2025 decadal mean. ~~Units are gC m^{-2} yr^{-1}. (~~Maps show the a) ~~The~~2024 bottom-up ~~anomaly in the net land flux combines both the anomaly in (~~DGVMs S_{LAND} ~~from DGVMs~~ and ~~in~~BKMs E_{LUC} ~~from bookkeeping models, although the E_{LUC} contribution to the anomaly is minimal. Panel (b) shows the mean anomaly in the net land flux across 14 inversions. Panel (c) shows the mean anomaly from GOBMs and fCO_2 product ensemble means. The mean anomaly~~ for land; GOBMs and fCO_2 products ~~is first calculated~~for ocean), b) 2024 top-down (atmospheric inversions), c) 2025 bottom-up, and ~~then the mean of the two products is shown. Panel (~~d) ~~shows the mean anomaly in ocean~~2025 top-down fluxes ~~across 14 inversions~~. Units are gC m^{-2} yr^{-1}.


a
CO2 effect
60°N
30°N
0°
30°S
60°S
150°W 120°W 90°W 60°W 30°W 0° 30°E 60°E 90°E 120°E 150°E
b
Climate effect
60°N
30°N
0°
30°S
60°S
150°W 120°W 90°W 60°W 30°W 0° 30°E 60°E 90°E 120°E 150°E
gC m−2 yr−1
160
80
40
20
10
5
2.5
0
−2.5
−5
−10
−20
−40
−80
−160

5386

5387

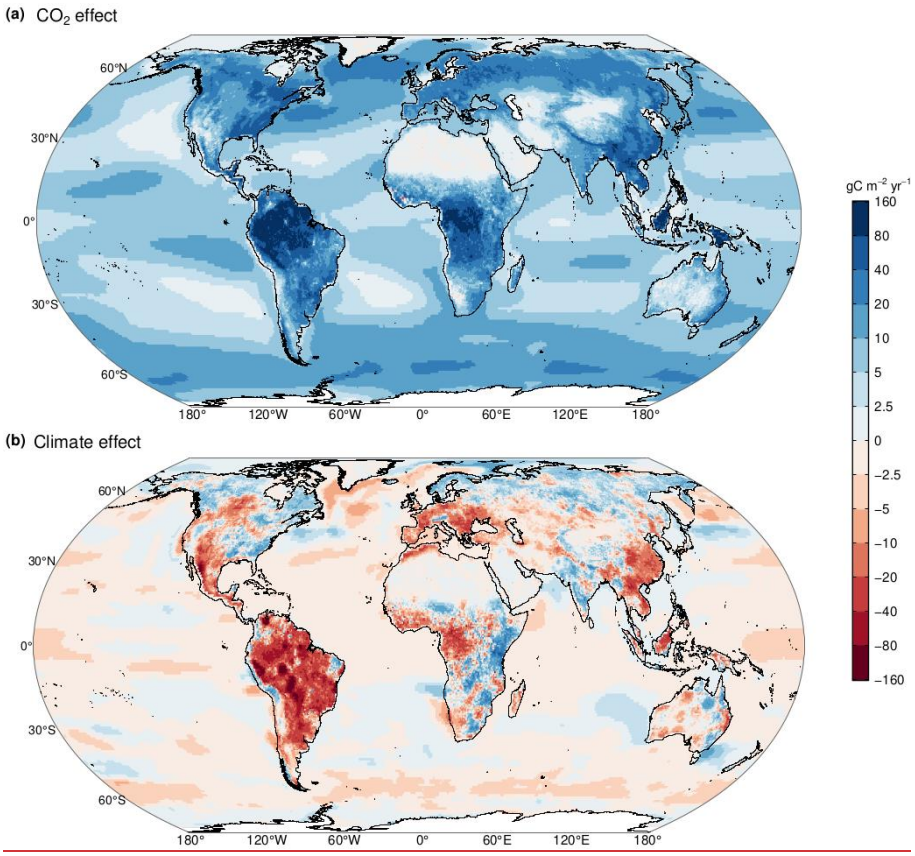
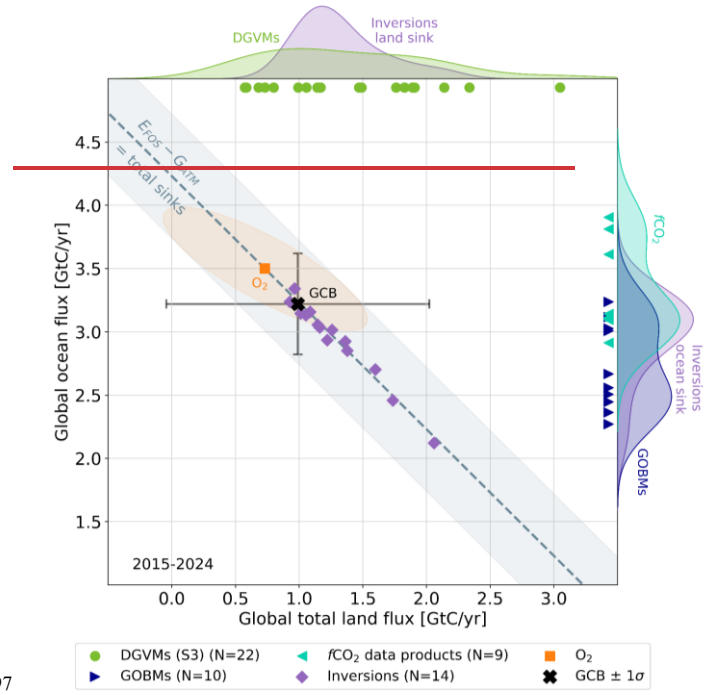


Figure 12. Attribution of the ~~atmosphere-~~anthropogenically-perturbed ocean (S_{OCEAN}) and ~~atmosphere-~~land (S_{LAND}) CO_2 ~~fluxes~~sinks to (a) increasing atmospheric CO_2 concentrations and (b) changes in climate, averaged over the ~~previous~~2016-2025 decade ~~2015–2024~~. All data shown is from the processed-based GOBMs, DGVMs, and ~~DGVMs. Note that the sum of ocean~~BKMs. The DGVM CO_2 ~~and climate effects shown here will not equal the ocean sink shown in Figure 6, which includes the fCO_2 products. No adjustments were applied to the DGVMs or GOBMs~~flux was adjusted for dL from the bookkeeping models. See Supplement S.3.2 and S.4.1 for attribution methodology. Units are in gC m^{-2} yr^{-1} (note the non-linear colour scale). Positive values (blue) are CO_2 sinks, negative values (red) are CO_2 sources.


DGVMs
Inversions land sink
Eros − Gatm = total sinks
O2
GCB
fCO2
Inversions ocean sink
GOBMs
Global ocean flux [GtC/yr]
Global total land flux [GtC/yr]
2015-2024
4.5
4.0
3.5
3.0
2.5
2.0
1.5
0.0
0.5
1.0
1.5
2.0
2.5
3.0
DGVMs (S3) (N=22)
GOBMs (N=10)
fCO2 data products (N=9)
Inversions (N=14)
O2
GCB ± 1σ

5397

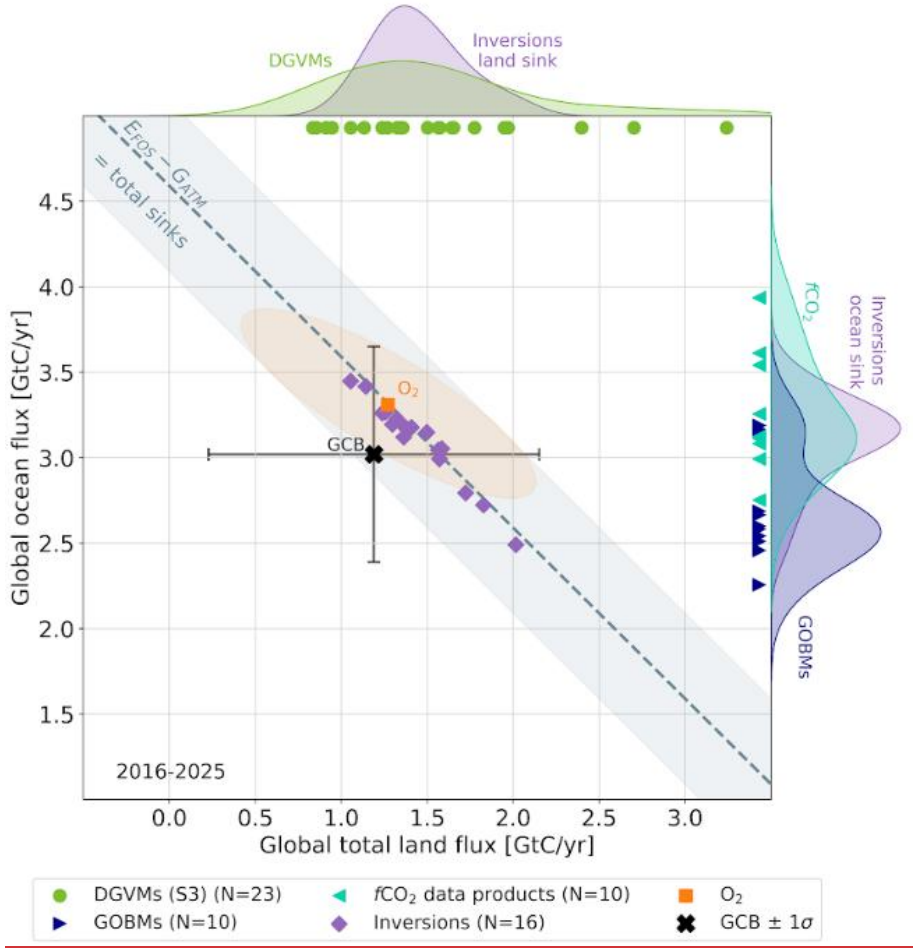
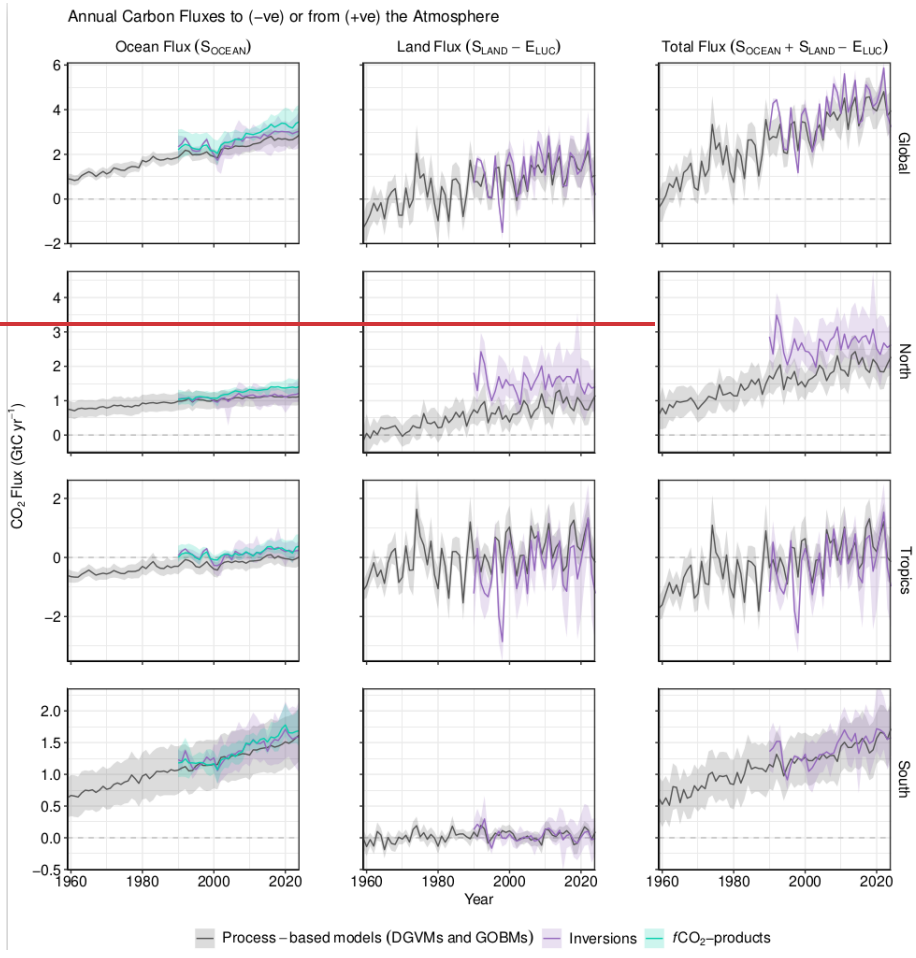

DGVMs
Inversions land sink
$E_{FOS} - G_{ATM}$ = total sinks
fCO_2
Inversions ocean sink
GOBMs
O_2
GCB
2016-2025
Global ocean flux [GtC/yr]
Global total land flux [GtC/yr]
4.5
4.0
3.5
3.0
2.5
2.0
1.5
0.0
0.5
1.0
1.5
2.0
2.5
3.0
DGVMs (S3) (N=23)
GOBMs (N=10)
fCO_2 data products (N=10)
Inversions (N=16)
O_2
GCB ± 1σ

Figure 13. The ~~2015-2024~~2016-2025 decadal mean global ~~net atmosphere-ocean~~S_{OCEAN} and net atmosphere-land fluxes derived from the ocean models and fCO_2 products (y-axis, right and left pointing blue triangles respectively), and from the DGVMs (x-axis, green symbols), and the same fluxes estimated from the atmospheric inversions (purple symbols). The shaded distributions show the densities of the ensembles of individual estimates. The black central cross ('GCB') is the mean (±1σ) of S_{OCEAN} and (S_{LAND} – E_{LUC}) as assessed in this budget. The grey diagonal line represents the constraint on the global land + ocean net flux, i.e. global fossil fuel emissions minus the atmospheric growth rate from this budget (E_{FOS} – G_{ATM}). The orange square represents the same global ~~net atmosphere-ocean~~S_{OCEAN} and atmosphere-land fluxes as estimated from the atmospheric O_2 constraint (the ellipse drawn around the central atmospheric O_2 estimate is a contour representing the 1σ uncertainty of the land and ocean fluxes as a joint probability distribution). Positive values are CO_2 sinks. Note that the inverse estimates have been scaled for a minor difference between E_{FOS} and ~~GridFEDv2025.1~~GridFEDv2026.0 (Jones et al., ~~2025~~2026). The 'GCB' central mean estimate includes the S_{LAND} ,E_{LUC}, and S_{OCEAN} global ~~adjustments.~~estimates from Table 7. The inversions and fCO_2 products include the river adjustment (see Section 2). No further adjustments or corrections were applied to the individual bottom-up estimates.


Annual Carbon Fluxes to (−ve) or from (+ve) the Atmosphere
Ocean Flux (S_{OCEAN})
Land Flux ($S_{LAND} - E_{LUC}$)
Total Flux ($S_{OCEAN} + S_{LAND} - E_{LUC}$)
Global
North
Tropics
South
CO_2 Flux (GtC yr^{-1})
Year
Process−based models (DGVMs and GOBMs)
Inversions
fCO_2−products

5415

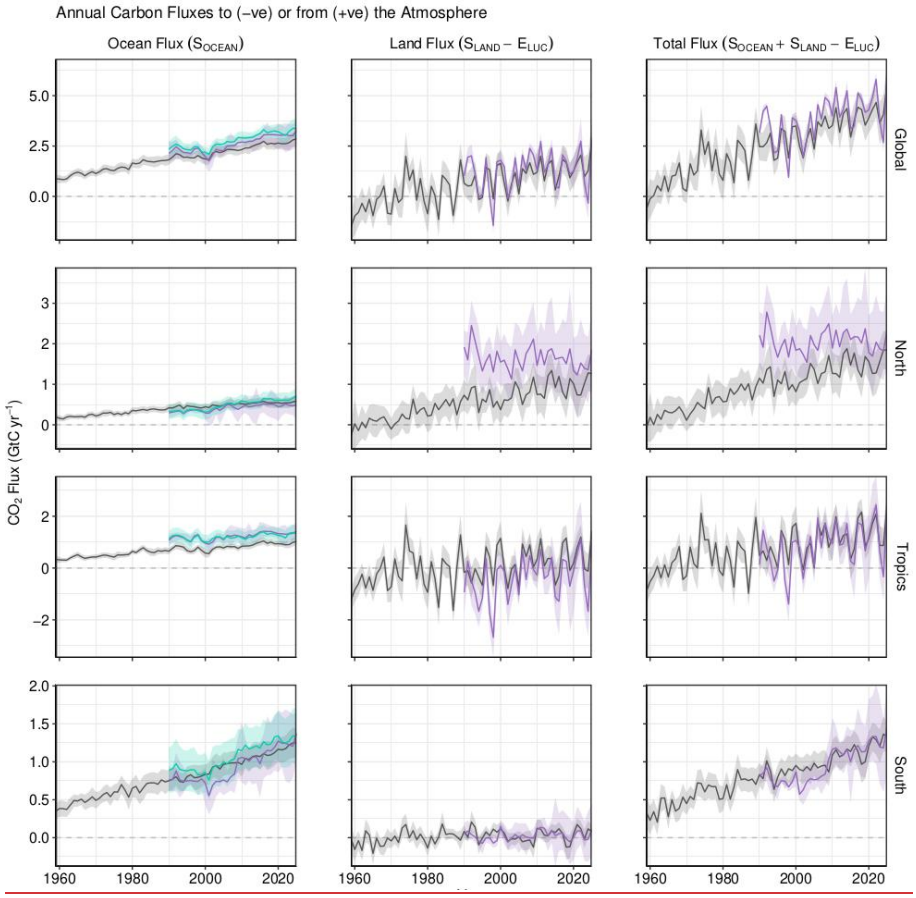
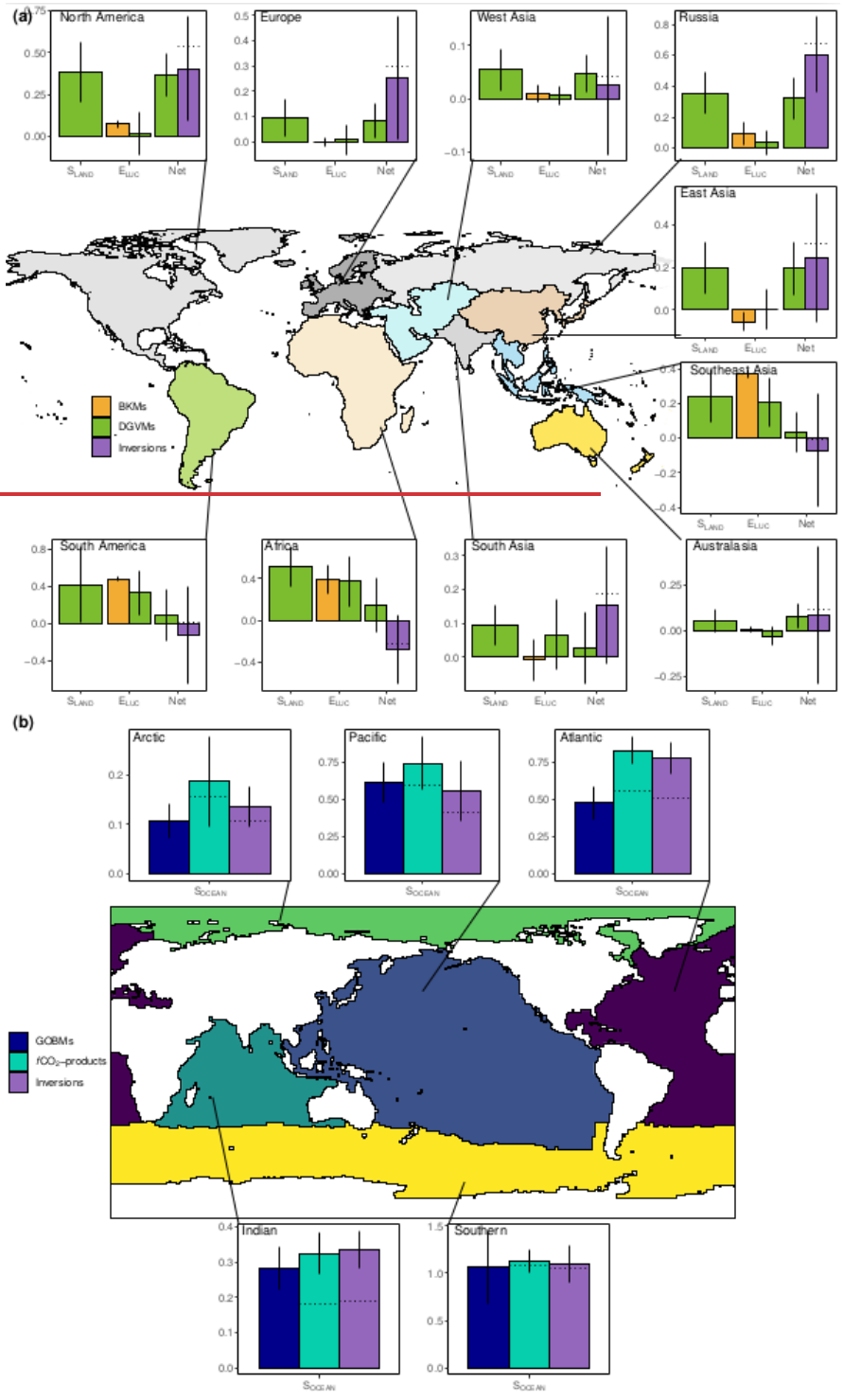


Figure 14. Anthropogenic CO_2 fluxes between the atmosphere and the Earth's surface separated between land and oceans, globally and in three latitude bands. The ocean flux is S_{OCEAN} and the land flux is the net atmosphere-land fluxes from the DGVMs. The latitude bands are (top row) global, (2nd row) north (>30°N), (3rd row) tropics (30°S-30°N), and (bottom row) south (<30°S), and over ocean (left column), land (middle column), and total (right column). Estimates are shown for: process-based models (DGVMs for land, GOBMs for oceans, simulation A minus B); inversion systems (land and ocean); and *f*CO_2-products (ocean only). Inversions and *f*CO_2-products are the contemporary fluxes minus the preindustrial natural steady-state and riverine fluxes (see Table S14). Positive values are CO_2 sinks. Mean estimates from the combination of the process models for the land and oceans are shown (black line) with ±~~1 σ~~1σ of the model ensemble (grey shading). For the total uncertainty in the process-based estimate of the total sink, uncertainties are summed in quadrature. Mean estimates from the atmospheric inversions are shown (purple lines) with their full spread (purple shading). Mean

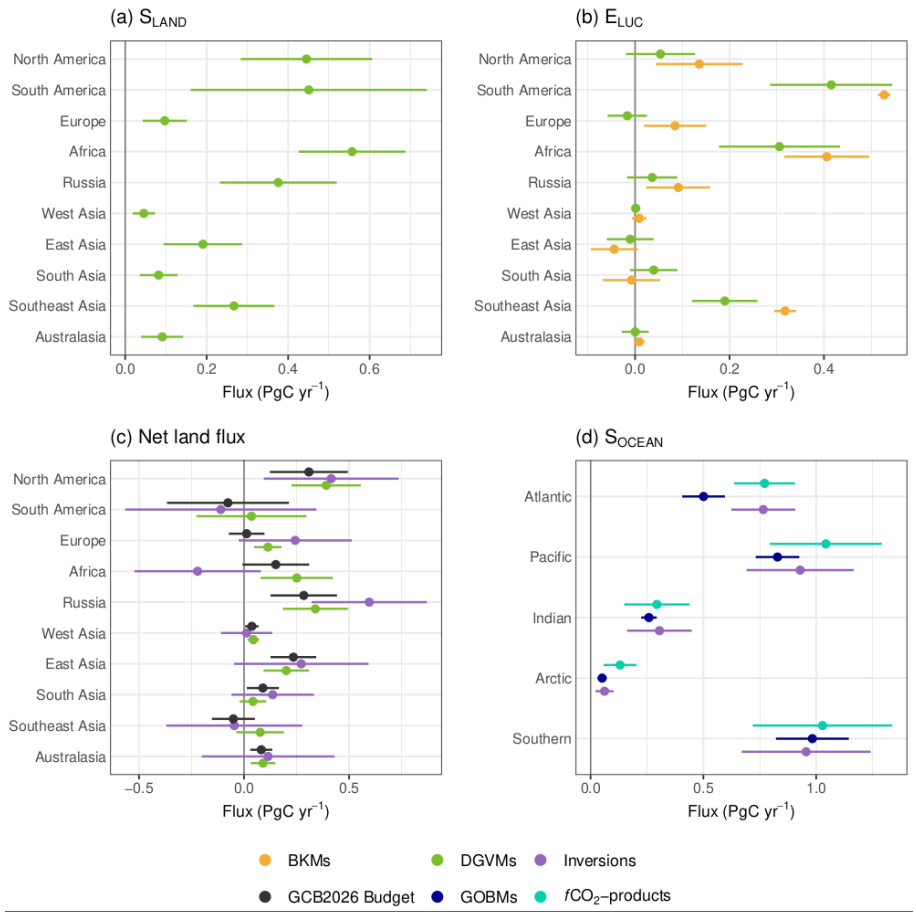
Formatted: Font: Not Bold

estimates from the fCO_2-products are shown for the ocean domain (light blue lines) with ~~full model spread (light blue shading). The global S_{OCEAN} (upper left) and the sum of S_{OCEAN} in all three regions represents the anthropogenic atmosphere-to-ocean flux based on the assumption that the pre-industrial ocean sink was 0 GtC yr^{-1} when riverine fluxes are not considered. This assumption does not hold at the regional level, where pre-industrial fluxes can be significantly different from zero. Hence, the regional panels for S_{OCEAN} represent a combination of natural and anthropogenic fluxes.~~uncertainty as the combination in quadrature of ±1σ of the model ensemble and the ±1σ of the GOBM preindustrial mean flux (Table S14). (light blue shading).

Formatted: Font: 10 pt


(a)
North America
Europe
West Asia
Russia
East Asia
Southeast Asia
South America
Africa
South Asia
Australasia
BIMs
DGVMs
Inversions
(b)
Arctic
Pacific
Atlantic
Indian
Southern
GOBMs
fCO2−products
Inversions

5435


(a) S_{LAND}
North America
South America
Europe
Africa
Russia
West Asia
East Asia
South Asia
Southeast Asia
Australasia
0.0
0.2
0.4
0.6
Flux (PgC yr^{-1})
(b) E_{LUC}
North America
South America
Europe
Africa
Russia
West Asia
East Asia
South Asia
Southeast Asia
Australasia
0.0
0.2
0.4
Flux (PgC yr^{-1})
(c) Net land flux
North America
South America
Europe
Africa
Russia
West Asia
East Asia
South Asia
Southeast Asia
Australasia
−0.5
0.0
0.5
Flux (PgC yr^{-1})
(d) S_{OCEAN}
Atlantic
Pacific
Indian
Arctic
Southern
0.0
0.5
1.0
Flux (PgC yr^{-1})
BKMs
DGVMs
Inversions
GCB2026 Budget
GOBMs
fCO_2–products

5436

Figure 15. Decadal mean (a-c) land and (bd) ocean fluxes for RECCAP-2 regions over 2015-20242016-2025. For land fluxes, S_{LAND} is estimated by the DGVMs (green bars), with the error bar as δL adjustment included. Uncertainty is the combination (in quadrature) of ±1σ spread among models.DGVMs for the sum of simulations S3-S4+S0 and the ±1σ spread among bookkeeping models (BKM) δL estimates. A positive S_{LAND} is a net transfer of carbon from the atmosphere to the land. E_{LUC} fluxes are shown for both DGVMs (green) and bookkeeping models (BKMs (orange), again with the). The BKM uncertainty calculated as the ±1σ spread.is defined as the ±1σ spread among BKMs. The DGVM uncertainty combines (in quadrature) the ±1σ spread among DGVMs for the sum of simulations S0-S4 and the ±1σ spread among BKM δL estimates. Note, a positive E_{LUC} flux indicates a loss of carbon from the land. For the DGVMs, S_{LAND} and E_{LUC} are adjusted for RSS bias. The The net land flux is shown for both DGVMs (green) and), atmospheric inversions (purple), including the full model spread for inversions.and the GCB2026 budget (black; DGVM S_{LAND} - BKM E_{LUC}). The ocean sink (S_{OCEAN}) is estimated by GOBMs (royal blue), fCO_2-products (cyan), and atmospheric inversions (purple). No adjustments were applied to GOBMs and fCO_2-products and atmospheric inversions have been adjusted for pre-industrial steady-state and river fluxes but the fCO_2-products were not corrected for the cool skin effect at regional scale. Uncertainty is estimated as the ±1σ spread for GOBMs, and the full model spread for the other two datasets. The dotted lines show the fCO_2 products and inversion results without river . For fCO_2-products and atmospheric inversions uncertainty is calculated as the combination in quadrature of ±1σ of the model ensemble and the ±1σ of the GOBM preindustrial mean flux adjustment. Positive values are CO_2 sinks. Region definitions can be found at: https://www.globalcarbonproject.org/reccap/

Formatted: Indent: Left: 0 cm, First line: 0 cm